Effect of the rhubarb anthraquinone Rhein on cardiac fibroblast to myofibroblast transition

Inaugural-Dissertation

zur Erlangung des Doktorgrades
der Mathematisch-Naturwissenschaftlichen Fakultät
der Heinrich-Heine-Universität Düsseldorf

vorgelegt von

David Monteiro Barbosa
aus Heinsberg

Düsseldorf, Mai 2019

aus dem Institut für Klinische Biochemie und Pathobiochemie
des Deutschen Diabetes-Zentrums
Leibniz-Zentrum für Diabetesforschung
an der Heinrich-Heine-Universität Düsseldorf

Gedruckt mit der Genehmigung der
Mathematisch-Naturwissenschaftlichen Fakultät der
Heinrich-Heine-Universität Düsseldorf

Berichterstatter:
1. Prof. Dr. Hadi Al-Hasani
2. Prof. Dr. Ulrich Rüther

Tag der mündlichen Prüfung: 02.07.2019

Zusammenfassung

Die manifestierte Fortschreitung myokardialer Fibrose in verschiedenen Formen der Kardiomyopathie, resultiert in der Versteifung des Herzgewebes und führt langfristig zur Dysfunktion des linken Herzventrikels. Die Persistenz dieses pathologischen Zustands beeinflusst dramatisch die Überlebensrate nach Herz-Kreislauf-Ereignissen und führt letztendlich zum Tod. Das Myokard besteht zu ca. 70-80% aus Herzfibroblasten, welche maßgeblich der Erhaltung der extrazellulären Matrix dienen. Fibroblasten sind in der Lage ihren Phänotypen hin zu Matrix akkumulierenden und aktiveren Myofibroblasten zu verändern, die die fibrotische Reaktion auf eine pathologische Umgebung ausführt. Obwohl Fibrosierung einen Heilungsvorgang darstellt, führt eine Maladaption durch exzessive extrazelluläre Matrixakkumulation zur Beschleunigung der kardialen Dysfunktion. Die Synthese und Freisetzung löslicher Mediatoren durch persistierende und hochaktive Myofibroblasten begünstigt die Verbreitung der Fibrosierung über das Myokard und verstärkt das maladaptive kardiale *Remodeling*. Die Erforschung einer antifibrotischen medikamentösen Behandlungsstrategie zur Reduktion der Fibroblast-zu-Myofibroblast Differenzierung und Unterbindung profibrotischer interzellulärer Kommunikation, zeugt demnach von dringender Notwendigkeit. Das Rhabarber-Anthraquinon Rhein, ein Wirkstoff, der bereits in der Behandlung von Osteoarthritis verwendet wird, wurde kürzlich mit heilsamen Eigenschaften im Kontext fibrotischer Krankheiten anderer Organe in Verbindung gebracht. Die Relevanz der potenziellen Behandlung im Bezug zur kardialen Fibrose und der genaue Wirkmechanismus wurden jedoch bislang nicht aufgeklärt. Das Ziel der vorliegenden Arbeit bestand demnach darin zu prüfen ob die Verabreichung von Rhein die Fibroblast-zu-Myofibroblast Differenzierung beeinträchtigen und die Verbreitung von fibrotischen Signalen in der pathophysiologischen Umgebung der chronischen Hypoxie unterbinden kann.

Die Charakterisierung der Sekretome von humanen primären Herzventrikelfibroblasten, die chronischer Hypoxie ausgesetzt wurden, zeigte eine moduläre Verschiebung der sekretorischen Produkte auf, die mit der differenziellen Regulation pro-fibrotischer Signalwege assoziierte. Rheinbehandlung milderte diese Hypoxie-vermittelte moduläre Verschiebung und mittels umfassender bioinformatischer Untersuchungen konnte die Auswirkung von Rhein auf die Modulation von Fibrose-assoziierten Signalwegen zurückgeführt werden. Darüber hinaus konnte die Einflussnahme von Rhein auf Veränderungen des Transkriptoms, die den kardialen Fibroblastenphänotypen determinieren, gezeigt und dessen Zusammenhang mit der Verschiebung des sekretorischen Profils umfangreich dargestellt werden. In einem holistischen Ansatz, durch die Kombination aus Sekretom- und Transkriptomsignalweganalysen, wurden die drei statistisch robusten, in der Determinierung des Herzfibroblastphänotyps beteiligten Upstreamregulatoren TGFβ1, p53 and p21 identifiziert.

Die detaillierte Untersuchung dieser Regulatoren zeigte die Rhein-vermittelte Minderung der Bioverfügbarkeit von TGFβ1 durch Herabsenkung dessen Sekretion. Funktional, erhöhte Rhein die Abundanz von p53 und p21, welche mit einer Verlängerung der G2/M Zellzyklusphase und im Einklang mit verminderter Proliferation einherging. Des Weiteren setzte Rhein die zelluläre Sensitivität zu exogenem TGFβ1 herab und hemmte auf intrazellulärem Wege den TGFβ/SMAD-Signalweg. Mechanistisch konnten die Rhein-vermittelten Effekte auf eine HDAC-abhängige Erhöhung der Abundanz von p53 und SMAD7 zurückgeführt werden. Schließlich konnte die antifibrotische Wirkung von Rhein durch eine Inhibition der Kollagenkontraktion als Antwort auf TGFβ1 und die damit verbundene gehemmte Fibroblastendifferenzierung funktional nachgewiesen werden.

Zusammenfassend, konnte anhand dieser Arbeit Rhein als neuer potenter HDAC-Inhibitor identifiziert werden und die Eignung von Rhein als Antifibrotikum in der Behandlung von kardialer Fibrose nachgewiesen werden. Die Verfügbarkeit von Rhein als bereits genehmigtes und auf Sicherheit geprüftes Medikament, lässt somit auf eine potenzielle Behandlung in der ergänzenden und protektiven Intervention von kardialer Fibrose schließen. Als mögliche unterstützende Maßnahme könnte somit die Verbreitung der kardialen Fibrose in Hochrisikopatienten unterbunden und langfristig die Erhaltung der Herzfunktion begünstigt werden.

Abstract

Myocardial fibrosis manifests progressively in several forms of cardiomyopathies leading to cardiac stiffness and left ventricle dysfunction. Persistence of this pathologic state dramatically affects the survival rate after cardiovascular events and ultimately leads to death. In the heart, cardiac fibroblasts account to approx. 70-80% of the resident cells, functioning as mediators of extracellular matrix maintenance. Fibroblasts are able to switch to the extracellular matrix-accumulating and more active myofibroblast phenotype, which drives the fibrotic response to pathologic environmental changes. Although fibrosis depicts a reparative mechanism, maladaptation of the heart due to excessive production of extracellular matrix accelerates cardiac dysfunction. Soluble signals generated by persistent and highly synthetic myofibroblasts exacerbate the progression of fibrosis throughout the myocardium, favoring maladaptive cardiac remodeling. Hence, an anti-fibrotic therapeutic approach leading to reduced fibroblast-to-myofibroblast transition and abrogation of profibrotic intercellular communication is of urgent interest. The rhubarb anthraquinone Rhein, a drug already used as treatment for osteoarthritis, has been reported to display beneficial properties in the setting of fibrotic pathologies of other organs. However, its relevance for the treatment of cardiac fibrosis and the exact mechanism have not been elucidated yet. The aim of this study, was to prove whether Rhein administration could interfere with fibroblast-to-myofibroblast transition and dissemination of fibrotic signals in the pathophysiological environment of chronic hypoxia.

Compositional characterization of primary human ventricular cardiac fibroblast secretomes subjected to chronic hypoxia revealed a modulatory shift of secretory products in association to differential regulation of profibrotic pathways. Rhein administration mitigated this hypoxia-mediated modulatory shift and via comprehensive bioinformatic examination the implication of Rhein in the modulation of fibrosis-associated pathways was identified. Further, the influence of Rhein on the alteration of the transcriptome linked to the cardiac fibroblast phenotype was elaborately demonstrated to associate to changes in the secretory profile. In a holistic approach, the combination of secretomic and transcriptomic pathway analyses, robustly identified the three upstream regulators TGFβ1, p53 and p21 to be involved in the determination of cardiac fibroblast phenotypes.

Detailed investigation of these regulators demonstrated the involvement of Rhein in the decrease of active TGFβ1 bioavailability via mitigation of its secretion. Functionally, Rhein increased p53 and p21 associated to a prolongation of the G2/M cell cycle phase and in line with decreased proliferation. Furthermore, Rhein was shown to reduce cellular sensitivity to exogenous TGFβ1 and to intracellularly abrogate TGFβ/SMAD-signaling. Mechanistically, Rhein-mediated effects were linked to the HDAC-dependent increase of p53 and SMAD7 abundance. Finally, Rhein was demonstrated to abolish collagen contraction in response to

TGFβ1 associated to inhibited cardiac fibroblast-to-myofibroblast transition, thus functionally proving its anti-fibrotic property.

In conclusion, this study identifies Rhein as a novel potent HDAC inhibitor and provides evidence that Rhein may contribute to the treatment of cardiac fibrosis as anti-fibrotic agent. As readily available drug with approved safety, Rhein constitutes a promising potential therapeutic approach in the supplemental and protective intervention of cardiac fibrosis. As complementary therapy, thus Rhein could prevent cardiac fibrosis propagation in high risk patients and aid in the preservation of cardiac function.

Table of contents

List of Figures

List of Tables

List of acronyms

αSMA	Alpha-smooth-muscle actin
ACTA2	Actin-alpha 2
ADP	Adenosine Diphosphate
AnA	Anacardic acid
ANOVA	Analysis of Variation
APP	Amyloid Precursor Protein
APS	Ammonium Persulfate
ATP	Adenosine Triphosphate
BCA	Bicinchoninic Acid
BSA	Bovine Serum Albumin
BZ	Bortezomib
CDKN1A	cyclin-dependent kinase inhibitor 1
cDNA	complementary DNA
CF	Cardiac fibroblast
CM	Cardiomyocyte
CO_2	Carbondioxide
CoA-SH	Coenzyme A thioester
COL	Collagen
CTGF	Connective Tissue Growth Factor
Cu^{2+}	Copper ion
CV	Coefficient of Variation
DDA	data dependent acquisition
DIA	data independent acquisition
DMEM	Dulbecco's Modified Eagle Medium
DMSO	Dimethyl sulfoxide
DNA	Deoxyribonucleic Acid
DNMT	DNA methyltransferase
NTP	nucleoside triphosphate
DTT	Dithiothreitol
ECM	Extracellular Matrix
EDTA	Ethylenediaminetetraacetic Acid
EGFR	Epidermal Growth Factor Receptor
EIF2	Eukaryotic Initiation Factor 2
ELISA	Enzyme Linked Immunosorbent Assay
EMT	Epithelial-to-mesenchymal transition
EndMT	Endothelial-to-mesenchymal transition

ER	Endoplasmic Reticulum
ERK	Extracellular Signal-Regulated Kinase
FCS	Fetal Calf Serum
FDR	False discovery rate
FMT	Fibroblast-to-myofibroblast transition
FN1	Fibronectin 1
FPCL	Fibroblast populated collagen lattice
GAPDH	Glyceraldehyde 3-phosphate dehydrogenase
GLUT1	Glucose transporter 1
GO	GeneOntology
HAT	Histone Acetyltransferase
HCF-v	Human cardiac fibroblast (ventricular)
HDAC	Histone Deacetylase
HF	Heart Failure
HIF	Hypoxia Inducible Factor
HRE	Hormone-Responsive Element
HRP	Horseradish Peroxidase
IC50	half maximal inhibitory concentration
IL1β	Interleukin 1 beta
IL-6	Interleukin 6
IPA	Ingenuity pathway analysis
iRT	indexed Retention Time
JNK	C-Jun N-Terminal Kinase
LAP	Latency-Associated Peptide
LC-MS	Liquid chromatography–mass spectrometry
LFQ	label-free quantification
LLC	large latent complex
LTBP	latent TGF-beta binding protein
MeT	Methyltransferase
Mg^{2+}	Magnesium ion
$MgCl_2$	magnesium chloride
MI	Myocardial Infarction
MMP	Matrix Metalloproteinase
MSF	matched spectra file
MW	Molecular Weight
Na_2HPO_4	Disodium phosphate
$Na_4P_2O_7$	Tetrasodium pyrophosphate

NaCl	sodium chloride
NAD	Nicotinamide Adenine Dinucleotide
Na-DOC	Sodium Deoxycholate
NaH_2PO_4	Monosodium phosphate
$NaHCO_3$	Sodium bicarbonate
NAM	Nicotinamide
NP-40	Nonidet P-40
O_2	Oxygen
PAI1	Plasminogen Activator Inhibitor 1
PBS	Phosphate Buffered Saline
PCR	Polymerase Chain Reaction
PiQ	Precursor Ions Quantifier
PLS-DA	Partial least square-discriminant analysis
PSM	Peptide-spectra match
PTM	Posttranslational Modification
PVDF	Polyvinylidene Difluoride
RFU	Relative fluorescent unit
RLU	Relative luminescent unit
RIPA	Radioimmunoprecipitation assay buffer
RNA	Ribonucleic Acid
RT	Reverse Transcriptase
RT-qPCR	Real-time quantitative polymerase chain reaction
SAH	S-adenosyl homocysteine
SAM	S-Adenosyl methionine
SB	Sodium Butyrate
SD	Std. Deviation
SDS	Sodium Dodecyl Sulfate
SIRT	Sirtuin
SLC	Small latent complex
SMAD	small Mothers Against Decapentaplegic
SP	signal peptide
TBS-T	tris-buffered saline, Tween 20
TCA	tricarboxylic acid
TEMED	Tetramethylethylenediamine
TGF	Transforming Growth Factor
TGFβR1	TGF beta receptor 1
TIMP	Tissue inhibitor of metalloproteinase

TSA	Trichostatin A
VEGF	Vascular endothelial growth factor

1 Introduction

Heart disease today is considered the most common death cause in both first- as well as third-world countries. Cardiac pathologies are most often associated to multifactorial cardiomyocyte decay resulting in decreased cardiac function and compromised blood supply. In the past, most research has been invested in the amelioration and therapy of cardiac physiology to decrease mortality, however only with minor success. The main focus has been laid on the prevention of cardiomyocyte loss and maintenance of extant heart muscle cells, neglecting the potential role of non-cardiomyocyte cells populated in the heart. Nevertheless, the higher number of non-cardiomyocytes and the heterogeneity of cells populating the heart suggests a tightly regulated network including inter- and intracellular communication (Souders et al., 2009). Furthermore, this might indicate non-cardiomyocytes as therapeutic target in the prevention of heart disease progression.

1.1 Heart failure

Heart failure (HF) is a complex clinical syndrome defined by malfunction of the heart in pumping blood (Coronel et al., 2001). In 2014, at least 26 million people worldwide were affected (Ponikowski et al., 2014) and its increasing prevalence indicates that HF is a major and growing public health problem worldwide (Savarese and Lund, 2017). The increased prevalence is thought to be assigned to a generally prolonged lifespan, but also associated to the increased life expectancy of HF patients due to improving therapeutic approaches. Still, HF is a disease with a poor prognosis marked by a mortality rate around 50% over 5 years after diagnosis comparable to that of the most common cancers (Pons et al., 2010).

Physiologically speaking, HF is characterized by compromised cardiac output unable to meet the demand of the body resulting from systolic dysfunction (decreased contractility of the myocardium) and/or diastolic dysfunction (inadequate filling of the heart) (Tan et al., 2010). Several clinical conditions have been identified to contribute to HF such as myocardial infarctions (MI), chronic ischemia, dilated cardiomyopathy, chronic pressure overload, valvular heart disease and congenital heart disease (Pazos-López et al., 2011). Collectively, any of these pathologies ultimately interferes with the myocardial contractility and inevitably promotes cardiomyocyte loss. In contrast to other organs, the heart muscle lacks the ability of self-renewal failing the regeneration of cardiomyocytes (Davidson et al., 2018). However, in order to compensate for physiological and pathological challenges, the heart features the ability to undergo morphological changes maintaining a certain degree of its contractile function. This process is referred to as cardiac remodeling.

1.1.1 Cardiac remodeling

Cardiac remodeling is the process by which ventricular size, shape, and function are modulated driven by neurohormonal, mechanical, and genetic parameters (Sutton and Sharpe, 2000). Herein, remodeling may be physiological and adaptive during normal growth or pathological due to cardiac injury. Cardiac remodeling in terms of hypertrophy e.g. occurs during development, which is associated with the normal growth of the heart after birth until adulthood (Figure 1). However, also the adult heart may develop hypertrophy as response to extensive aerobic conditioning through chronic exercise (Dickhuth et al., 2004), considered physiological hypertrophy. Both developmental and physiological hypertrophy are characterized by a uniform ventricular growth featuring an even enlargement of chamber, septum and ventricular wall (Heineke and Molkentin, 2006). As an adaptive state, exercise-induced physiological hypertrophy is reversible in the long term and does not negatively affect cardiac function. Contrarily, pathological hypertrophy most often induced by chronic hypertension and aortic valve stenosis involves concentric growth of the septum and the ventricular wall leading to decreased chamber size, which directly affects diastolic function. The concentric growth is not only mediated by one-dimensional enlargement of cardiomyocytes but also caused by the onset of fibrosis, making the pathological hypertrophy only partly reversible.

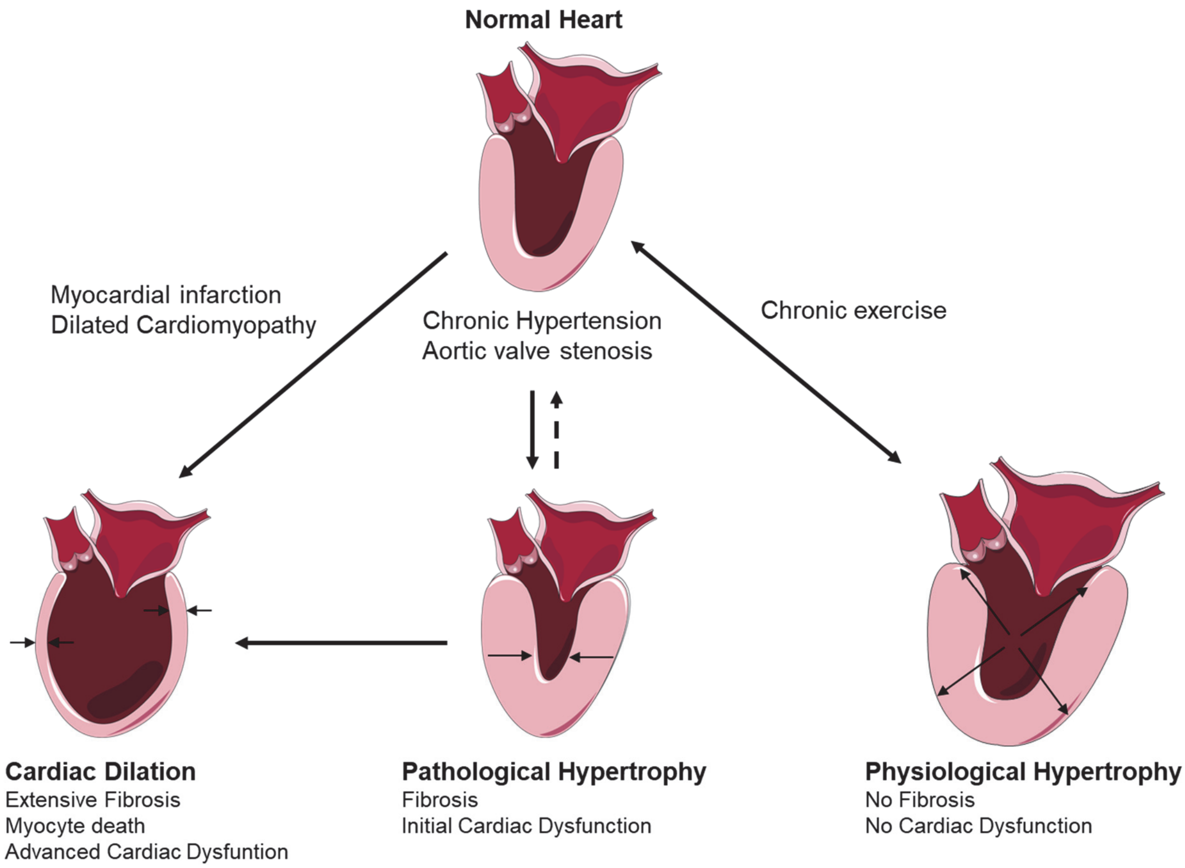

Figure 1: Overview of physiological and pathological cardiac remodeling

Modified after: Heineke and Molkentin (2006)

Persistence of pathological hypertrophy consequently produces cardiac dilation due to cardiomyocyte death and pronounced cardiac wall thinning leading to increased ventricular chamber volume. In consequence to these structural modifications, the heart shows strongly impaired systolic and diastolic function progressively resulting in HF. Independently of precedent hypertrophy, cardiac dilation also occurs directly as product of acute stimuli such as MI and dilated cardiomyopathy. An important determinant of the severity and propagation of cardiac remodeling-associated HF is the extent of cardiac fibrosis.

1.1.2 Cardiac fibrosis

Cardiac fibrosis is a complex process that involves each cellular component of the myocardial tissue (Mewton et al., 2011). The heart is composed of cardiomyocytes, endothelial cells, vascular smooth muscle cells and fibroblasts interconnected in a compacted network of extracellular components (Figure 2), the so-called extracellular matrix (ECM). Under physiological conditions, the ECM is in intimate contact with the cardiac cells and plays a critical role in the maintenance of ventricular shape, size, and function. To guarantee the integrity of this network, the ECM undergoes constitutive degradation and synthesis mediated by the turnover of the extracellular components. During cardiac fibrosis an imbalance of this homeostasis results in the formation of excess fibrous connective tissue (Birbrair et al., 2014). Depending on the pathological stimulus, cardiac fibrosis is discriminated between a reactive or reparative process. As in the case of chronic hypertension and aortic valve stenosis the present pressure overload promotes reactive interstitial fibrosis defined by progressive deposition of ECM (Creemers and Pinto, 2011). As an adaptation to increased workload, interstitial fibrosis supports the cardiomyocytes by stabilizing the ventricular wall, however at the expense of ventricular stiffness and impaired diastole. Following the acute incident of MI and as a consequence of progressive manifestation of interstitial fibrosis, the loss of cardiomyocytes initiates inflammatory cell response and drives the replacement of dead cells by increased collagen deposition (Russo and Frangogiannis, 2016). Fibrotic scar formation in the ventricle is associated with increased mechanical stiffness and hence contributes to both systolic and diastolic dysfunction (Murtha et al., 2017). Conclusively, although fibrosis constitutes an essential reparative and compensatory mechanism, maladaptation of the heart due to excessive production of ECM aggravates cardiac dysfunction and accelerates HF. Thus, an anti-fibrotic approach leading to reduced adverse remodeling will be of relevant therapeutic interest.

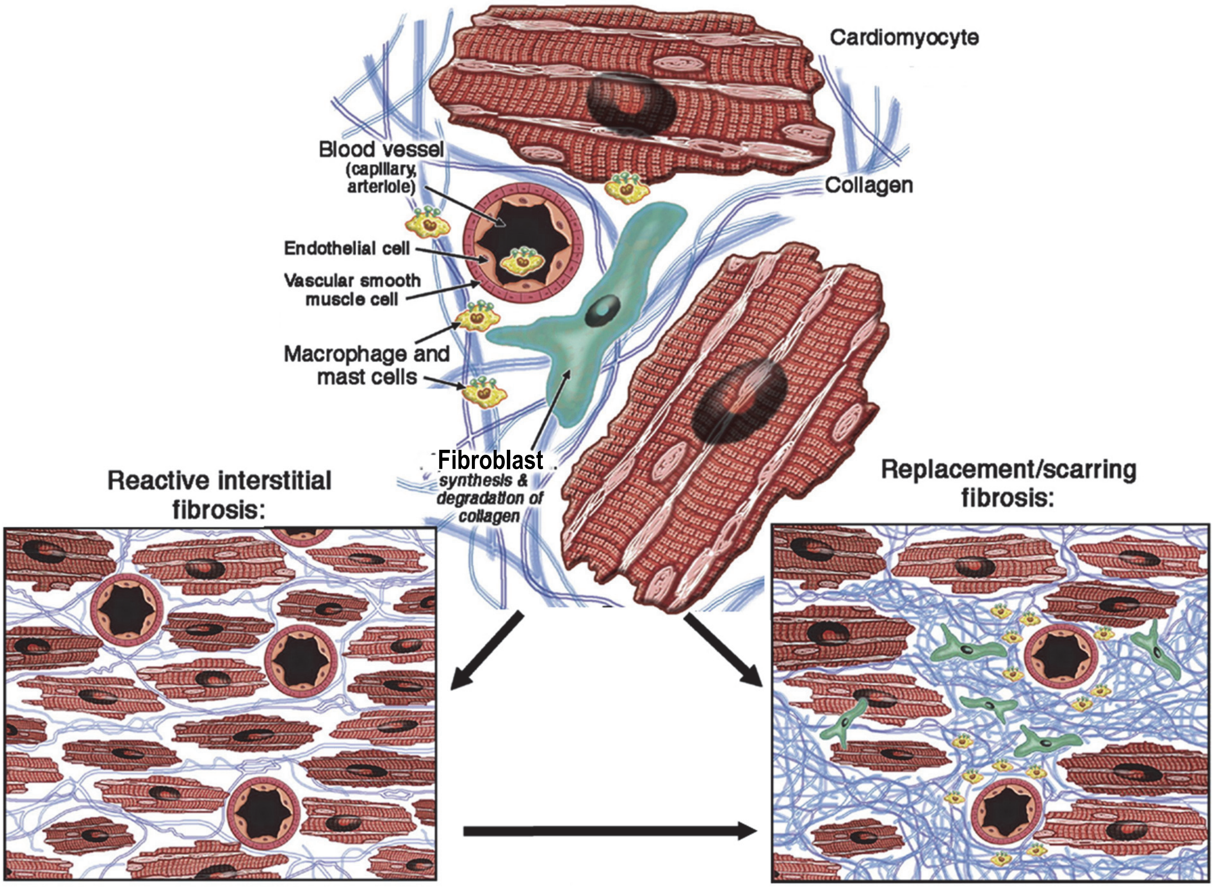

Figure 2: Etiology of cardiac fibrosis

Modified after Mewton et al. (2011)

1.2 Mediators of fibrosis

1.2.1 Cellular effectors of fibrosis

Independent of the etiology of fibrosis, myofibroblast (MF) activation is the hallmark of the cardiac fibrotic response (Kong et al., 2014). Activation MFs in the remodeling myocardium requires the co-operation of growth factors and specific matrix proteins, which signal through cell surface receptors to activate intracellular signaling pathways resulting in the synthesis of contractile proteins and production of matrix macromolecules (Shinde and Frangogiannis, 2017).

Cardiomyocyte dysfunction or death is often the initial event responsible for direct or indirect activation of fibrogenic signals in the myocardium, respectively. In the case of MI, acute death of cardiomyocytes results in inflammatory response, characterized by the activation of innate immune pathways including release of inflammatory cytokines, leukocyte recruiting to the infarcted site and activation of neutrophils (Zymek et al., 2006). After resolution of the primary inflammatory phase, the proliferative phase is initiated by secreted growth factors from mononuclear cells and macrophage subpopulations recruiting reparative cells including fibroblasts and MFs to the site of injury (Frangogiannis, 2014). In other cases, such as pressure overload or chronic myocardial inflammation, viable cardiomyocytes may directly promote reactive fibrosis by activating interstitial fibroblasts (Sassi et al., 2014). Further, neurohumoral and growth factor-mediated pathways may play an important role in activation of cardiomyocyte-derived fibrogenic signals (Kong et al., 2014).

Endothelial cells in the myocardium are also thought to contribute to the induction of MFs playing a bivalent role. On the one hand, endothelial cells, promote the recruitment of macrophages and lymphocytes with fibrogenic actions through the release of pro-inflammatory cytokines and chemokines (Van Linthout et al., 2014). On the other hand, endothelial cells may undergo endothelial-mesenchymal transition (EndMT) (Zeisberg et al., 2007), thus directly contributing to expansion of the fibroblast population in the remodeling heart.

Most interestingly, another cellular effector of MF induction constitutes the myofibroblast itself. Soluble signals generated by persistent and highly synthetic MFs at the injured site are capable of traversing neighboring interstitial space to distant sites where they provoke quiescent fibroblasts into collagen synthesis (Weber et al., 2012b) and ultimately to trans-differentiation. Via coronary arteries, circulating signals might be transported to even more remote sites exacerbating to the progression of fibrosis throughout the myocardium. This process depicts a possible explanation for maladaptive cardiac remodeling and favoring progressive HF. Thus, investigation of the cardiac MF secretome is proposed as one area of interest to develop antifibrotic therapies to ameliorate cardiac preservation after injury (Weber and Diez, 2016).

1.2.2 Physiological effectors of fibrosis

1.2.2.1 Chronic hypoxia

Following tissue injury, vascular perfusion is compromised creating acute hypoxic conditions in a microenvironment. Sustained local hypoxic conditions in damaged tissue further may evolve from high demand for oxygen by resident cells or infiltrated inflammatory cells and mesenchymal cells (Remensnyder and Majno, 1968). Acute hypoxia constitutes a key factor essential for processes involved in tissue repair, such as angiogenesis and energy homoeostasis. However, prolonged or chronic hypoxia may play a role in both pathological repair and adverse fibrosis (Darby and Hewitson, 2016).

Most of the cellular responses in the presence of hypoxia occur through activation of the transcription factor hypoxia-inducible factor 1 (HIF1). HIF1 transcriptionally upregulates the expression of several targets including glucose transporter (GLUT)1 and vascular endothelial growth factor (VEGF), enabling physiologic adaptation to hypoxia through the promotion of angiogenesis, increased glucose metabolism and increased survival. Furthermore, HIF1 targets the transcription of adhesion proteins (integrins), extracellular matrix components (type

I collagen and fibronectin) and connective tissue growth factor (CTGF), to enhance the repair process (Higgins et al., 2004; Semenza, 1999).

Although oxygen-sensing by HIF1 is a key factor in the physiological response in consequence of ischemia and reperfusion injury in the heart, its activation may be both cardioprotective or derogatory (Townley-Tilson et al., 2015). Characteristically, fibrosis-associated diseases feature chronic tissue hypoxia, caused by microvascular obstruction (Kischer et al., 1982) and high oxygen consumption (Ichioka et al., 2008) and it has been demonstrated that HIF1α actively participates in the pathogenesis of fibrosis (Ho et al., 2014). Herein, overrepresentation of HIF1α in fibrotic tissues has been shown to correlate with upregulation of profibrotic factors involved in excessive ECM production (Distler et al., 2007; Higgins et al., 2004). Contrastingly, ablation of HIF1α in age-related ischemic wounds was associated to diminished adaptive hypoxia responses and impaired wound healing (Liu et al., 2008b). However, accumulating evidence points to a strong correlation between HIF-1 stabilization and TGF-β signaling during enhanced fibroblast function in hypoxic tissue (Lokmic et al., 2012).

1.2.3 Epigenetic and posttranslational contributors to fibrosis

Epigenetics refers to alterations of gene expression without manipulation of the native DNA sequence, whereas posttranslational modifications (PTM) relate to the covalent addition of a functional group to a protein after completed translation by ribosomes. Recently, a vast number of studies reported that the activation of CF in the development of cardiac fibrosis may be attributed to epigenetic and posttranslational changes, adding a novel perspective to the mechanistic comprehension of the disease (Grimaldi et al., 2017). The most characterized and associated regulators in this context include DNA methylation, histone deacetylases (HDACs), sirtuins (SIRTs) and histone acetyltransferases (HATs), which are introduced in detail in the following sections.

1.2.3.1 DNA methylation

DNA methylation plays an essential role in epigenetic regulation including genomic imprinting and gene silencing (Tao et al., 2013). Methylation of DNA occurs at the fifth carbon of cytosine (m5C) within phosphate-linked cytosine guanine (CpG). Relatively rare throughout the genome accounted as whole, CpGs appear in clusters referred to as CpG islands (Tan et al., 2013). Around 70% of genes are estimated to have a CpG island in their proximal promoter regions (Estécio and Issa, 2011), which can be hypermethylated and thus impede transcription of genes at those sites (Yang et al., 2012). DNA methylation is effectuated by at least three different DNA (cytosine-5)-methyltransferases (DNMTs) identified to have functional activity in mammals, namely, DNMT1, DNMT3A, and DNMT3B (Yao and Li, 2015). While DNMT1 is primarily known as a maintenance DNMT important for maintaining the DNA methylation patterns during replication (Clements et al., 2012), DNMT3A and DNMT3B belong to *de novo* methyltransferases able to methylate non-methylated CpG sequences (Sharma et al., 2012).

The implication of DNA methylation in the development of cardiac fibrosis has been demonstrated by Metes-Kosik et al. (2012) in an *in vivo* approach, where mice were either deprived or supplemented with selenium, which reduced methylation levels and DNMT activity. The authors reported that both manipulations resulted in reactive myocardial fibrosis and systolic dysfunction, indicating that imbalance of the DNA methylation state is involved in the prevalence of cardiac complications. *In vitro*, inhibition of DNA methylation in human ventricular CFs using 5-azacytidine resulted in decreased TGFβ1-induced expression of collagen I, collagen III, and α-smooth muscle actin (αSMA) (Watson et al., 2016). A quite interesting finding, linking hypoxia with DNA methylation and activation of human cardiac fibroblasts was published by the very same group around Watson et al. (2014). Here, the authors reported that prolonged hypoxia-induced stabilization of HIF1α directly led to increased transcription levels of DNMT1 and DNMT3a/3b. Consequently, as a result of elevated DNA methylation levels, increased synthesis of collagen I and αSMA were observed.

1.2.3.2 Acetylation – HAT, HDAC and SIRT

Reversible acetylation and deacetylation of ε-amino groups on lysine residues constitutes a PTM, which significantly participates in the regulation and determination of stability and function of proteins (Drazic et al., 2016). Acetylation plays a role in the regulation of gene expression as histone acetylation/deacetylation of the N-terminal tail leads to alteration of the chromatin structure, leaving the DNA accessible or inaccessible for transcriptional activation (Allfrey et al., 1964; Bannister and Kouzarides, 2011). Regulation of gene transcription also occurs via acetylation of non-histone proteins, like transcriptional factors, by affecting their DNA binding affinity (Das and Kundu, 2005). Further, acetylation of lysine residues competitively blocks them for ubiquitin ligases, protecting cytoplasmic proteins from ubiquitination and subsequent degradation by the proteasome, while deacetylation unmasks the lysine residue and destabilizes the protein (Caron et al., 2005).

The balance between the acetylated/deacetylated states of both histone and non-histone proteins is mediated by the competition between HATs and HDACs. The acetyl group adding HAT family members are classified in nuclear type A HATs, including MYST, NRCF, GNAT, basal TF and the most studied p300/CBP, and cytoplasmic type B HATs comprised of HAT1, HAT2, HatB3.1, Rtt109, and HAT4 (Wang et al., 2014). HDACs, as deacetylating counterpart to HATs, include 4 different classes (class I-IV), whereas class III is often referred to as distinct class named SIRT. Although all HDAC classes have the same deacetylating function, SIRTs (SIRT1-7) require NAD^+ for catalytic activity, whereas Class I (HDACs 1, 2, 3 and 8), IIa

(HDACs 4, 5, 7 and 9), IIb (HDACs 6, 10) and IV (HDAC11) are Zn^{2+}-dependent (Gallinari et al., 2007). While Class I and IIb statically act in the nucleus or mainly in the cytoplasm, respectively, all other HDAC classes are able to shuttle between the nucleus and the cytoplasm (Caron et al., 2005; Morris and Monteggia, 2013).

Using chemical inhibitors to individually block HATs, HDACs and SIRTs, the implication of acetylation and deacetylation activity in the development of fibrosis has been shown in numerous studies. Mechanistically, HDAC inhibition seems to abrogate cardiac fibrosis by multiple mechanisms such as inhibition of fibroblast proliferation, induction of genes that suppress extracellular matrix production from fibroblasts and reduced differentiation (Schuetze et al., 2014). Despite catalyzing a similar reaction, SIRTs exhibit, unlike HDACs, opposite protective effects in the setting of cardiovascular diseases. Exemplarily, resveratrol-mediated SIRT3 activation was demonstrated to suppress Ang II-induced MF activation by inhibiting the TGF-β/Smad3 pathway and SIRT3-knockout potentiated pathological outcome (Chen et al., 2015a).

1.2.4 Molecular mediators of fibrosis

1.2.4.1 Transforming growth factor β

TGFβ is considered a master molecule in tissue remodeling and activation of MFs and a strong association with tissue injury in general has been shown (Kane et al., 1991). TGF-β is a cytokine with diverse and often contradictory functions, with both profibrotic and hypertrophic actions (Edgley et al., 2012). In the setting of cardiac pathologies, increased TGFβ expression levels are robustly correlated with cardiac hypertrophy (Huntgeburth et al., 2011), MI (Vilahur et al., 2011) in combination with reduced ventricular ejection fractions (Talasaz et al., 2013) and most importantly with cardiac fibrosis (Liu et al., 2017). TGFβs are pleiotropic factors and exist in three different isoforms (TGFβ1, β2, and β3) encoded by distinct genes (Schiller et al., 2004). Herein, TGFβ1 is the dominant isoform and ubiquitously found in nearly all cells, while the other isoforms are more tissue specific (Dobaczewski et al., 2011). Although *in vitro* studies have shown similar functions, *in vivo* effects of the three isoforms differ and activation of tissue fibrosis is primarily attributed to TGFβ1 (Ask et al., 2008).

Commonly, all three isoforms undergo gradual processing from inactive precursors to regulatory active molecules (Figure 3). TGFβs are synthesized as pro-TGFβ protein containing three domains: the carboxy-terminal mature peptide (MP), which constitutes the active cytokine, the latency-associated peptide (LAP) and the amino-terminal signal peptide (SP) that shuttles the protein through the rough endoplasmic reticulum. After cleavage of the SP, protein homodimers form and are proteolytically processed by furin producing LAP and mature TGFβ dimers (Dubois et al., 1995). After folding, the active TGFβ dimer remains non-covalently bound to LAP forming the small latent complex (SLC). In the Golgi apparatus, the SLC is covalently bound to the glycoprotein (Miyazono et al., 1988) latent TGFβ-binding protein (LTBP) producing the large latent complex (LLC). Finally, LLC is enveloped in vesicles and secreted into the extracellular space, where it associates to the ECM via LTBP (Taipale et al., 1994) and to integrins by LAP (Henderson et al., 2013) constituting a stored bioavailable pool of inactive TGFβ. Mechanical stress, either caused by the cell itself or by a neighboring cell (Wipff et al., 2007), results in contractile forces applied to either site (integrin or ECM) of the LLC and active TGFβ is mechanically released in a 'straightjacket' manner (Shi et al., 2011). Another mechanism associated with bioavailability of active TGFβ represents the enzymatic degradation of LAP by several proteases including plasmin, thrombin, elastase, matrix metalloproteinase (MMP)-2 and MMP-9 (Jenkins, 2008). Free active TGFβ, independent of its origin, is recognized by TGFβ receptor, stimulating the synthesis of TGFβ and its activators, amplifying the response in an autocrine fashion (Bouche et al., 2000). Furthermore, TGFβ binding to its receptor initiates the canonical SMAD-dependent TGFβ-signaling cascade resulting in the activation of the fibrogenic gene program (Knittel et al., 1996).

Although TGFβ mainly signals through the canonical SMAD-dependent pathway, it also exerts the activation of other signaling pathways including ERK, JNK and p38 pathways (Zhang et al., 2006b), collectively referred to as non-canonical or SMAD-independent pathways. However, these pathways are believed to be involved in the basal regulation of ECM production, cell migration and apoptosis (Papageorgis, 2015), other than in the direct activation of MFs.

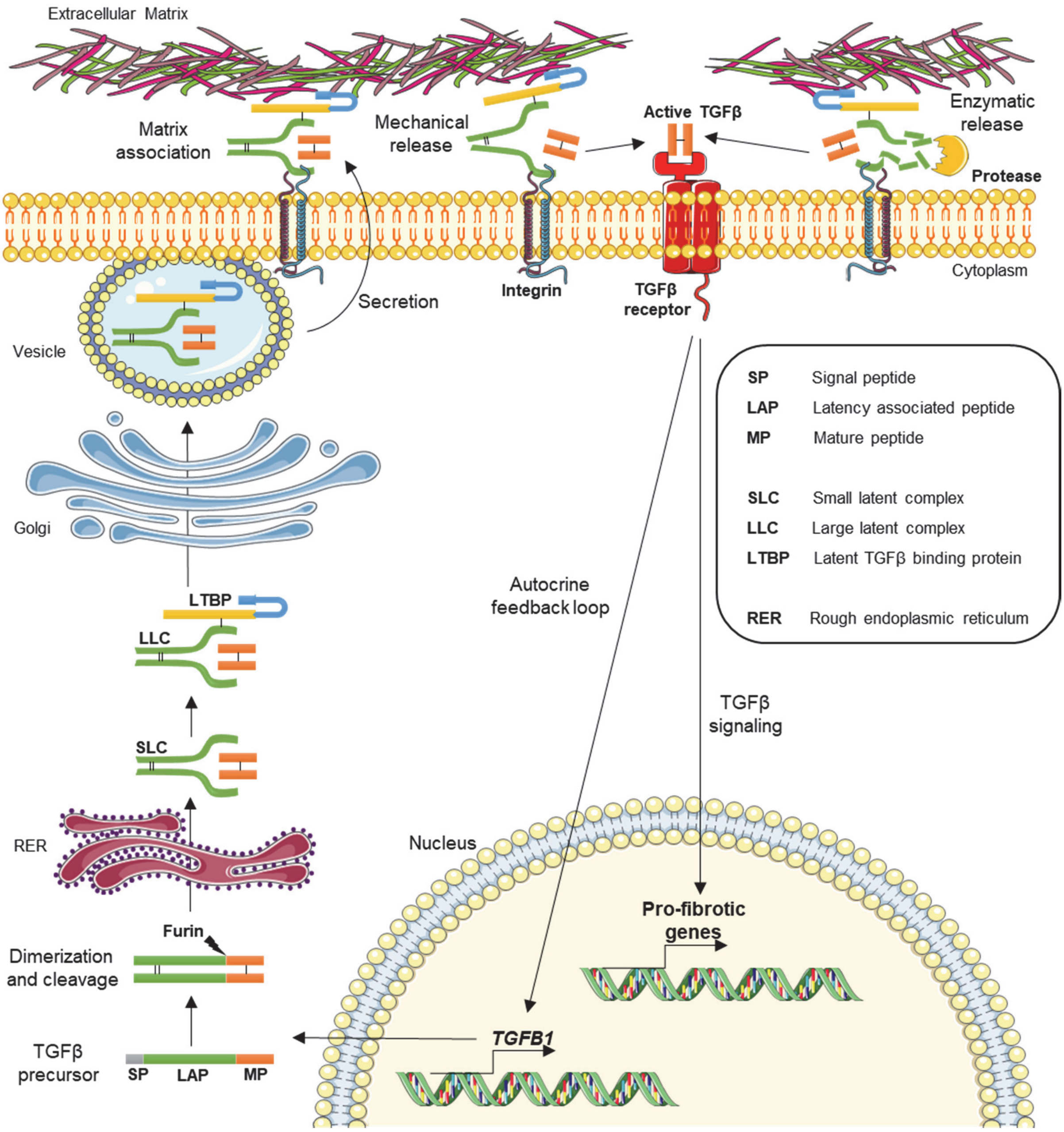

Figure 3: TGFβ synthesis, secretion and activation

1.3 Cardiac fibroblasts

Fibroblasts are ubiquitously found in every organ and tissue and originate from mesenchymal stem cells or multipotent progenitor cells during embryonic development displaying multiple morphologies depending on their location (Baum and Duffy, 2011a). In the heart, although cardiomyocytes account for 70-85% of the volume (Tang et al., 2009), non-cardiomyocytes such as endothelial cells and cardiac fibroblasts (CF) dominate numerically. Despite prior studies suggested that CFs make up to 60-70% of cells in the myocardium (Aoyagi and Matsui, 2011; Camelliti et al., 2005), recent publications indicate that in the mouse heart CFs may comprise less than 20% of cellular heart components (Pinto et al., 2016). CFs - in analogy to other fibroblasts - identify as single-nucleated, spindle-shaped cells, which reside in the self-secreted extracellular matrix organized in sheets and strands enveloping the neighboring cardiomyocytes (Snider et al., 2009). Under physiological conditions, CFs play a key role in the maintenance of the heart's structural integrity by controlled proliferation and ECM turnover (Brown et al., 2005). Herein, CFs synthesize and deposit collagen types I, III, V and VI, laminin, elastin, proteoglycans and glycosaminoglycan (Banerjee et al., 2007; Creemers and Pinto, 2011), and secrete several MMPs specialized in enzymatically degrading respective ECM components and the activity is fine-tuned by tissue inhibitors of metalloproteinases (TIMPs) secretion (Mishra et al., 2013). The CFs not only preserve the ECM, but also participate in the moderation of mechanical stress in the heart through their tight connection to cardiomyocytes by gap junctions and to the ECM via integrins (Kanekar et al., 1998; Spinale, 2007). In addition, the CF-synthesized ECM acts as a natural electrical insulator, which allows for proper ventricular contraction due to gradual distribution of the electrical excitement throughout the cardiac tissue (Snider et al., 2009). Moreover, CFs release a series of growth factors and cytokines, such as TGFβ, CTGF, interleukin-1-beta (IL-1β), interleukin-6 (IL-6), natriuretic peptides and VEGF acting in an autocrine and paracrine manner to promote migration, differentiation, proliferation and further secretion of release factors by surrounding CF and other cells (Travers et al., 2016).

1.3.1 Fibroblast-to-myofibroblast transition

The CF features the property of phenotypic plasticity in response to pathological stimuli. Following cardiac injury, normal 'quiescent' CFs dramatically enhance the ECM production and become so-called 'activated fibroblasts' (Figure 4). The incidence of enhanced biosynthetic characteristics, such as a prominent rough endoplasmic reticulum and a prominent nucleolus and Golgi complex, identifies these cells as activated fibroblasts (Souders et al., 2009). The persistence of this state and the upregulation of various pro-inflammatory cytokines and pro-fibrotic factors eventually increases proliferation rates and ultimately mediates the trans-differentiation to the MF phenotype (Kawaguchi et al., 2011), referred to as fibroblast-to-myofibroblast transition (FMT). In comparison to CFs, MFs are larger in size, obtain ruffled membranes and contain a highly active endoplasmic reticulum due to extensive production of ECM and cytokines (Baum and Duffy, 2011a). Furthermore, MFs are characterized by tremendously increased motility, migration and adhesion (Bagalad et al., 2017). A distinct feature of MFs over CFs is the gain of contractile function due to the *de novo* formation of α-smooth muscle actin (αSMA) fibers, important for wound closure and structural integrity during scar formation (Brown et al., 2005; Souders et al., 2009). Apart from FMT of resident CFs, other origins of MFs have been discussed. For example, bone marrow-derived fibrocytes have been shown to accumulate in the myocardium after ischemic injury recruited via the circulatory system (Chu et al., 2010). Another source of MFs has been described to evolve from epithelial cells of the epicardium undergoing epithelial-mesenchymal-transition (EMT) after cardiac injury (Zhou and Pu, 2011). Furthermore, lineage tracing analysis after pressure overload has revealed EndMT that partially drives the accumulation of MFs (Zeisberg et al., 2007).

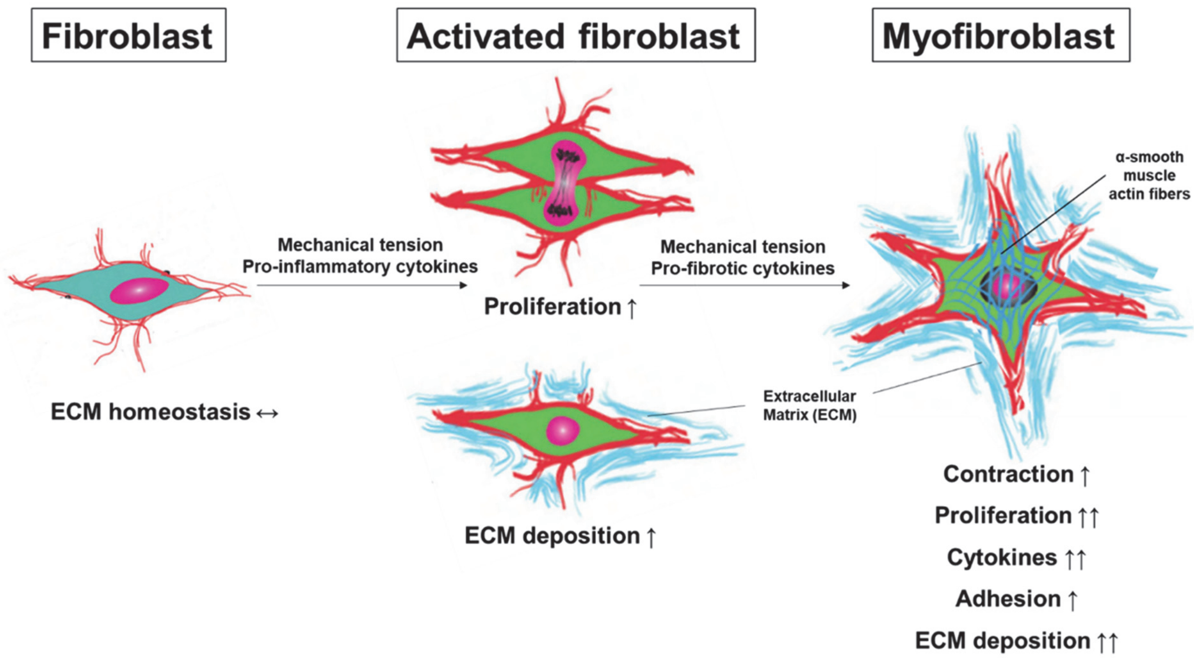

Figure 4: Two-stage model of cardiac fibroblast-to-myofibroblast transition

In the case of MI, MFs were thought to persist for a long time (months or years) in the mature infarct scar (Willems et al., 1994). However, other studies reported that a majority of MFs undergo apoptosis leaving a mature scar composed of condensed and cross-linked ECM (Gurtner et al., 2008). Most recently, Fu et al. (2018) presented that MFs lose their contractile αSMA-expressing properties and remain in the mature scar resistant of repeated pathological challenges using a genetic fibroblast lineage-tracing approach. This kind of cells is characterized by chondrocyte-and osteoblast-like signatures expressing markers of bone, connective tissue, cartilage, and tendon, thus considered as newly identified phenotype referred to as ‘matrifibrocyte’. The authors assume that matrifibrocytes could be important for the preservation of mature scars in the long-term.

1.4 Intercellular Communication

Intercellular communication depicts a fundamental process for radiation of cellular signals between neighboring and remote cells to coordinate metabolism, maintenance and adaptation as a functional tissue and organ. The crosstalk between cells is mediated via the exchange of chemical, electrical, and mechanical signals through direct cell–cell interactions or the secretion of factors such as cytokines and growth factors (Takeda and Manabe, 2011).

Secretion of proteins occurs via multiple pathways. In the classical pathway, proteins containing the N-terminal signal peptide sequence shuttle through the endoplasmic reticulum (ER) and the Golgi apparatus and are subsequently secreted after secretory vesicles fuse with the plasma membrane (Stein et al., 2014). Another pathway depicts the non-classical secretion pathway, in which proteins without SP are delivered to the plasma membrane and the extracellular space without entering the ER–Golgi conventional pathway of secretion (Rabouille, 2017). These leaderless proteins either exit the cell by pore-mediated translocation across the plasma membrane, specific transporter-based secretion or membrane-bound organelle-based release (Rabouille, 2017). A third way of cell-to-cell communication, which does not require direct cell contact, constitute extracellular vesicles that are released by a donor cell and absorbed by a recipient cell. These so-called exosomes not only shuttle proteins, but also contain bioactive particles, lipids, metabolites and different types of nucleic acids such as DNA, mRNA, and microRNA (Plotnikov et al., 2017). Independent of the secretory pathway, extracellular signals can act in a paracrine, autocrine or, when released into the circulatory system, in an endocrine manner.

The heart is nowadays accepted as an organ capable of releasing factors into the circulation and one of the first so-called cardiokines to be discovered leading to the consideration of endocrine function was the atrial natriuretic peptide (Frohlich, 1985). Other identified cardiokines include TGFβ, angiotensin II, tumor necrosis factor α (TNFα), IL-1β or CTGF, which may contribute to hypertrophic growth, survival or apoptosis of CM and promote FMT or regulate inflammation (Bang et al., 2015). Cardiokines are secreted from all types of cells found in cardiac tissue, including myocytes, fibroblasts, and endothelial and vascular cells (Planavila et al., 2017). Physiologically, cardiokines are important in the maintenance of normal cardiac function. Herein, paracrine and autocrine signaling within cardiac cells marks the pivotal way of communication in the instrumentation of this process (Tirziu et al., 2010). However, in pathological conditions, including MI or HF, a coordinated response of the heart via cardiokine secretion triggers pro- or antihypertrophic, fibrotic, and/or angiogenic compensating reactions (Doroudgar and Glembotski, 2011; Planavila et al., 2017). Thus, identification of changes in the composition of the secretory profile under pathological conditions constitutes an interesting point of investigation to develop new therapeutic approaches and strategies. Furthermore, considering their presence in the circulatory system, cardiokines also feature the potential property as diagnostic and prognostic biomarkers with clinical value (Doroudgar and Glembotski, 2011).

1.5 Rhein: A potential anti-fibrotic agent.

Rhein (4,5-dihydroxyanthraquinone-2-carboxylic acid), a lipophilic anthraquinone, is a pharmaceutically active component predominantly found in rhubarb (*Rheum palmatum* L.), but also in the medicinal herbs *Cassia tora L.*, *Polygonum multiflorum* Thunb. and *Aloe barbadensis* Miller, which have been extensively used in traditional Chinese medicine (Zhou et al., 2015). Since the early 1990s, Rhein in its diacetylated pro-drug form, Diacerein, has found clinical appreciation in the treatment of osteoarthritis by decreasing inflammation and cartilage destruction (Spencer and Wilde, 1997). Rhein, as a natural compound, is well-tolerated and merely displays a mild laxative side effect, which is associated with diarrhea or soft stools in 20 to 30% of patients only after the first few doses (Nguyen et al., 1994). Pharmacologically, Diacerein is rapidly deacetylated to active Rhein (Figure 5), which exerts linear kinetics in a range between 50 and 200mg (Layek et al., 2008) with a half-life of 4-10h (Nicolas et al., 1998). Herein, free Rhein is either directly eliminated by the kidney (20%) or primarily conjugated to Rhein glucuronide (60%) or Rhein sulfate (20%) in the liver before renal elimination and excretion via urine (Nicolas et al., 1998).

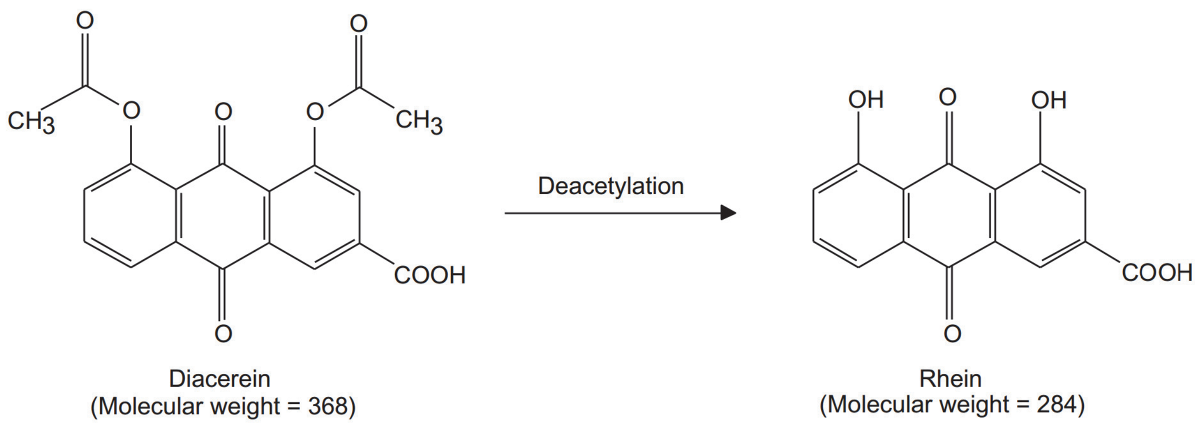

Figure 5: Chemical structures of Diacerein and Rhein
Adapted from Nicolas et al. (1998)

Besides anti-inflammatory properties in the setting of osteoarthritis, multiple pharmacological effects have been ascribed to Rhein including hepatoprotective, nephroprotective, antidiabetic, lipid-lowering, antioxidant, anticancer, and antimicrobial activities (Zhou et al., 2015). Based on the wide potential applicability, disposition of Rhein as treatment for several other pathologies besides osteoarthritis has been considered and numerous studies have been conducted in the recent past. Particularly, increasing evidence suggests Rhein as anti-fibrotic agent. In a rat model of carbon tetrachloride-induced liver fibrosis, Rhein administration exerted protective effects expressed by reduced alanine aminotransferase, hyaluronic acid and procollagen type III levels and decreased expression of αSMA and TGFβ1 (Guo et al., 2002). Anti-fibrotic properties were also demonstrated in the setting of pancreatic fibrosis, where prolonged Rhein application significantly decreased immunoreactivities of αSMA, TGFβ, FN1 and COL1α1 on murine pancreatic sections and in TGFβ1-treated cultured cells (Tsang et al., 2013a). Most of studies supporting Rhein as anti-fibrotic compound have been conducted in kidney in the context of chronic kidney disease and obstructive nephropathy. Herein, in rodent animal experiments, Rhein markedly ameliorated glomerular hypertrophy (Sheng-Nan et al., 2013), improved renal function after transplantation (Su et al., 2013) and alleviated renal tissue cell apoptosis in glomerulosclerosis (Ji et al., 2005). Collectively with further publications, the nephroprotective activities of Rhein were also assigned to reductions of αSMA, TGFβ, FN1 and COL1α1, suggesting Rhein as a potent inhibitor of kidney fibrosis (He et al., 2011; Peng et al., 2013). The role of Rhein in cardiac pathology has been scarcely investigated, yet one study has been published demonstrating that Diacerein administration improves left ventricular remodeling and cardiac function after MI (Torina et al., 2015). Herein, the authors linked preserved heart function to reduced replacement fibrosis reporting lower levels of caspase-3 activity and NF-κB p65 transcription.

On the molecular level, the Rhein-mediated biological network is vast and complex, affecting a broad variety of signaling pathways including MAPK, PI3K-AKT, ERK and JNK signaling, to name a few. This suggests that Rhein action is the synergistic result of temporal and spatial crosstalk between multiple signaling networks (Sun et al., 2016). In regard to anti-fibrotic properties of Rhein, the TGFβ signaling cascade has attracted much attention as potential target pathway. So far, Rhein was shown to reduce ECM deposition and α-SMA expression (Guo et al., 2002; He et al., 2011; Peng et al., 2013; Tsang et al., 2013a) and to inhibit the expression of TGFβ and its type I receptor (He et al., 2011). Further, Rhein was reported to dose-dependently block TGFβ-stimulated *PAI1* mRNA expression (Zhu et al., 2003).

Despite Rhein has repeatedly been shown to reduce fibrosis in multiple organs and to exert beneficial effects associated with the heart, the exact mechanism of how Rhein as small molecule interferes with the progression of fibrosis has not been sufficiently addressed. Further understanding of its molecular mode of action, could provide new insights for precise treatment and individualized drug administration.

1.6 Aim of the study

Myocardial fibrosis manifests progressively in several forms of cardiomyopathies leading to cardiac stiffness and left ventricle dysfunction. Persistence of this pathologic state dramatically affects the survival rate after cardiovascular events or leads to death. In the heart, CFs account to approx. 70-80% of the resident cells, functioning as mediators of ECM maintenance. CFs are able to switch to the ECM-producing and more active MF phenotype, which drives the fibrotic response to pathologic environmental changes like MI (acute) or chronic hypertension (progressive). Cardiac remodeling and fibrosis-associated morbidities have been attributed to TGFβ, the most potent inducer of collagen-production and fibroblast differentiation. Physiologically, sustained hypoxia and the associated modulation of secretory factors have also been identified, contributing to the radiation of MFs from the point of lesion towards the remote interstitium.

Although fibrosis depicts a reparative mechanism, maladaptation of the heart due to excessive production of ECM accelerates cardiac dysfunction. Hence, an anti-fibrotic therapeutic approach leading to reduced FMT is of relevant investigative interest. The rhubarb anthraquinone Rhein, a drug already used as clinical treatment for osteoarthritis has been reported to display beneficial properties in the setting of kidney fibrosis. However, its relevance for the treatment of myocardial fibrosis and the principally underlying mechanism have not been fully elucidated yet. Therefore, in this study the effect of Rhein administration on fibroblast-to-myofibroblast differentiation of hypoxia-treated primary human ventricular cardiac fibroblasts (HCF-v) was investigated.

2 Materials & Methods

2.1 Materials

2.1.1 Instruments and disposables

Table 1: Instruments

Instruments	Manufacturer (name, location)
AE31 Trinocular inverted microscope	Motic, Wetzler, Germany
Analytical Balance	Sartorius, Göttingen, Germany
ChemiDoc XRS	Biorad Laboratories, Munich, Germany
Electronic Precision Balance U4100	Sartorius, Göttingen, Germany
GeneAmp PCR System 9700 thermocycler	Thermo Fisher Scientific, Darmstadt, Germany
Heracell™ 240i CO_2 incubator	Thermo Fisher Scientific, Darmstadt, Germany
Heraeus LaminAir HB 2448 S GS	Thermo Fisher Scientific, Darmstadt, Germany
Heraeus™ Multifuge™ X3 Zentrifuge	Thermo Fisher Scientific, Darmstadt, Germany
iMark Microplate Reader	Biorad Laboratories, Munich, Germany
Maxwell® 16 Instrument	Promega, Mannheim, Germany
Mini PROTEAN Tetra System	Biorad Laboratories, Munich, Germany
Mini Trans-Blot®	Biorad Laboratories, Munich, Germany
Molecular Imager® VersaDoc™ MP 4000	Biorad Laboratories, Munich, Germany
Moticam Pro 282B	Motic, Wetzler, Germany
NanoDrop™ 2000/2000c spectrometer	Thermo Fisher Scientific, Darmstadt, Germany
Neubauer counting chamber	BRAND®, Wertheim, Germany
Orbital shaker	Assistent GmbH, Altnau, Switzerland
Power Pac Basic power supply	Biorad Laboratories, Munich, Germany
PURA water bath	Julabo, Seelbach, Germany
Quantstudio 7 flex	Applied Biosystems, Darmstadt, Germany
Reaxtop shaker	Heidolph, Schwabach, Germany
Spacer plates for SDS gels	Biorad Laboratories, Munich, Germany
Sprout® Mini Centrifuge, HS120301	Heathrow Scientific, Vernon Hills, IL, USA
StepOnePlus Real-time PCR system	Applied Biosystems, Darmstadt, Germany
Table centrifuge 5417 R	Eppendorf, Wesseling-Berzdorf, Germany
Tecan Infinite 200 reader	Tecan, Maennersdorf, Germany

Thermomixer comfort	Eppendorf, Wesseling-Berzdorf, Germany
VersaDoc MP 4000	Biorad Laboratories, Munich, Germany
Xvivo System X3 Hypoxia Hood	Biospherix, Parish, NY, USA
PyroMark Q96 ID	Qiagen, Hilden, Germany
PyroMark Q96 Vacuum Workstation	Qiagen, Hilden, Germany

Table 2: Disposables

Disposables	Manufacturer (name, location)
96-well high-binding assay plates	Sarstedt, Nümbrecht, Germany
Cell culture plates, sterile (6-, 96-well)	Greiner Bio-One, Frickenhausen, Germany
Cell scraper	Sarstedt, Nümbrecht, Germany
Electrode paper NovaBlot™	GE Healthcare, Freiburg, Germany
Falcon® cell culture dishes, sterile	VWR, Darmstadt, Germany
Immobilon-P Membran, PVDF, IPVH00010	Merck Chemicals GmbH, Darmstadt, Germany
MicroAmp® Fast Optical 96-Well Reaction Plate	Thermo Fisher Scientific, Darmstadt, Germany
MicroAmp® Optical Adhesive Film	Thermo Fisher Scientific, Darmstadt, Germany
Rotlabo®-syringe filter, sterile, P666.1	Carl Roth, Karlsruhe, Germany
Steritop™ filter unit	Merck Chemicals GmbH, Darmstadt, Germany
Surgical blades	VWR, Darmstadt, Germany
Perfusor syringes 50 ml	VWR, Darmstadt, Germany
175cm² flasks	Sarstedt, Nümbrecht, Germany
96-Well Polystyrene Microplate, clear flat bottom, white	Corning, New York, USA
96-Well Polystyrene Microplate, clear flat bottom, black	Corning, New York, USA
Amicon® Ultra 15, Ultracel -3K	Merck Chemicals GmbH, Darmstadt, Germany

2.1.2 Chemicals

Table 3: Chemicals

Chemicals	Manufacturer (name, location)
Ammonium persulfate (APS)	Roth, Karlsruhe Germany
Antibiotic-Antimycotic Solution (100x)	Gibco®, Thermo Fisher Scientific, Darmstadt, Germany
Bovine serum albumin (BSA) Fraction V, fatty acid free	Carl Roth, Karlsruhe, Germany
Bromophenol Blue	AppliChem GmbH, Darmstadt, Germany
BSA Fraction V, very low endotoxin	Carl Roth, Karlsruhe, Germany
Complete Protease Inhibitor Cocktail	Roche, Mannheim, Germany
Dimethyl sulfoxide (DMSO)	Sigma-Aldrich, Darmstadt, Germany
Disodium hydrogen phosphate dihydrate ($Na_2HPO_4 \cdot 2H_2O$)	Sigma-Aldrich, Darmstadt, Germany
Dithiothreitol (DTT)	VWR, Darmstadt, Germany
Fetal calf serum (FCS)	Biochrom GmbH, Berlin, Germany
GlutaMAX™ (100x)	Gibco®, Thermo Fisher Scientific, Darmstadt, Germany
Hepes PUFFERAN®	Carl Roth, Karlsruhe, Germany
Insulin from porcine pancreas	Sigma-Aldrich, Darmstadt, Germany
Nonfat dried milk powder	AppliChem GmbH, Darmstadt, Germany
Nonidet P-40 (NP-40)	Sigma-Aldrich, Darmstadt, Germany
PhosSTOP Phosphatase Inhibitor	Roche, Mannheim, Germany
Precision Plus Protein™ Standard	Biorad Laboratories, München, Germany
Rat tail type-I collagen stock (4 mg/ml)	CellSystems®, Troisdorf, Germany
SDS (sodium dodecyl sulfate)	AppliChem GmbH, Darmstadt, Germany
Sodium bicarbonate ($NaHCO_3$)	Merck Chemicals GmbH, Darmstadt, Germany
Sodium bicarbonate ($NaHCO_3$) solution (7.5%)	Thermo Fisher Scientific, Darmstadt, Germany
Sodium deoxycholate	AppliChem GmbH, Darmstadt, Germany
Sodium dihydrogen phosphate monohydrate ($NaH_2PO_4 \cdot H_2O$)	Sigma-Aldrich, Darmstadt, Germany
Tetraethylethylenediamin (TEMED)	Roth, Karlsruhe Germany
Tetrasodium Pyrophosphate Decahydrate ($Na_4P_2O_7 \cdot 10H_2O$)	Sigma-Aldrich, Darmstadt, Germany

Tris(hydroxymethyl)aminomethane (TRIS)	Roth, Karlsruhe Germany
Trypan blue solution (0.4%)	Sigma Aldrich, St Louis, MO, USA
Tween® 20	AppliChem GmbH, Darmstadt, Germany
β-Mercaptoethanol	Thermo Fisher Scientific, Darmstadt, Germany
0.05% Trypsin-EDTA	Gibco®, Thermo Fisher Scientific, Darmstadt, Germany
Trypsin inhibitor from soybean	AppliChem GmbH, Darmstadt, Germany
Rhein	Sigma Aldrich, St Louis, MO, USA

2.1.3 Buffers and solutions

Table 4: Buffers and solutions

Buffers and solutions	Formulation
0.2% trypan blue working solution	1:2 (v/v) dilution of 0.4% trypan blue solution in 1x phosphate-buffered saline (PBS)
5x Laemmli sample buffer	312.5 mM Tris-HCl (pH 6.8), 10% SDS, 50% glycerol, 500 mM DDT, 0.01% bromophenol blue
Complete Protease working solution	1 tablet dissolved in 1 ml $H_2O_{bidest.}$
Membrane Stripping buffer	20 ml 10% SDS, 12.5 ml 0.5 M Tris-HCl (pH 6.8), 67.5 ml H_2O, 0.8 ml β-mercaptoethanol
PhosSTOP working solution	1 tablet dissolved in 1 ml $H_2O_{bidest.}$
Rat tail type-I collagen	stock: 4mg/ml (CellSystems®, Troisdorf, Germany)
RIPA lysis buffer	30 mM Tris-HCl (pH 7.5), 1 mM EDTA, 150 mM NaCl, 0.5% Triton X-100, 0.5% Na-deoxycholate (Na-DOC) supplemented with 1:10 (v/v) of Complete Protease Inhibitor working solution and 1:10 (v/v) PhosStop Phosphatase Inhibitor cocktail working solution

SDS-PAGE running buffer (1x)	25 mM Tris, 190 mM glycine, 0.1% SDS
TBS-T (Tris-buffered saline with Tween® 20) wash buffer	20 mM Tris-HCl (pH 7.5), 150 mM NaCl, 0.1% Tween® 20
Western Blot transfer buffer (1x)	25 mM Tris, 190 mM glycine, 20% methanol
0.025% Trypsin-EDTA	1:2 (v/v) dilution of 0.05% Trypsin-EDTA in 1x phosphate-buffered saline (PBS)
0.025% Trypsin inhibitor	0.025g/L trypsin inhibitor from soybean in 1x phosphate-buffered saline (PBS)

2.1.4 Cell culture media and cells

Table 5: Media

Media	Supplements
Human cardiac fibroblast growth medium	Dulbecco's modified Eagle's medium (DMEM), 22320-022 (Gibco®, Thermo Fisher Scientific, Darmstadt, Germany), 10% FCS, 1% GlutaMAX™, 1% antibiotic-antimycotic mixture, 5µg/ml insulin and 5ng/ml basic fibroblast growth factor (hFGF-b)
Human cardiac fibroblast growth medium (for Normoxia and Hypoxia)	Dulbecco's modified Eagle's medium (DMEM), 22320-022 (Gibco®, Thermo Fisher Scientific, Darmstadt, Germany) 10% FCS, 1% GlutaMAX™, 1% antibiotic-antimycotic mixture
Human cardiac fibroblast maintenance medium	Dulbecco's modified Eagle's medium (DMEM), 11880-028 (Gibco®, Thermo Fisher Scientific, Darmstadt, Germany), 1% GlutaMAX™, 1% antibiotic-antimycotic mixture
Human cardiac fibroblast cultivation medium	FGM™ 3 Cardiac Fibroblast Growth Medium-3 BulletKit™, CC-4526 (Lonza, Basel, Switzerland)
Serum-free medium (for secretome collection)	Dulbecco's modified Eagle's medium (DMEM), 11880-028 (Gibco®, Thermo Fisher Scientific, Darmstadt, Germany),

	1% GlutaMAX™, 1% antibiotic-antimycotic mixture
Freezing solution	Dulbecco's modified Eagle's medium (DMEM), 22320-022, 20% FCS, 10% DMSO

Table 6: Human cardiac fibroblast donors

Donor	age (y)	sex	race	alcohol use	smoke use	Lot no.	Catalog #	Manufacturer
1462	32	f	Caucasian	yes	yes	0000401462	CC-2904	Lonza, Basel, Switzerland
2836	31	f	Caucasian	yes	no	0000402836	CC-2904	Lonza, Basel, Switzerland
1712	52	m	Caucasian	yes	no	0000421712	CC-2904	Lonza, Basel, Switzerland
3042	54	m	Caucasian	NA	NA	3042901.1	C-12375	Promocell, Heidelberg, Germany
1050	57	m	caucasian	NA	NA	1050401.11	C-12375	Promocell, Heidelberg, Germany

2.1.5 Kits

Table 7: Kits

Kits	Manufacturer (name, location)
CellTiter-Glo® Luminescent Cell Viability	Promega, Mannheim, Germany
CellTox™ Green Cytotoxicity Assays	Promega, Mannheim, Germany
GoScript™ Reverse Transcription System	Promega, Mannheim, Germany
GoTaq® qPCR Master Mix	Promega, Mannheim, Germany
Immobilon Western HRP Substrate	Merck Chemicals GmbH, Darmstadt, Germany
Maxwell® 16 LEV simplyRNA Kit	Promega, Mannheim, Germany
Pierce™ BCA Protein Assay Kit	Thermo Fisher Scientific, Darmstadt, Germany
Proteasome-Glo™ Cell-Based Assay	Promega, Mannheim, Germany
SIRT-Glo™ Assay System	Promega, Mannheim, Germany

HDAC-Glo™ I/II Assays and Screening System	Promega, Mannheim, Germany
MTase-Glo™ Methyltransferase Assay	Promega, Mannheim, Germany
HAT Activity Assay Kit II	PromoKine, Heidelberg, Germany
RT² Profiler PCR array Fibrosis	Qiagen, Hilden, Germany
Human LAP (TGF-beta 1) Quantikine ELISA	R&D systems, Wiesbaden, Germany
GeneChip™ Human Transcriptome Array 2.0	Applied Biosystems, California, USA
EpiTect® Fast DNA Bisulfite Kit	Qiagen, Hilden, Germany
PyroMark PCR Kit	Qiagen, Hilden, Germany
EpiTect® PCR Control DNA Set	Qiagen, Hilden, Germany
PyroMark Gold Q96 Reagents	Qiagen, Hilden, Germany
DNeasy® Blood & Tissue Kit	Qiagen, Hilden, Germany

2.1.6 Primers

Table 8: Primers

Target	Accession	Forward 5’->3’	Reverse 5’->3’
ACTA2	NM_001613	GCTATTCCTTCGTTACTACTG	CAAAGTCCAGAGCTACATAAC
CCL11	NM_002986	ACCCCTTCAGCGACTAGAGA	CCACTTCTTCTTGGGGTCGG
COL1A2	NM_000089	ACCTTATGCCTAGCAACATGC	GGCCCTTTCTTACAGTTTCCT
CTGF	NM_00190	AACATTAAGAAGGGCAAAAAGT	TCGGTATGTCTTCATGCTGG
EIF4A2	NM_001967	TGTGCAACAAGTGTCTTTGGTT	CACCTTTCCTCCCAAATCGAC
LTBP1	NM_206943	GGCAGCTAAAGACCAGTGTGAA	TTCCTGCACTGCCCATGA
SERPINE1	NM_000602	AATGTGTCATTTCCGGCTGC	GAGCTGCCTGTCTCTCTCAC
SMAD7	NM_005904	GGCATTCGTCGGAAGTCAAG	AGAGTCGGCTAAGGTGATGG
TGFB1	NM_000660	GTTAAAAGTGGAGCAGCACG	GATAACCACTCTGGCGAGTC
TGFBR1	NM_004612	ACCATCGAGTGCCAAATGAA	ATGGTAAACCTGAGCCAGAAC
YWHAZ	NM_003406	TCTGGCTCCACTCAGTGTCT	CTGTGGGATGCAAGCAAAGG

ACTA2: Actin, Alpha 2, Smooth Muscle, Aorta; CCL11: C-C Motif Chemokine Ligand 11; COL1A2: Collagen Type I Alpha 2 Chain; CTGF: Connective Tissue Growth Factor; EIF4A2: Eukaryotic Translation Initiation Factor 4A2; LTBP1: Latent Transforming Growth Factor Binding Protein 1; SERPINE1: Serpin Family E Member 1; SMAD7: SMAD Family Member 7; TGFB1: Transforming

Growth Factor Beta 1; TGFBR1: Transforming Growth Factor Beta Receptor 1; YWHAZ: 14-3-3 protein zeta/delta

2.1.7 Antibodies

Table 9: Antibodies

Antibodies	**Origin**	**Dilution**[1]	**Product number**	**Manufacturer (name, location)**
Primary				
Acetyl-p53 (Lys382), polyclonal	rabbit	1:1000 (v/v) 5% BSA	2525	Cell Signaling Technology, Danvers, MA, USA
DNMT1, polyclonal	rabbit	1:1000 (v/v) 5% BSA	5032	Cell Signaling Technology, Danvers, MA, USA
GAPDH, monoclonal	rabbit	1:5000 (v/v) 5% MP	2118	Cell Signaling Technology, Danvers, MA, USA
HIF1α, monoclonal	mouse	1:500 (v/v) 5% MP	NB100-105	Novus Biologicals, Littleton, CO, USA
LTBP1, polyclonal	rabbit	1:500 (v/v) 5% MP	PA5-45075	Thermo Fisher Scientific, Waltham, MA
p21 Waf1/Cip1, polyclonal	rabbit	1:1000 (v/v) 5% BSA	2947	Cell Signaling Technology, Danvers, MA, USA
p53, polyclonal	rabbit	1:1000 (v/v) 5% MP	9282	Cell Signaling Technology, Danvers, MA, USA
phospho-SMAD2 (Ser465/Ser467), polyclonal	rabbit	1:1000 (v/v) 5% BSA	3108	Cell Signaling Technology, Danvers, MA, USA
SMAD7, monoclonal	mouse	1:500 (v/v) 2.5% MP	MAB2029	R&D Systems, Wiesbaden, Germany
TGFβ1, polyclonal	rabbit	1:1000 (v/v) 5% BSA	3709	Cell Signaling Technology, Danvers, MA, USA

TGFβR1, polyclonal	rabbit	1:250 (v/v) 5% MP	sc-398	Santa Cruz Biotechnology, Santa Cruz, CA, USA
α-SMA, monoclonal	mouse	1:2000 (v/v) 5% BSA	A2547	Sigma-Aldrich, Darmstadt, Germany
Secondary				
Anti-mouse IgG, HRP-linked	horse	1:1000 (v/v) 5% MP or (v/v) 5% BSA	7076	Cell Signaling Technology, Danvers, MA, USA
Anti-rabbit IgG, HRP-linked	goat	1:1000 (v/v) 5% MP or (v/v) 5% BSA	7074	Cell Signaling Technology, Danvers, MA, USA

[1]5% non-fat dry milk powder (MP) or 5% bovine serum albumin (BSA) were dissolved in 1x TBS-T; HRP, horseradish peroxidase; IgG, immunoglobulin G

2.1.8 Recombinant proteins and inhibitors

Table 10: Recombinant proteins

Recombinant protein	solved in	Manufacturer (name, location)
Human transforming growth factor β1 (hTGFβ1)	0.04M HCl, 1% BSA	Peprotech, Hamburg, Germany
human fibroblast growth factor, basic (hFGF-b)	5 mM Tris pH 7.6, 0.1% BSA	Peprotech, Hamburg, Germany

Table 11: Inhibitors

Inhibitor/Reagent	Solvent	Manufacturer (name, location)
Bortezomib (BZ)	DMSO	Merck Chemicals GmbH, Darmstadt, Germany
Anacardic acid (AnA)	DMSO	Sigma-Aldrich, Darmstadt, Germany
sodium butyrate (SB)	H_2O	Sigma-Aldrich, Darmstadt, Germany
Nicotinamide (NAM)	H_2O	Sigma-Aldrich, Darmstadt, Germany

2.2 Methods

2.2.1 Cell culture techniques

2.2.1.1 Primary human ventricular cardiac fibroblast culture

Primary HCF-v were purchased from Lonza (Basel, Switzerland) or Promocell (Heidelberg, Germany) and stored in gaseous nitrogen upon arrival. HCF-v were expanded from passage (P)2 to P5 (and P5 to P7) before undergoing experimental use and were cultured as follows: cells were resuspended in HCF-v culture media (2.1.4) and seeded at a density of 3,500 cells/cm² in 175cm² flasks (612,500 cells/flask). HCF-v were cultured in a humidified incubator at 37°C with 5% CO_2 and media was changed every second day until sub-confluent (80% confluency, 5-7 days). Confluent flasks were rinsed twice with 1x PBS before 0.25% trypsin was added to the cells for 2 min at 37°C. To detach all cells from the surface, the flask was gently tapped or knocked. Trypsin inhibitor (ratio 1:1 to trypsin) was added to stop trypsin activity and transferred to 50 ml conical tubes. Subsequently, the cell suspension was centrifuged (220x g, RT, 5 min) and the pellet was resuspended in fresh growth medium. Cells were counted and viability was assessed using a Neubauer cell counting chamber and trypan blue staining for dead cell exclusion. After reaching P5, HCF-v were cryopreserved in aliquots (3.6x 10^6 cells) using freezing medium (2.1.4) and stored in gaseous nitrogen until experimental use.

2.2.1.2 Chronic Hypoxia treatment

To study the impact of chronic hypoxia on CF phenotype, cells were subjected to a chronic hypoxic environment (0.5% O_2) and compared to control cells grown under normal oxygen concentrations (21% O_2, = normoxic conditions).

In detail, for chronic hypoxia treatment, P7 HCF-v were seeded in 145 mm petri dishes in HCF-v growth medium at a density of 10,000 cells per cm² (approx. 1.5x 10^6 cells per dish) and let adhere for 16h. Cells were then introduced to hypoxic conditions for a total of 4 days (96h) initiated by changing the media to N_2-pre-gassed growth media (for normoxia and hypoxia, 2.1.4) and transferring the cells to a humidified incubator of the hypoxic workstation (Xvivo System, Biospherix, Parish, NY, USA) set to 0.5% O_2, 5% CO_2, 94.5% N_2 and 37°C. Under these conditions the cells were allowed to grow, with the media changed once after 30h, until a confluency of 80% was reached (60h). At this point, further proliferation was stopped by washing once with pre-warmed N_2-pre-gassed 1x PBS and adding nitrogenated serum-free media (2.1.4) for 36h. Analogously, normoxic HCF-v were treated equally as a time-matched control. In contrast to cells undergoing chronic hypoxia, these cells were cultivated in non-gassed growth media in a second humidified incubator of the hypoxic workstation set to 21% O_2, 74% N_2, 5% CO_2 and 37°C. For the final 36h, media was changed to non-gassed serum-free media for secretome collection. In Rhein treated samples, 35 µM Rhein was added to the respective media and replenished upon every media change resulting in a total incubation time 4d (96h). In total, 6 replicates for each condition from 4 different donors were generated. After the treatment the conditioned serum-free media was collected, filtered through a 0.8 µM syringe filter and immediately stored at -80°C before subjected to secretome analysis via LC-MS (2.2.3.7). Subsequently, the cells were washed twice with 1x PBS and either frozen dry (2x replicates) or directly processed for RNA isolation (2.2.2.1), protein extraction for Western blot analysis (2x replicates, 2.2.3.1) or protein extraction for enzyme activity assays (2.2.3.2)

2.2.1.3 TGFβ1-stimulated differentiation of cardiac fibroblasts

The phenotype of CFs and MFs and the effect of Rhein were studied using human recombinant TGFβ1 (Peprotech, Hamburg, Germany) as a potent stimulator of differentiation. Herein, P5 HCF-v were seeded in 6-well plates at a density of 15,000 cells per cm² in HCF-v growth media (2.1.4) and grown until 80%-90% confluency (3-4d) with the media changed every 48h. Subsequently, cells were washed once with 1x PBS and incubated with 10 ng/ml TGFβ1 alone or in combination with the specified Rhein concentration in HCF-v maintenance media (2.1.4) for 24h. At the end of incubation cells were washed twice with ice-cold 1x PBS and immediately processed for RNA or protein isolation or frozen at -20°C until further use.

2.2.1.4 Collagen gel contraction assay

Collagen contractility, due to *de novo* formation of αSMA fibers, is a distinct characteristic of MFs which can be evaluated by the 3D collagen matrix gel contraction assay. Herein, fibroblasts are seeded in floating collagen gel lattices. Increasing number of MFs, is proportional to increasing contraction (or lower surface area) of the gel over time in this assay.

In detail, collagen media was prepared by mixing 1 part of rat-tail collagen type I (CellSystems, Troisdorf, Germany) with 3 parts (v/v) of growth media and kept on ice. HCF-v (P6) were trypsinized, counted and resuspended in growth media (6x 10^6 cells/ml). Polymerization was started by neutralizing the acidified environment by adding 1:25 NaOH (1M) (v/v) to the collagen media and immediately mixed with the cell suspension. 500 µl of the collagen/cell suspension per well (final concentrations: 1 mg/ml collagen I; 300,000 cells/ml) were quickly transferred to a 24-well plate to cast the fibroblast populated collagen lattices. Collagen gels were allowed to solidify for 15 min at 37°C in a humidified incubator. Polymerized lattices were released using a pipette tip and transferred to a 6-well plate containing 2 ml of serum-free media per well. Floating collagen lattices were treated in triplicates with 10 ng/ml human recombinant TGFβ1 or different doses of Rhein for 5d. Overhead pictures were taken at day d0 (before treatment) and d5 using the ChemiDoc System (BioRad, Munich, Germany) and respective surface areas were determined by manual circling using ImageJ software.

Relative contraction given in percent was calculated by dividing final area (d5) by starting area (d0).

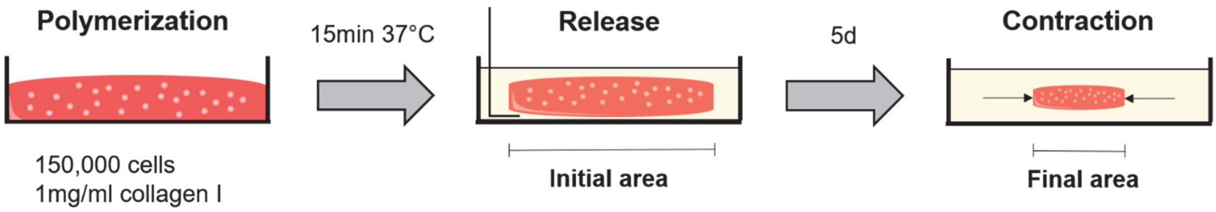

Figure 6: Principle of collagen gel contraction assay
A mixture of cells and collagen is spontaneously polymerized when placed in an incubator (37°C, 5% CO_2, 21% O_2, 74% N_2) for 15 min. The lattices are then mechanically released from the culture dish wells and transferred to a new well containing HCF-v maintenance media. The floating lattice allows the cells to contract the collagen matrix over the experimental duration of 5 days. The amount of contraction can then be measured and quantified by assessing the initial and final area.

2.2.2 Molecular biological methods

2.2.2.1 RNA extraction

RNA extraction was performed using the Maxwell® 16 low elution volume (LEV) automated system in combination with the LEV simplyRNA Purification Kit (Promega, Madison, USA) according to the manufacturer's instructions. This system employs RNA-binding paramagnetic particles that allow RNA isolation via a built-in magnetic rod in fully-automated serial steps. Frozen cells were homogenized in 200 µl 1-thioglycerol containing homogenization buffer, before lysis buffer (1:1, (v/v) was added. The extraction solutions containing cartridges were prepared and placed into the machine's rack prior the cell lysate was transferred into the first well of respective cartridge. RNA elution volume was set to 30 µl and concentration and purity were determined photometrically (NanoDrop 2000, Thermo Scientific, Wilmington, USA) at a wavelength of 260 nm. RNA samples were directly transcribed into cDNA (2.2.2.2) or stored at -80°C.

2.2.2.2 cDNA synthesis

Reverse transcription of RNA was performed using the Go Script Reverse Transcription System (Promega, Madison, USA) according to the manufacturer's instructions. RNA was mixed with 1 µl Oligo-dT Primer and denatured at 70°C for 5 min, before reverse transcription buffer was added (Table 12). Annealing, cDNA synthesis and dissociation of the reverse transcriptase were performed in the GeneAmp PCR System 9700 thermocycler.

Table 12:cDNA synthesis preparation

Sample Mix:

11.3	µl	800 ng RNA in H_2O_{bidest}
1	µl	Oligo-dT

RT mix:

4	µl	5x reaction buffer
1.2	µl	$MgCl_2$
1	µl	Reverse Transcriptase
0.5	µl	RNAse inhibitor
1	µl	dNTP mix

Profile:

Name	Time	Temperature
Denaturation	5 min	70°C
Addition of RT mix		
Annealing	5 min	25°C
Synthesis	60 min	42°C
Dissociation	15 min	70°C

2.2.2.3 Realtime-Quantitative Polymerase-Chain-Reaction (RT-qPCR)

In quantitative PCRs (qPCR) a fluorescent reporter molecule (e.g. SYBR green), which intercalates into double stranded DNA, is employed to quantify the amplicons during the exponential phase of amplification. Proportionally, the fluorescent intensity increases with every amplification cycle and data is collected by a PCR cycler system. The threshold cycle (C_t) gives information about the first cycle in which fluorescent intensity exceeds the background intensity of the sample. C_t values are inversely proportional to the initial cDNA template concentration of the sample. At the end of the RT-qPCR a melting curve is performed to control the specificity of the primers and to exclude unspecific amplification. RT-qPCRs were carried out using the StepOnePlus qPCR System and the GoTaq® qPCR master mix (Promega, Madison, USA) according to the manufacturer's instructions. cDNA was diluted 1:40 with dH_2O and the samples RT-qPCR was accomplished under following conditions:

Table 13: qPCR sample mix and profile.

Sample Mix:

5 µl	2x GoTaq® qPCR Master Mix
0.5 µl	forward primer
0.5 µl	reverse primer
4 µl	***cDNA (1ng/µl)***

PCR profile:

Name	Time	Temperature	Cycles
Hot Start	2 min	95°C	1x
Denaturation	15 s	95°C	40x
Annealing/Extension	60 s	60°C	
Dissociation (Melting)		60-95°C	1x

2.2.2.4 RT² Profiler qPCR Fibrosis Array

The RT² Profiler PCR Fibrosis Array (Qiagen, Hilden, Germany) is a RT-qPCR-based microarray with the ability of detecting the expression of many genes simultaneously. Herein, the kit includes a pre-designed 384-well plate (4x 96) containing 4 replicate primer assays for each of 89 pathway- or disease-focused genes including 5 housekeeping genes and internal controls for data normalization, genomic DNA contamination detection, RNA sample quality and general PCR performance. For each sample 400 ng RNA were transcribed to cDNA as previously described (2.2.2.2) and 10 µl of 1:70 diluted cDNA was added to each well of one set (1x 96). RT-qPCR was performed as previously described (2.2.2.3) using the same parameters with exception of applying the QuantStudio 7 Flex Real-Time PCR System.

2.2.2.5 Affymetrix microarray

Transcriptome analysis was performed using the Affymetrix microarray technology. Basically, mRNA is first transcribed into cDNA using fluorescence labeling, before the native strand is removed and the fluorescent strand is hybridized with complementary probes spotted on a microarray chip. In this study the GeneChip™ Human Transcriptome Array 2.0 was employed, which covers 68,000 probe sets from both non-coding and coding-RNA. RNA was extracted from cells as previously described (2.2.2.1) and purified RNA was handed over to the Genomics Core Facility of the German Diabetes Center (Head: Dr. Knebel). S. Jacob and Dr. Knebel performed RNA quality controls and the Affymetrix microarray workflow to generation and extraction of raw data. Processed raw data were received from the Core facility for analyses. Experimental groups were analyzed using the Transcriptome Analysis Console

(TAC) software version 4.0 to determine differential expression using the restrictions: 1.5-fold differences and p-value 0.05. Further bioinformatic analysis was performed using the knowledge-based Ingenuity® Pathway Analysis (IPA®) (release summer 2018 (Qiagen, Hilden, Germany)).

2.2.2.6 DNA-Methylation analysis

2.2.2.6.1 DNA isolation

Isolation of DNA from HCF-v challenged with chronic hypoxia (2.2.1.2) was conducted using the DNeasy® Blood & Tissue Kit (Qiagen, Hilden, Germany). Isolation procedure was carried out according to the manufacturer' protocol. Briefly, 1x PBS washed and dry frozen cell pellets were resuspended in 200 µl PBS and 20 µl proteinase K before 200 µl buffer AL was added to each sample. Samples were incubated for 20 minutes at 56°C followed by addition of 200 µl ethanol (100%) prior being vortexed and subjected to DNeasy Mini spin columns. Loaded DNA underwent a series of washing step as described in the manufacturer' instructions and purified DNA was eluted in 200 µl 10 mM Tris-HCl, pH 7.8. DNA concentration was measured using the NanoDrop™ 2000/2000c spectrometer (Thermo Fisher Scientific, Darmstadt, Germany) via OD260 measurement and quality was visually assessed after separation by 1.5% agarose-gel electrophoresis.

2.2.2.6.2 Bisulfide conversion of isolated DNA

The EpiTect® Fast DNA Bisulfite Kit (Qiagen, Hilden, Germany) was used for DNA bisulfite conversion of 1 µg isolated DNA from each condition. To each sample 85 µl bisulfite solution and 35 µl DNA protect buffer was added followed by incubation for two cycles with 5 minutes denaturation at 95°C and 10 minutes at 60°C to proceed DNA conversion. Subsequently, the bisulfite converted DNA was purified using the provided purification protocol. Therefore, converted DNA samples were combined with 310 µl buffer BL and 250 µl ethanol (100%) vortexed for 15 seconds and subjected to MinElute DNA spin columns. After several washing steps described in detail in the manufacturers' instructions bisulfite converted DNA was eluted from spin columns using 15 µl elution buffer. Concentration of purified DNA was measured using the NanoDrop™ 2000/2000c spectrometer (Thermo Fisher Scientific, Darmstadt, Germany).

2.2.2.6.3 Amplification of sequence to analyze

Methylation analysis was performed from Homo Sapiens chromosome 14 (complete sequence, ID: ng_029606) positions 4895, 4892, 4869, 4863, 4857, 4854. First, the sequence to analyze (Table 14) was amplified using the PyroMark PCR Kit. Briefly, 10 ng of bisulfite converted DNA (2.2.2.6.2) from each sample and controls was combined with PyroMark PCR master mix, CoralLoad® concentrate and primers (Table 14). The PCR was performed using different stages including 15 minutes at 95°C for polymerase activation followed by 45 cycles of 30 seconds denaturation at 94°C, 30 seconds annealing at 56°C, 30 seconds extension at 72°C and an additional final extension step for 10min. Final PCR products were loaded and separated on a 2% agarose-gel electrophoresis for visual quality assessment using 3 µl of each PCR reaction. As internal control, DNA provided in the EpiTect® PCR Control DNA Set was also amplified in addition to experimental samples. Primers were designed using the PyroMark Assay Design Software.

Table 14: Sequences used for methylation analysis of *HIF1A* hypoxia response element

Sequence to analyze	RCCRCTAAACACAAACRAACACRTAAACRTCRC
Forward primer (biotinylated)	TAGGAGGAGGTTAGTTGAGGTATAGTT
Reverse primer	ACCCCCATCTCCTTTCTCT
Sequencing primer	CCTTTCTCTTTCCTCC

R: Methylation site

2.2.2.6.4 Pyrosequencing

Pyrosequencing was conducted in the PyroMark Q96 ID device (Qiagen, Hilden, Germany). Using the PyroMark Q96 Vacuum Workstation (Qiagen, Hilden, Germany), the amplified bisulfite DNA samples were purified by sepharose beads binding the biotinylated primer attached to the amplicons. PyroMark Gold Q96 Reagents (Qiagen, Hilden, Germany) required for analysis were loaded to the device according to manufacturers' instructions. Finally, the purified PCR products were processed and mixed with reaction buffer and sequencing primer according to the manufacturers' protocol before pyrosequencing.

2.2.3 Biochemical methods

2.2.3.1 Protein extraction for Western blot analysis

For protein extraction, cells were washed twice with ice-cold 1x PBS and immediately processed or frozen at -20°C until further processing. To each well of a 6-well-plate 100µl or to each 145 mm dish 500µl of ice cold RIPA-buffer (containing 1:10 protease and phosphatase buffer each) was added, respectively, and cells were lysed using cell scrapers. Lysates were transferred to 1.5 ml Eppendorf vials and incubated on ice for 10 min prior centrifugation at 14,000x g and 4°C for 15 min. The protein-containing supernatant was transferred into a new reaction tube and stored at -20°C until further use.

2.2.3.2 Protein extraction for enzyme activity assay analysis

For enzyme activity assays (2.2.5), cells were washed twice with ice-cold 1x PBS and protein extraction was performed by lysing the cells in 1x PBS supplemented with 1% NP-40. Subsequently, lysates were transferred to 1.5 ml vials and incubated on ice for 10 min prior undergoing centrifugation (14,000x g, 4°C, 15min). The protein-containing supernatant was transferred into a new reaction tube and stored at -20°C until further use.

2.2.3.3 Measurement of protein concentration

Protein concentrations of cleared lysates were determined using the BCA Protein Assay Kit (Pierce, Rockford) according to the manufacturer's prescription. The assay is based on the reduction of Cu^{2+} ions to Cu^{+} ions by proteins in alkaline medium (biuret reaction). The chelating agent bicinchoninic acid (BCA) forms a complex with Cu^{+} ions, leading to a color change of the solution from green to purple. The extinction of the color change can be measured at 560 nm and is directly proportional to the protein content. To determine the protein concentration, lysates were diluted with dH_2O 1:5 and pipetted in a 96-well plate in duplicates. After addition of 200 µl of BCA reagent, the samples were incubated at 37°C for 30 min and the absorption was measured with an iMark microplate absorbance reader. A BSA standard ranging from 0.125 mg/ml to 2 mg/ml was used for protein content estimation via linear regression.

2.2.3.4 Sodium dodecyl sulfate polyacrylamide gel electrophoresis (SDS-PAGE)

Sodium dodecyl sulfate polyacrylamide (SDS) binds to hydrophobic residues of proteins and applies negative charges to the proteins proportionally to its mass facilitating the electrophoretic separation of proteins according to their molecular weight. Separation was carried out via the fine-pored matrix of polyacrylamide gels, which are formed by the polymerization and crosslinking of acrylamide molecules under catalysis of ammonium persulfate (APS) radicals and the stabilizer tetramethylethylenediamine (TEMED). The percentage of polyacrylamide in the gels was selected depending on the molecular weight of the target protein (Table 15).

Laemmli sample buffer (Table 4), containing SDS as denaturing and linearizing agent and dithiothreitol (DTT) for disulfide bond reduction, was added to 20µg of lysate in a ratio of 1:5. Subsequently, the samples were boiled for 5 min at 95°C before loaded onto the SDS gel. Samples were first electrophoretically focused in the stacking gel for 10-15 min at 100V and subsequently run through the separating gel at 150V.

Table 15: Composition of polyacrylamide gels

Stacking gel buffer
0.5 M Tris
0.4% SDS; pH 6.8

Separation gel buffer
1.5 M Tris
0.4% SDS; pH 8.8

Separation gel	8%	10%	12%
Separation gel buffer	1.56 ml	1.56 ml	1.56 ml
Acrylamide (30%)	1.60 ml	2.00 ml	2.40 ml
dH_2O	2.84 ml	2.44 ml	2.04 ml
Ammonium persulfate (APS)	6 mg = 12 µl	12 µl	12 µl
TEMED	6 µl	6 µl	6 µl

Stacking gel	
stacking gel buffer	520 µl
Acrylamide (30%)	260 µl
dH_2O	1.22 ml
Ammonium persulfate (APS)	2 mg = 4 µl
TEMED	2 µl

2.2.3.5 Western blot

Separated proteins were blotted from SDS-gels to polyvinylidene fluoride (PVDF) membranes via Tank-Blot technology. Gels and membranes were placed in a tank filled with cold transfer buffer and proteins were transferred from the polyacrylamide gel to the membrane by horizontal electrophoresis at 0.2A for 3h.

2.2.3.6 Antibody staining and detection

Transferred proteins were targeted with epitope-specific primary antibodies and subsequently stained with IgG-binding peroxidase-coupled secondary antibodies. Antibody solutions were prepared in 5% skim milk/ TBS-T (Table 4) or 5% BSA/TBS-T, respectively. After blocking of membranes for 1h 5% skim milk/TBS-T or 5% BSA/TBS-T, the primary and secondary antibody were successively incubated for 1h at RT or o/n at 4°C.

For detection, horseradish-peroxidase substrate solution (Merck Millipore, Burlington, USA), was applied to the membrane as described in the manufacturer's instructions. The peroxidase coupled to the secondary antibody, oxidizes the substrate leading to a flash signal. The light evolving from this reaction was detected by a light-sensitive camera in the VersaDoc^{TM} System (BioRad, Munich, Germany) and analyzed using Image Lab software.

Table 16: Western blot parameters according to target protein

Target Protein	MW (kDa)	Percentage of Separation gel (%)
HIF1α	120	8
αSMA	42	10
DNMT1	200	8
TGFβ1	45	10
TGFβR1	52	10
pSMAD2	60	10
SMAD7	49	10
p53	53	10
p21	21	12

Bands were manually edged with rectangles and relative intensity was automatically calculated by the software (Quantity One, ImageLab 5.2). Normalization was performed by calculating the ratio between the intensities of target protein/GAPDH using GAPDH as loading control.

2.2.3.7 Secretome analyses

The pre-filtered HCF-v secretomes from chronic hypoxia experiments (2.2.1.2) were centrifuged (45min, 85,000xg, 4°C) prior undergoing a protein-binding based concentration process by centrifugation in Amicon® Ultra 15 Ultracel column tubes (Merck Millipore, Burlington, USA) with an exclusion of protein <3kDa to increase the concentration of the proteins to be analyzed.

Further sample preparation and mass spectrometry running both data dependent acquisition (DDA) and data-independent acquisition (DIA) strategies were performed by Dr. S. Hartwig and U. Kettel at the Proteomics Core Facility (Head: Dr. S. Lehr) of the Institute of clinical biochemistry and pathobiochemistry at the German Diabetes Center.

DDA run data files were analyzed using Proteome Discoverer™ 2.2 software (ThermoFisher Scientific) and Sequest HT search was performed against the FASTA database (SwissProt Homo sapiens (TaxID=9606, version 2018-05-25)). In the processing workflow, Sequest HT parameters were set to trypsin as digestion enzyme with maximum tolerance of 2 miscleavages, a peptide length of 5-144 and maximum 10 peptides per spectrum. Allowed modifications were cysteine carbamidomethylation static and N-terminal acetylation and methionine oxidation as dynamic modifications. In the Percolator node Peptide-spectrum-match (PSM) analysis was performed setting q-values to 0.01 (strict) and 0.05 (relaxed) false discovery rate (FDR). Q-values are a statistical means, giving the percentage of significant tests that will statistically result in false positives and thus representing FDR adjusted p-values.

Resulting matched spectra file (MSF) was subjected to the consensus workflow, where PSMs were grouped, validated and identified peptides filtered before protein confidence scores were calculated. In the protein grouping node parsimony was applied excluding all protein groups not strictly explaining identified peptides. Furthermore, scored proteins were filtered according to a FDRs 0.01/0.05 (strict/relaxed) and annotated using the standard Gene Ontology term annotations. For label-free protein quantification, peptides linked to proteins were quantified using the Precursor Ions Quantifier (PiQ). Importantly, Imputation Mode parameter in the PiQ node was selected to Low Abundance Resampling, which replaces missing values with random values sampled between the minimum and the lower 5 percent of all detected values. This step allows for low abundant proteins to be tagged as identified providing a more complete picture of present and non-present proteins in the secretome.

As Proteome Discoverer™ does not give absolute signal intensities, but only relative abundances and information about peak identification in the individual conditions and donors, another analyses software package, i.e. MaxQuant, was employed as alternative tool for DDA run analysis. MaxQuant enables label-free quantification (LFQ) using the procedure MaxLFQ, which determines and normalizes the intensities based on the assumption that the presence of quantifiable peptides varies from sample to sample. Herein, protein abundance profiles are assessed by extracting the maximum ratio information from peptide signals in arbitrary numbers of samples. Using this approach, not only information is retrieved whether a protein is present, but also its abundance in the respective secretome. MaxQuant analysis was performed using the FASTA database (SwissProt Homo sapiens (TaxID=9606, version 2018-05-25)) and parameters were mainly left at default settings with a few alterations. In the group-specific parameters section digestion was set to trypsin, oxidation and N-terminal acetylation were allowed as modifications and LFQ option was enabled. For PSM analysis and protein identification the q-value was set to 0.01 FDR and advanced ratio estimation was enabled for protein quantification.

For a more reliable quantification of label-free probe sets LC/MS runs were performed also in DIA scan mode and spectral data was analyzed using Spectronaut™ Pulsar X software (Biognosys, Zürich, Switzerland). DIA runs are evaluated using a self-performed spectral library based on DDA runs analyzed with the Proteome Discoverer™ in Sequest HT mode (see above). Additionally, normalization and quantification of the secretomes was granted by spiking the samples with indexed Retention Time (iRT) standard, containing eleven non-naturally occurring synthetic peptides, which allows for calibration of the chromatographic system. Based on the standard parameter settings, the software identified the proteins in the secretome and calculated the folds between set numerator and denominator groups including p-value and FDR.

2.2.3.8 TGFβ1 ELISA

Secreted TGFβ1 levels from normoxia versus chronic hypoxia treated HCF-v were measured using the Human LAP (TGF-β1) Quantikine ELISA Kit (R&D systems, Wiesbaden, Germany) with a detection range of 3.4 - 1,500 pg/ml according to the manufacturer's instructions. As input for the ELISA, 10 µl of previously concentrated secretome (2.2.3.7) were employed and resulting TGFβ1 levels were normalized to total protein used from input.

2.2.4 Cell-based assays

2.2.4.1 Cell toxicity assay

To determine the working dose range of Rhein and inhibitors used in this study, the non-toxic concentrations were analyzed using the cell-based CellTox™ Green Cytotoxicity Assay (Promega, Madison, IA, USA) according to the instruction manual. The principle of the assay is based on a fluorescent DNA-binding dye that is excluded from viable cells, but preferentially enters non-viable cells due to their lack of membrane integrity. The resulting fluorescent signal is directly proportional to the stained cells and cytotoxicity. 10,000 HCF-v cells per well were seeded into black opaque 96-well cell culture plates in growth media and let adhere overnight. Cells were washed once with PBS and dose range of respective substance of interest was applied to the cells in serum-free media for 24h at 37°C in a humidified incubator (74% N_2, 21% O_2, 5% CO_2). For assaying, 100 µl of dye-containing assay buffer (1:1 to medium (v/v)) was added to the cells and incubated for 15 min RT prior measurement of fluorescent signals at E_{Ex} = 485nm/E_{Em} = 530nm using the Infinite 200 PRO microplate reader. A maximum toxicity control was employed by addition of 4µl lysis reagent to the cells.

2.2.5 Enzyme activity assays

Measurement of respective enzyme-activities in this study were carried out using bioluminescent- or fluorescence-based enzyme-specific activity assays. For all activity assays used, 5 µg of whole cell extracts as enzyme source were diluted in 50 µl of respective assay buffer and added to white-walled (luminescence) or black-walled (fluorescence) opaque 96-well plates. If applicable, to monitor whether Rhein has a modulating effect on respective enzyme activity, 5 µg of control cell lysates (24h serum-free media) were preincubated with 35µM Rhein or with specific inhibitor for 1h. Luminescence was measured using the Infinite 200 PRO microplate reader. Detailed parameters of the single activity assays are specified in the following sections.

2.2.5.1 HDAC I/II activity

HDACs are enzymes that deacetylate acetylated lysine residues of histones and non-histone proteins. HDAC class I/II activity was analyzed using the HDAC-Glo™ I/II Assay and Screening System (Promega, Madison, IA, USA). The assay uses HDAC I/II-specific substrates that are conjugated to aminoluciferin. Upon catalyzation of the substrate by the enzyme of interest, aminoluciferin is released from the complex by a developer reagent provided protease, and subsequently oxidized by luciferase creating a light signal. The acquired luminescence is directly proportional to HDAC class I/II activity. In practice, cell lysates were incubated with HDAC I/II substrate for 45 min at RT before luminescence was determined. In experiments performed to study the imminent effect of Rhein on HDAC activity, 1 mM of sodium butyrate (SB), an HDAC class I and IIa inhibitor, was applied as HDAC inhibition control.

2.2.5.2 SIRT activity

Sirtuins (SIRTs) are considered as class III HDACs and also function as deacetylases, however, unlike HDAC class I/II, SIRTs are NAD^+-dependent and therefore directly coupled to the metabolic state of the cell. For activity determination of SIRTs, the SIRT-Glo™ Assay (Promega, Madison, IA, USA) was applied according to the manufacturer’s instructions. Consistent with the HDAC-Glo™ I/II Assay and Screening System, the SIRT assay is based on SIRT-specific aminoluciferin-conjugated substrate that promotes luminescence upon SIRT deacetylase reaction. Briefly, cell lysates were incubated with SIRT substrate for 15 min before luminescence measurement. As reference for testing the direct influence of Rhein on SIRT activity, 10 mM nicotinamide (NAM) was used as comparative SIRT inhibitor.

2.2.5.3 Methyltranferase activity

Methylation is a process mediated by methyltransferases that can modify a broad range of substrates such as DNA, RNA, proteins and small molecules. To determine global methyltransferase activity the MTase-Glo™ Methyltransferase Assay (Promega, Madison, IA, USA) was used. The assay monitors the formation *S*-adenosylhomocysteine (SAH) from methyl donor *S*-adenosylmethionine (SAM) during the methyltransferase reaction. Upon addition of the MTase-Glo™ Reagent, SAH is converted to ADP. Subsequently, MTase-Glo™ Detection Solution is added to convert ADP to ATP, which is detected as luminescence via the luciferase reaction. Briefly, cell lysates were incubated with 2.5 mM SAM for 30 min at RT, succeeded by 30 min incubation with MTase-Glo™ Reagent. Next, MTase-Glo™ Detection Solution was added, followed by 30 min incubation at RT before luminescence was read.

2.2.5.4 HAT activity

As counterpart of HDACs and SIRTs, histone acetyltransferases (HATs) are able to acetylate lysine residues of both histones and non-histone proteins. The HAT activity assay Kit II was used (PromoKine, Heidelberg, Germany) to assess HAT activity in lysates according to the instructions. In this assay, HATs catalyze the transfer of acetyl groups from acetyl-CoA to the target protein. The resulting CoA-SH reacts with the developer producing a fluorometrically detectable signal, directly proportional to HAT activity in the sample. In black opaque-walled 96-well plates, total protein lysates were incubated with 50µl HAT substrate solution for 45min at RT, before fluorescence was measured at E_{Ex}/E_{Em} = 535nm/587nm using the Infinite 200 PRO microplate reader (Tecan Group AG, Männedorf, Zürich, Switzerland). To determine whether Rhein has an immediate effect on HAT activity, 35 µM Rhein or 1 µM of HAT inhibitor anacardic acid were added to control cell extracts for 1h before assaying.

2.2.6 Statistical analysis

Statistical analysis was performed with GraphPad Prism 7.04 (GraphPad Software Inc., La Jolla, USA). To confirm significant differences unpaired two-tailed t-tests, One-way-ANOVA or Two-way-ANOVA with Sidak´s multiple comparison test was used as detailed in the legends of the figures. Values are presented as means with standard error of mean (SD).

2.2.7 Bioinformatic analysis

To identify whether proteins in the secretome are secreted via the classical secretion pathway, the non-classical secretion pathway or whether they secretion of the proteins is unknown, the web-based tools SignalP 4.1 (http://www.cbs.dtu.dk/services/SignalP/) and SecretomeP 2.0 (http://www.cbs.dtu.dk/services/SecretomeP/) were employed. Therefore, only proteins that were identified by MaxQuant in at least 3 out of 4 donors within one condition were subjected to further analysis. FASTA files of proteins passing this data restriction were retrieved from https://www.uniprot.org/ and loaded into the SignalP server. SignalP 4.1 predicts the presence and location of signal peptide cleavage sites in amino acid sequences and tags a protein signal peptide positive (SP+) or negative (SP-). Since this approach only identifies SP+ proteins that are secreted by the classical secretion pathway, further dissection of non-classical pathway (SP-) and unknown pathway secretion (NP) proteins was conducted. Therefore, SP- proteins from SignalP analysis were subjected to SecretomeP 2.0, which obtains information on various post-translational and localizational aspects of the protein integrating them into the final secretion prediction.

Partial least square-discriminant (PLS-D) analysis was conducted in Metaboanalyst 4.0 (http://www.metaboanalyst.ca/) using the pre-filtered secretome lists containing MaxQuant LFQ intensities of proteins present in either all 4 donors of one condition or in three donors of at least two conditions of one comparison.

GeneOntology (GO) term analysis of secretomes was conducted in the web-based PANTHER classification system (version 13.1 Released 2018-02-03, http://www.pantherdb.org/) using the Homo sapiens reference proteome and Fisher's Exact testing with Bonferroni correction for multiple testing.

For pathway enrichment analyses and upstream regulator analysis of differential abundant transcripts (1.5-fold, p-value ≤ 0.05) and secretory proteins (2.6-fold, p-value ≤ 0.05) were performed with Ingenuity® Pathway Analysis (IPA®) software (Qiagen, Hilden, Germany).

3 Results

3.1 Chronic hypoxia-mediated modulation of the secretome and its impact on the cardiac fibroblast phenotype

Persistent local hypoxia after cardiac injury results in the radiation of MFs from the point of lesion towards the remote interstitium. Based on this observation, the question of a local cellular dissemination of information is justified and one possible mechanism constitutes the direct intercellular crosstalk through different secretion profiles.

The first part of the study is focused on the characterization of HCF-v maintained to chronic hypoxia in comparison to normoxic cells, grown under regular oxygen conditions (Figure 7). Further, it was investigated whether hypoxia interferes with the FMT, and how it might be modulated in concert with fibrotic features.

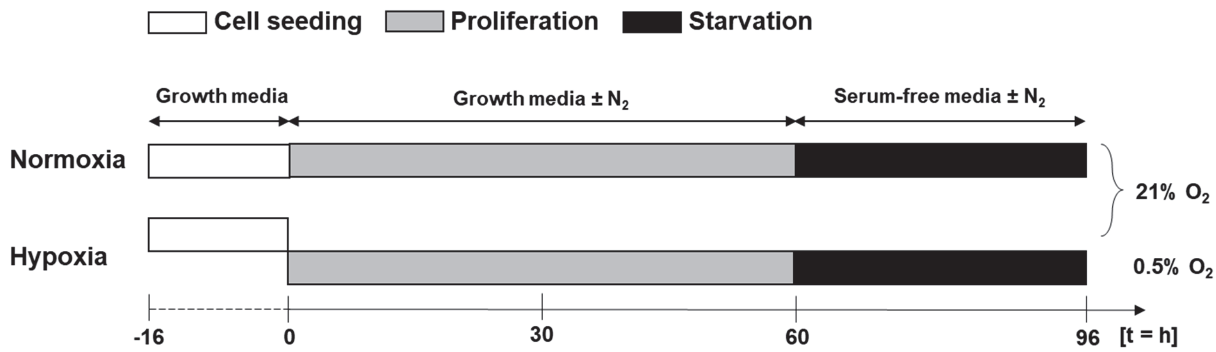

Figure 7: Schematic overview of chronic hypoxia experimental setup

Primary human ventricular cardiac fibroblasts (HCF-v) were seeded at 10% confluency. After 16h medium was changed and cells were cultured in growth media at 21% O_2 for additionally 60h before maintained for 36h in serum-free media for secretome collection. For hypoxic treatment cells were seeded at 10% confluency and let adhere for 16h at 21% O_2 before being challenged for 60h with 0.5% O_2. Media were changed from growth to serum-free media for 36h secretome collection.

To validate whether the hypoxic treatment was functional, the protein abundance of hypoxia-activated HIF1α was determined in hypoxia treated versus normoxic HCF-v (Figure 8). HIF1α was significantly increased by approx. 7-fold ($p < 0.0001$) in cells subjected to chronic hypoxia in comparison to normoxic control cells.

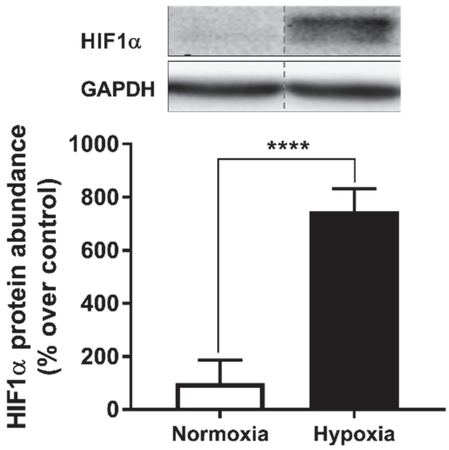

Figure 8: Chronic Hypoxia stabilizes HIF1α.

Primary human ventricular cardiac fibroblasts (HCF-v) were cultivated for 4d at 21% O_2 (normoxia) or 4d at 0.5% O_2 (hypoxia). Representative Western blot and quantitative analysis of HIF1α. n = 4, Mean ± SD, two-tailed unpaired t-Test **** $p < 0.0001$ as indicated.

3.1.1 Effect of chronic hypoxia on cardiac fibroblast secretome profile

To study the impact of chronic hypoxia on the secretory profile of HCF-v secretome analysis was performed as described in the methods section (2.2.3.7). Secretome analysis based on the data-dependent (DDA) acquired LC-MS runs using the MaxQuant software (2.2.3.7), identified a total of n = 707, which were found at least in 3 out of 4 supernatants of each normoxic or hypoxic HCF-v or at least 4 times in one of both conditions. Herein, n = 535 proteins were commonly secreted, whereas n = 43 proteins were specifically found under normoxic conditions and hypoxic secretomes comprised n = 129 unique proteins. For the normoxic secretomes, SecretomeP and SignalP (2.2.7) predicted a contribution of 39.7% of proteins that were secreted according to the classic secretion pathway (SP+), 12.9% according to the non-canonical secretion pathway (SP-) and the resembling 47.4% were labeled with unknown secretion (NP). In the secretome of hypoxia-treated cells, distribution depicted 38.1% SP+, 11.4% SP- and 50.4% NP.

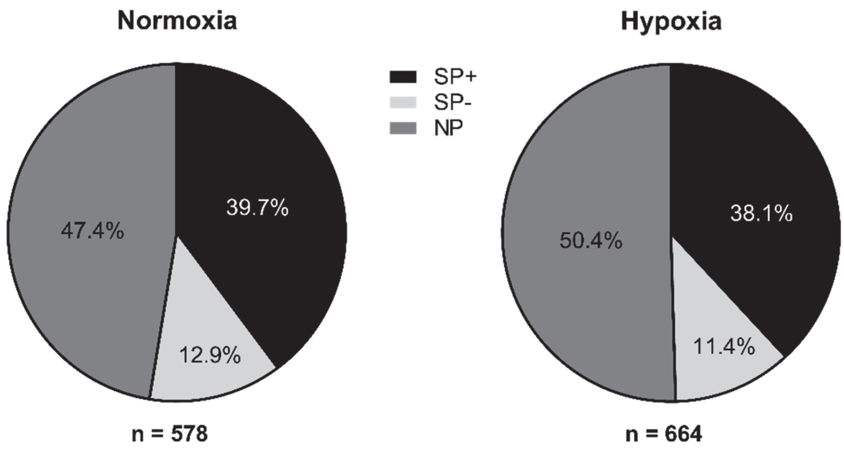

Figure 9: Number of secreted proteins in normoxia- and hypoxia-treated cells
Proteins identified using MaxQuant analysis of DDA mode LC-MS runs and classified by SecretomeP and SignalP according to secretion pathway. SP+: canonical secretion pathway, SP-: non-canonical secretion pathway, NP: secretion unknown.

For further characterization and quality assessment of the generated secretomes, bioinformatical analyses were performed using the *cellular component* (CC) module of the GeneOntology (GO) web-based tool (Table 17). The normoxic secretome contained proteins of predominantly extracellular nature revealing GO terms such as ‘extracellular region part’ ($p = 1.31 \times 10^{-249}$), ‘extracellular vesicle’ ($p = 2.80 \times 10^{-244}$), ‘extracellular organelle’ ($p = 3.89 \times 10^{-244}$), ‘extracellular exosome’ ($p = 1.06 \times 10^{-240}$), ‘extracellular space’ ($p = 1.42 \times 10^{-240}$), ‘extracellular region’ ($p = 3.61 \times 10^{-226}$), ‘vesicle’ ($p = 1.58 \times 10^{-189}$) and ‘extracellular matrix’ ($p = 2.37 \times 10^{-61}$). Similar observations were made after analysis of hypoxic secretomes, which revealed most significant enrichment for terms as ‘extracellular region part’ ($p = 4.74 \times 10^{-272}$), ‘extracellular vesicle’ ($p = 7.61 \times 10^{-266}$), ‘extracellular organelle’ ($p = 1.10 \times 10^{-265}$), ‘extracellular space’ ($p = 5.88 \times 10^{-265}$), ‘extracellular exosome’ ($p = 8.53 \times 10^{-264}$), ‘extracellular region’ ($p = 2.01 \times 10^{-248}$) and ‘vesicle’ ($p = 4.56 \times 10^{-202}$).

Table 17: Top 10 enriched cellular component terms found in secretomes of normoxia- and hypoxia-treated HCF-v

Normoxia		
GO cellular component	**Fold Enrichment**	**P value**
extracellular region part	4.97	1.31×10^{-249}
extracellular vesicle	7.01	2.80×10^{-244}
extracellular organelle	7	3.89×10^{-244}
extracellular exosome	7.01	1.06×10^{-240}
extracellular space	5.1	1.42×10^{-240}
extracellular region	4.13	3.61×10^{-226}
vesicle	4.22	1.58×10^{-189}
extracellular matrix	8.53	2.37×10^{-61}

collagen-containing extracellular matrix	10.92	2.04 $x10^{-60}$
cytoplasm	1.58	3.66 $x10^{-56}$
	Hypoxia	
GO cellular component	**Fold Enrichment**	**P value**
extracellular region part	4.86	4.74 $x10^{-272}$
extracellular vesicle	6.84	7.61 $x10^{-266}$
extracellular organelle	6.83	1.10 $x10^{-265}$
extracellular space	5.01	5.88 $x10^{-265}$
extracellular exosome	6.86	8.53 $x10^{-264}$
extracellular region	4.06	2.01 $x10^{-248}$
vesicle	4.1	4.56 $x10^{-202}$
cytoplasm	1.59	4.06 $x10^{-67}$
cytoplasmic part	1.74	1.42 $x10^{-65}$
membrane-bounded organelle	1.51	3.08 $x10^{-61}$

Next, the proteins identified via LC-MS runs based on the more reliable data-independent acquisition (DIA) mode using the Spectronaut® software, which directly compares differentially regulated proteins, were evaluated. Using the standard settings (2.2.3.7), the secretomes of normoxic versus hypoxia treated cells revealed a total of n = 1662 commonly present proteins, wherein n = 638 were significantly ($p < 0.05$) regulated targets of which n = 390 were upregulated and n = 248 were downregulated by at least 1.5-fold (Figure 10). A list of top 50 up- and downregulated proteins is given in the appendix (Table 27).

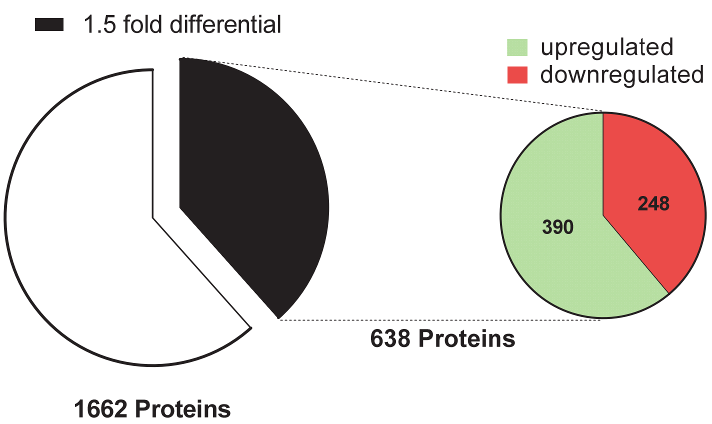

Figure 10: Number of differentially regulated proteins in the comparison between normoxic and hypoxic HCF-v secretomes.

Pie chart showing the fraction of 1.5-fold differentially abundant proteins (p-value <0.05) found in the secretomes of normoxia and chronic hypoxia treated HCF-v. Right handed pie diagram depicts up- and downregulated fractions and respective numbers are given.

As proof of principle and to describe the quality of differential secretomes, an enrichment analysis of cellular component annotations was conducted using the respective PANTHER database (Table 18). As expected, the 6 most significantly enriched components featured extracellular components containing ‘extracellular exosome’ (p = 5.03 x10^{-147}, n = 334, 52.4% of total molecules found in list), ‘extracellular vesicle’ (p = 8.31 x10^{-147}, n = 335, 52.5%), ‘extracellular organelle’ (p = 1.08 x10^{-146}, n = 335, 52.5%), ‘extracellular region part’ (p = 1.22 x10^{-139}, n = 401, 62.9%), ‘extracellular space’ (p = 6.02 x10^{-138}, n = 390, 61.1%) and ‘extracellular region’ (p = 3.57 x10^{-134}, n = 431, 67.6%). However, also proteins with intracellular character were found to be enriched according to the top 15 cellular component annotations, such as ‘cytoplasmic part’ (p = 9.17 x10^{-62}, n = 510, 79.9%), ‘cytoplasm’ (p = 2.49 x10^{-56}, n = 550, 86.2%), ‘membrane-bounded organelle’ (p = 1.01 x10^{-47}, n = 557, 87.3%), ‘organelle’ (p = 1.44 x10^{-42}, n = 574, 90.0%) and ‘cytosol’ (p = 1.65 x10^{-41}, n = 320, 50.2%).

Table 18: Top 15 enriched cellular component terms found in differential secretomes of normoxia versus hypoxia treated HCF-v

PANTHER cellular component	P value	Fold Enrichment	Molecules *n*	% of total molecules
extracellular exosome	5.03 x10^{-147}	5.14	334	52.4
extracellular vesicle	8.31 x10^{-147}	5.1	335	52.5
extracellular organelle	1.08 x10^{-146}	5.1	335	52.5
extracellular region part	1.22 x10^{-139}	3.7	401	62.9
extracellular space	6.02 x10^{-138}	3.8	390	61.1
extracellular region	3.57 x10^{-134}	3.23	431	67.6
vesicle	5.09 x10^{-113}	3.25	382	59.9
cytoplasmic part	9.17 x10^{-62}	1.7	510	79.9
cytoplasm	2.49 x10^{-56}	1.54	550	86.2
membrane-bounded organelle	1.01 x10^{-47}	1.45	557	87.3
organelle	1.44 x10^{-42}	1.37	574	90.0
cytosol	1.65 x10^{-41}	2.03	320	50.2
vesicle lumen	9.18 x10^{-34}	6.79	71	11.1
cytoplasmic vesicle lumen	4.97 x10^{-33}	6.71	70	11.0
secretory granule lumen	9.5 x10^{-32}	6.75	67	10.5

PANTHER protein class analysis of differential secretomes (Table 19) revealed a significant enrichment of ECM regulating enzymes with the terms ‘hydrolase’ (p = 3.80 x10^{-28}, n = 238, 37.3% of total molecules found in list), ‘protease’ (p = 3.25 x10^{-18}, n = 141, 22.1%), ‘metalloprotease’ (p = 6.13 x10^{-13}, n = 54, 8.5%), ‘enzyme modulator’ (p = 3.97 x10^{-12}, n = 153, 24%) and ‘protease inhibitor’ (p = 4.21 x10^{-17}, n = 79, 12.4%). Furthermore, annotations associated with structural components such as ‘cytoskeletal protein’ ($p = 4.21 \times 10^{-17}$, n = 87, 13.6%), ‘actin family cytoskeletal protein’ ($p = 8.59 \times 10^{-11}$, n = 53, 8.3%) and ‘extracellular matrix protein’ ($p = 3.05 \times 10^{-10}$, n = 49, 7.7%) were more frequently annotated. Additionally, translation-related ‘ribosomal protein’ and ‘RNA binding protein’ ($p = 2.21 \times 10^{-09}$, n = 98, 15.4%) were identified among the top 15 enriched protein classes ($p = 3.83 \times 10^{-09}$, n = 39, 6.1%).

Table 19: Top 15 enriched protein classes found in differential secretomes of normoxia versus hypoxia treated HCF-v

PANTHER Protein Class	P value	Fold Enrichment	Molecules *n*	% of total molecules
hydrolase	3.80×10^{-28}	2.24	238	37.3
protease	3.25×10^{-18}	2.35	141	22.1
protease inhibitor	4.21×10^{-17}	3.25	79	12.4
transcription factor	8.95×10^{-14}	0.3	26	4.1
metalloprotease	6.13×10^{-13}	3.44	54	8.5
chaperone	3.81×10^{-12}	4.53	37	5.8
enzyme modulator	3.97×10^{-12}	1.87	153	24.0
serine protease inhibitor	1.62×10^{-11}	4.65	34	5.3
cytoskeletal protein	5.55×10^{-11}	2.27	87	13.6
actin family cytoskeletal protein	8.59×10^{-11}	2.99	53	8.3
extracellular matrix protein	3.05×10^{-10}	3.03	49	7.7
oxidoreductase	4.88×10^{-10}	2.31	77	12.1
RNA binding protein	2.21×10^{-09}	2	98	15.4
ribosomal protein	3.83×10^{-09}	3.25	39	6.1
extracellular matrix glycoprotein	6.32×10^{-09}	3.94	30	4.7

To acknowledge the principal molecular functions underlying in the differential secretomes between normoxia and chronic hypoxia, a second annotation enrichment analysis using the PANTHER molecular function database was performed (Table 20). Consistent with the identification of translation-related proteins in the cellular component analysis (Table 19), most significant enrichment of the term ‘structural constituent of ribosome’ ($p = 8.62 \times 10^{-18}$, n = 32, 5.0% of total molecules found in list) alongside ‘aminoacyl-tRNA ligase activity’ ($p = 7.09 \times 10^{-04}$, n = 7, 1.1%) were found. However, most differentially abundant secretory proteins contained a catalytic function exhibited by the terms ‘peptidase activity’ (6.13×10^{-13}, n = 44, 6.9%), ‘catalytic activity’ ($p = 3.49 \times 10^{-12}$, n = 208, 32.6%), ‘hydrolase activity’ ($p = 1.92 \times 10^{-08}$, n = 103, 16.1%), ‘isomerase activity’ ($p = 1.92 \times 10^{-08}$, n = 103, 16.1%), ‘oxidoreductase activity’ ($p = 9.12 \times 10^{-06}$; n = 36, 5.6%) and ‘lyase activity’ ($p = 4.77 \times 10^{-04}$, n = 17, 2.7%).

Table 20: Top 15 enriched molecular function annotations found in differential secretomes of normoxia versus hypoxia treated HCF-v

PANTHER Molecular Function	P value	Fold Enrichment	Molecules *n*	% of total molecules
structural constituent of ribosome	8.62 $x10^{-18}$	8.17	32	5.0
structural molecule activity	5.77 $x10^{-13}$	3.31	52	8.2
peptidase activity	6.13 $x10^{-13}$	3.79	44	6.9
catalytic activity	3.49 $x10^{-12}$	1.59	208	32.6
hydrolase activity	1.92 $x10^{-08}$	1.8	103	16.1
isomerase activity	2.69 $x10^{-06}$	4.69	15	2.4
oxidoreductase activity	9.12 $x10^{-06}$	2.3	36	5.6
calcium ion binding	1.83 $x10^{-05}$	3.12	20	3.1
sequence-specific DNA binding transcription factor activity	3.76 $x10^{-05}$	0.28	7	1.1
antioxidant activity	2.36 $x10^{-04}$	6.43	7	1.1
protein kinase activity	4.35 $x10^{-04}$	0.16	2	0.3
lyase activity	4.77 $x10^{-04}$	2.64	17	2.7
DNA binding	5.24 $x10^{-04}$	0.45	15	2.4
aminoacyl-tRNA ligase activity	7.09 $x10^{-04}$	5.24	7	1.1
signal transducer activity	7.41 $x10^{-04}$	0.44	13	2.0

To further characterize the differential secreted proteins between normoxia and hypoxia-treated HCF-v, a fourth enrichment study was performed using the PANTHER biological process database (Table 21). In line with the previous finding, that the differential secretomes are mainly comprised of catabolic function proteins (Table 20), mostly terms related to metabolism were found to be most significantly enriched. As such, annotations like ‘protein metabolic’ ($p = 1.14 x10^{-12}$, n = 105, 16.5% of total molecules found in list), ‘process primary metabolic process’ ($p = 1.35 x10^{-12}$, n = 229, 35.9%) and ‘metabolic process’ ($p = 2.12 x10^{-11}$, n = 264, 41.4%) were highly frequent. Furthermore, the terms ‘glycolysis’ (p = 1.31 x10-09, n = 12, 1.9%) and ‘carbohydrate metabolic process’ ($p = 9.42 x10^{-07}$, n = 29, 4.5%) were enriched.

Table 21: Top 15 enriched biological process annotations found in differential secretomes of normoxia versus hypoxia treated HCF-v

PANTHER Biological Process	P value	Fold Enrichment	Molecules *n*	% of total molecules
protein metabolic process	1.14 $x10^{-12}$	2.13	105	16.5
primary metabolic process	1.35 $x10^{-12}$	1.55	229	35.9
metabolic process	2.12 $x10^{-11}$	1.45	264	41.4
proteolysis	4.44 $x10^{-11}$	3.23	45	7.1

translation	5.81 x10^{-11}	4.71	29	4.5
glycolysis	1.31 x10^{-09}	13.79	12	1.9
cellular amino acid metabolic process	5.30 x10^{-09}	3.92	28	4.4
generation of precursor metabolites and energy	9.68 x10^{-08}	4.14	22	3.4
carbohydrate metabolic process	9.42 x10^{-07}	2.92	29	4.5
tricarboxylic acid cycle	2.12 x10^{-06}	11.7	8	1.3
transcription, DNA-dependent	1.37 x10^{-05}	0.32	10	1.6
cellular component biogenesis	1.52 x10^{-05}	1.99	48	7.5
catabolic process	2.45 x10^{-05}	1.75	64	10.0
sulfur compound metabolic process	2.54 x10^{-05}	4.71	12	1.9
monosaccharide metabolic process	6.01 x10^{-05}	4.66	11	1.7

To further dissect differences in the secretome of normoxia- and chronic hypoxia-challenged cells more in detail, Ingenuity pathway analysis® (IPA®) was performed, identifying canonical pathways affected that may contribute to the modulation of fibroblast phenotypes and the secretome itself. In line with precedent observations (Table 21), IPA® core analysis mostly detected metabolism-related pathways to be affected among the most significant top 20 canonical pathways (Figure 11). In detail, predominantly glucose metabolism-associated pathways such as glycolysis ($-\log_{10}$ p = 8.88, ratio: 0.39), gluconeogenesis ($-\log_{10}$ p = 7.57, ratio: 0.35), pentose phosphate pathways ($-\log_{10}$ p = 5.10, ratio: 0.46) and TCA-cycle ($-\log_{10}$ p = 4.31, ratio: 0.25) were affected. Furthermore, consistent with anterior findings (Table 19), highest significance was found in relation to pathways involved in translational regulation, namely regulation of eIF4 and p70S6K signaling ($-\log_{10}$ p = 22.70, ratio: 0.24), mTOR signaling ($-\log_{10}$ p = 16.10, ratio: 0.17), protein ubiquitination pathway ($-\log_{10}$ p = 12.50, ratio: 0.13) and p70S6K Signaling ($-\log_{10}$ p = 3.92, ratio: 0.10) and ER stress-related canonical pathways EIF2 Signaling ($-\log_{10}$ p = 30.70, ratio: 0.23) and NRF2-mediated oxidative stress response ($-\log_{10}$ p = 4.32, ratio: 0.09). Additionally, apoptosis-associated pathways like phagosome maturation ($-\log_{10}$ p = 8.74, ratio: 0.14), antigen presentation pathway ($-\log_{10}$ p = 4.98, ratio: 0.21), Myc mediated apoptosis signaling ($-\log_{10}$ p = 4.50, ratio: 0.14) and HIPPO signaling ($-\log_{10}$ p = 4.39, ratio: 0.13) were detected by IPA®. Most interestingly in relation to fibrosis, ECM remodeling-affiliated inhibition of matrix metalloproteases ($-\log_{10}$ p = 3.95, ratio: 0.18) and osteoarthritis pathway ($-\log_{10}$ p = 3.82, ratio: 0.08) were determined differentially affected between normoxic and hypoxic cells.

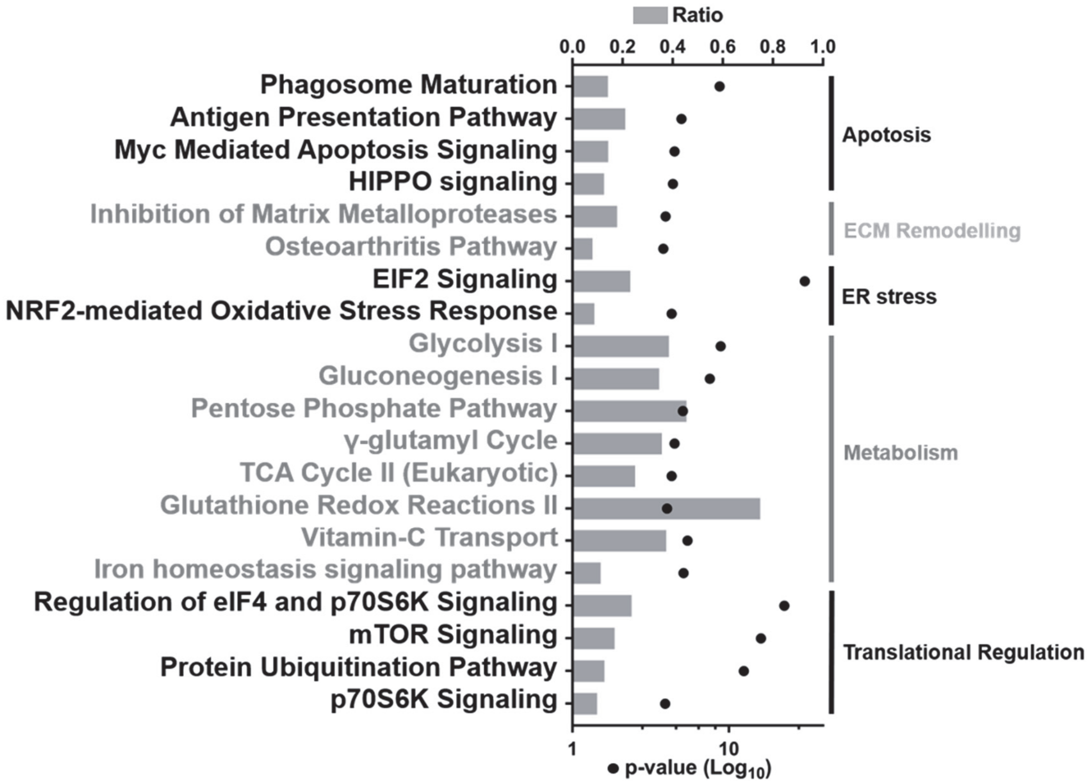

Figure 11: Top 20 canonical pathway annotations of differential secreted proteins in the comparison of normoxia versus chronic hypoxia treated HCF-v.

Affected pathways from secreted proteins were grouped in biological function terms. Grey bars give the ratio of in-data regulated proteins to total pathway associated proteins. Black dots indicate Log_{10} transformed p-value.

Upstream regulator analysis of differentially secreted proteins (Table 22) most robustly identified cell fate- and cell cycle-determining MYC ($p = 2.34 \times 10^{-41}$), MYCN ($p = 3.51 \times 10^{-39}$) and TP53 ($p = 2.72 \times 10^{-14}$). Particularly interesting, also TGFB1 ($p = 2.32 \times 10^{-16}$) associated with pathological fibrosis and FMT was identified as probable mediator between the normoxic and hypoxic fibroblast phenotypic secretome.

Table 22: Top 10 upstream regulators of differential secreted proteins of normoxia versus chronic hypoxia HCF-v.

Upstream Regulator	p-value	n
MYC	2.34×10^{-41}	127
MYCN	3.51×10^{-39}	65
RICTOR	1.03×10^{-32}	57
APP	1.56×10^{-16}	75
TGFB1	2.32×10^{-16}	118
NFE2L2	8.05×10^{-16}	48
TFEB	5.73×10^{-15}	16
MAPT	8.89×10^{-15}	36

PSEN1	1.58×10^{-14}	44
TP53	2.72×10^{-14}	103

p-value: significance for enrichment of category molecules in the data set; n: number of target molecules in data set

3.2 The impact of Rhein on chronic hypoxia-mediated modulation of cardiac fibroblast phenotypic profiles

After showing that chronic hypoxia modulates the secretome, next it was tested whether this associates with phenotypic changes of the fibroblast. In addition, it was investigated whether Rhein, a natural compound already found to act as antifibrotic agent in kidney fibrosis, would alter the phenotype of CFs or at least the secretory profile.

3.2.1 Effect of Rhein on HIF1α signaling and cardiac fibroblast to myofibroblast transition

To determine a working, non-toxic concentration of Rhein, toxicity was assessed performing a 24h Rhein dose-course (1-100 µM) with end-point measurement of HCF-v cell decay (Figure 12A). A concentration up to 100 µM did not increase cell death compared to lysis control. However, due to a slight non-significant increase in toxicity signal observed from 50 µM on, concentrations below 50 µM were used throughout this study. Subsequently, to examine whether Rhein is able to modulate the hypoxic or normoxic HCF-v phenotype, cells where cultivated in 21% or 0.5% O_2 for 4 days in the absence or presence of 35 µM Rhein. Western Blot analysis of HIF1α revealed 9-fold increased protein levels in cells exposed to prolonged hypoxia (H) in comparison to normoxic (N) conditions, wherein Rhein treatment under neither normoxic (NR) nor hypoxic (HR) environment did not further affect HIF1α abundance (Figure 12B). In contrast to that, in the presence of Rhein, cells contained substantially decreased αSMA amounts (Figure 12C) independently of whether exposed to normoxia (20% abundance, $p < 0.001$) or hypoxia (15% abundance, $p < 0.05$).

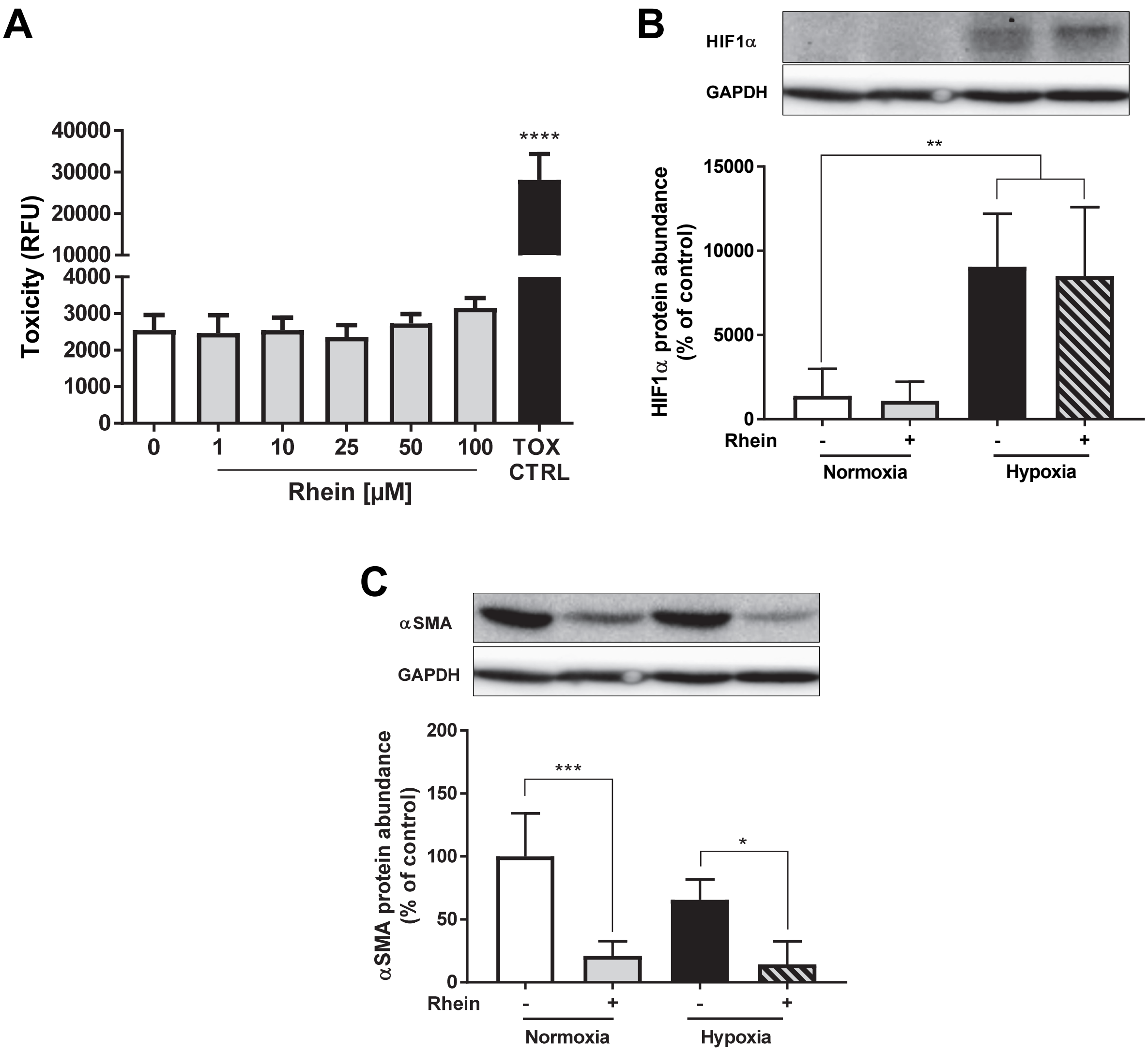

Figure 12: Effect of Rhein αSMA and HIF1α after chronic hypoxia treatment.

(A) HCF-v were treated with different Rhein doses (1-100 µM) for 24h and toxicity was assessed by a fluorescent cell-based assay. Toxicity is given in relative fluorescent units (RFU). HCF-v were cultivated for 4d at 21% O_2 (normoxia) or 4d at 0.5% O_2 (hypoxia) both with or without 35 µM Rhein. Representative Western blots and densitometric analysis of HIF1α (B) and αSMA (C). n = 4, Mean ± SD, One-way ANOVA with Sidak's multiple comparisons test * $p < 0.05$, ** $p < 0.01$, *** $p < 0.001$, **** $p < 0.0001$ as indicated.

3.2.2 Effect of Rhein on the secretome of cardiac fibroblast under normoxic and hypoxic environments

As indicated by previous findings in this study, Rhein treatment effectively reduced the expression of α-SMA, suggesting inhibition of FMT under both hypoxic or normoxic environments, respectively. Consequently, data raised the question whether Rhein was able to modulate both, pathological and physiological secretomes. In order to comprehensively study the impact of Rhein on the modulation of HCF-v secretory phenotypes in the context of normoxia and hypoxia, logical comparison groups (lists) between the four conditions were defined (Figure 13). Based on the initial hypothesis that hypoxia mediates a phenotypic switch and in consequence modulates the fibroblast secretome, the set reference list comprised the comparison between normoxic cells and hypoxic cells (N vs H). The second list was created to address the question whether Rhein treatment of normoxic cells maintain the normoxic phenotype or render a different one (N vs NR). Similarly, the third list was defined in order to determine whether Rhein prevents hypoxia-mediated phenotype modulation or if it mediates another quality of phenotype (H vs HR). Lastly, the list NR vs HR was used to determine whether Rhein-treated cells share the same phenotype independently from normoxic or hypoxic environments. Resulting lists of top 50 up- and downregulated proteins in the respective comparisons of the secretomes are given in the appendix (Table 27-Table 30).

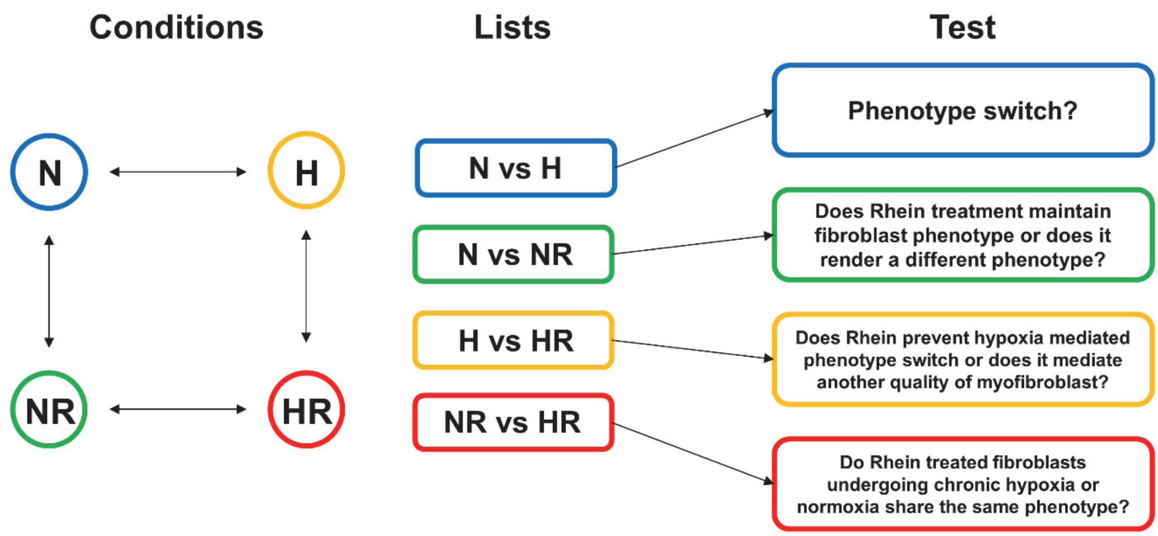

Figure 13: Assignment of comparison groups for differential secretome analysis. Differential protein lists were generated by comparing the 4 conditions (N: Normoxia, H: Hypoxia, NR: Normoxia+Rhein, HR: Hypoxia+Rhein) according to biologically reasonable hypotheses.

Based on the created comparison lists and the proteins observed within each single donor in each condition, it was aimed to evaluate the comparability between normoxic, hypoxic and respective Rhein treated HCF-v secretomes. Providing information about classification and interrelation of present phenotypes, a *partial least square-discriminant* (PLS-D) analysis was performed using the lists generated from LC-MS runs in DDA mode analyzed with Proteome Discoverer^{TM} 2.2 software (2.2.3.7). This approach depicted 4 distinct populations within our dataset and clearly distinguished between the experimental conditions (Figure 14). The influence of the two main components of variation in the data separate the secretome of hypoxia treated cells (red) from the normoxia group (blue). Rhein treatment during hypoxia (green) converged the variation in the secretomes towards the variation in the normoxic phenotype. Of further notice, the variation in the normoxic cells (turquois) secretome is also influenced by Rhein treatment and apparently shifted the secretome in the same direction. However, this group resembles the highest variation in comparison.

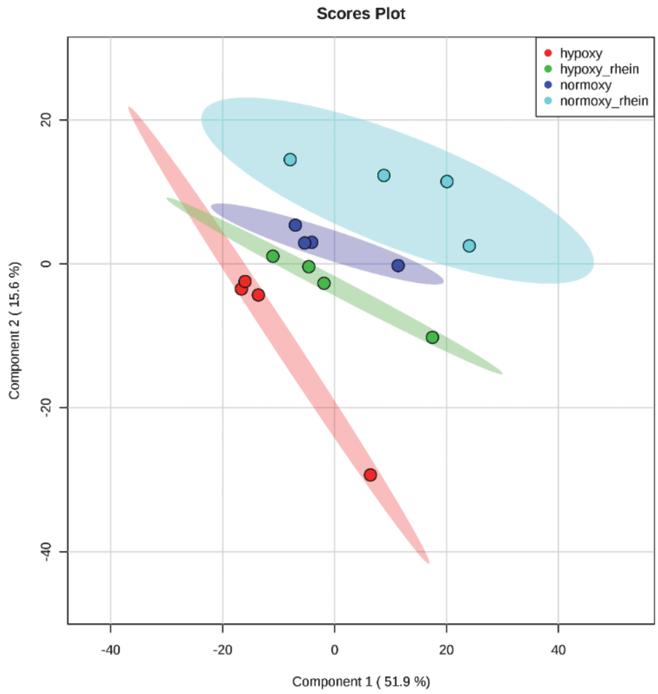

Figure 14: PLS-D analysis of experimental HCF-v secretomes.

Graph generated from secretome intensity signals in Metaboanalyst 4.0 (http\\www.metaboanalyst.ca). Data restriction: signal must be present in all 4 samples of one condition or in three samples of at least two conditions of one comparison. Colored dots indicate single donors of each experimental condition (red: hypoxia, green: hypoxia + Rhein, blue: normoxia, turquois: normoxia + Rhein) and corresponding colored shade depicts the coefficient of variance (%CV), respectively.

To identify which proteins determine the diverse phenotypes, Venn analyses were performed (Figure 15). In total, 638 proteins were differentially regulated (>1.5 fold, p-value < 0.05) within N vs H of which 95 proteins were unique in this comparison, whereas 46 out of 619 were found in the comparison of NR vs HR. Further, 170 proteins out of 1010 in total were solely observed in N vs NR and 74 out of 590 in H vs HR, respectively. Overall, 126 differentially abundant proteins were identified to overlap in all 4 lists.

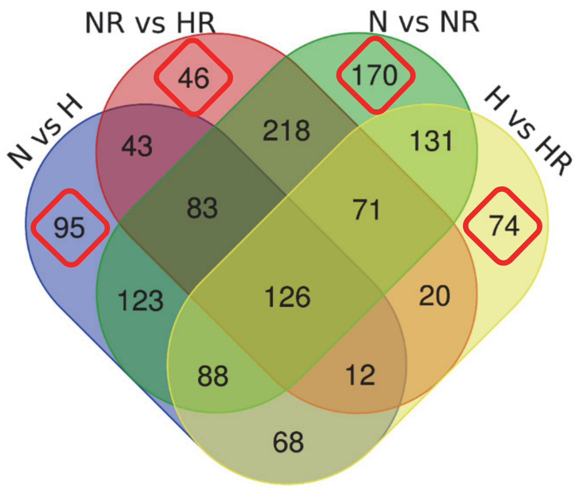

List	number of elements
N vs H	638
N vs NR	1010
H vs HR	590
NR vs HR	619

Figure 15: Venn analysis of differential secreted proteins.
Proteins with differential abundance in the comparison of normoxic versus hypoxic HCF-v treated with or without Rhein (>1.5-fold, one-way ANOVA posthoc p-value < 0.05) were analyzed for overlap to determine group specific or independent alterations. Table below provides information on total number of elements found in respective list. N: Normoxia, H: Hypoxia, NR: Normoxia + Rhein, HR: Hypoxia + Rhein; N vs H (blue; n = 638), N vs NR (green; n = 1010), H vs HR (yellow; n = 590), NR vs HR (red; n = 619).

Using the protein lists harboring uniquely found proteins specific for respective comparison group, IPA® was performed. In the group N vs H, IPA® revealed translational regulation associated pathways (Table 23) like tRNA charging (6.31×10^{-04}), regulation of eIF4 and p70S6K Signaling (6.92×10^{-04}) and mTOR Signaling (2.00×10^{-03}) and metabolic pathways involving matrix proteoglycans such as Heparan Sulfate Biosynthesis (5.50×10^{-03} and 4.27×10^{-03} respectively) and Dermatan Sulfate Biosynthesis (1.66×10^{-02}) to be most significantly affected. Most interestingly, analogies in the top 10 affected pathways between the comparison groups N vs NR and H vs HR were identified. Although, the inserted lists were comprised of different proteins uniquely found in respective group, IPA® computed out the same fibrosis-related pathways for both N vs NR and H vs HR namely Hepatic Fibrosis/ Hepatic Stellate Cell Activation (1.17 $x10^{-04}$ and 4.27 $x10^{-04}$), Remodeling of Epithelial Adherens Junctions (1.70 $x10^{-05}$ and 1.66 $x10^{-03}$), Epithelial Adherens Junction Signaling (2.51 $x10^{-05}$ and 1.66 $x10^{-03}$). Whereas, further ECM remodeling-associated pathways were enlisted in N vs NR like Actin Cytoskeleton Signaling (1.62 $x10^{-05}$), Regulation of Cellular Mechanics by Calpain Protease (1.38 $x10^{-04}$), Inhibition of Matrix Metalloproteases (2.45 $x10^{-04}$) and Axonal Guidance Signaling (2.75 $x10^{-04}$), in the group H vs HR the other affected pathways involved metabolism-related L-cysteine Degradation II (3.39 $x10^{-03}$), Antioxidant Action of Vitamin C (5.89 $x10^{-03}$), Taurine Biosynthesis, Palmitate Biosynthesis I and Fatty Acid Biosynthesis Initiation II (all 6.76 $x10^{-03}$). Differential proteins solely found in the comparison between Rhein treated cells subjected either to normoxia or hypoxia (NR vs HR) mainly suggested metabolic pathways to be most significantly affected such as S-adenosyl-L-methionine Biosynthesis (6.17 $x10^{-03}$), N-acetylglucosamine Degradation I (6.17 $x10^{-03}$), NAD Biosynthesis from 2-amino-3-carboxymuconate semialdehyde (1.45 $x10^{-02}$) and Ketolysis (2.04 $x10^{-02}$).

Table 23: Pathway analysis of comparison group-specific differential proteins

N vs H		
Pathway	**p-value**	**Ratio**
tRNA Charging	6.31 $x10^{-04}$	0.08
Regulation of eIF4 and p70S6K Signaling	6.92 $x10^{-04}$	0.03
Pentose Phosphate Pathway	9.77 $x10^{-04}$	0.18
mTOR Signaling	2.00 $x10^{-03}$	0.02
EIF2 Signaling	2.95 $x10^{-03}$	0.02
Heparan Sulfate Biosynthesis (Late Stages)	4.27 $x10^{-03}$	0.04
Heparan Sulfate Biosynthesis	5.50 $x10^{-03}$	0.04
Spermidine Biosynthesis I	8.51 $x10^{-03}$	0.50
Coagulation System	1.00 $x10^{-02}$	0.06
Dermatan Sulfate Biosynthesis (Late Stages)	1.66 $x10^{-02}$	0.04
N vs NR		
Pathway	**p-value**	**Ratio**
Protein Ubiquitination Pathway	1.86 $x10^{-07}$	0.05
Actin Cytoskeleton Signaling	1.62 $x10^{-05}$	0.04
Remodeling of Epithelial Adherens Junctions	1.70 $x10^{-05}$	0.09
Epithelial Adherens Junction Signaling	2.51 $x10^{-05}$	0.05
Unfolded protein response	7.76 $x10^{-05}$	0.09
GP6 Signaling Pathway	9.33 $x10^{-05}$	0.05
Hepatic Fibrosis / Hepatic Stellate Cell Activation	1.17 $x10^{-04}$	0.04
Regulation of Cellular Mechanics by Calpain Protease	1.38 $x10^{-04}$	0.08
Inhibition of Matrix Metalloproteases	2.45 $x10^{-04}$	0.10
Axonal Guidance Signaling	2.75 $x10^{-04}$	0.03
H vs HR		
Pathway	**p-value**	**Ratio**

Acute Phase Response Signaling	3.24 x10^{-04}	0.03
Hepatic Fibrosis / Hepatic Stellate Cell Activation	4.27 x10^{-04}	0.03
LXR/RXR Activation	7.59 x10^{-04}	0.03
Remodeling of Epithelial Adherens Junctions	1.66 x10^{-03}	0.04
Epithelial Adherens Junction Signaling	1.66 x10^{-03}	0.03
L-cysteine Degradation II	3.39 x10^{-03}	1.00
Antioxidant Action of Vitamin C	5.89 x10^{-03}	0.03
Taurine Biosynthesis	6.76 x10^{-03}	0.50
Palmitate Biosynthesis I (Animals)	6.76 x10^{-03}	0.50
Fatty Acid Biosynthesis Initiation II	6.76 x10^{-03}	0.50
	NR vs HR	
Pathway	**p-value**	**Ratio**
S-adenosyl-L-methionine Biosynthesis	6.17 x10^{-03}	0.33
N-acetylglucosamine Degradation I	6.17 x10^{-03}	0.33
N-acetylglucosamine Degradation II	8.32 x10^{-03}	0.25
NAD Biosynthesis from 2-amino-3-carboxymuconate semialdehyde	1.45 x10^{-02}	0.14
Death Receptor Signaling	1.58 x10^{-02}	0.02
Protein Ubiquitination Pathway	1.78 x10^{-02}	0.01
Ketogenesis	2.04 x10^{-02}	0.10
Ketolysis	2.04 x10^{-02}	0.10
Mevalonate Pathway I	2.69 x10^{-02}	0.08
Isoleucine Degradation I	2.88 x10^{-02}	0.07

p-value: significance for enrichment of category molecules in the data set; Ratio: coverage of in-data regulated proteins to total pathway associated proteins

The upstream regulator analysis module of IPA®, with input of the individually observed differential proteins in the secretome comparison of respective groups, was used to identify putative regulated upstream targets. Analysis revealed several upstream regulators of decent confidence in all groups (Table 24). However, regulators yielded relatively low numbers of overlapping target molecules (n) in the data-set, which was to be expected due to the low number of elements in the comparison specific lists. In the comparison between N vs H, NPPC (1.76 x10^{-05}), a cardiac natriuretic peptide associated with chronic heart failure was predicted as top upstream regulator candidate, along with GTPase activity-regulating HRAS (1.26 x10^{-03}) and TSC2 (2.12 x10^{-04}) as well as EGFR signaling-related ERBB3 (6.18 x10^{-04}) and ERBB4 (5.91 x10^{-04}). Among the most probable upstream regulators predicted in N vs NR, HTT (1.68 x10^{-09}) a protein highly associated with Huntington’s disease, ECM modulator MMP12 (7.84 x10^{-07}) and cell cycle and cell fate-determining TP53 (2.47 x10^{-07}), MYC (5.97 x10^{-06}) and MYCN (2.64 x10^{-06}) were found. Likewise, IPA® predicted MYC (1.93 x10^{-05}) and TP53 (7.84 x10^{-05}) as top upstream regulator candidates for the group H vs HR. Putatively affected upstream regulators discriminating the NR vs HR secretomes included POLR3G (2.89 x10^{-04}) as top candidate and mainly ER stress and unfolded protein response-involved targets such as ICMT (2.11 x10^{-03}), MKNK1 (1.30 x10^{-03}), NFE2L2 (1.89 x10^{-03}) and ERN1 (2.29 x10^{-03}). Most interestingly, TGFB1 was predicted among the top 3 upstream regulators for all comparison groups except for H vs HR (top 35, 6.87 x10^{-03}, data not shown) with high significance (N vs H: 2.30 x10^{-04}, N vs NR: 1.04 x10^{-08} and NR vs HR: 1.01 x10^{-03}) and highest overlapping number of target molecules in data set in respective analysis (N vs H: n = 19, N vs NR: n = 38 and NR vs HR: n = 11).

Table 24: Upstream regulator analysis of comparison group-specific differential proteins

	N vs H	
Upstream Regulator	**p-value**	**n**
NPPC	1.76 x10^{-05}	3
TSC2	2.12 x10^{-04}	5
TGFB1	2.30 x10^{-04}	19
UCP1	3.50 x10^{-04}	5
ERBB4	5.91 x10^{-04}	4
ERBB3	6.18 x10^{-04}	4
KDR	8.36 x10^{-04}	3
FOXF1	1.23 x10^{-03}	2
HRAS	1.26 x10^{-03}	9
TGFBR2	1.49 x10^{-03}	5
	N vs NR	
Upstream Regulator	**p-value**	**n**
HTT	1.68 x10^{-09}	24
TGFB1	1.04 x10^{-08}	38
TP53	2.47 x10^{-07}	33
CD 437	7.13 x10^{-07}	11
MMP12	7.84 x10^{-07}	7
COLQ	1.18 x10^{-06}	7
MYCN	2.64 x10^{-06}	12
MYC	5.97 x10^{-06}	24
CD3	4.65 x10^{-05}	16
NFE2L2	1.23 x10^{-04}	12
	H vs HR	
Upstream Regulator	**p-value**	**n**
MYC	1.93 x10^{-05}	14
TP53	7.84 x10^{-05}	16
PKD1	3.95 x10^{-04}	5
FOS	5.52 x10^{-04}	8
EPAS1	6.80 x10^{-04}	5
COL6A1	1.03 x10^{-03}	2
STAT4	1.03 x10^{-03}	5
SYVN1	1.23 x10^{-03}	4
Srebp	1.35 x10^{-03}	2

CBS/CBSL	1.35 x10^{-03}	2
	NR vs HR	
Upstream Regulator	**p-value**	**n**
POLR3G	2.89 x10^{-04}	2
TGFB1	1.01 x10^{-03}	11
MKNK1	1.30 x10^{-03}	3
NFE2L2	1.89 x10^{-03}	5
ICMT	2.11 x10^{-03}	2
Lamin b	2.13 x10^{-03}	1
KPNB1	2.13 x10^{-03}	1
SLC25A5	2.13 x10^{-03}	1
MECP2	2.13 x10^{-03}	3
ERN1	2.29 x10^{-03}	3

p-value: significance for enrichment of category molecules in the data set; n: number of target molecules in data set

The next goal was to evaluate which pathways play a global role in the context of chronic hypoxia and intervention via Rhein administration. Therefore, pathway analyses using complete lists containing all differentially abundant proteins within each comparison group were performed and commonly annotated pathways were explored (Figure 16). Noteworthy, all top 30 cumulative pathways were identified in all 4 comparison groups. In conformity with previous findings regarding observations in individual protein lists (Table 25), among the top 30 commonly enlisted canonical pathways, ER stress-associated EIF2 signaling ($-\log_{10}$ p = ∑108.8) and translational regulation-related pathways such as, Regulation of eIF4 and p70S6K Signaling ($-\log_{10}$ p = ∑71.1), mTOR signaling ($-\log_{10}$ p = ∑52.5) and Protein Ubiquitination Pathway ($-\log_{10}$ p = ∑46.8) showed highest cumulative significance. Further, enrichment in ECM modulation and fibrosis-involved pathway annotations like Hepatic Fibrosis/ Hepatic Stellate Cell Activation ($-\log_{10}$ p = ∑33.7), Remodeling of Epithelial Adherens Junctions ($-\log_{10}$ p = ∑23.2), Epithelial Adherens Junction Signaling ($-\log_{10}$ p = ∑20.5), Axonal Guidance Signaling ($-\log_{10}$ p = ∑19.5), Osteoarthritis Pathway ($-\log_{10}$ p = ∑16.9) and Inhibition of Matrix Metalloproteases ($-\log_{10}$ p = ∑14.7) was identified. In addition, hypoxic metabolism-associated pathways such as Glycolysis I ($-\log_{10}$ p = ∑30.9), Gluconeogenesis I ($-\log_{10}$ p = ∑30.3) and TCA Cycle II ($-\log_{10}$ p = ∑18.5) were represented among the most significant predicted pathways. Also, a cluster of apoptosis-associated pathways comprised of Phagosome Maturation ($-\log_{10}$ p = ∑25.1), Myc Mediated Apoptosis Signaling ($-\log_{10}$ p = ∑15.6) and Antigen Presentation pathway ($-\log_{10}$ p = ∑14.4) was listed among the most probable pathways.

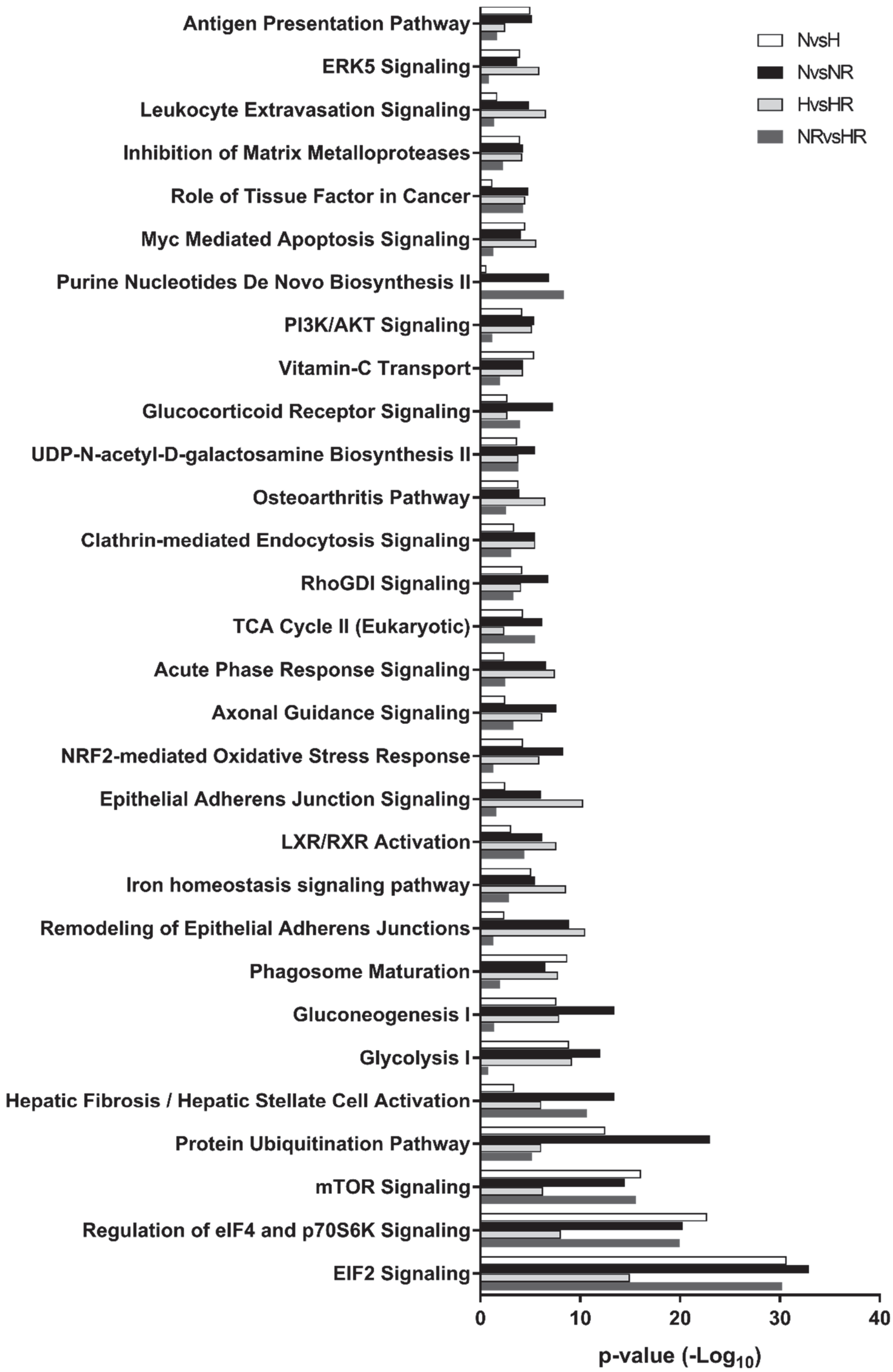

Figure 16: Top 30 canonical pathway annotations of differential secreted proteins.
Comparison of commonly annotated pathways between normoxic and hypoxic HCF-v treated with or without Rhein, sorted by ascending cumulative p-value ($-\log_{10}$) > 1.3 ≙ p = 0.05. N vs H: Normoxia vs Hypoxia, N vs NR: Normoxia vs Normoxia+Rhein, H vs HR: Hypoxia vs Hypoxia+Rhein, NR vs HR: Normoxia+Rhein vs Hypoxia+Rhein.

Analogously to the general pathway analysis described above, upstream regulator analyses using the complete lists of differential abundant proteins were performed and common hits were summarized in Figure 17. In line with previous findings (Figure 14), cell fate- and cell cycle-determining MYC ($-\log_{10}$ p = ∑175.8), MYCN ($-\log_{10}$ p = ∑135.1) and TP53 ($-\log_{10}$ p = ∑114.7) constituted the most significant upstream regulators in the context of chronic hypoxia and intervention via Rhein administration. Again, TGFB1 ($-\log_{10}$ p = ∑101.7) was robustly predicted to be involved in the shaping of the condition-dependent secretome. Moreover, RICTOR ($-\log_{10}$ p = ∑96.4) as mTOR signaling-involved regulator and ER stress-associated NFE2L2 ($-\log_{10}$ p = ∑77.1) were listed in the common top 10 upstream regulators.

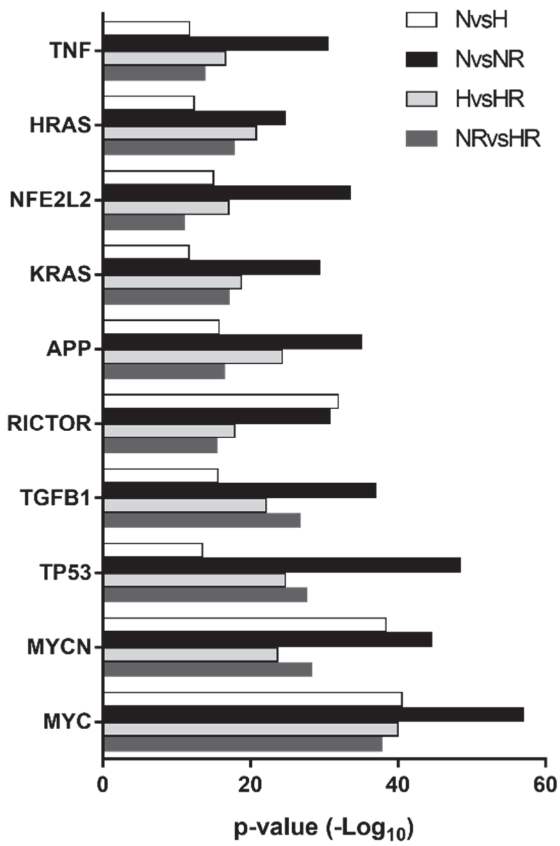

Figure 17: Upstream regulator analysis of differential secretomes.

Commonly predicted upstream regulators in the comparison of normoxic versus hypoxic HCF-v treated with or without Rhein. List of upstream regulators sorted by ascending cumulative p-value ($-\log_{10}$) > 1.3 ≙ p = 0.05. N vs H: Normoxia vs Hypoxia, N vs NR: Normoxia vs Normoxia+Rhein, H vs HR: Hypoxia vs Hypoxia+Rhein, NR vs HR: Normoxia+Rhein vs Hypoxia+Rhein.

3.2.3 Influence of Rhein administration on transcriptomic profiles in cardiac fibroblasts under normoxic and hypoxic conditions

To further dissect how chronic hypoxia and Rhein treatment are able to modulate the secretome of CFs, the potential role of the transcriptome as direct modifier of secretory profiles was studied. Therefore, RNA, isolated from the same HCF-v of which the secretome was collected from and investigated before (3.2.2), was subjected to Affymetrix microarray technology and the expression of known pro-fibrotic markers and HIF1α target genes as a control for hypoxic treatment was evaluated using the microarray data (2.2.2.5).

As shown in the upper part of Figure 18, the Rhein-mediated decrease of αSMA under normoxia was accompanied by an overall reduction in the expression of profibrotic response targets (*ACTA2*, *CTGF*, *COL1A1*, *COL3A1*, *OGN*, *ITGA8*, *TIMP3*; $\Delta\log_2$: -1.66 to -3.42). Differently, *MMP1* expression was increased resulting in a higher MMP:TIMP ratio (data not shown). In the comparison between NR and HR both treated with Rhein, gene levels showed the same negative regulatory direction but did not score the same intensity. However, addition of Rhein during prolonged hypoxia resulted in strongly opposing regulatory effects when set against hypoxia treated cells. Surprisingly, although HIF1α protein abundance was unaffected by Rhein, gene expression of HIF1α targets during prolonged hypoxia seemed to be potentiated by Rhein (Figure 12D, lower part). Interestingly, hypoxia responsive genes *SLC2A1* and *VEGFA* were upregulated in Rhein treated samples, which did not experience hypoxia. Furthermore, in NR and HR treated CFs *HMOX1* expression was inversely regulated compared to hypoxia only cells.

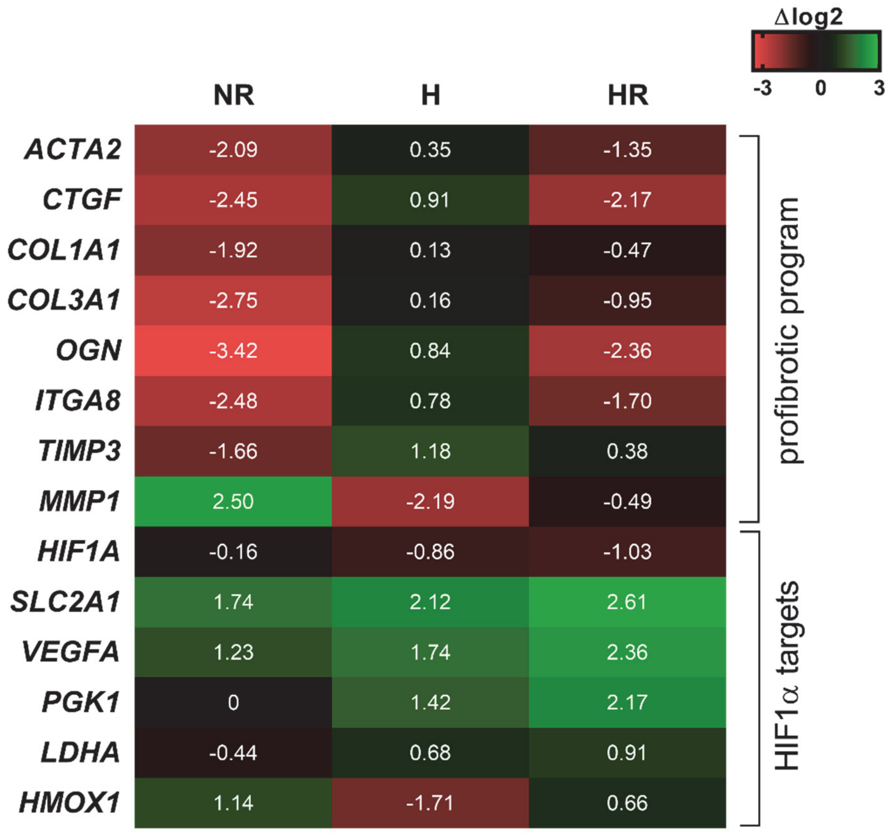

Figure 18: Influence of chronic hypoxia and Rhein treatment on fibrotic program and HIF1α target expression

Heatmap of differentially regulated fibrogenic and HIF1a targets determined by Affymetrix microarray (**D**). Given values are interpreted as $\Delta log_2 = Log_2(x)-Log_2(Normoxia)$ with x=NR (Normoxia+Rhein), H (Hypoxia), HR: Hypoxia+Rhein; $\Delta log_2 \geq 0.58 \triangleq 1.5$-fold (linear); n = 4

Differential transcripts were analyzed using IPA software according to the afore-mentioned comparison strategy (3.2.2, Figure 13), using the same defined assignments in analogy to the secretome analysis. Resulting lists of top 50 up- and downregulated transcripts in the respective comparisons of the transcriptomes are given in the appendix (Table 31-Table 34).

Venn analysis identified 136 out of 325 differentially regulated transcripts (>1.5-fold, p-value < 0.05) solely identified in H vs N, while the comparison HR vs NR harbored 719 out of 2175 transcripts uniquely found (Figure 19). In comparison to that, 1210 out of 2916 mRNAs and 247 out of 803 transcripts were exceptionally observed within the group of N vs NR and H vs HR, respectively.

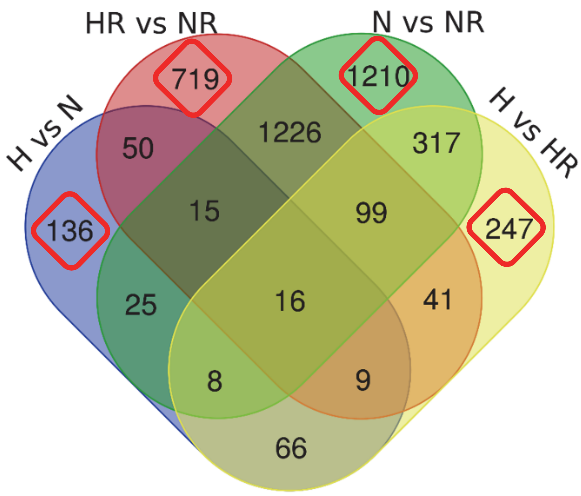

List	number of elements
H vs HR	803
H vs N	325
HR vs NR	2175
N vs NR	2916

Figure 19: Venn analysis of differential transcripts.
Differentially expressed transcripts in the comparison of normoxic versus hypoxic HCF-v treated with or without Rhein (>1.5-fold, one-way ANOVA posthoc p-value < 0.05) were analyzed for overlap to determine group specific or independent alterations. Table below gives information on total number of elements found in respective list. N: Normoxia, H: Hypoxia, NR: Normoxia+Rhein, HR: Hypoxia+Rhein; H vs N (blue; n = 325), N vs NR (green; n = 2916), H vs HR (yellow; n = 803), HR vs NR (red; n = 2175).

Next, the specific lists harboring the transcripts uniquely observed to be differentially abundant in respective comparison group were subjected to IPA® core analysis (Table 25). Pathway analysis revealed regulation of eIF4 and p70S6K Signaling (1.66 x10^{-05}), EIF2 Signaling (1.66 x10^{-05}) and mTOR Signaling (1.66 x10^{-05}) to be affected in the comparison between H vs N, which corresponded to pathways identified the differential secretome (Table 23). Interestingly, enrichment was found in Mitochondrial Dysfunction (2.09 x10^{-04}) in association to chronic hypoxia treatment (H vs N), however annotation of mitochondrial stress-relieving ketone body metabolism-involved Ketogenesis and Ketolysis (both 1.07 x10^{-03}) was also observed. In regard to specifically affected N vs NR transcripts, enrichment of elements involved in heart failure-associated pathways such as Relaxin Signaling (3.98 x10^{-05}), Endothelin-1 Signaling (1.26 x10^{-04}), Cardiac Hypertrophy Signaling (4.47 x10^{-04}) and Corticotropin Releasing Hormone Signaling (5.62 x10^{-04}). On the other hand, H vs HR included enriched pathways related to metabolism such as Alanine Biosythesis III (9.77 x10^{-03}), Iron homeostasis signaling pathway (1.10 x10^{-02}) and D-myo-inositol-5-phosphate Metabolism (2.09 x10^{-02}), besides fibrosis-related mechanisms like Regulation of Cellular Mechanics by Calpain Protease (2.34 x10^{-02}) and Osteoarthritis Pathway (1.74 x10^{-02}). Specific discrepancies between HR vs NR, mirroring the influence of chronic hypoxia affected pathways such as tRNA Charging (7.94 $x10^{-11}$), Protein Ubiquitination Pathway and Cholesterol Biosynthesis I-III (all 5.01 $x10^{-04}$). Of further notice, senescence-associated Sirtuin Signaling Pathway (2.82 $x10^{-04}$) and Telomere Extension by Telomerase (9.12 $x10^{-04}$) seemed to play a role in the discrimination of both conditions.

Table 25: Top 10 pathway analysis of comparison group-specific differential transcripts

H vs N		
Ingenuity Canonical Pathways	**p-value**	**Ratio**
Regulation of eIF4 and p70S6K Signaling	1.66 $x10^{-05}$	0.04
EIF2 Signaling	1.74 $x10^{-05}$	0.04
Mitochondrial Dysfunction	2.09 $x10^{-04}$	0.04
mTOR Signaling	5.75 $x10^{-04}$	0.03
Ketogenesis	1.07 $x10^{-03}$	0.20
Ketolysis	1.07 $x10^{-03}$	0.20
Mevalonate Pathway I	1.82 $x10^{-03}$	0.15
Isoleucine Degradation I	2.14 $x10^{-03}$	0.14
Glutaryl-CoA Degradation	2.75 $x10^{-03}$	0.13
Superpathway of Geranylgeranyldiphosphate Biosynthesis I	3.16 $x10^{-03}$	0.12
N vs NR		
Ingenuity Canonical Pathways	**p-value**	**Ratio**
Relaxin Signaling	3.98 $x10^{-05}$	0.13
Endothelin-1 Signaling	1.26 $x10^{-04}$	0.12
Breast Cancer Regulation by Stathmin1	3.72 $x10^{-04}$	0.11
Cardiac Hypertrophy Signaling	4.47 $x10^{-04}$	0.10
Gap Junction Signaling	4.68 $x10^{-04}$	0.11
Sphingosine-1-phosphate Signaling	4.90 $x10^{-04}$	0.13
Corticotropin Releasing Hormone Signaling	5.62 $x10^{-04}$	0.12
Molecular Mechanisms of Cancer	7.24 $x10^{-04}$	0.09
CXCR4 Signaling	9.12 $x10^{-04}$	0.11
Lysine Degradation II	1.15 $x10^{-03}$	0.60
H vs HR		
Ingenuity Canonical Pathways	**p-value**	**Ratio**
Alanine Biosynthesis III	9.77 $x10^{-03}$	1.00
Iron homeostasis signaling pathway	1.10 $x10^{-02}$	0.04
Agranulocyte Adhesion and Diapedesis	1.15 $x10^{-02}$	0.03
Aryl Hydrocarbon Receptor Signaling	1.23 $x10^{-02}$	0.04
GADD45 Signaling	1.45 $x10^{-02}$	0.11
Hereditary Breast Cancer Signaling	1.55 $x10^{-02}$	0.03
Osteoarthritis Pathway	1.74 $x10^{-02}$	0.03

D-myo-inositol-5-phosphate Metabolism	2.09 x10^{-02}	0.03
Regulation of Cellular Mechanics by Calpain Protease	2.34 x10^{-02}	0.05
Antiproliferative Role of TOB in T Cell Signaling	2.63 x10^{-02}	0.08
HR vs NR		
Ingenuity Canonical Pathways	p-value	Ratio
tRNA Charging	7.94 x10^{-11}	0.33
Protein Ubiquitination Pathway	2.45 x10^{-05}	0.08
Tetrahydrofolate Salvage from 5,10-methenyltetrahydrofolate	2.75 x10^{-04}	0.60
Sirtuin Signaling Pathway	2.82 x10^{-04}	0.07
Cholesterol Biosynthesis I	5.01 x10^{-04}	0.31
Cholesterol Biosynthesis II (via 24,25-dihydrolanosterol)	5.01 x10^{-04}	0.31
Cholesterol Biosynthesis III (via Desmosterol)	5.01 x10^{-04}	0.31
Zymosterol Biosynthesis	5.37 x10^{-04}	0.50
Telomere Extension by Telomerase	9.12 x10^{-04}	0.27
Dolichol and Dolichyl Phosphate Biosynthesis	9.33 x10^{-04}	1.00

p-value: significance for enrichment of category molecules in the data set; Ratio: coverage of in-data regulated proteins to total pathway associated proteins

Confirmative of pathways identified in the comparison group H vs N (Table 25), upstream regulators RICTOR (2.49 x10-04), NFE2L2 (3.50 x10-03) and MTOR (3.94 x10-03) were significantly predicted matching the observed enrichment of translation regulation-related respective pathways (Table 26). Furthermore, cell cycle regulators E2f (2.93 x10-04), TP53 (2.85 x10-03) and CIP2A (3.07 x10-03) were listed among the top 10 upstream regulators specific for H vs N. Upstream regulator analysis of differential transcripts unique for N vs NR presented ESR1 (3.92 x10-08) as most significant putative target. However most interestingly, TP53 (2.64 x10-04) and TGFB1 (3.49 x10-04), already significantly predicted in the group-specific (Table 24) as well as in the global secretome analysis (Figure 17) of N vs NR, were confidently identified to be responsible for transcriptome modulation. Similar findings were made in the comparison group H vs HR, where TGFB1 (1.21 x10-05) was also annotated. Although in this case cell cycle-determining TP53 did not hit the top 10 upstream regulators, CDKN1A (1.20 x10-05), which plays an inhibitory role in the network of TP53, alongside E2F8 (2.93 x10-06) as most significant target and E2F7 (1.55 x10-05) was enlisted. Lastly, in HR vs NR uniquely differential transcripts IPA considered CST5 (2.58 x10-09), EIF2AK3 (3.79 x10-09) and ATF4 (6.63 x10-08) as most significant upstream regulators.

Table 26: Top 10 upstream regulator analysis of comparison group-specific differential transcripts

	H vs N	
Upstream Regulator	**p-value**	**n**
RICTOR	2.49×10^{-04}	7
E2f	2.93×10^{-04}	5
INSR	5.36×10^{-04}	8
PLIN1	2.19×10^{-03}	2
TP53	2.85×10^{-03}	16
CIP2A	3.07×10^{-03}	3
NFE2L2	3.50×10^{-03}	7
EMD	3.52×10^{-03}	2
MTOR	3.94×10^{-03}	6
FOXO1	4.19×10^{-03}	7
	N vs NR	
Upstream Regulator	**p-value**	**n**
ESR1	3.92×10^{-08}	111
NEUROG1	3.38×10^{-06}	14
TP53	2.64×10^{-04}	111
TGFB1	3.49×10^{-04}	121
KLF3	4.07×10^{-04}	32
NR4A1	6.62×10^{-04}	20
PKD1	8.18×10^{-04}	20
HNF4A	1.03×10^{-03}	137
NUPR1	1.07×10^{-03}	42
IFITM1	1.19×10^{-03}	5
	H vs HR	
Upstream Regulator	**p-value**	**n**
E2F8	2.93×10^{-06}	4
FOXO3	3.65×10^{-06}	14
IKBKB	5.15×10^{-06}	13
ESR1	5.89×10^{-06}	31
CDKN1A	1.20×10^{-05}	11
TGFB1	1.21×10^{-05}	37
Vegf	1.32×10^{-05}	17
E2F7	1.55×10^{-05}	4
YY1	2.29×10^{-05}	12
RABL6	4.48×10^{-05}	6
	HR vs NR	
Upstream Regulator	**p-value**	**n**

CST5	2.58 x10^{-09}	30
EIF2AK3	3.79 x10^{-09}	18
ATF4	6.63 x10^{-08}	20
MYC	8.34 x10^{-07}	64
HNF4A	1.55 x10^{-06}	103
UCP1	5.09 x10^{-06}	16
SCAP	7.59 x10^{-06}	12
TRIB3	1.00 x10^{-05}	7
CLOCK	1.50 x10^{-05}	16
NRIP1	1.56 x10^{-05}	10

p-value: significance for enrichment of category molecules in the data set; Ratio: coverage of in-data regulated proteins to total pathway associated proteins

Analogous to previous analyses conducted regarding differential secretomes (3.2.2), IPA was also applied to explore globally and commonly affected pathways using the respective complete lists of differential transcripts within each assigned comparison (Figure 20). The pathway scoring the highest cumulative significance according to IPA was Glycolysis I ($-\log_{10}$ p = ∑19.4), although mostly H vs N ($-\log_{10}$ p = 12.1) and HR vs NR ($-\log_{10}$ p = 4.0) accounted for the high p-value. Similarly, regarding Gluconeogenesis I (11.8) most of the accumulated p-value fell upon H vs N ($-\log_{10}$ p = 7.2) and HR vs NR ($-\log_{10}$ p = 2.4). Most interestingly, Cell Cycle: G2/M DNA Damage Checkpoint Regulation ($-\log_{10}$ p = ∑15.4) associating to previously identified TP53 and CDK1NA (Table 26) was annotated and seemed to play a particular role in Rhein intervention of hypoxic cells (H vs HR, $-\log_{10}$ p = 9.4). Further cell cycle-related pathways contributing to the top 30 by IPA were p53 Signaling ($-\log_{10}$ p = ∑10.1), Mitotic Roles of Polo-Like Kinase ($-\log_{10}$ p = ∑7.5) and Role of CHK Proteins in Cell Cycle Checkpoint Control ($-\log_{10}$ p = ∑6.1). Of further notice, in the groups N vs NR and H vs HR most strikingly the pathways, small molecule-responsive Aryl Hydrocarbon Receptor Signaling ($-\log_{10}$ p = 3.7 and $-\log_{10}$ p = 3.1), cell cycle-determining ATM Signaling ($-\log_{10}$ p = 3.0 and $-\log_{10}$ p = 4.0), cancer-related Pancreatic Adenocarcinoma Signaling ($-\log_{10}$ p = 3.6 and $-\log_{10}$ p = 3.1) and Molecular Mechanisms of Cancer ($-\log_{10}$ p = 4.4 and $-\log_{10}$ p = 2.9) were found. Particularly interesting, also fibrosis-associated pathways like Hepatic Fibrosis/ Hepatic Stellate Cell Activation ($-\log_{10}$ p = 4.8 and $-\log_{10}$ p = 4.0), Osteoarthritis Pathway ($-\log_{10}$ p = 3.1 and $-\log_{10}$ p = 2.6) and Actin Cytoskeleton Signaling ($-\log_{10}$ p = 3.1 and $-\log_{10}$ p = 3.0) were revealed to participate in the Rhein-mediated modulation of the transcriptome.

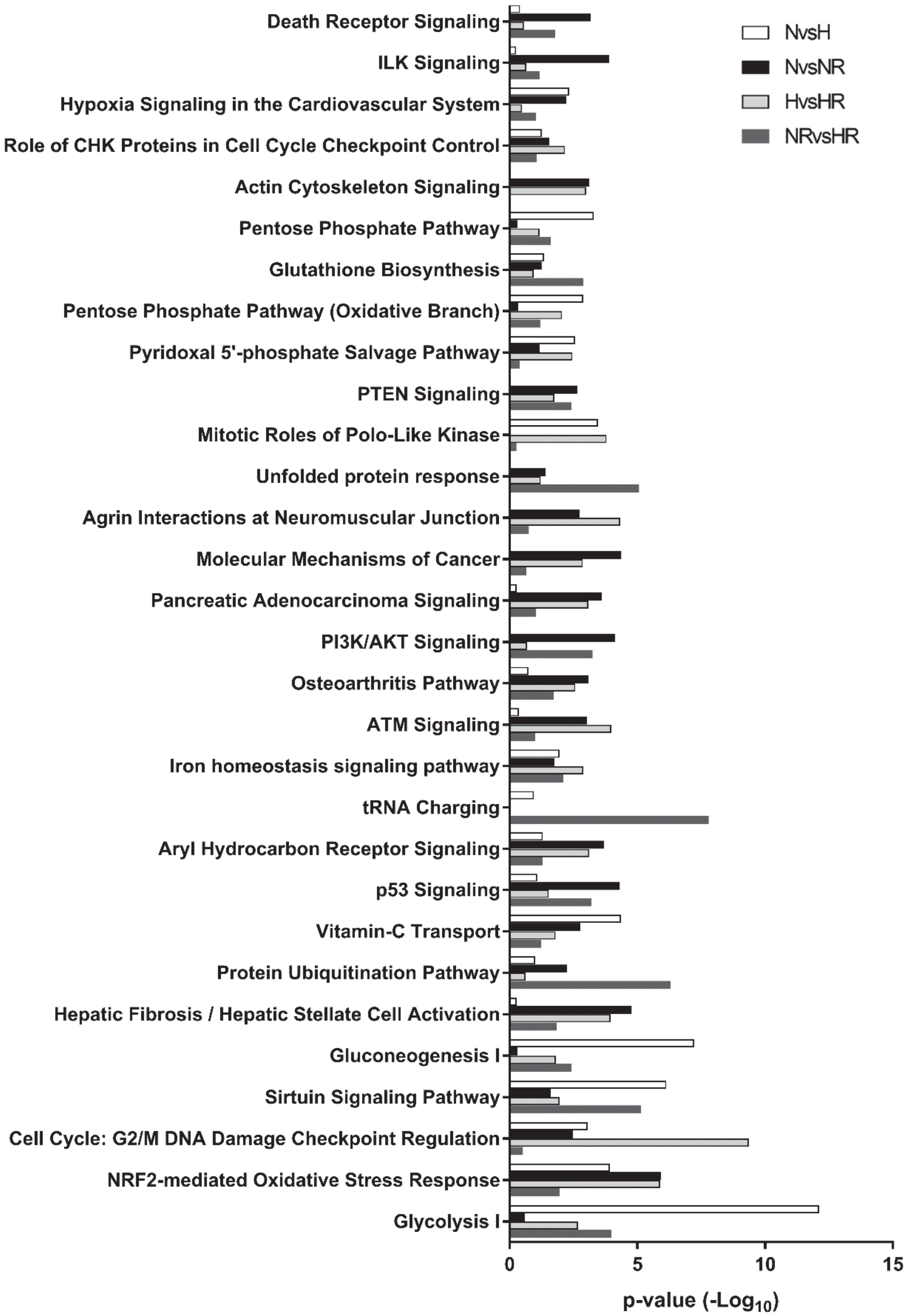

Figure 20: Top 30 canonical pathway annotations of differential transcripts.

Comparison of commonly annotated pathways between normoxic and hypoxic HCF-v treated with or without Rhein, sorted by ascending cumulative p-value ($-\log_{10}$) > 1.3 ≙ p = 0.05. N vs H: Normoxia vs Hypoxia, N vs NR: Normoxia vs Normoxia+Rhein, H vs HR: Hypoxia vs Hypoxia+Rhein, NR vs HR: Normoxia+Rhein vs Hypoxia+Rhein.

Upstream regulator analysis of complete differential transcript lists (Figure 21) expectedly identified TP53 ($-\log_{10}$ p = ∑81.4) as top affected target in all phenotypes. Also, HIF1A ($-\log_{10}$ p = ∑43.0), responsible for transcriptomic activation of hypoxia-related genes (3.2.1, Figure 12), was identified as upstream regulator, as anticipated, playing a particular role in the comparisons between normoxic and hypoxic conditions (H vs N: $-\log_{10}$ p = 17.3; HR vs NR: $-\log_{10}$ p = 14.2). Of utmost interest, and as already suggested by previous other analyses (Figure 17, Table 24, Table 26), TGFB1 ($-\log_{10}$ p = ∑48.4) was predicted as common upstream regulator especially in the context of Rhein treatment independent from environmental condition (N vs NR: $-\log_{10}$ p = 16.9; H vs HR: $-\log_{10}$ p = 18.4). Moreover, CDKN1A ($-\log_{10}$ p = ∑34.0) was identified to be significantly affected. Interestingly, CDKN1A was not predicted at all as upstream regulator in the comparison group HR vs NR and yielded low significance in N vs NR ($-\log_{10}$ p = 1.7). However, significance levels were high in H vs N ($-\log_{10}$ p = 11.8) and H vs HR ($-\log_{10}$ p = 20.6), suggesting CDKN1A as common denominator and principal regulator in regard to chronic hypoxia-driven modulation and Rhein-mediated intervention of fibrotic phenotypes.

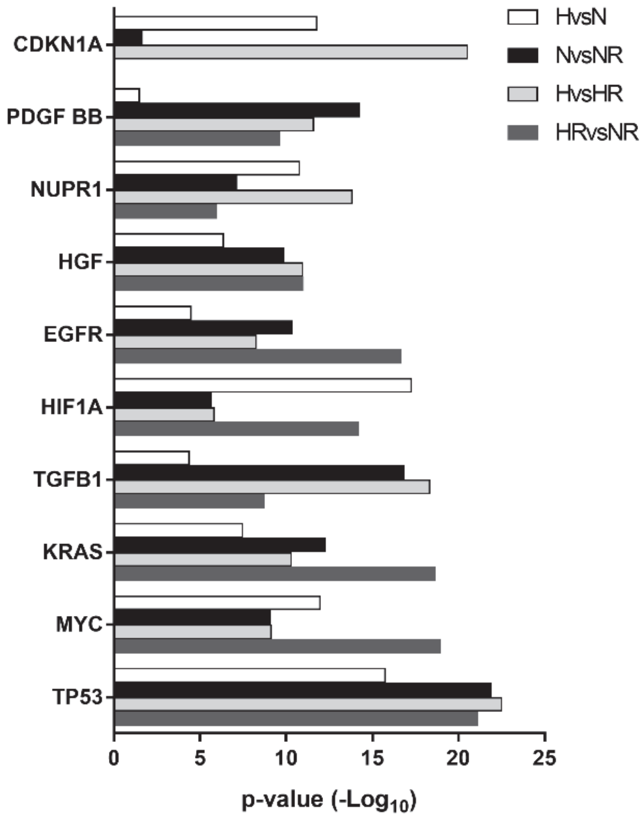

Figure 21: Upstream regulator analysis of differential transcripts.

Commonly predicted upstream regulators in the comparison of normoxic versus hypoxic HCF-v treated with or without Rhein. List of upstream regulators sorted by ascending cumulative p-value ($-\log_{10}$) > 1.3 ≙ p = 0.05. N vs H: Normoxia vs Hypoxia, N vs NR: Normoxia vs Normoxia+Rhein, H vs HR: Hypoxia vs Hypoxia+Rhein, NR vs HR: Normoxia+Rhein vs Hypoxia+Rhein.

3.2.4 Effect of Rhein on proliferation markers and cell cycle regulation

IPA® analysis of both, the transcriptome and secretome (3.2.2, 3.2.3), strongly suggested the regulation of the cell cycle to participate in the determination of hypoxia- and Rhein-mediated phenotype modulation. To determine the role of cell cycle progression in our setup, first the proliferation, as feature increased under pro-fibrotic conditions, by analyzing the expression of *MKI67*, *CDK1*, *CCNA2* and *CCNB1* (Figure 22), was investigated. As assumed, chronic hypoxia strongly induced the expression of the surrogate proliferation markers (*MKI67*: 6.6-fold, *CDK1:* 1.8-fold, *CCNA2*: 2.2-fold and *CCNB1*: 1.5-fold) underlining the pro-fibrotic character of this phenotype. Most interestingly, exposure to Rhein during chronic hypoxia decreased expression levels to baseline (normoxia) pointing towards complete inhibition of the hypoxia-mediated effect.

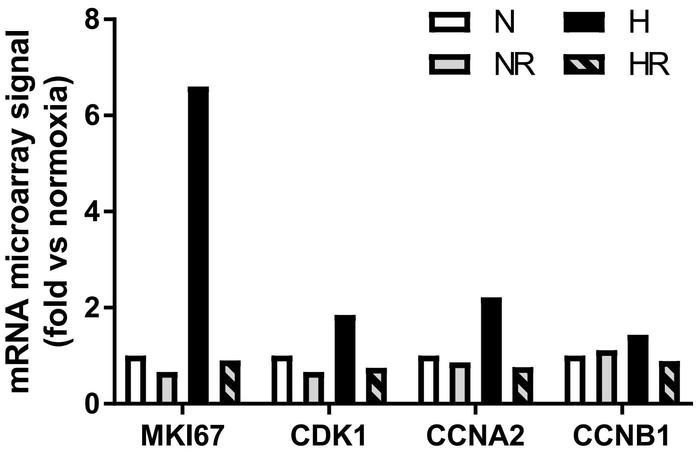

Figure 22: Rhein decreases chronic hypoxia-induced expression of proliferation markers. Expression of surrogate proliferation markers *MKI67*, *CDK1*, *CCNA2* and *CCNB1* was determined from Affymetrix microarrays and plotted as relative mRNA microarray signal folds over the normoxic control. N: Normoxia, H: Hypoxia, NR: Normoxia+Rhein, HR: Hypoxia+Rhein

Subsequently, the expression status of genes involved in the regulation of the G2/M phase, the point which strongly determines the cell cycle progression and thus the proliferation rate of cells, was investigated. Several positive and negative regulators of the G2/M phase, according to Hasvold et al. (2016), were determined from Affymetrix microarrays and plotted as relative mRNA microarray signal normalized to normoxic control (Figure 23). Analysis revealed that chronic hypoxia (H) considerably increased the expression of negative regulators *PLK1* (Δlog_2: 1.79), *CCNA2* (Δlog_2: 1.15), *CDK1* (Δlog_2: 0.89) and *CCNB2* (Δlog_2: 0.87). Contrarily, under the influence of Rhein (HR), activation of negative regulators was abolished, marked by mildly decreased to non-regulated gene expression. Under normoxic conditions (NR), with exception of CDK1 (Δlog_2: -0.60), Rhein did not further affect expression of negative G2/M phase regulators. As regards the positive regulators, only CLSPN (Δlog_2: 0.82) was increased under hypoxic conditions; other factors were not affected. Interestingly, administration of Rhein under normoxic conditions upregulated *RAD9A* (Δlog_2: 0.61), *HUS1* (Δlog_2: 0.89) and *PALB2* (Δlog_2: 0.78) and downregulated *CHEK1* (Δlog_2: -0.73) and *ATM* (Δlog_2: -0.67). In consent with normoxic cells exposed to Rhein, simultaneous treatment with chronic hypoxia and Rhein equally affected *CHEK1* (Δlog_2: -0.69) and *ATM* (Δlog_2: -0.51), but exceptionally downregulated *BRCA2* (Δlog_2: -0.66) and *ATR* (Δlog_2: -0.65) among the positive regulators. Particularly interesting, *CDKN1A*, a potent inhibitor of G2/M cell cycle progression and predicted upstream regulator (Figure 21), was strongly induced by Rhein under normoxic conditions (Δlog_2: 1.15) and differentially regulated between H (Δlog_2: -0.48) and HR (Δlog_2: 0.43). *TP53,* which was also predicted as one of the key upstream regulators before (3.2.2, 3.2.3), did not display any differential regulation between the conditions and was only weakly decreased in comparison to normoxic control.

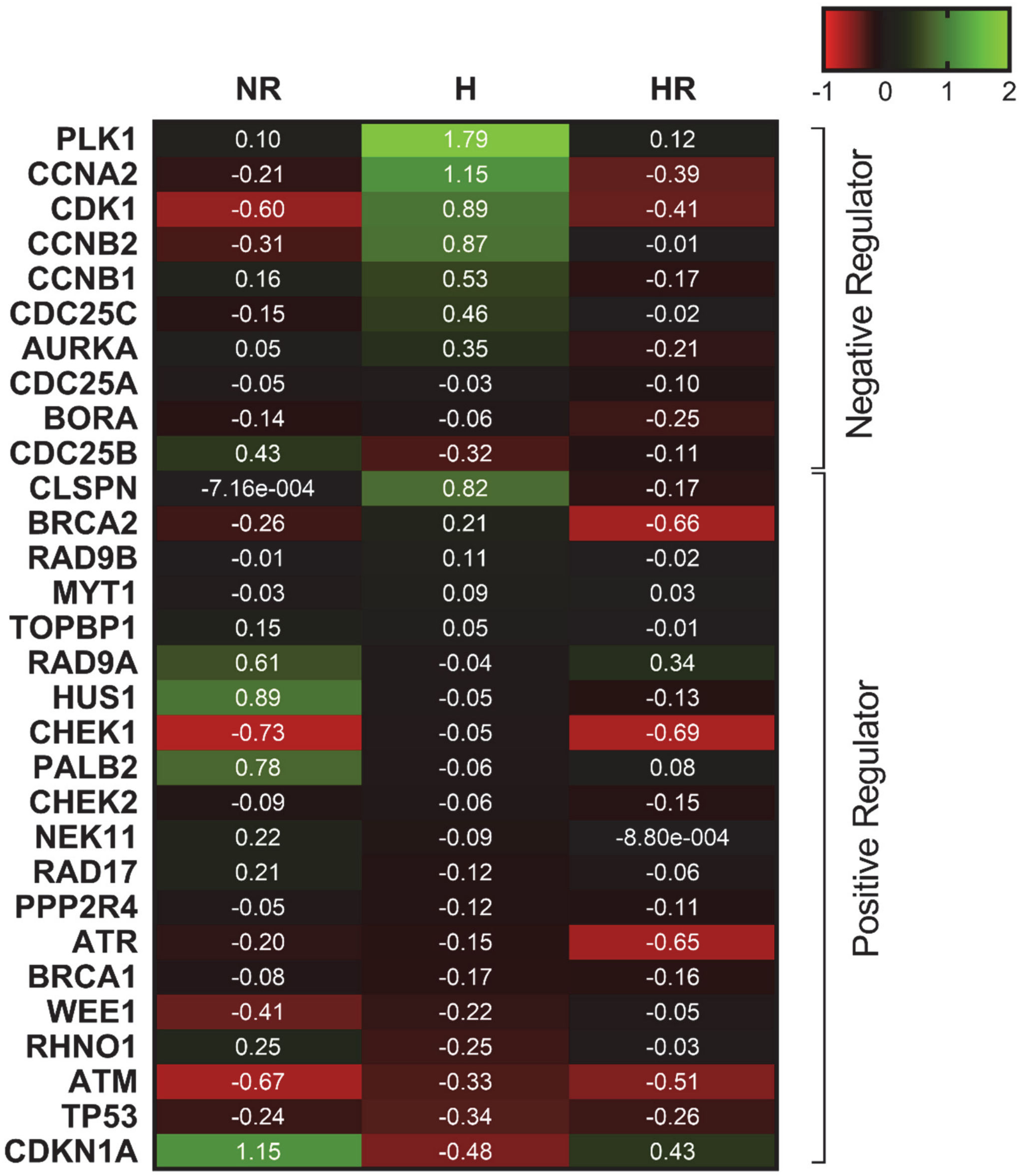

Figure 23: Rhein reverses hypoxia-mediated regulation of G2/M cell cycle phase

Transcriptome analysis of positive and negative regulators of G2/M phase according to *Hasvold et al., 2016*. The heatmap shows transcriptional expression scaled as $\log_2$ in relation to normoxic control as $\Delta\log_2 = \mathrm{Log}_2(x)-\mathrm{Log}_2(\mathrm{Normoxia})$ with x=NR (Normoxia+Rhein), H (Hypoxia), HR: Hypoxia+Rhein; $\Delta\log_2 \geq 0.58 \triangleq 1.5$-fold (linear).

To confirm whether Rhein-induced upregulation of *CDKN1A* was also functional on the protein level, and to clarify whether *TP53*, as predicted by upstream regulator analysis, is influenced, abundances of the *CDKN1A* gene-encoded protein p21 and p53 were determined via Western blot. Following Rhein treatment under normoxic conditions, p21 protein abundance was significantly increased by 1.8-fold ($p < 0.01$), whereas under hypoxic conditions Rhein application produced a less prominent, however non-significant increment, pointing towards restoring of protein abundances to normoxic control levels (Figure 24A). Similar observations were made as regards p53 (Figure 24B), where Rhein administration under normoxia significantly induced p53 protein abundance by 2.5-fold ($p < 0.0001$) and hypoxia showed a trend towards p53 depression. Likewise, under hypoxic conditions restoration of p53 to normoxic control protein levels modulated by Rhein was observed, still this finding was also not significant.

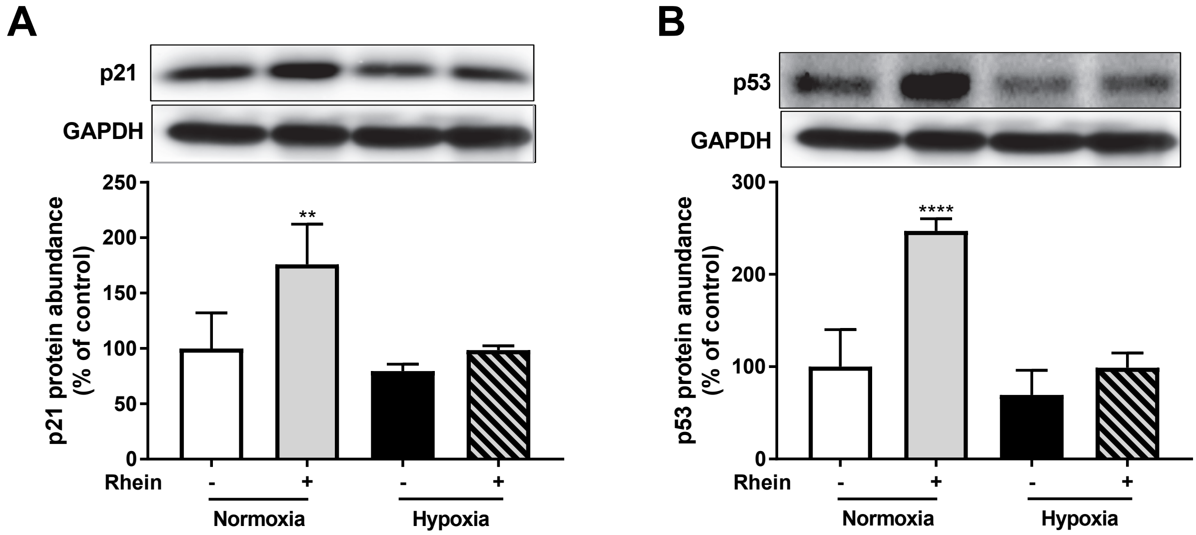

Figure 24: Rhein increases abundance of p21 and p53 under normoxic conditions
HCF-v were cultured for 4d at 21% O_2 (normoxia) or 4d at 0.5% O_2 (hypoxia) both with or without 35 µM Rhein. Representative Western blot and quantitative analysis of p21 (A) and p53 (B). Mean ± SD, two-way ANOVA statistical test ns = not significant, ** $p < 0.01$, **** $p < 0.0001$ as indicated.

Since *CDKN1A* transcript and p21 protein abundance was shown to be upregulated upon Rhein treatment, it was investigated how Rhein as a small molecule could increase *CDKN1A* expression and generally-speaking modulate the transcriptome. To address this question, upstream regulators associated with *CDKN1A* expression were explored using IPA®. Herein, several HDACs were identified to be correlated with *CDKN1A* expression (appendix,

Figure 47) and the interrelation of both factors in the focus of Rhein treatment was presented by the example of HDAC5 upstream regulator analysis. According to IPA®, *CDKN1A* is negatively regulated by HDAC5, which matched the observed decreased *CDKN1A* mRNA expression in the comparisons N vs NR (Figure 25A) and H vs HR (Figure 25B). However, IPA® marked this finding as inconsistent with state of downstream molecule, because HDAC5 itself was predicted with very low confidence to be inhibited in respective untreated cells (N and H). Of further notice, HDAC5 seemed to be associated with FMT marker *ACTA2*, which was observed to be downregulated by Rhein (3.2.1).

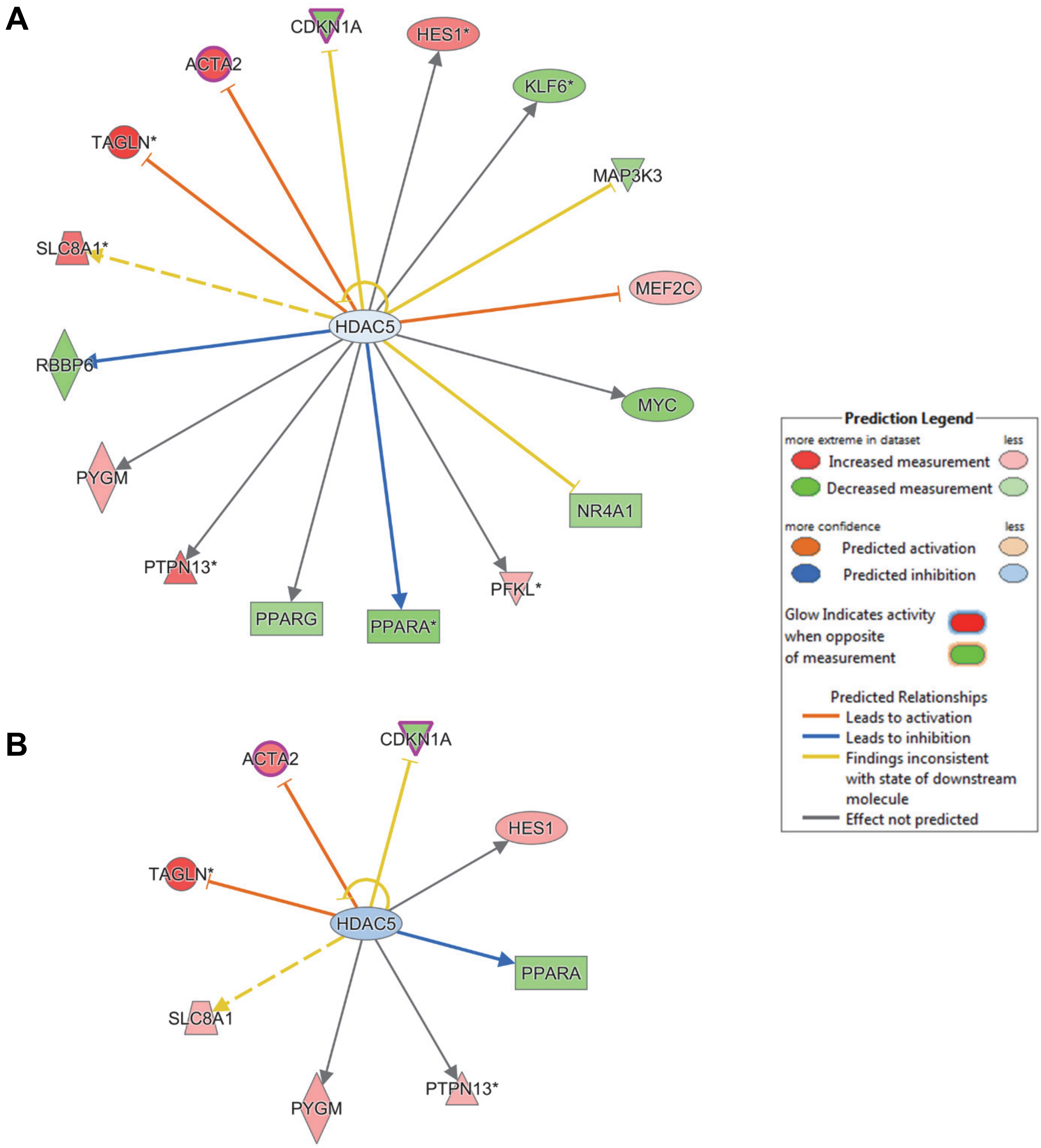

Figure 25: HDAC5 regulated downstream targets in transcriptome analyses.

Rhein mediated effects were analyzed in the comparison groups N vs NR (A) and H vs HR (B). Fold changes of up- and down-regulated genes are scaled in shades of red (higher expression in first condition of comparison) and green (lower in first condition), respectively. Blue color of upstream target indicates predicted inhibition. Orange and blue arrows indicate indirect activation and inhibition; yellow and gray arrows represent inconsistent effects and no prediction, respectively.

To study the correlation between HDAC and *CDKN1A*, experiments using the specific HDAC inhibitor sodium butyrate (SB) were performed and compared to Rhein treatment. Therefore, prior testing, a working non-toxic concentration of SB was determined by treating HCF-v cells a dose range 0.001-10 mM for 24h. Toxicity testing revealed that a concentration up to 10 mM SB did not affect cell viability after 24h exposure (Figure 26A). HDAC inhibition using SB for 24h did not reveal a significant increase of p21 abundance (Figure 26B), however exposure of HCF-v to Rhein for 24h significantly increased protein levels by 1.4-fold ($p < 0.05$).

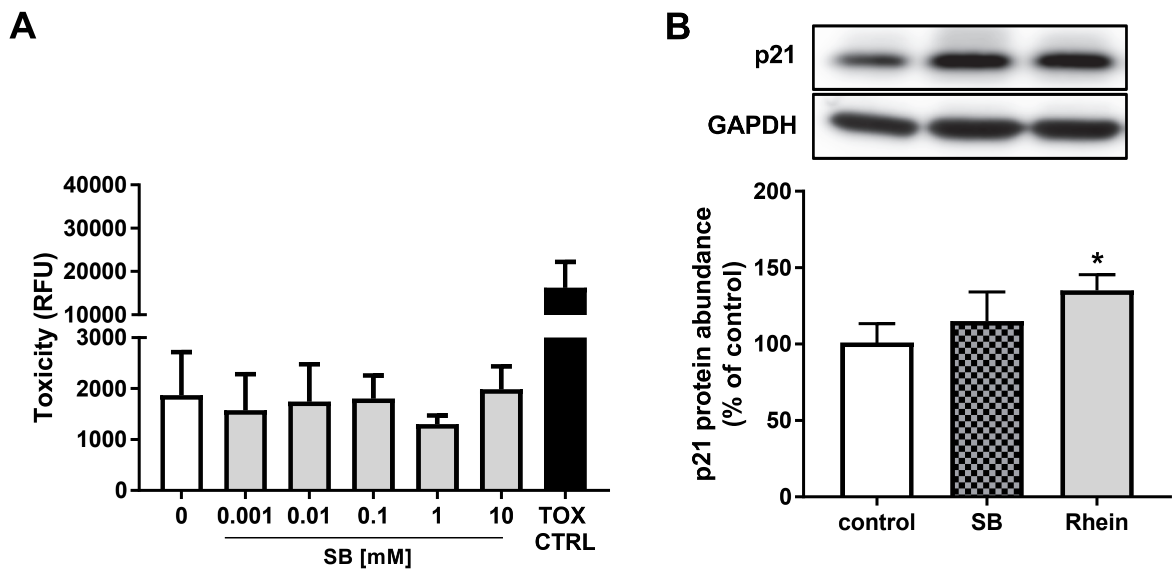

Figure 26: Effect of Rhein and HDAC-inhibitor sodium butyrate on p21 protein abundance
Toxicity of sodium butyrate (SB) on HCF-v was determined by performing a dose course (range: 0.001-10 mM) for 24h (A). HCF-v were treated with 1 mM sodium butyrate (SB) or 35 µM Rhein for 24h and p21 protein abundance was determined by Western blot (B) and normalized to GAPDH as loading control. Representative blots are shown and protein abundance is presented as % over control. Mean ± SD, n = 3, one-way ANOVA * $p < 0.05$ as indicated.

p53, as one inducer of *CDKN1A* transcription, is regulated by HDAC, which negatively affects its stability and regulatory activity via deacetylation of lysine residue Lys382. To test whether increased p53 levels (Figure 24) evolved from increased acetylation via HDAC inhibition, cells were treated with SB and Rhein. In Western blot analyses HDAC inhibition via SB showed a trend ($p=0.056$) towards increased p53 acetylation at Lys382 normalized to GAPDH as loading control, whereas following Rhein treatment enhanced acetylation (1.2-fold) was significant ($p < 0.05$) (Figure 27B). However, total p53 normalized to GAPDH was equally increased (1.2-fold, $p < 0.05$) by Rhein treatment (Figure 27C), while SB-mediated HDAC inhibition did not significantly promote higher presence of p53. When normalizing acetyl(Lys382)-p53 ratios (B) to total p53 ratios (C), the levels were equalized (Figure 27D).

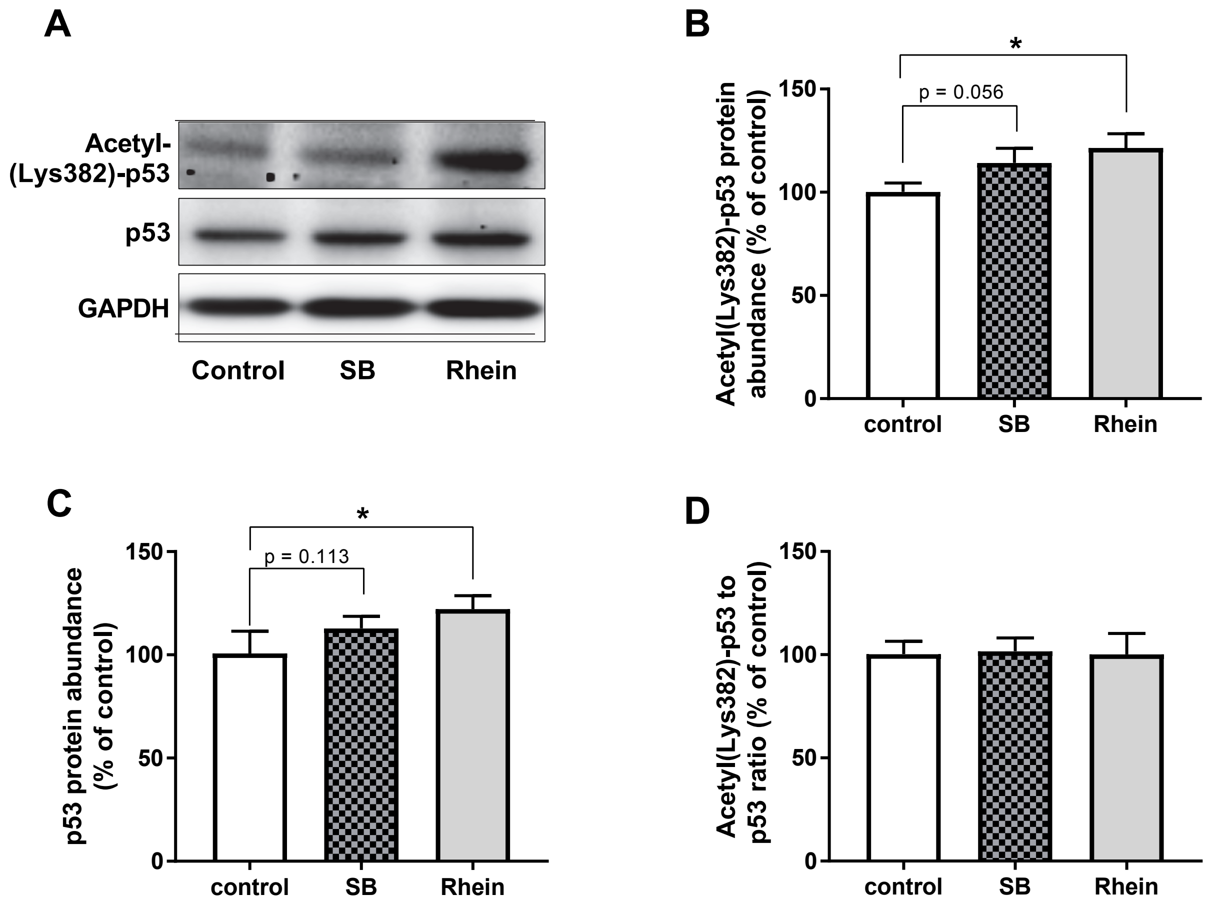

Figure 27: Effect of Rhein on p53 protein and its acetylation at Lys382

HCF-v were treated with 1 mM sodium butyrate (SB) or 35 µM Rhein for 24h and protein lysates were subjected to Western blot analysis. Representative blots are shown (A) and protein abundance of acetyl(Lys382)-p53 (B) and total p53 (C) are presented as % over control normalized to GAPDH as loading control. Protein abundance (D) with normalization of acetyl(Lys382)-p53 to total p53 given as % over control. Mean ± SD, n = 3, one-way ANOVA * $p < 0.05$ as indicated.

3.2.5 Effect of Rhein on epigenetic regulators during chronic hypoxia and normoxia

Analysis of transcriptomic data revealed that cell cycle genes, particularly the ones negatively regulating the progression of the G2/M phase, are affected by chronic hypoxia and inversely modulated in the presence of Rhein (Figure 23). Since further analysis demonstrated that HDACs might be involved in the Rhein-driven p53-dependent regulation of the cell cycle arrest-determinant gene *CDK1NA* in concert with myofibroblast marker *ACTA2* (Figure 25), the role of several epigenetic regulators was analyzed. Alongside HDACs, also the closely-related family of sirtuins (SIRTs) are known histone-deacetylases and modulators of DNA transcription, whereas both their effects are counteracted by histone-acetyltransferases (HATs). In contrast, methyltransferases (MeT) immediately influence transcription and translation by mRNA and DNA methylation. Therefore, the activity of expression-regulating HDACs, SIRTs, HATs and MeTs was tested. Herein, it was determined (1) whether long-term exposure to Rhein under normoxic and hypoxic conditions (2.2.1.2, 3.1) permanently and irreversibly affected activity and (2) whether Rhein exerts acute and imminent effects on activities in comparison to respective reference inhibitors.

To analyze potential long-term effects on HDAC activity, the intact protein lysates (2.2.3.2) of normoxic and hypoxic cells that had experienced 4d Rhein treatment were subjected to HDAC class I/II enzyme activity assays (2.2.5.1) in the absence of Rhein during the activity test. Interestingly, no significant changes in HDAC activity between the experimental lysates were detected (Figure 28A), which was in accordance to unchanged expression levels (average: NR: Δlog_2: 0.08, H: Δlog_2: -0.14, HR: Δlog_2: 0.03) throughout all members of the HDAC family (Figure 28B). However, when HDAC activity was tested in control cell lysates in the direct presence of Rhein (Figure 28C), deacetylase activity was significantly inhibited by 70% ($p < 0.0001$), which was superior ($p < 0.05$) to the SB-mediated HDAC inhibition by 0.57-fold ($p < 0.01$). These results implicated that Rhein directly affected HDAC enzyme activity, but that this effect was reversible when Rhein was removed from the system. Determination of the potency of Rhein regarding HDAC class I/II inhibition (Figure 28D) determined an inhibitory concentration IC_{50} = 57.88 µM (n = 1).

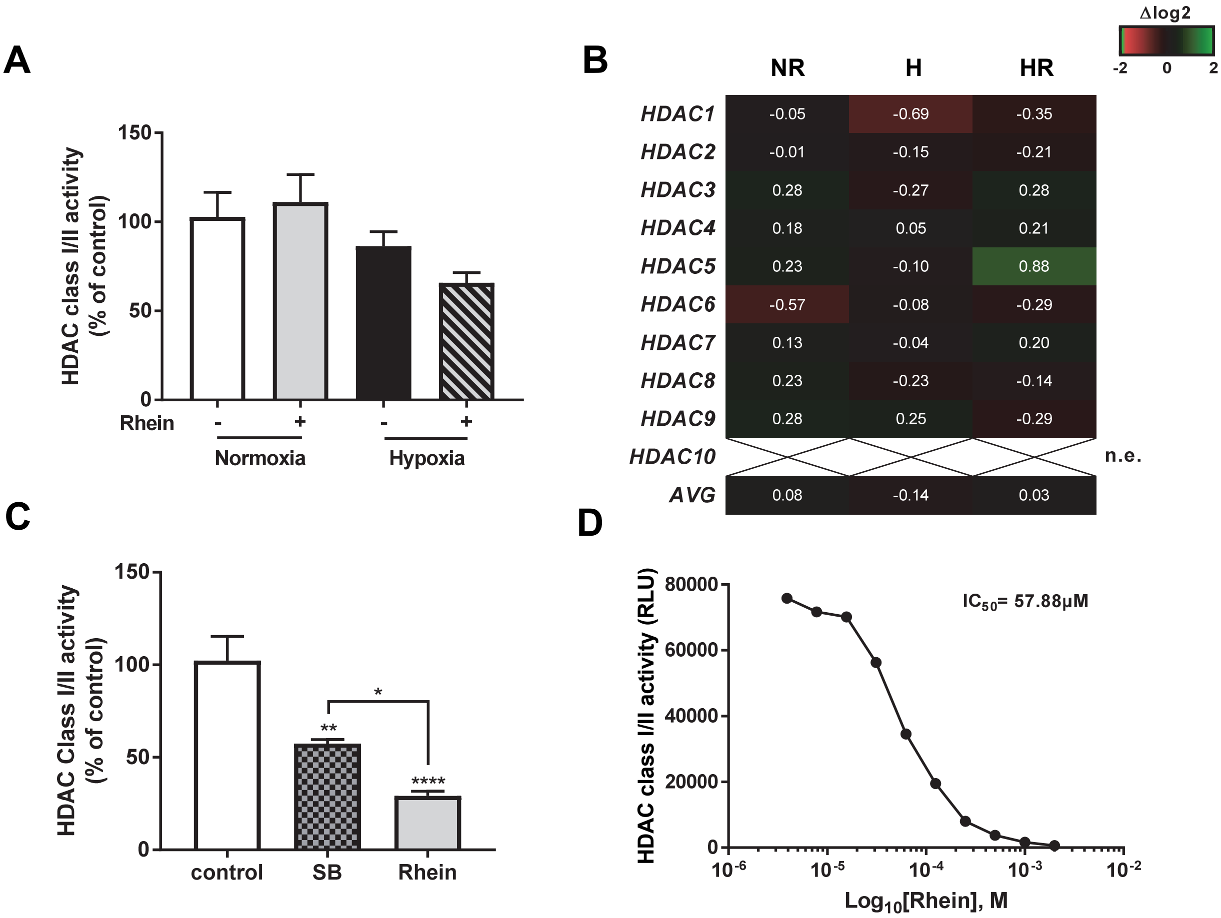

Figure 28: Effect of Rhein on HDAC enzyme activity

HDAC Class I/II luminescent activity assays were carried out using 5µg of total protein lysate, respectively. (A) HDAC activity in HCF-v lysates after 4d culture at 21% O_2 (normoxia) or 4d at 0.5% O_2 (hypoxia) both with or without 35 µM Rhein. (B) Heatmap showing transcriptional expression of all HDAC family members in relation to normoxic control. Given values are interpreted as $\Delta log_2 = Log_2(x) - Log_2(Normoxia)$ with x=NR (Normoxia+Rhein), H (Hypoxia), HR: Hypoxia+Rhein *n.e.:* not expressed. *AVG*: average regulation of gene family. $\Delta log2 > 0.58 \triangleq 1.5$-fold (linear). (C) HDAC activity in control cell lysates directly exposed to 35 µM Rhein or 1 mM sodium butyrate (SB) during measurement. (D) The potency of Rhein as HDAC inhibitor was assessed by a performing a dose-course. IC_{50} was calculated via non-linear regression after log_{10} transformation. n = 1-4, Mean ± SD, One-way ANOVA with Sidak's multiple comparisons test ** $p < 0.01$, **** $p < 0.0001$ as indicated.

Similarly, to the observations made regarding HDACs, SIRT activity was also not significantly affected in any of the experimental lysates (Figure 29A). Opposingly, however, upregulation of SIRT1 (Δlog_2: 0.73), SIRT6 (Δlog_2: 0.88) and SIRT7 (Δlog_2: 0.73) in NR was observed (Figure 29B). Nonetheless, overall average regulation of the SIRT family was considerably low (NR: Δlog_2: 0.31, H: Δlog_2: -0.08, HR: Δlog_2: 0.19). Again, the presence of Rhein during activity measurement in control lysates (Figure 29C), inhibited SIRT deacetylase activity by 60% ($p < 0.0001$) compared to inhibition via nicotinamide by 23% ($p < 0.001$). For

SIRT activity (Figure 29D), an inhibitory concentration of IC_{50} = 31.41 µM Rhein was determined.

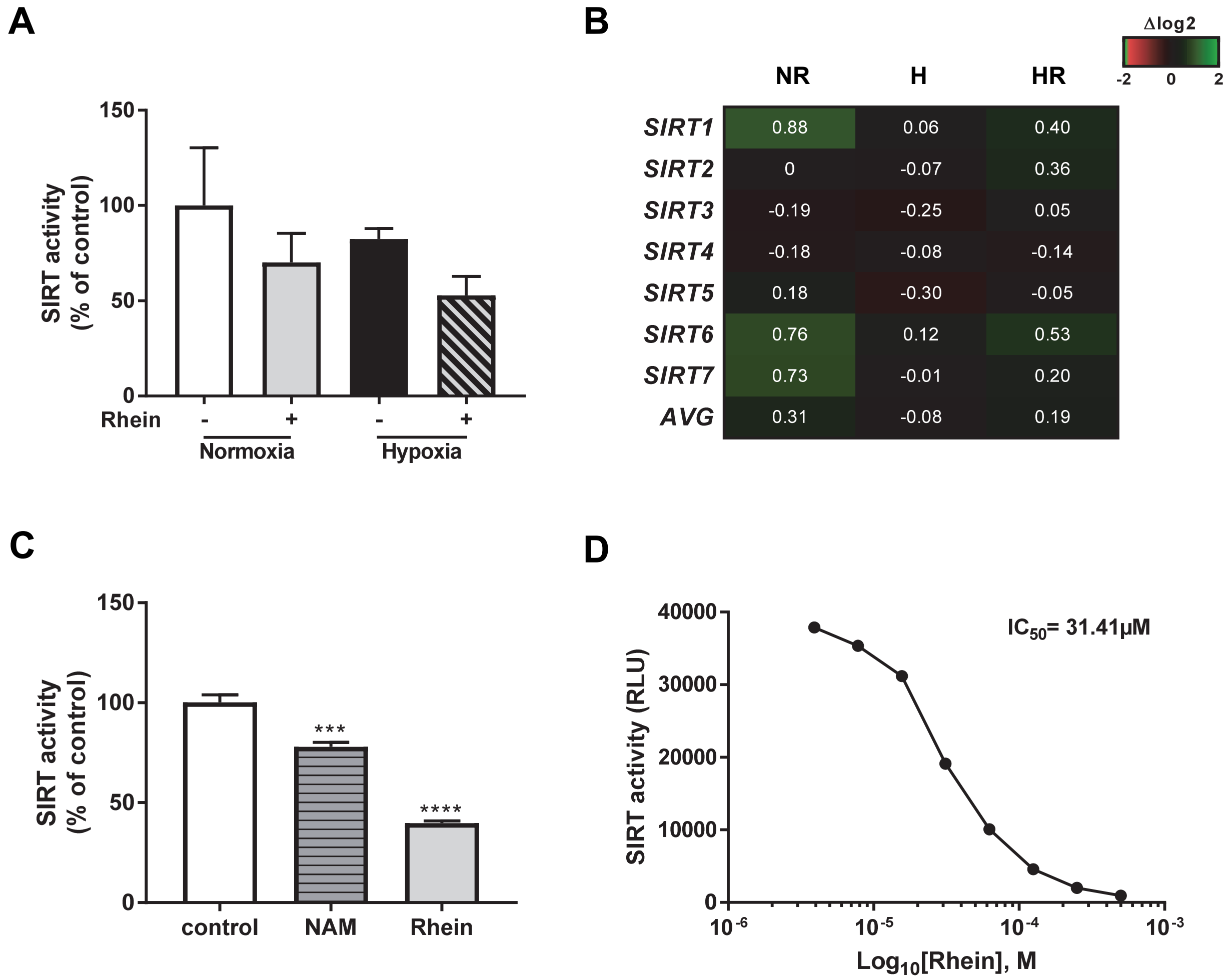

Figure 29: Effect of Rhein on SIRT activity

SIRT activity assays were carried out with 5µg of total protein lysate using the SIRT-Glo assay kit. (A) SIRT activity in HCF-v lysates after 4d culture at 21% O_2 (normoxia) or 4d at 0.5% O_2 (hypoxia) in the presence or absence of 35 µM Rhein. (B) Heatmap showing transcriptional expression of all SIRT family members in relation to normoxic control. Given values are interpreted as Δlog2= Log_2(x)-Log_2(Normoxia) with x=NR (Normoxia+Rhein), H (Hypoxia), HR: Hypoxia+Rhein. *AVG*: average regulation of gene family. $\Delta log_2 > 0.58 \triangleq 1.5$-fold (linear). (C) SIRT activity in control cell lysates directly exposed to 35 µM Rhein and 10 mM nicotinamide (NAM) during assay was performed. (D) The inhibitory potency of Rhein as SIRT inhibitor was measured by a dose-course. IC_{50} was calculated via non-linear regression after log_{10} transformation. n = 1-4, Mean ± SD, One-way ANOVA with Sidak's multiple comparisons test *** $p < 0.001$, **** $p < 0.0001$ as indicated.

As counteracting partner of histone deacetylases, histone acetyltransferase activity was tested in parallel. HAT activity was significantly depressed ($p < 0.01$) in lysates of normoxic specimens treated with Rhein (NR) by 55% (Figure 30A). Similarly, in lysates from cells that experienced hypoxic conditions (H) HAT enzyme activity was decreased by 40% ($p < 0.05$) and 4d Rhein treatment (HR) significantly pronounced this reduction resulting in 28% activity ($p < 0.05$). However, mRNA expression (Figure 30B) of HAT family members (KATs) showed mild average upregulation (Δlog_2: 0.37) and selectively more pronounced effects in KAT3A (Δlog_2: 0.69), KAT3B (Δlog_2: 1.11) and KAT6A (Δlog_2: 1.09) in NR. In hypoxia-treated HCF-v cells no considerable cumulative alteration was observed (AVG: Δlog_2: -0.17), however HR cells, still negligible, displayed opposed regulation. Most interestingly, Rhein did not display any inhibitory capacity on HAT activity, when directly applied to lysates of unbiased control cells (Figure 30C), opposed by specific HAT inhibitor anacardic acid (AnA)-mediated suppression by 28% ($p < 0.05$).

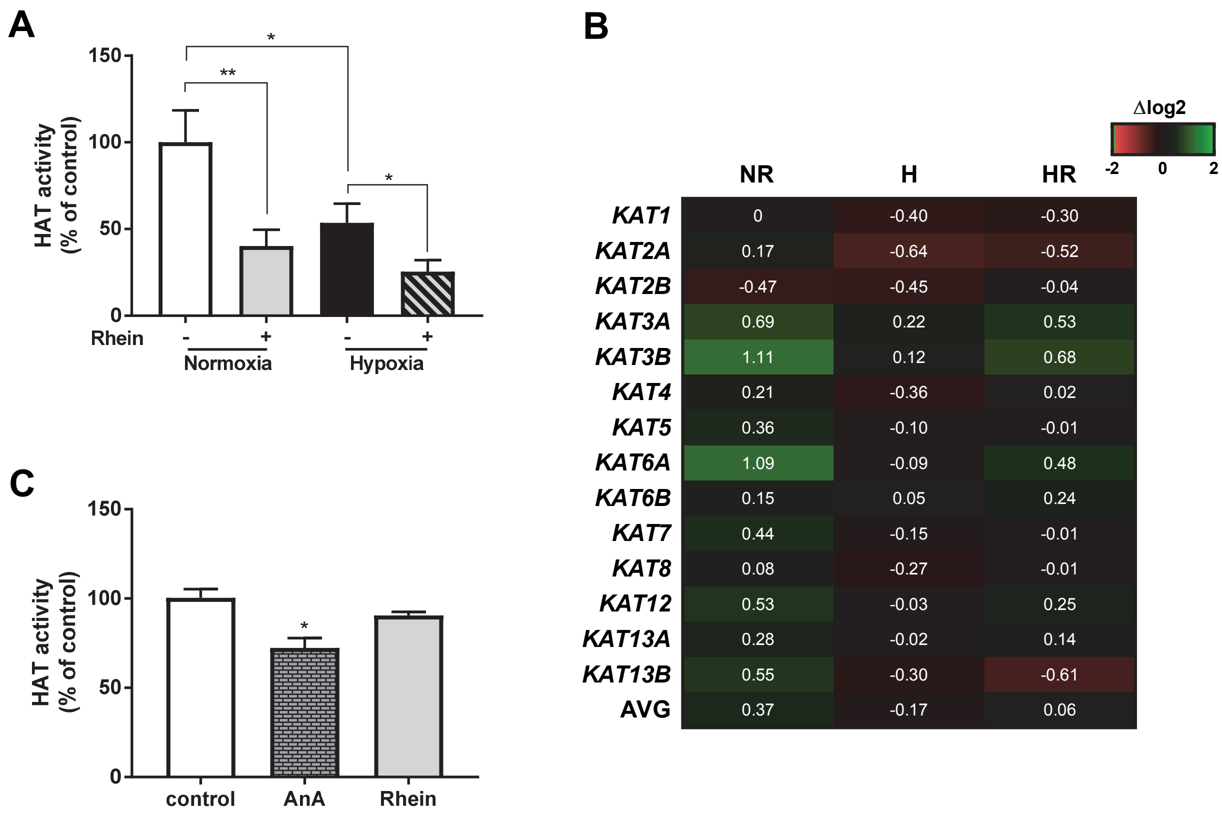

Figure 30: Effect of Rhein on HAT activity.

HAT activity assays were performed using 5µg of total protein lysate using the HAT activity assay II kit. (A) Activity in HCF-v lysates after 4d culture at 21% O_2 (normoxia) or 4d at 0.5% O_2 (hypoxia) both with or without 35 µM Rhein. (B) Heatmap showing transcriptional expression of all KAT family members in relation to normoxic control. Given values are interpreted as $\Delta log2 \triangleq Log_2(x)-Log_2(Normoxia)$ with x=NR (Normoxia+Rhein), H (Hypoxia), HR: Hypoxia+Rhein. *AVG*: average regulation of gene family. $\Delta log2>0.58$ = 1.5-fold (linear). (C) HAT activity in control cell lysates directly exposed to 35 µM Rhein or 1 µM anacardic acid (AnA) during measurement. n = 4, Mean ± SD, One-way ANOVA with Sidak's multiple comparisons test * $p < 0.05$, ** $p < 0.01$ as indicated.

Epigenetic regulation via increased DNA-methylation has been shown to be associated to chronic hypoxia. Pointing towards this interrelation, a significant 3-fold increased global methyltransferase (MeT) activity ($p < 0.05$) in lysates of cells subjected to chronic hypoxia (Figure 31A) was found, whereas lysates from cells after long-term Rhein treatment did not display any differential effect independently from normoxic or hypoxic conditions. Unexpectedly, the abundance of hypoxia-sensitive DNA-methyltransferase DNMT1 was unaltered in our hypoxic system (Figure 31B), but after treatment with Rhein independent from employed environment (NR and HR) protein levels were significantly decreased by approx. 60% (both $p < 0.01$). Exemplarily, to check whether Rhein influenced DNA-methylation rates, the methylation of *HIF1A* in the region of its hypoxia responsive element (HRE) was exemplarily assessed. Neither Rhein alone (NR) nor chronic hypoxia in the presence (HR) or absence (H) of Rhein did differentially change methylation rates in any of the six investigated methylation sites (Figure 31C).

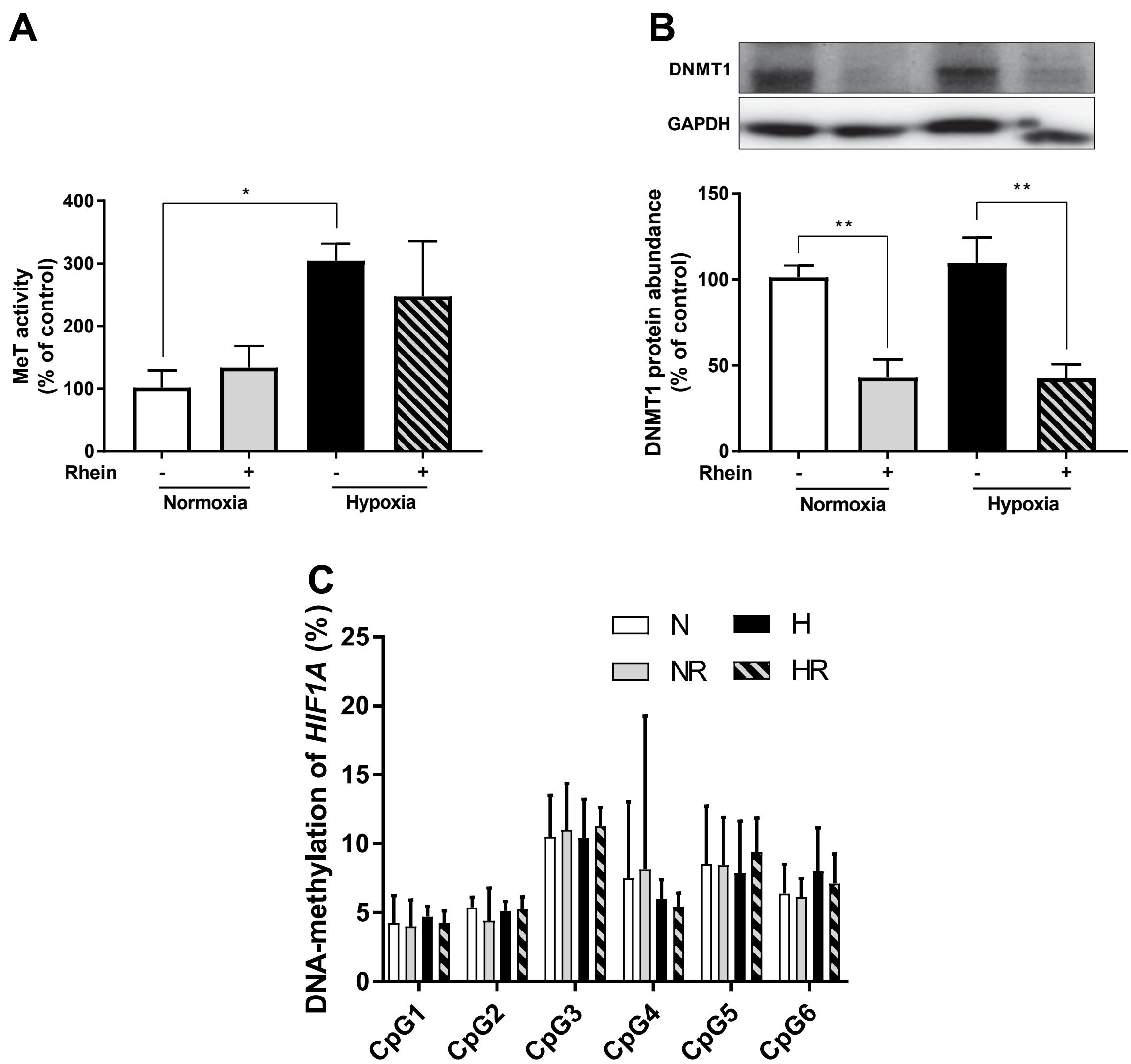

Figure 31: Methyltransferase activity potentiated by chronic hypoxia was not affected by Rhein administration.

HCF-v were cultured for 4d at 21% O_2 (normoxia) or 4d at 0.5% O_2 (hypoxia) both with or without 35 µM Rhein. (A) Methyltransferase (MeT) activity assay was measured in 5µg of total protein lysate, respectively. (B): Representative Western blots and quantitative analysis of DNMT1. (C) DNA-methylation at respective CpG methylation site (1-6) of HIF1A in the region of its hypoxia responsive element. n = 3-4, Mean ± SD, One-way ANOVA with Sidak's multiple comparisons test * $p < 0.05$, ** $p < 0.01$ as indicated.

3.2.6 Effect of Rhein on cardiac fibroblast TGFβ production and secretion under chronic hypoxia and normoxia

Regarding the modulation of secretome as well as transcriptome under chronic hypoxia and in the presence of Rhein, TGFβ1 was predicted as one of the most probable common and condition-specific upstream regulator candidates as previously shown (3.2.2, 3.2.3). In this context, the role of TGFβ1 was investigated in the system with a focus on its secretory mechanism and in relation to other TGFβ family members.

TGFβ1 protein abundance was upregulated by 1.5-fold ($p < 0.05$) in normoxic Rhein-treated cells and was unaltered in specimens subjected to chronic hypoxia with or without Rhein (Figure 32A). Of further notice, a shift in the band signal patterns of TGFβ was observed, marked by a more prominent lower band in both normoxic and hypoxic cells exposed to Rhein in comparison to evenly pronounced bands in their respective untreated controls. Abundance of LTBP1 (latent TGFβ binding protein 1), which regulates the secretion of TGFβ1 by their association to latent complexes, was approximately 25-30% less in Rhein treated specimens of both normoxic and hypoxic cells, however this effect was not significant (Figure 32B). To determine the abundance of secreted TGFβ1, latency associated protein (LAP) ELISA, which detects total (active + inactive) TGFβ1 and serves as surrogate marker to circumvent detection limitations of the instable activated form, was performed in the supernatants. Most interestingly, a detrimental decrease of LAP from 6pg/µg in normoxic cells to 3pg/µg in Rhein-treated cells ($p < 0.001$) and a reduction from 7pg/µg in hypoxic cells to 3.7pg/µg in hypoxic cells treated with Rhein ($p < 0.01$) was observed (Figure 32C). In accordance to reduced LTBP1 protein abundance, mRNA levels of all latent TGFβ binding protein isoforms were rather downregulated (Figure 32D) after Rhein administration with *LTBP4* being most strikingly affected (NR $\Delta\log_2$: -2.12 and HR $\Delta\log_2$: -0.68). Likewise, *TGFB1* levels corresponded to protein abundances and were remarkably increased in Rhein-treated specimens (NR $\Delta\log_2$: 0.68 and HR $\Delta\log_2$: 0.95), however the expression of the isoform *TGFB3* was downregulated (NR $\Delta\log_2$: -2.16 and HR $\Delta\log_2$: -1.36). Of further interest, expression of TGFβ receptor kinase *TGFBR1* was inversely regulated in Rhein treated cells compared to hypoxic cells (NR $\Delta\log_2$:

-0.47, H Δlog_2: 0.50, HR Δlog_2: -0.71), whereas *TGFBR2* was only upregulated in Rhein-treated samples (NR Δlog_2: 0.94 and HR Δlog_2: 0.58). Comparably, TGFβ antagonist *TGFBR3* mRNA was also more abundant in the presence of Rhein and mildly decreased in hypoxia-only treated cells (NR Δlog_2: 0.91, H Δlog_2: -0.31, HR Δlog_2: 0.64).

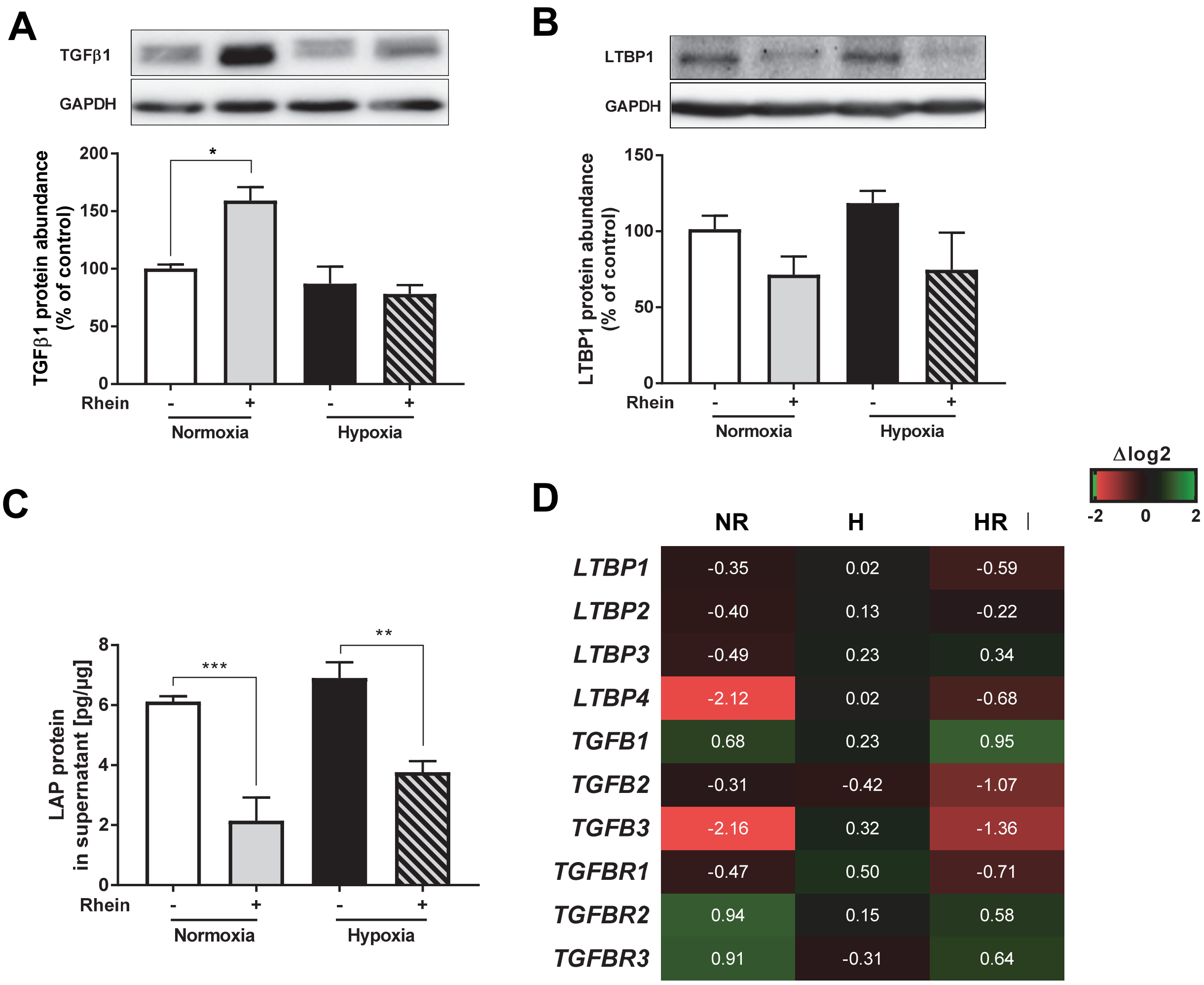

Figure 32: Rhein treatment leads to intracellular TGFβ1 sequestration.

HCF-v were cultured for 4d at 21% O_2 (normoxia) or 4d at 0.5% O_2 (hypoxia) both with or without 35 µM Rhein. Representative Western blot and quantitative analysis of inactive pro-TGFβ1 (A) and LTBP1 (B). (C) Latency associated Protein (inactive pro-TGFβ1) concentration was assessed in concentrated supernatants via sandwich-ELISA. (D) Heatmap of transcriptional expression of TGFβ secretion- and signaling-related targets normalized to normoxic control. Given values are interpreted as Δlog2= $Log_2(x)-Log_2(Normoxia)$ with x=NR (Normoxia+Rhein), H (Hypoxia), HR: Hypoxia+Rhein. n = 4, Mean ± SD, One-way ANOVA with Sidak's multiple comparisons test, * $p < 0.05$ as indicated.

3.3 The impact of Rhein on TGFβ-stimulated differentiation of cardiac fibroblasts

Our previous findings consistently suggested TGFβ1 as solid upstream regulator in the hypoxia- and Rhein-induced modulation of both the secretome and transcriptome. Therefore, the role of Rhein as a potential inhibitor in TGFβ1-mediated FMT was tested.

3.3.1 TGFβ activates cardiac fibroblast to myofibroblast transformation by activating profibrotic program

First, the working concentration of human recombinant TGFβ1, the most prominent isoform related to FMT, sufficient to promote the induction of αSMA as representative marker for fibroblast differentiation was determined. As shown in Figure 33, treatment of HCF with 1 ng/ml TGFβ1 for 24h already lead to a mild 1.5fold upregulation of *ACTA2*, however, 10 ng/ml TGFβ1 was necessary to pronouncedly induce the transcription of the marker (3.5 fold). Consequently, 10 ng/ml TGFβ1 was set as standard concentration for MF activation in this study.

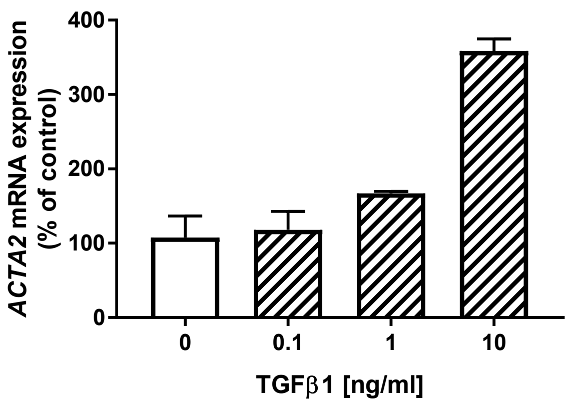

Figure 33: TGFβ1 induces alpha-smooth muscle actin mRNA *expression*.
HCF-v were incubated with 0.1-10 ng/ml human recombinant transforming growth factor β1 for 24h. *ACTA2* (alpha-smooth muscle actin) mRNA levels were analyzed using RT-qPCR. n = 2, Mean ± SD

Next, downstream targets regulated by TGFβ1 in HCF-v cells were tested. Therefore, the transcription levels of 84 key genes subdivided in 4 categories (ECM components and remodeling enzymes, cell adhesion molecules, cytokines and growth factors, signal transduction) involved in dysregulated tissue remodeling were tested. RT-qPCR array analysis revealed 27 genes significantly (p-value <0.05) up- or downregulated in cells treated with 10 ng/ml TGFβ1 for 24h compared to untreated control cells (Figure 34). Among the ECM components, only *COL1A2* and collagen binding *HSP47* were found to be significantly upregulated (1.5-fold and 2-fold) by TGFβ1, whereas in the ECM regulating group *MMP13* (5.5-fold) and matrix metalloproteinase inhibitor *TIMP3* (1.7-fold) were increased. As regards the plasmin system as part of ECM remodeling enzymes, expectedly, TGFβ1 significantly stimulated *PAI1* (4-fold) and inhibited *PLG* by 60% and *PLAT* by 80%. While TGFβ1 markedly enhanced the transcription of several integrins (1.5-2-fold), examined cytokine and growth factor expression was bidirectionally regulated. Transcript numbers of profibrotic and proliferation stimulating factors were increased, with *CTGF* and *CCL11* scoring the highest folds (3-fold and 4.4-fold). Contrarily, the mRNA expression of antiproliferative *IL1B* and *HGF* were proven repressed by 60%. Interestingly, not only did TGFβ1 promote the expression of itself (1.6-fold) and its receptor kinase *TGFBR1* (1.5-fold), but it also increased the transcription of the canonical TGFβ/SMAD pathway inhibitor *SMAD7* by 2.4-fold.

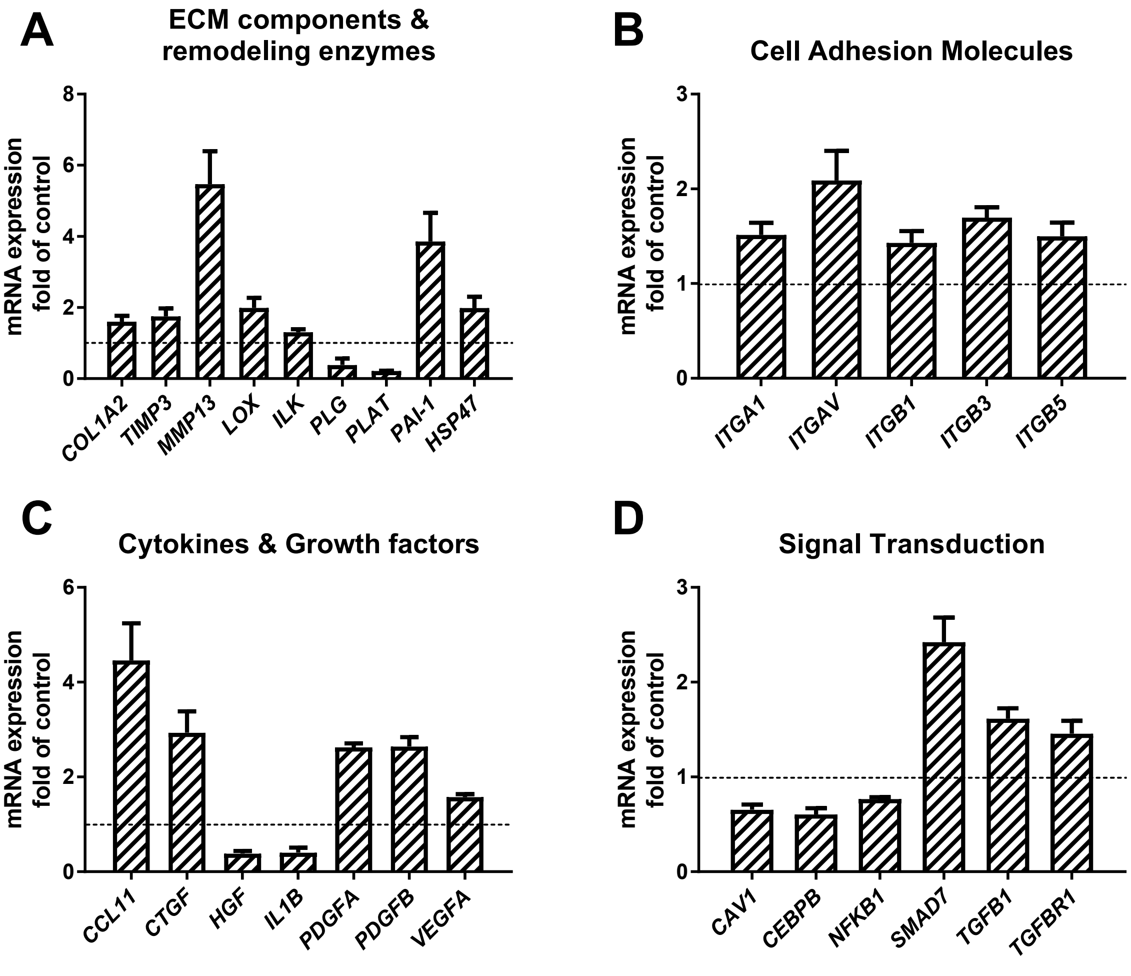

Figure 34: TGFβ1-mediated pro-fibrotic target genes.

HCF-v cells were incubated with 10 ng/ml human recombinant transforming growth factor β1 for 24h. Bar graphs show folds of significantly TGFβ1-regulated genes ($p < 0.05$) involved in ECM remodeling (**A**), cell adhesion (**B**), released cytokines (**C**) and signaling transduction (**D**). The mRNA levels of fibrotic response genes were analyzed using a RT-qPCR array. n = 4, ±SD, two-tailed unpaired t-test

3.3.2 Rhein dose-dependently reduces TGFβ1-mediated upregulation of myofibroblast markers

To evaluate whether Rhein affects FMT, cells were exposed to a dose-range of 10-50 μM Rhein for 24h in the presence of human recombinant TGFβ1 followed by assessment of TGFβ1-responsive targets. Rhein treatment counteracted the stimulating effect of TGFβ1 and dose-dependently decreased protein abundance and mRNA expression of the myofibroblast marker αSMA (gene name: *ACTA2*). On protein level a concentration between 10 and 20 μM Rhein was sufficient to completely abrogate TGFβ1-induced upregulation ($p < 0.01$, Figure 35A), whereas *ACTA2* gene expression achieved baseline levels when a dose between 30-50 μM Rhein was applied to the cells ($p < 0.0001$, Figure 35B). Likewise, transcription rates of selected TGFβ1 targets were similarly affected by Rhein administration (Figure 35C): Whereas TGFβ1-mediated *PAI-1* upregulation was not completely abolished, but significantly downregulated by approx. 30% at dose higher than 30 μM Rhein ($p < 0.05$), mRNA of fibrosis-associated cytokines *CTGF* and *CCL11* depicted a similar dose-dependent decrease ($p < 0.05$) as *ACTA2* (baseline expression: 30-50 μM Rhein). In contrast, induction of the most prominent collagen isoform in fibrotic pathologies *COL1A2* was already significantly repressed with a dose of Rhein as little as 10 μM ($p < 0.05$).

Due to the observation that administration of a dose between 10-20 μM and between 30-50 μM Rhein during stimulation of HCF-v with TGFβ1 lead to baseline αSMA protein levels and mRNA expression, respectively, from this point 15 μM and 35 μM Rhein were used as low- and high-dose treatment for all following experiments in this study.

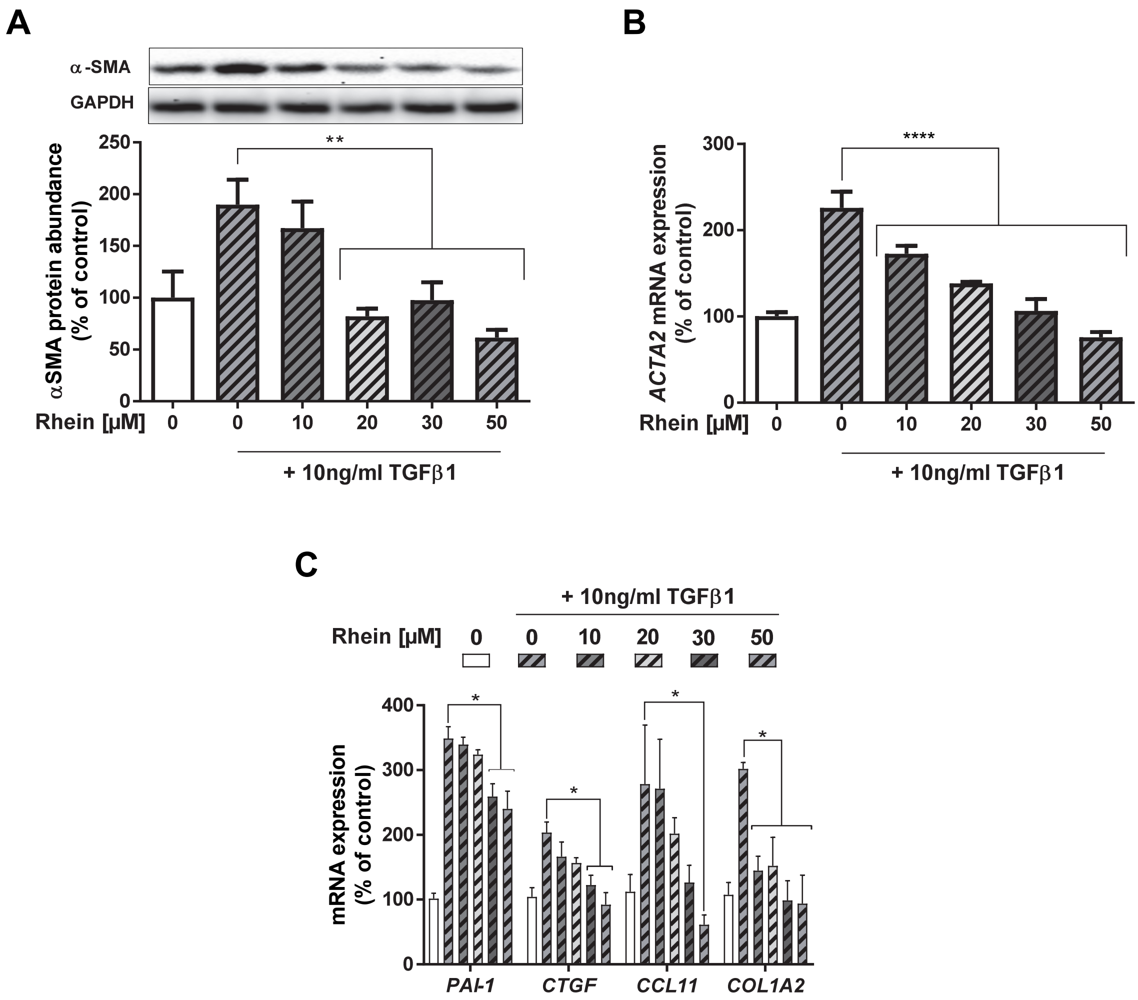

Figure 35: Rhein reduces TGFβ1-induced upregulation of fibrogenic targets in a dose-dependent way.

HCF-v cells were incubated with 10 ng/ml human recombinant transforming growth factor β1 alone or in combination with increasing doses of Rhein for 24h. (A) Representative Western blot and quantitative analysis of myofibroblast marker αSMA. The mRNA levels of *ACTA2* (B) and selected genes (C) were analyzed via RT-qPCR analysis. n = 4, Mean ± SD, One-way ANOVA with Sidak's multiple comparisons test * $p < 0.05$, ** $p < 0.01$, **** $p < 0.0001$ as indicated.

3.3.3 Rhein does not interfere with TGFβ1 autocrine self-induction

Given that Rhein significantly counteracted the expression of fibrotic targets upon TGFβ1 exposure (3.3.2), the question arose whether Rhein directly affected the expression and whether it influenced the induction of the TGFβ1 autocrine loop. Treatment of CFs with TGFβ1 significantly promoted auto-induction of TGFβ1 protein (Figure 36A) and mRNA (Figure 36B) by 2.6-fold ($p < 0.05$) and 2-fold ($p < 0.001$), respectively. Nonetheless, Rhein administration did not display any differential effect on protein level neither under stimulated nor unstimulated conditions. Intriguingly, transcriptional abrogation of TGFβ1 auto-induction was observed by 15 µM Rhein but was absent in cells treated with a higher dose of 35µM Rhein. However, the elevated expression of *LTBP1*, which is important for the secretion of latent TGFβ1, upon stimulation was significantly influenced by Rhein and completely abolished by both 15 µM ($p < 0.05$) and 35 µM Rhein ($p < 0.01$).

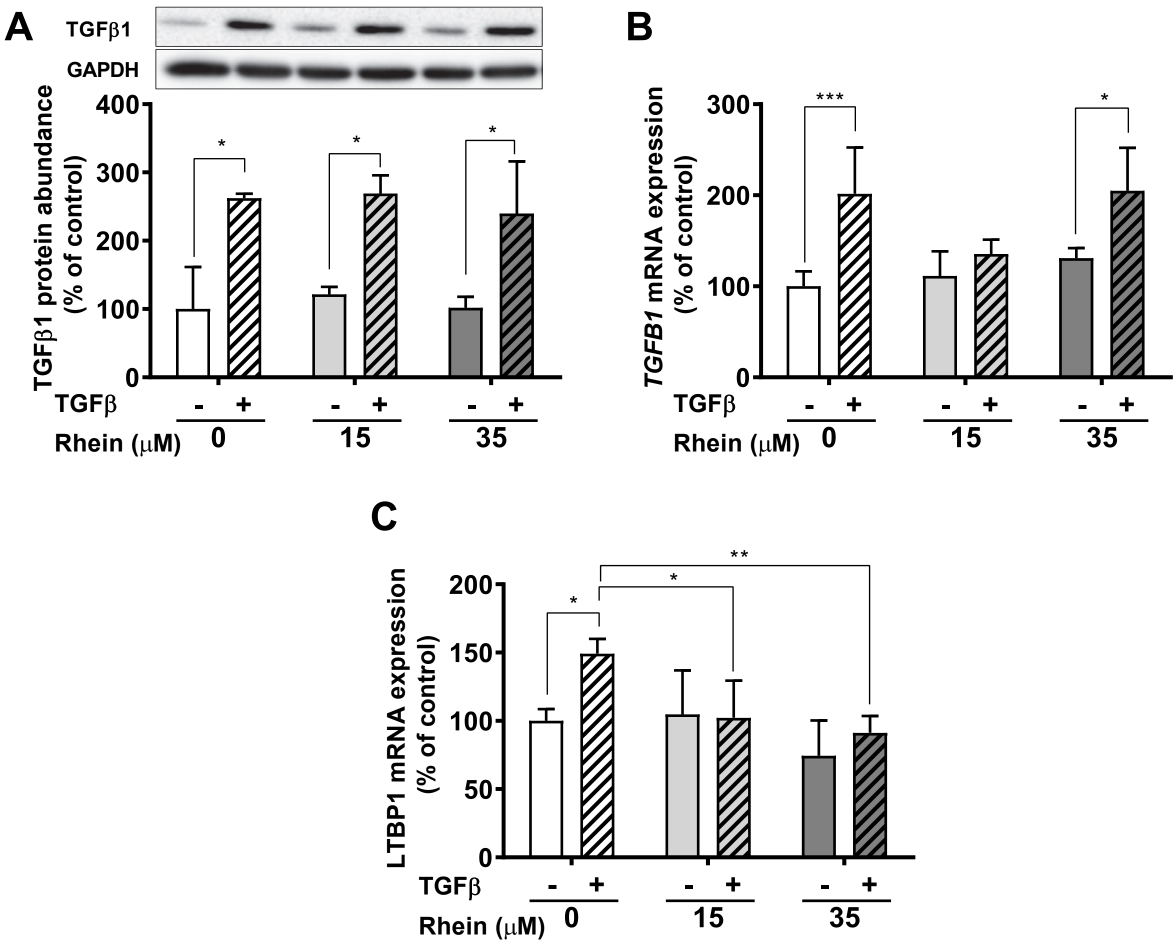

Figure 36: Rhein treatment does not modulate the TGFβ autocrine induction but decreases latent TGF binding protein 1 mRNA expression.

Primary human ventricular fibroblasts (HCF-v) were treated with 15 µM and 35 µM of Rhein alone or in combination with 10 ng/ml TGFβ1 for 24h. Expression levels of TGFβ1 and LTBP1 were assessed by (A) Western blot technique and/or (B, C) RT-qPCR analysis. Mean ± SD, n = 4, Two-way ANOVA statistical test, * $p < 0.05$, ** $p < 0.01$, *** $p < 0.001$ as indicated.

3.3.4 Rhein interferes with TGFβ1-SMAD signaling pathway

TGFβ1-mediated FMT is associated with the activation of the canonical SMAD-dependent TGFβ-signaling pathway. Herein, active TGFβ binding triggers the kinase TGFβR1 to phosphorylate SMAD2/3 complexes, which propagate the transcription of profibrotic genes. As part of the positive feedback loop and as shown before (0, Figure 34) TGFβ1 increases the levels of *TGFBR1*, to sensitize and enhance the signaling cascade. Accordingly, Western blot analysis revealed a trend towards accumulation of TGFβR1 protein upon TGFβ1-stimulation (Figure 37A), however, this trend was significantly mitigated when 35 µM Rhein was added to

TGFβ1-stimulated cells ($p < 0.05$). On transcriptional level, this observation was even more pronounced (Figure 37B) as indicated by a 2-fold increase of *TGFBR1* expression levels in TGFβ1-only treated ($p < 0.001$) and a significant decrease to baseline levels in 35 µM Rhein additionally treated cells. Most interestingly, comparison of untreated cells with cells treated with 35 µM Rhein but without TGFβ1 revealed a significant downregulation of *TGFBR1* transcripts by approx. 40% ($p < 0.05$).

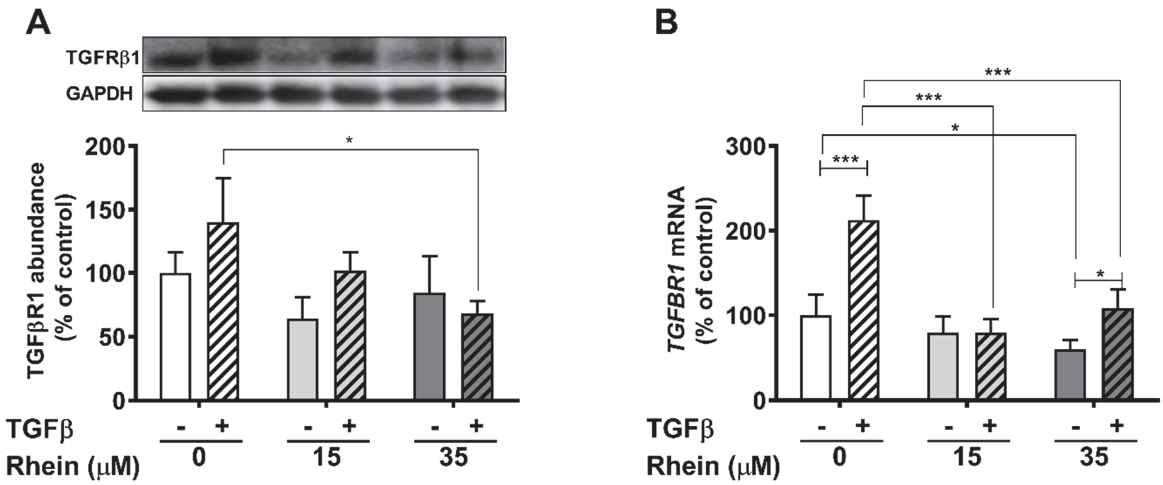

Figure 37: Rhein reduces TGFβR1 protein and gene expression.

HCF-v were treated with 15 µM and 35 µM of Rhein alone or in combination with 10 ng/ml TGFβ1 for 24h. TGFβR1 (A) and mRNA levels of TGFBR1 (B) were determined by Western blot analysis and via RT-qPCR, respectively. Mean ± SD, n = 4, Two-way ANOVA statistical test, * $p < 0.05$, *** $p < 0.001$ as indicated.

According to the observation of decreased abundance of TGFβR1 in cells treated with Rhein, it was examined whether the propagation of TGFβ signaling was impaired by analyzing the phosphorylation of the TGFβ receptor downstream target SMAD2. Therefore, HCF-v cells were pre-treated with low- and high-dose Rhein concentrations for 24h before cells were challenged for 30min or 1h with human recombinant TGFβ1 and phosphorylation was determined by Western blot analysis. As expected, short-term stimulation with TGFβ1 strongly increased phosphorylation of SMAD2 at Ser465/467 (Figure 38A+B), reaching its peak of action after 30 min. Rhein low-dose pre-treatment was sufficient to significantly decrease this peak of SMAD2 phosphorylation after 30min of TGFβ1 stimulation by 50% (Figure 38A), which was not further depressed by 35 µM Rhein (both $p < 0.05$). However, a marked difference between 15 µM and 35 µM Rhein treatment was noticed 1h after exposure to TGFβ1 (Figure 38B): While high-dose treated specimens continuously displayed a significant 50% decrease in TGFβ1-mediated SMAD2 phosphorylation ($p < 0.05$), 15 µM treatment was not able to significantly mitigate the signal propagation anymore.

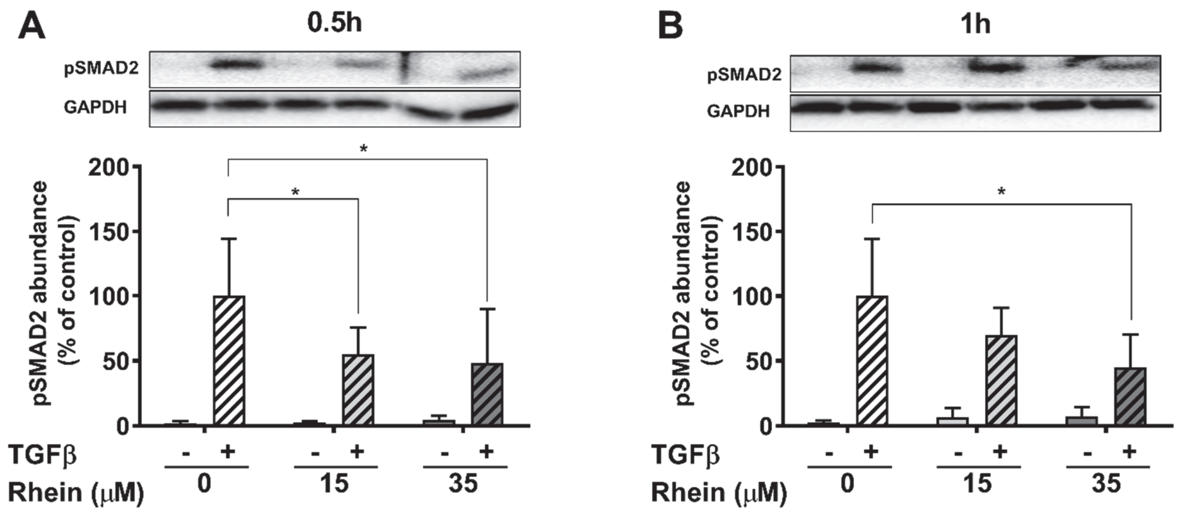

Figure 38: Rhein mitigates TGFβ/SMAD signaling.

HCF-v cells were incubated with Rhein for 24h prior exposure to 10 ng/ml TGFβ1 for 0.5 (A) and 1h (B), respectively. SMAD2 phosphorylation at Ser465/467 was determined by Western blot analysis and normalized to GAPDH as loading control. Mean ± SD, n = 4, Two-way ANOVA statistical test, * $p < 0.05$ as indicated.

3.3.5 Rhein upregulates endogenous SMAD-signaling inhibitor SMAD7 in a post-translational manner

The activity of the canonical SMAD-dependent TGFβ pathway is not only well-orchestrated by the positive feedback loop as shown in 3.3.4 (*TGFBR1* upregulation) but also comprises endogenous inhibitory regulation by the TGFβ1-mediated upregulation of inhibitory SMAD family member SMAD7. To test the implication of Rhein on this system SMAD7 mRNA expression and protein abundance were analyzed.

Stimulation of HCF-v cells with TGFβ1 for 24h expectedly activated the negative feedback loop marked by upregulation of *SMAD7* (Figure 39A) by 1.7-fold ($p < 0.01$) and a 1.6-fold increase of protein levels ($p < 0.05$) in comparison to untreated controls (Figure 39B). Treatment of cells in combination with Rhein, however, did not potentiate TGFβ1-mediated transcription (not significant) and exposure of cells to 15 µM or 35 µM Rhein alone did not affect mRNA expression either. Most interestingly, a Rhein-mediated dose-dependent SMAD7 protein accumulation in unstimulated cells was observed, displaying 2.5-fold higher protein levels in 35 µM Rhein treated cells ($p < 0.0001$). Administration of Rhein to cells treated with TGFβ1 showed a trend towards elevated protein abundance, although these observations were not significant (15 µM: p=0.1; 35 µM: p=0.08).

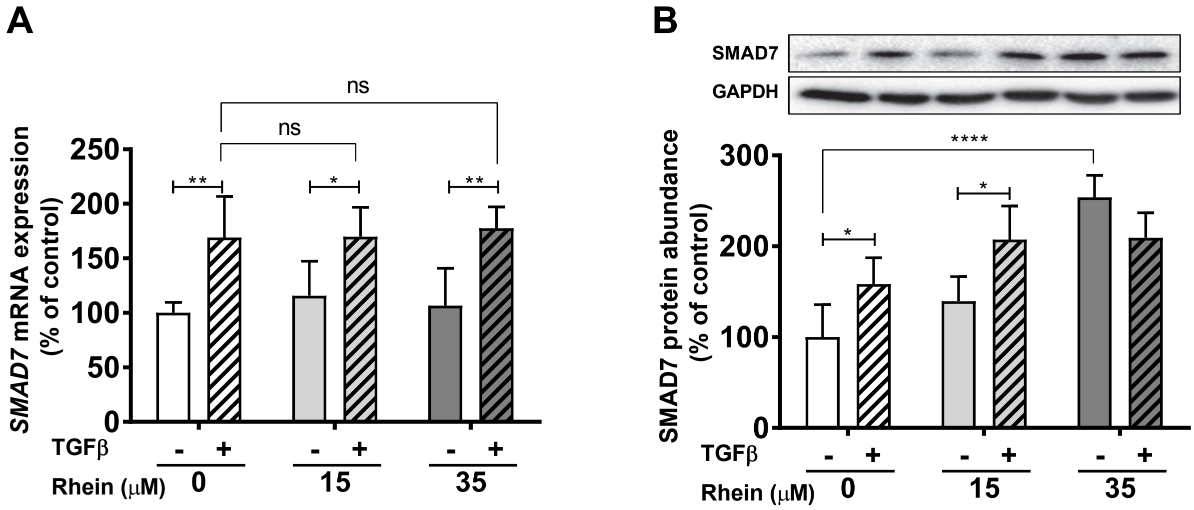

Figure 39: Rhein increases SMAD7 protein but not mRNA levels.

HCF-v cells were exposed to Rhein alone or combined with 10 ng/ml TGFβ1 for 24h. *SMAD7* mRNA expression (A) and protein abundance (B) were determined by qPCR analysis or Western blot, respectively. Mean ± SD, n = 4, Two-way ANOVA statistical test ns = not significant, * p < 0.05, ** p < 0.01, **** p < 0.0001 as indicated.

Given that Rhein treatment did not alter mRNA levels of *SMAD7*, but accumulation on the protein level was observed. To study whether SMAD7 is prone to acetylation or deacetylation in our system, the influence of respective inhibitors was studied and set into relation to Rhein treatment. First, the influence of nicotinamide (NAM), a commonly used SIRT inhibitor, on SMAD7 abundance was analyzed. Therefore, prior testing, a working non-toxic concentration of NAM was determined by treating HCF-v a dose range 0.1-10 mM for 24h (Figure 40A). Analogously to literature, viability of cells was not affected up to 10 mM NAM. Against expectations, inhibition of SIRT by 10 mM NAM did not affect SMAD7 abundance after 24h (Figure 40B), excluding sirtuins as mediators of Rhein-mediated SMAD7 accumulation. However, in this experiment Rhein-mediated SMAD7 enrichment was not significant and did not achieve previously observed magnitude.

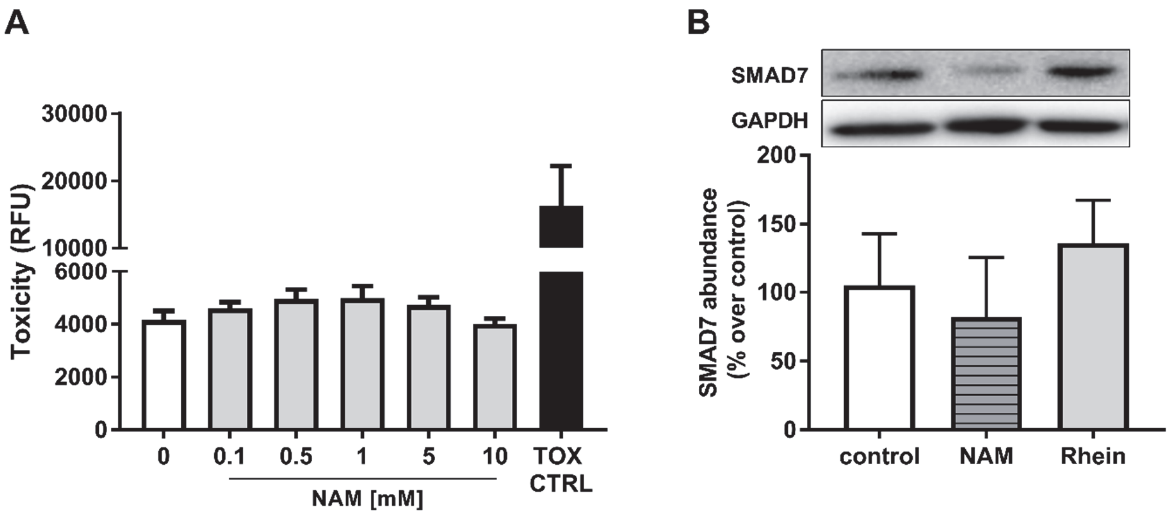

Figure 40: SIRT inhibitor nicotinamide does not affect SMAD7 abundance.
HCF-v were incubated with different doses (range 0.1-10 mM) of nicotinamide (NAM) and toxicity was determined after 24h using CellTox-green assay (A). HCF-v were exposed to 10 mM NAM or 35 µM Rhein for 24h (B). SMAD7 abundance was determined by Western blot and normalized to GAPDH as loading control. Representative blot is shown and abundance was plotted as % over control. Mean ± SD, n = 2-4

Next, it was tested if HAT inhibition using anacardic acid (AnA) would negatively affect SMAD7 abundance. Consequently, the maximum non-toxic concentration of AnA to employ for 24h on HCF-v was initially tested. In our study, 1 µM anacardic acid was found to be safe (Figure 41A) and used for the next experiment. The exposure of cells to HAT inhibitor AnA, did not display any effect on SMAD7 protein levels (Figure 41B).

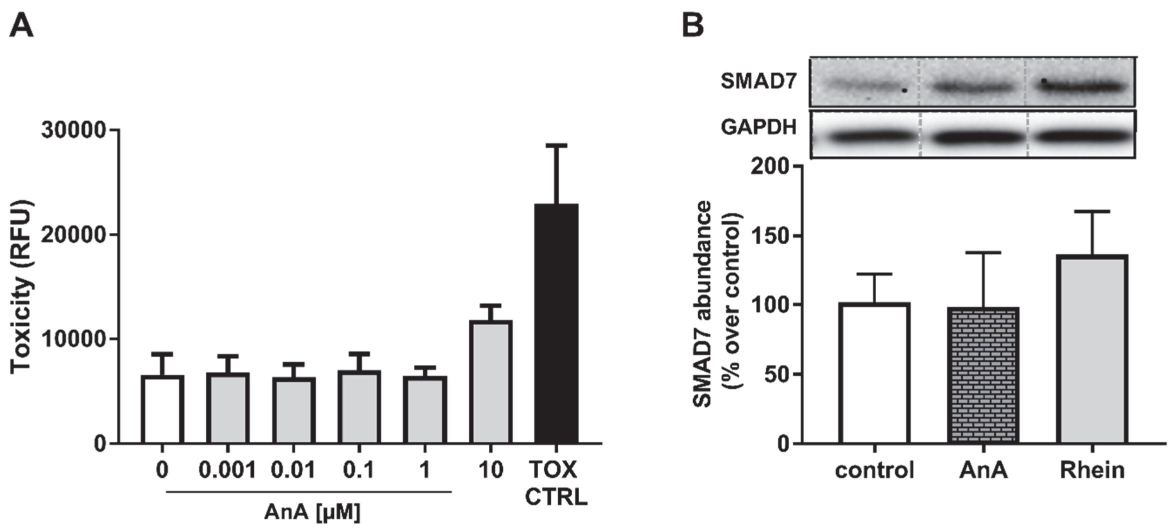

Figure 41: Inhibition of HAT by anacardic acid does not modulate SMAD7 protein abundance.

HCF-v were exposed to a dose range from 0.001-10 µM anacardic acid (AnA) for 24h and toxicity was assessed via CellTox-green kit (A). To determine SMAD7 abundance 1 µM anacardic acid or 35 µM Rhein were added to cells for 24h and lysates were measured using Western blot technique (B). SMAD7 was normalized to GAPDH and abundance is given as % over control. Mean ± SD, n = 2-4

Lastly, the effect of HDAC inhibition by sodium butyrate (SB) on SMAD7 was tested. As anticipated, HDAC inhibition effectively increased SMAD7 protein abundance by 1.5-fold ($p < 0.01$), whereas a 1.7-fold induction was reached after Rhein administration ($p < 0.01$). Considering that Rhein efficiently inhibited HDAC activity (3.2.5, Figure 28), this finding suggests Rhein to operate via HDACs to increased SMAD7 abundance.

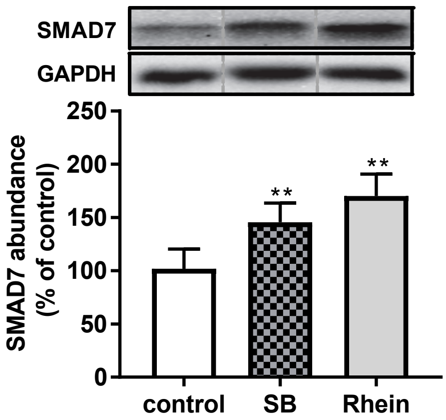

Figure 42: SMAD7 abundance increases upon HDAC inhibition via sodium butyrate.
HCF-v were treated with 1 mM sodium butyrate (SB) or 35 µM Rhein for 24h. SMAD7 protein abundance was determined by Western blot and normalized to GAPDH as loading control. A representative blot is shown and SMAD7 abundance is presented as % over control. Mean ± SD, n = 4, one-way ANOVA ** $p < 0.01$ as indicated.

3.3.6 Rhein inhibits collagen gel contraction and *de novo* synthesis of α-smooth muscle actin

According to the principle of *de novo* formation of αSMA fibers as distinct myofibroblast feature and source of the gain of contractile function, the collagen contraction assay was performed as functional assay providing information about the degree of FMT in relation to contraction.

Therefore, HCF-v cells were seeded into collagen gel lattices and treated for 5 days with 15 µM and 35 µM Rhein with or without TGFβ1 and gel size was assessed on day 0 and day 5 (Figure 43A). The incubation with TGFβ1 induced 3-fold contraction of collagen gels in relation to baseline (Figure 43B), which was significant in comparison to the contraction degree (2-fold) of untreated cell-populated gels ($p < 0.001$). Opposingly, a significant ($p < 0.001$) dose-dependent decrease of contraction was observed in Rhein treated gel lattices when compared to TGFβ1-incubated specimens. Notably, TGFβ1-mediated contraction in relation to respective unstimulated control was abolished upon administration of 15 µM (163% versus 208% to baseline) and 35 µM Rhein (133% versus 141% to baseline). Another interesting finding constituted the observation that untreated collagen gels experienced a diminution in size (Figure 43A), suggesting a general background differentiation when cells are exposed to experimental conditions. Most surprisingly, this degree of baseline FMT observed in untreated samples (208% to baseline) was significantly ($p < 0.001$) decreased in unstimulated cells exposed to 35 µM Rhein (133% to baseline).

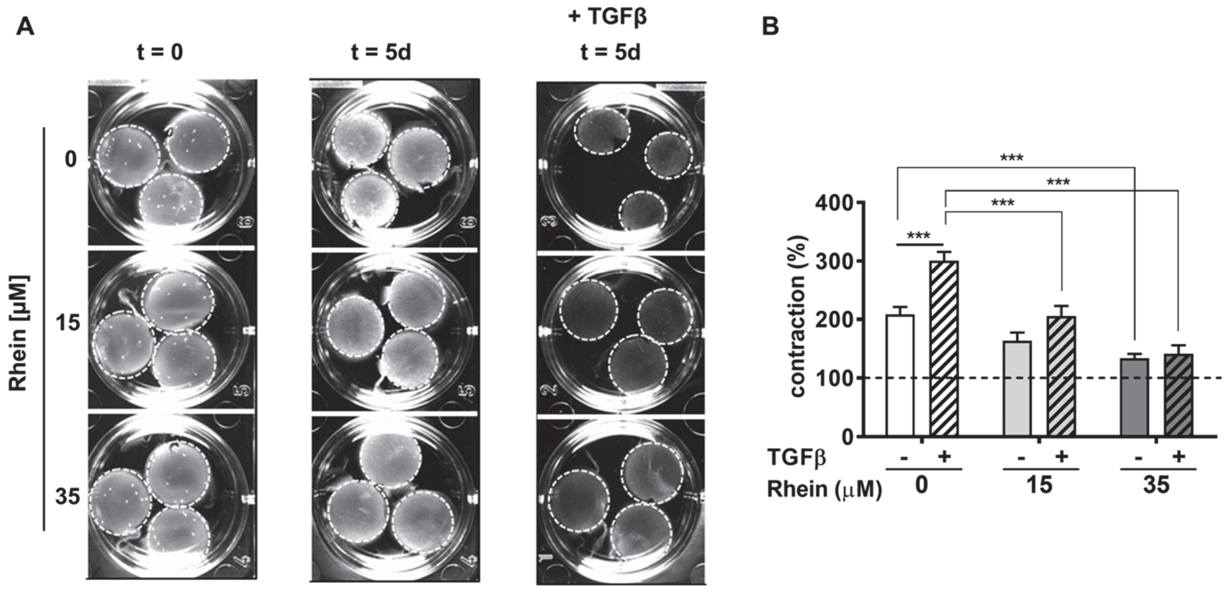

Figure 43: Rhein treatment inhibits TGFβ-induced collagen gel contraction.
Human ventricular cardiac fibroblasts (HCF-v) were embedded in collagen gel lattices and incubated with 15µM or 35µM Rhein alone or in combination with TGFβ1 10 ng/ml for 5d. Images of collagen lattices were taken at d0 and d5 (A) and relative contraction was calculated (B). Dashed line indicates baseline (start point at d0). Mean ± SD, n = 4, Two-way ANOVA, *** $p < 0.001$ as indicated.

To confirm the finding that decreased contractibility of cells treated with Rhein went in line with decreased abundance and expression of αSMA, Western blot and qPCR analysis was performed from cells treated with 15µM and 35µM of Rhein alone or in combination with TGFβ1 for 24h. The protein abundance of αSMA (Figure 44A) was dose-dependently decreased in stimulated cells additionally treated with 15 µM (153% versus 113%; $p < 0.05$) and 35 µM Rhein (153% versus 49%; $p < 0.0001$). Further, 35 µM Rhein completely abrogated the cellular response of TGFβ1-induced accumulation of αSMA. Similar observations were made in regard to transcription rates of αSMA (Figure 44B). Equally, Rhein treatment dose-dependently reduced TGFβ1-promoted induction of *ACTA2* by 1.7-fold at 15 µM Rhein and 3.5-fold at 35 µM. Moreover, the abrogation of TGFβ1-response to accumulation of αSMA was consistently found on transcriptional level in stimulated cell treated with 35 µM Rhein as well.

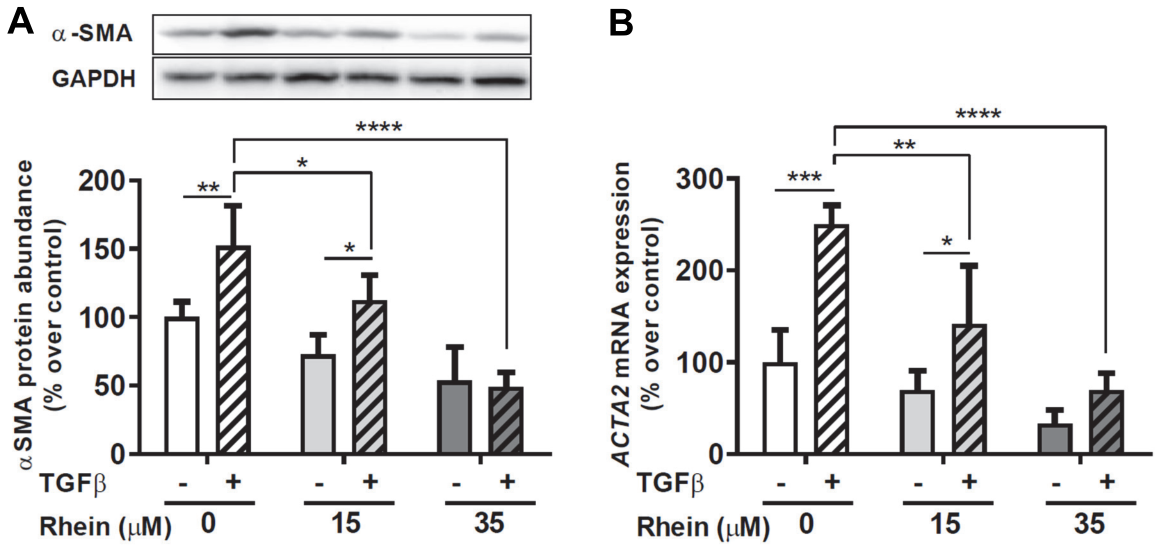

Figure 44: Rhein treatment attenuates TGFβ-induced transdifferentiation of HCF-v. Primary human ventricular fibroblasts (HCF-v) were treated with 15μM and 35μM of Rhein alone or in combination with 10 ng/ml TGFβ1 for 24h. Expression levels of α-smooth muscle actin were determined by (A) Western blot analysis (α-SMA) and (B) RT-qPCR (*ACTA2*). Mean ± SD, n = 4, Two-way ANOVA statistical test * $p < 0.05$ as indicated.

Taken together, Rhein was able to decrease TGFβ1-activated collagen contraction, which correlated with a Rhein-mediated decrease of αSMA.

4 Discussion

Heart failure accounts for the most deaths in both first- as well as third-world countries. A hallmark of heart failure is maladaptive cardiac remodeling following cardiac injury, which is characterized by dysregulated fibrosis. This process is mediated by the persistent differentiation of resident cardiac fibroblasts to myofibroblasts and their dissemination beyond the point of lesion towards the remote interstitial space.

The purpose of this thesis was to study the role of the rhubarb anthraquinone Rhein as anti-fibrotic agent in the setting of cardiac fibrosis. To address this question, an *in vitro* model of sustained hypoxia as physiological mediator of a profibrotic environment using primary human ventricular cardiac fibroblasts was employed. Herein, to understand the role of the pathological radiation of myofibroblasts in the context of paracrine as well as autocrine signaling, the impact of hypoxia and the potential intervention by Rhein on secretory profiles was investigated. Further, the influence of Rhein on the alteration of the cardiac fibroblast phenotype was elaborately studied by transcriptome analysis and set into relation to changes in the secretory profile. The present thesis provides evidence that Rhein prevents the differentiation of cardiac fibroblasts and the modulation of a pathological secretome under hypoxic conditions. Functionally, this study clearly ascribes Rhein a potent role as anti-fibrotic agent via inhibition of HDAC activity. Rhein-associated HDAC inhibition was identified in the regulation of p53 and increased p21 expression, resulting in the mitigation of hypoxia-induced proliferation. Further, Rhein was demonstrated to act as antagonist of the TGFβ/SMAD signaling via a HDAC inhibition-mediated mechanism involved in the stabilization of SMAD7. Individual findings and observations are further discussed in detail in the following sections.

4.1 Chronic hypoxia associates with alteration of HCF-v secretory profiles

The local intercellular crosstalk through different secretion profiles constitutes a possible mechanism driving the radiation of myofibroblasts from the point of lesion towards the remote interstitium. Chronic or prolonged periods of hypoxia have been hypothesized to be involved in adverse fibrosis, directly associating to changes of fibroblast behavior including the modulation of release factors secreted by CFs (Darby and Hewitson, 2016; Weber et al., 2012a; Weber and Diez, 2016). However, the connection between the impact of chronic hypoxia on secretome modulation and autocrine/paracrine induction of FMT have currently not been addressed, yet. To comparatively characterize the CF secretome under normal (normoxic) and pathological (hypoxic) conditions, the validity of the presently employed protocol was initially evaluated.

4.1.1 Establishment and quality control of secretome analysis approach

HIF1α is regarded the master regulator in response to hypoxic environment, essential for mediating adaptive reactions and is commonly used as marker for hypoxia (Le and Courter, 2008). Overrepresentation of HIF1α in tissues has been critically associated to fibrotic features (Darby and Hewitson, 2016; Distler et al., 2007; Liu et al., 2008b; Lokmic et al., 2012). The regulation of HIF1 activity is determined by the degradation or stabilization of the HIF1α subunit. Both subunits HIF1α and HIF1β are constitutively expressed and translated in all cells, but under normoxic conditions, HIF1α is posttranslationally hydroxylated by prolyl hydroxylases (PHDs) labeling it for ubiquitination by the pVHL (Von-Hippel-Lindau) ligase (Bruick and McKnight, 2001; Kamura et al., 2000). Following polyubiquitination, HIF1α is subsequently recruited to the proteasome and instantly degraded. Hypoxia however, limits O_2-dependent PHD-mediated hydroxylation of HIF1α resulting in rapid accumulation (Nakayama et al., 2004).

Accordingly, in the present study, HIF1α was used as positive marker for hypoxia. Following chronic hypoxia, cellular HIF1α protein abundance was significantly increased, demonstrating the cells were indeed experiencing a hypoxic environment and proving the validity of the presently employed protocol.

To verify the feasibility of the experimental workflow and the comparability between hypoxic and normoxic secretomes, quality of sample preparation was assessed using bioinformatic tools. Herein, SignalP identified secretory proteins with signal peptides traversing via the classical pathway (Petersen et al., 2011), while SecretomeP predicted proteins lacking the signal peptide, which are secreted through the non-classical pathway (Bendtsen et al., 2004). Computational analysis revealed indifferent proportional composition between the normoxic and hypoxic group, with approx. 50% of released factors identified as classically (SP+) and non-classically (SP-) secreted and the other 50% of proteins not associated with any know secretion pathway (NP). The latter possibly originated from exosomes that were explicitly not depleted in the preparation of secretomes. Cellular component analysis underlined this finding and revealed partial enrichment of proteins with intracellular character as they are often found in exosomes such as plasma membrane, endocytic pathway, and cytosolic proteins (Mathivanan and Simpson, 2009). Proteins passively released by dead cells into the media might mask and contaminate the actually secreted proteins impeding their genuine interpretation (Chevallet et al., 2007; Mukherjee and Mani, 2013). However, in both normoxic and hypoxic secretomes the analyses identified extracellular components as most significant overrepresentation, supporting the feasibility of this approach and negligible abundance of cell debris in the procedure. Furthermore, these findings indicate, that both oxygen conditions display comparable secretome complexities.

4.1.2 Chronic hypoxia-mediated modulation of HCF-v secretome associates with differential pathway regulation

After proving the feasibility of the present experimental setup, the impact of hypoxia on the secretory profile of CFs, was studied by differential secretome analyses and characterization using proteomic and bioinformatic approaches. The present comprehensive study clearly ascribed hypoxia a role as driver of CF behavior alterations and modulator of secretory profiles. As a novelty, these data factually described the hypoxic CF secretory profile as contextual result of glucose metabolism, ECM synthesis and ER stress.

Correspondingly, the cellular component composition analyses of differential secretomes revealed most significant enrichment of proteins of extracellular, exosomal or secretory vesicle character. This finding confirms that the differential secretory profile consists of proteins that are indeed actively secreted in a multiple secretion pathway fashion. Further, *in silico* characterization of the differential secretome's molecular and biological function demonstrated enrichment of the GO terms extracellular matrix protein, metalloprotease and hydrolase associating with catalytic modulation of ECM. These findings are in line with the report by Cosme et al. (2017), concluding that in the secretomes of murine CFs exposed to hypoxia, particularly ECM proteins were upregulated including multiple collagen types, perlecan and fibronectin (FN1). Furthermore, differentially abundant proteins showed high correlation with catabolic process-involving glycolysis and carbohydrate metabolism, pointing towards an alteration of glucose metabolism during chronic hypoxia. This observation is consistent with the physiological shift of cells towards a glycolytic phenotype in response to the absence of sufficient oxygen levels to enable oxidative metabolism (Bartrons and Caro, 2007; Essop, 2007; Heather and Clarke, 2011), mediated by HIF1α accumulation and activation of glycolysis-related proteins (Fulda and Debatin, 2007; Kim et al., 2006; Zhou et al., 2008). Expectedly and in support of these findings, canonical pathway analysis also detected predominant involvement of metabolism-related pathways. Herein, particularly the glucose metabolism-associated pathways glycolysis, gluconeogenesis and TCA-cycle were highly significant, playing a crucial role in the preservation of energy homeostasis under hypoxic conditions (Mirtschink and Krek, 2016; Robin et al., 1984). Besides contribution of glucose metabolism to the modulation of the hypoxic CF secretome, inhibition of matrix metalloproteases was predicted to be involved, which has been associated to ECM accumulation (Bonnema et al., 2007; Li et al., 2000), a key feature of fibrosis. Other predicted affected pathway branches constitute translational regulation and ER stress involving mTOR and EIF2 signaling, which have been reported to be activated under prolonged hypoxia, leading to the repression of mRNA translation and unfolded protein response (Koritzinsky et al., 2006; Liu et al., 2006; Spriggs et al., 2010). This represents a major protective strategy to maintain energy metabolism under challenging conditions (Storey and Storey, 2004; Wouters et al., 2005).

Of further interest, using bioinformatical upstream regulator analysis for the prediction of robust molecular mediators linking these potentially affected pathways and the differentially abundant proteins, TGFβ1, a potent inducer of cardiac fibrosis (Meng et al., 2016), was identified. This observation will be further discussed in the next sections.

4.2 Rhein inhibits FMT and leads to modification of secretory and transcriptomic profiles

4.2.1 Rhein administration prevents FMT under normoxic and hypoxic conditions

The data of this thesis provided primary evidence, that Rhein also exerts anti-fibrotic actions in the setting of cardiac fibrosis. The impact of Rhein on FMT was investigated under both normoxic and hypoxic conditions. The presently utilized non-toxic concentration of 35µM Rhein was within the range reported by other Rhein studies (range 1-100µM, (Zhou et al., 2015)). The key finding that exposure to Rhein substantially reduced αSMA protein abundance in HCF-v was in line with several observations made in other tissues (Martin et al., 2003, 2004; Sanchez et al., 2003; Sheng-Nan et al., 2013; Tsang and Bian, 2015; Tsang et al., 2013b). Interestingly, this effect was observed in an oxygen condition independent fashion. Together with the finding that Rhein administration displayed no differential effect on HIF1α stabilization, at this point one could propose the Rhein effect to be unrelated to HIF1 signaling.

In cell culture, several studies indicated that both acute hypoxia (24-72h) and prolonged hypoxia (4-8d) enhanced fibroblast activity including ECM remodeling, increased profibrotic gene transcription and, most interestingly, directly initiated FMT marked by pronounced αSMA expression (Clancy et al., 2007; Gao et al., 2014; Misra et al., 2010; Ugolini et al., 2017; Watson et al., 2014). Further, the evidence of hypoxia-induced pro-fibrotic changes was confirmed in human cardiac biopsies, in which the degree of hypoxia was positively correlated with collagen I and αSMA expressions (Watson et al., 2014). Although the present study employed a similar protocol using the same cell system and the exposure period of 4d as reported by Watson et al. (2014), chronic hypoxia did not significantly affect αSMA and even showed a slight trend to decreased protein abundance. A possible explanation for this discrepancy could be the use of 0.5% O_2 tension instead of 1% O_2 or the employment of different culture conditions (media, cell density, etc.), which were not further specified in the author’s publication. Considering a report demonstrating that more severe conditions, such as anoxia, repressed HIF1 transcriptional activity (Schmid et al., 2004), at this point one could also speculate that the slight reduction of αSMA is also in part due to HIF1 transcriptional repression.

4.2.2 Rhein modulates normoxic and hypoxic secretomes and affects fibrosis-associated pathways

The present thesis reported a potential role of Rhein as modulator of CF behavior and CF secretory profiles. *Partial least square-discriminant* analysis demonstrated clear delineation between the 4 conditions and a modulatory shift of the secretomes of both normoxic and hypoxic cells in the presence of Rhein. To further elucidate the processes underlying the condition-dependent modulation of the secretomes, two bioinformatic approaches were selected. On the one hand, a comprehensive analysis of pathways responsible for the distinct secretory profiles from differential proteins solely found within a comparison set was performed. Individual pathway analysis ascribed a particular implication of translational control pathways and proteoglycan biosynthesis in the differential modulation between N vs H secretomes, which is in line with previous reports in chondrocytes, macrophages and corneal fibroblasts (Asplund et al., 2010; Lee et al., 2011; Pfander et al., 2003). Although, the inserted lists were comprised of different proteins uniquely found in respective comparison, individual analysis of both N vs NR and H vs HR, predicted association with fibrosis-related pathways, strongly ascribing Rhein a role independent of the environment. Interestingly, specific discrepancies between HR vs NR, consisted predominantly of metabolic pathways, presumably mirroring the pure metabolic influence of chronic hypoxia on CFs. Notably, in all conditions *TGFB1* was predicted from the individual protein sets, respectively, pointing towards a general engagement. Furthermore, *TP53* stood out and was robustly associated with solely differential proteins in both Rhein-involved comparisons N vs NR and H vs HR. Both findings support already published work, showing the interaction between Rhein and TGFβ1 (Guo et al., 2002; He et al., 2011; Peng et al., 2013; Tsang and Bian, 2015) and p53 (Hsia et al., 2009; Panigrahi et al., 2015; Zhao et al., 2014), collectively proving the functionality of Rhein and its action in the presently applied system.

The second bioinformatic approach concentrated on the exploration of pathways playing a global role in the context of chronic hypoxia and intervention via Rhein administration. Cumulatively, data provided evidence that several pathways involving ER stress, translational regulation, glucose metabolism and ECM modulation most significantly contribute to the modulation of respective differential secretomes. Noteworthy, with exception of the ER stress- and translational regulation-related pathways, in the comparison group NR vs HR commonly identified pathways yielded relatively low p-values, suggesting marginal importance of these pathways in the discrimination between these phenotypes. Also, this might indicate a more similar phenotype between both Rhein treated conditions and a more pronounced impact of

Rhein over the global influence of hypoxia alone. Of particular interest, upstream analysis from the cumulative perspective, again identified TGFβ1 and p53 as confident mediators in the orchestration of the secretory profiles confirming the previous observations.

Collectively, these data identify a pharmacological role of Rhein in the alteration of the hypoxia-induced secretome, potentially preventing the paracrine and autocrine dissemination of profibrotic signals. In this context, TGFβ1 and p53 might play a central role.

4.2.3 Rhein attenuates profibrotic transcriptome and potentiates transcription of HIF1α targets

The activation of cardiac fibroblasts to myofibroblast features the induction of several genes to promote proliferation, differentiation, migration and cytokine release (Schuetze et al., 2014; Travers et al., 2016). Aside of αSMA as main marker of mature myofibroblasts, other genes including cytokines, ECM components such as collagens and proteoglycans and ECM interacting enzymes like integrins, MMPs and their inhibitors TIMPs (Frangogiannis, 2012; Kong et al., 2014; Porter and Turner, 2009) are activated and may be used as marker of myofibroblast activity.

In the present study, chronic hypoxia induced the expression of representative genes of the profibrotic response program. For example, *CTGF* – a cytokine highly associated with cardiac fibrosis (Lipson et al., 2012) and marker of myofibroblast activity (Dorn et al., 2018) – was significantly upregulated under hypoxic conditions. Further, the transcription of osteoglycin (*OGN*), a proteoglycan linked to increased proliferation and cardiac diseases (Deckx et al., 2016; Zuo et al., 2018) was increased, along with elevated levels of integrin-8α (*ITG8A*), a cell surface receptor, which acts in both cellular adhesion/signaling and ECM interaction (Chen et al., 2016). Although, expression of collagen I and III, the predominant collagen forms in the fibrotic heart (Ely et al., 2010; Fan et al., 2012), were only slightly elevated, the observed reduced *MMP1* and upregulated *TIMP3* levels suggest an overall increased accumulation of ECM products due to elevated TIMP/MMP ratios as described elsewhere (Polyakova et al., 2011).

The key findings involving tremendously reduced expression levels of αSMA, CTGF, collagen I and III in the presence of Rhein, support its effect in the prevention of pathologic ECM accumulation as reported in other tissues (Guo et al., 2002; Su et al., 2013). Another new insight, reveals the opposite regulation MMP and TIMP after Rhein treatment under normoxic conditions as compared to chronic hypoxia, reportedly resulting in relativization and restoration of the hypoxia-mediated TIMP/MMP imbalance promoting preservation of the ECM status (Polyakova et al., 2011). Overall, addition of Rhein during prolonged hypoxia resulted in strongly opposing regulatory effects, supporting the potential therapeutic role of Rhein as anti-fibrotic compound.

Upon hypoxia-triggered HIF1α stabilization, HIF1 heterodimers are capable to translocate into the nucleus and in cooperation with co-factor p300 to exert transcriptional activity binding to genes carrying hypoxia response elements (HREs) (Jiang et al., 1996). In the present study, chronic hypoxia induced transcription of *SLC2A1* (GLUT1), phosphoglycerate kinase 1 (*PGK1*) and lactate dehydrogenase A (*LDHA*), genes associating with glycolytic metabolism and HIF1α activity (Benita et al., 2009; Semenza, 2012). HIF1 also targets the transcription of factors that increase the distribution of oxygen supply such as angiogenic *VEGFA* (Dengler et al., 2014; Takeda et al., 2004), which was also promoted following hypoxic treatment. Consistent with the precedent finding of hypoxia-driven HIF1α stabilization, these observations actually prove HIF1α transcriptional activity and underline the validity of the employed hypoxia protocol. The presence of an HRE in the core promoter sequence of *HIF1A* allows for its autoregulation by the HIF1 transcription factor during hypoxia (Asby et al., 2014; Minet et al., 1999). Contrarily, this was not the case in the present study, indicated by downregulation under hypoxic conditions, a feature thought to evolve from additional regulatory mechanisms under prolonged forms of hypoxia (Lafleur et al., 2014; Schmid et al., 2004; Uchida et al., 2004).

Surprisingly, the presence of Rhein under hypoxic conditions even potentiated the transcription of HIF1α targets, indicating enhancement of HIF1α transcriptional activity aside from oxygen-dependent pathways (Lisy and Peet, 2008). Of utmost interest, Rhein administration under normoxia also displayed activation of hypoxia-induced targets in the absence of HIF1α accumulation. This novel observation leads to the hypothesis that, at least in part, Rhein mimics metabolic adaptation to hypoxia independently from HIF1α, accrediting Rhein a potential role as preconditioning agent in the protection of cells from hypoxia-induced injury (Zhuonan et al., 2015).

4.2.4 Rhein administration modulates transcriptomic signatures and interferes with fibrosis-associated pathways

Transcriptome analyses using microarray- or sequencing-based technologies, allow the generation of comprehensive gene expression profiles of cells under pathological and experimental conditions (Casamassimi et al., 2017; Kukurba and Montgomery, 2015). Although upregulated secretory products may be independent of elevated mRNA levels (Eichelbaum and Krijgsveld, 2014; Shimwell et al., 2013), global secretory alterations might be the result of differential gene expression profiles affecting regulatory pathways. Thus, transcriptome assessment constitutes a complementary approach to secretome analysis, reflecting the intracellular status of cells. The combination of both, secretome and transcriptome, but also transcriptome analysis alone, enables a more accurate picture of underlying pathways. Consequently, in the present thesis the determination of transcriptomic changes in the context of chronic hypoxia and Rhein intervention was conducted. Herein, a special focus was laid on the revelation of overlapping pathways correlating between the differential secretome and the transcriptome, but also on the determination of 'transcriptome-only' pathways.

In analogy to the secretome analysis, solitary differential transcripts consistently revealed similarly regulated pathways related to hypoxic metabolism, translational control and fibrosis for respective comparison groups. Further, in agreement with observations made in solitary secreted proteins, again the bioinformatic tool IPA® predicted *TP53* and *TGFB1* as solid upstream mediators. These findings allow for the speculation that both chronic hypoxia and Rhein treatment interfere with the transcriptome. Furthermore, this justifies the direct correlation between transcriptomic changes and alteration of the secretory profiles.

Global transcriptomic analysis indicated that pathways identified in the secretome were also differentially regulated on gene expression level, presenting overlaps in regulated pathways involved in hypoxic metabolism, translational regulation and fibrosis. Interestingly, glycolysis and gluconeogenesis scored the highest cumulative significance, although mostly the comparisons between hypoxic and normoxic conditions accounted for the high p-value. Together with the findings in differential secretomes, this may indicate glucose metabolism as minimal and essential pathway in cells undergoing chronic hypoxia independently from Rhein treatment. In this context, *MYC*, which was predicted as upstream regulator, might be involved in the activation of glucose metabolism as indicated in several publications (Dang; Miller et al., 2012; Stine et al., 2015). Furthermore, *MYC* associates with regulation of HIF1α activity (Doe et al., 2012), which depicts a possible mechanism of Rhein in increasing hypoxic target transcription under normoxic conditions. On the other hand, according to the p-values of both secretome and transcriptome analysis, fibrosis-related pathways seemed to play a particular role in the Rhein-treated conditions, which also associated with *TGFB1* as predicted mediator. Apart from high coverage of pathways identified, the global approach using total differential transcript lists enabled the revelation of mitotic roles of polo-kinases, ATM and p53 signaling and most interestingly G2/M checkpoint regulation to significantly participate in the phenotype modulation. These pathways are associated to collectively contribute to the regulation of proliferation and cell cycle. Computational analysis also predicted *CDKN1A* (p21) together with p53 as upstream regulators, which might be implicated as key mediators of those pathways (Lin et al., 2011; Yang et al., 2010; Yosef et al., 2017).

4.2.5 Rhein mitigates chronic hypoxia-mediated cell cycle progression and proliferation

Proliferation of myofibroblasts is a key feature of wound healing and adverse fibrosis (Bagalad et al., 2017; Baum and Duffy, 2011b; Fan et al., 2012; Kong et al., 2014; Weber et al., 2012b). In the present study, the expression of gene markers related to proliferation (Fu et al., 2018; Whitfield et al., 2006), showed dramatically increased levels of *MKI67* and other genes under hypoxic conditions. An interesting finding was, that the hypoxia-induced expression of proliferation markers was inhibited in the presence of Rhein. Consistent with other reports, the association of increased proliferation rates and hypoxia was demonstrated in cardiac (Gao et al., 2014) and pulmonary fibroblasts (Das et al., 2008; Senavirathna et al., 2018; Wilson et al., 2015). The key observation, that Rhein inhibits expression of proliferation markers strongly ascribes Rhein a novel anti-proliferative property in regard to cardiac fibrosis, supported by reports in the context of cancer (Aviello et al., 2010) and scar fibroblasts (Wang et al., 2012b).

In the present study, hypoxia increased the expression of negative regulators of the G2/M checkpoint, suggesting increased cell cycle progression and confirming observed elevated proliferation marker expression. Constituting a novel finding, in the presence of Rhein this hypoxia-mediated effect was abrogated and under normoxic conditions, Rhein administration even promoted the expression of positive regulators. The switch between cell proliferation and cell cycle arrest is defined by a sensitive balance between a variety of direct and indirect negative and positive regulators (Hanahan and Weinberg, 2011; Hasvold et al., 2016). The alteration of G2/M checkpoint, which terminally decides the transition of a cell from a quiescent to proliferative state, has been shown to be modulated by hypoxia (Hasvold et al., 2016). Thus, Rhein-mediated opposite regulator expression indicates a prolongation of the G2/M phase. Most interestingly, Rhein induced the expression of *CDKN1A*, a well-known regulator of the cell cycle, which functions as inhibitor of cyclin-dependent kinases promoting the arrest of cell cycle progression (Dutto et al., 2015; Gartel et al., 1996). This key finding is underlined by a previous report, where Rhein-mediated suppression of proliferation in chondrocytes was associated to increased p21 levels (Legendre et al., 2009). Another prominent contributor to G2/M cell cycle arrest is p53, protecting cells from entering mitosis with damaged DNA by activation of DNA repair mechanisms (Taylor and Stark, 2001). Contrarily, depletion of p53 leads to cell cycle progression and promotes the entrance into the mitotic phase. Although p53 was multiply predicted as robust upstream regulator throughout all conditions, *TP53* mRNA levels were not affected in any experimental group. However surprisingly, p53 protein levels, were increased under normoxic conditions in the presence of Rhein, in line with other reports (Hsia et al., 2009; Ip et al., 2007; Kuo et al., 2004; Panigrahi et al., 2015; Zhao et al., 2014). Similarly, elevated p21 protein levels in Rhein-treated normoxic cells were found, and together with the increased *CDKN1A* mRNA expression, this supports the well-known fact that p53 is a transcriptional regulator of p21 (Beckerman and Prives, 2010). In another study, moderate hypoxia (2% O_2) was found to increase the proliferation of normal human lung fibroblasts through the suppression of p21 without affected p53 abundance (Mizuno et al., 2009). Collectively, these findings indicate that transcriptional activity of p53 might be involved in the Rhein-induced upregulation of p21.

Interestingly, HDACs have been demonstrated to be implicated in the cell cycle regulation of cardiac fibroblasts and inhibition resulted in decreased proliferation by induction of cell cycle arrest-associated proteins such as p53 and p21 (Nural-Guvener et al., 2014; Schuetze et al., 2017; Williams et al., 2014). Actually, it has been reported that acetylation of p53 at lysine K382 by HDAC inhibition increases p53-dependent p21 expression (Condorelli et al., 2008; Taniguchi et al., 2012; Wang et al., 2012a; Zhao et al., 2006). In the present study, comparable to effects of HDAC inhibition using the reference inhibitor SB, application of Rhein indeed significantly increased both p21 and p53 protein abundance. Of utmost interest, this key finding implicatively alludes to the novel possible connection between HDAC inhibition and Rhein. However, to confirm this assumption final proof would be required by HDAC knockdown or knockout studies. Although, acetylation of p53 at lysine K382 was shown to be increased by Rhein when normalizing to GAPDH as loading control, normalization of acetyl(K382)-p53 ratios to p53 ratios demonstrated equalized levels. On the one hand, this result could point towards a correlation between increased acetylation and posttranslational p53 stabilization (Muñoz-Fontela et al., 2011; Reed and Quelle, 2014; Tang et al., 2008). In this concern further investigation will be required, e.g. by immunoprecipitation studies employing antibodies against acetyl-lysine, to rule out whether the fraction of acetylated p53 is increased following Rhein treatment. On the other hand, increased mRNA translation could be responsible for the higher protein abundance. Still, as long-term Rhein treatment did not affect p53 mRNA levels, this explanation seems only likely in the case of an improved translational efficiency.

Altogether, these data highlight the hypoxia-mediated shift towards negative G2/M regulation, which is counteracted and rebalanced by Rhein treatment via differential regulation of positive regulator and normalization of negative regulator gene expression. Further, this study identified, p21 and p53 as most likely effectors in the Rhein-mediated inhibition of pathologic proliferation, presumably in a HDAC-dependent manner.

4.2.6 Rhein inhibits HDAC and SIRT activity, but does not affect HAT and MeT activity

The involvement of epigenetic and posttranslational modifications in the development of cardiac fibrosis has recently attracted substantial interest, adding a novel perspective to the mechanistic comprehension of the disease (Grimaldi et al., 2017). Herein, especially acetylation and DNA methylation have become a central focus of investigation. However, the implication of Rhein as modulator of these regulators has not been addressed yet. Therefore, the role of Rhein in the interaction with the predominant PTMs present in the setting of fibrosis were explored.

The present thesis demonstrates for the first time that Rhein directly inhibits HDAC and SIRT enzymatic activity. While inhibition was not permanent as shown in lysates of long-term Rhein treated cells, the acute application of Rhein on lysates and its presence during the assay performance strongly reduced respective activities. Supported by the observation that expression of HDACs and SIRTs was unchanged and that their enzymatic activity was seemingly restored as Rhein was excluded during the measurement, this implicatively indicates Rhein as immediate and reversible inhibitor. Interestingly, Rhein even exhibited a higher inhibitory potency for HDAC and SIRT than the presently used specific inhibitors SB and NAM, respectively.

Eventually, HDAC inhibition has drawn a lot of interest and different HDAC inhibitors are currently investigated in clinical trials (Yoon and Eom, 2016). In basic research for example, *in vivo* treatment of rats with valproic acid or tributyrin for 4 weeks revealed attenuation of cardiac fibrosis when administered 24 h after coronary artery ligation-mediated MI (Lee et al., 2007). In a streptozotocin-induced diabetic mouse model, *ad libitum* treatment with sodium butyrate (SB), a potent HDAC inhibitor, was reported to reduce diabetes related cardiac remodeling (Chen et al., 2015b). Furthermore, it was shown that the pan-HDAC inhibitor trichostatin A (TSA) blocks αSMA induction associated with reduced activation of Akt in lung fibroblasts (Guo et al., 2009) and inhibits TGFβ1-induced collagen synthesis in cultured rat cardiac fibroblasts (Yu and Xu, 2015). Administration of MGCD0103 even demonstrated reversion of αSMA expression in $CD90^{+}/cKit^{-}$ cardiac fibroblasts (Nural-Guvener et al., 2014). Similar findings were made in SIRT6-knockdown rat fibroblasts revealing promoted Ang II-stimulated differentiation of cardiac fibroblasts into myofibroblasts via activation of NF-κB signaling (Tian et al., 2015). Inconsistently, specific inhibition of SIRT1, however, diminished the protective effects of L-arginine against myocardial fibrosis in streptozotocin-induced diabetic rats (Rizk et al., 2014).

HATs, exhibiting acetylase activities, depict the counterpart of deacetylating enzymes. The interplay between both HAT and HDAC (including SIRT) activity results in a dynamic balance in the acetylation state of non-histone proteins and provides a major contribution to the modulation of signaling pathways. In this thesis, although expression was unaffected, global HAT activity was decreased under hypoxic levels, a novel observation which has not been reported yet, leaving the underlying mechanism to be deciphered in the future. Based on these observations and under consideration of unchanged HDAC enzyme activity under hypoxia, one can speculate that global acetylation levels might be lowered leading to destabilization of proteins susceptible to proteasomal degradation. A contrary example of such an effect associated with HAT activity is the p300-mediated acetylation and subsequent stabilization of SMAD7 at Lys64 and Lys70 conferring resistance to ubiquitination and degradation (Gronroos et al., 2002). Contrarily, HDAC1 (Simonsson et al., 2005) and SIRT1 (Kume et al., 2007) deacetylate SMAD7 facilitating its ubiquitylation and therefore negatively affecting its stability and activity as TGFβ signaling inhibitor. On the other hand, studies in cultured fibroblasts have also revealed a pro-fibrotic role for HATs. Knockdown of p300 in cultured fibroblasts (Bhattacharyya et al., 2005) or inhibition of HAT catalytic activity of PCAF, p300 and Tip60 by anacardic acid (AnA) was shown to significantly blunt TGFβ1-mediated profibrotic gene expression (Ghosh et al., 2013). Given their opposing catalytic reactions it seems paradox that either HAT or HDAC inhibitors block fibrosis. An explanation might be, that HDAC inhibition results in global alteration of the histone acetylation state, while HAT inhibitors feature more restricted manipulations in histone acetylation (Stratton and McKinsey, 2016). Interestingly, HAT activity was also decreased lysates of cells that experienced long-term Rhein treatment. Though, considering that Rhein did not display any direct interference when present during the HAT activity assay and compared to specific inhibitor AnA, it is tempting to speculate that this effect is secondary. Conceptively, this effect could evolve from a Rhein-mediated stably downregulated co-factor required for proper HAT function. Concluding, these findings implicate a secondary mechanism regarding the influence of Rhein on HATs, rather than an imminent effect on HAT enzyme activity itself.

DNA hypermethylation has also been linked to chronic hypoxia and myofibroblast differentiation (Robinson et al., 2012; Watson et al., 2014; Yao and Li, 2015). Accordingly, exposure of CFs to chronic hypoxia resulted in sustained methyltransferase activity, however contrarily, protein levels of DNMT1, one prominent effector of DNA methylation, were unaffected following hypoxic exposition. While DNMT1 plays a pivotal role in the maintenance of DNA methylation, DNMT3A and DNMT3B effectuate *de novo* methylation (Clements et al., 2012), suggesting that maybe these factors are upregulated and contribute to the increased methyltransferase activity. Most interestingly, DNMT1 protein was significantly decreased following Rhein treatment, although *DNMT1* mRNA expression was unaffected, which further empowers the implication of Rhein in posttranslational mechanisms. To finally clarify, whether elevated methyltransferase activity was attributed to increased DNA methyltransferase activity, the methylation of CpG sites within the HIF1α hypoxia response element (Asby et al., 2014; Minet et al., 1999) was exemplarily determined. Surprisingly, neither hypoxia nor Rhein treatment displayed any effect on the degree of CpG methylation. A possible explanation constitutes that other genes could be affected, that have not been investigated in this thesis. Another assumption is that since the employed activity assay does not discriminate between DNA, RNA or protein methyltransferases, increased global methyltransferase activity could just as well be attributed to any other kind of methyltransferases. Conclusively, these findings suggest that in this case activities of MeTs other than DNA-methyltransferases were affected by hypoxia and that DNMT1 abundance was secondarily downregulated by Rhein.

4.2.7 Rhein administration decreases TGFβ1 bioavailability by decreased secretion and intracellular sequestration

The central role of TGFβ1 in the pathogenesis of cardiac fibrosis has been already adequately recognized (Edgley et al., 2012; Kane et al., 1991; Liu et al., 2017). In the present study, its implication in the modulation of the secretome and transcriptome has been emphasized, since TGFβ1 was multiply predicted as upstream regulator. Elevated levels of active TGFβ1 by higher secretion and activation is associated with fibrosis (Fan et al., 2012; Travers et al., 2016). Cardiac fibroblasts contribute to the synthesis of TGFβ1, and its increased bioavailability promotes FMT by paracrine and autocrine signaling (Bomb et al., 2016). The measurement of active TGFβ1 is lowly reliable due to low sensitivity of ELISA (Khan et al., 2012), especially in combination with cell culture supernatants containing low levels of TGFβ1. Thus, since TGFβ1 is produced and secreted bound to the latency-associated peptide (Dubois et al., 1995), LAP measurement via ELISA depicts a surrogate approach to estimate the potential bioavailability of TGFβ1. To prove evidence, whether Rhein effects are indeed attributable to TGFβ1, the regulation of TGFβ1 secretion in the context of hypoxia was studied.

A key finding in the present study was that LAP levels in the supernatant were substantially decreased after Rhein treatment of both normoxic and hypoxic cells. Surprisingly however, intracellular TGFβ1 protein abundance was increased following Rhein treatment under normoxic conditions, markedly indicating intracellular sequestration due to defective secretion. Empowering this assumption, LTBP1, one of 4 different LTBPs essential for proper secretion and association of TGFβ1 to the ECM (Henderson et al., 2013; Taipale et al., 1994), showed a trend towards reduced abundance accompanied by a general mRNA suppression of all LTBPs. Another interesting observation depicts the reduced mRNA expression of *TGFBR1*, the intracellular kinase of the TGFβ-receptor (Nagaraj and Datta, 2010), and the increased transcription of its acceptor *TGFBR2*. These key findings allude to the speculation of increased reception of TGFβ1 but theorize an impeded signal transduction due to reduced presence of its kinase. Another striking finding was the tremendously increased expression of *TGFBR3* after Rhein treatment. *TGFBR3*, constitutes an accessory co-receptor of TGFβs with no apparent intrinsic signaling activity (López-Casillas et al., 1991). *TGFBR3* is recognized as a negative regulator of TGFβ-signaling by competitively binding free TGFβ impeding its availability for the other receptors (Chu et al., 2011; Eickelberg et al., 2002). Thus, *TGFBR3* constitutes a potential factor mediated by Rhein, which putatively leads to a certain degree of active TGFβ clearance.

Conclusively, the presented data give evidence that Rhein reduces TGFβ1 bioavailability and elucidate a possible mechanism that involves intracellular sequestration by decreased LTBP expression. Therapeutically, this displays a putative mode of action of Rhein in preventing the expansion of myofibroblast populations via inhibition of paracrine and autocrine signal transduction. Of further notice, observations of altered TGFβ-receptor expressions let assume the involvement of Rhein in signal sensitivity reduction, which is comprehensively discussed in the next sections.

4.3 Rhein disrupts TGFβ-mediated differentiation of human cardiac fibroblasts

In the present work, the implication of TGFβ1 has been robustly predicted by comprehensive secretome and transcriptome analyses. Further, present data provided evidence that Rhein decreased bioavailability of TGFβ1, and hints were given that the sensitivity to TGFβ might be diminished due to alteration of receptor expressions. As already discussed in the previous sections, TGFβ-signaling is strongly associated to cardiac fibrosis (Edgley et al., 2012; Kane et al., 1991), constituting a pivotal mechanism in the activation of the fibrogenic response (Knittel et al., 1996). Therefore, to prove and to translate the presented holistic findings into a more mechanistic setting, exploration whether Rhein interferes with the TGFβ1 signaling was conducted by experiments using exogenous human recombinant TGFβ1.

The following sections focus on the dissection of the Rhein effect on the TGFβ/SMAD-axis and their surrounding positive and negative feedback loops. Finally, a functional assay is employed, to verify whether Rhein is a valid anti-fibrotic agent.

4.3.1 Rhein prevents the TGFβ1-induced transcription of profibrotic targets

Active TGFβ dimers are recognized by the extracellular domain of TGFβ receptor type II (TGFβRII). Upon binding (Figure 45), TGFβ receptor type I (TGFβRI), the kinase of the TGFβ receptor, is recruited by TGFβRII to form heterodimeric complexes and in this process TGFβRI is activated (Nagaraj and Datta, 2010). TGFβRI kinase activity leads to phosphorylation of regulatory small Mothers Against Decapentaplegic ((R-)SMAD)2 at Ser465/467 and SMAD3 at Ser423/425 (Shi and Massague, 2003), enabling complex formation with SMAD4 (co-SMAD). Subsequently, the SMAD2/3/4 complex is translocated into the nucleus, where it acts as transcription factor promoting the expression of profibrotic targets including αSMA, collagens, CTGF, MMPs and TIMPs (Desmouliere et al., 1993).

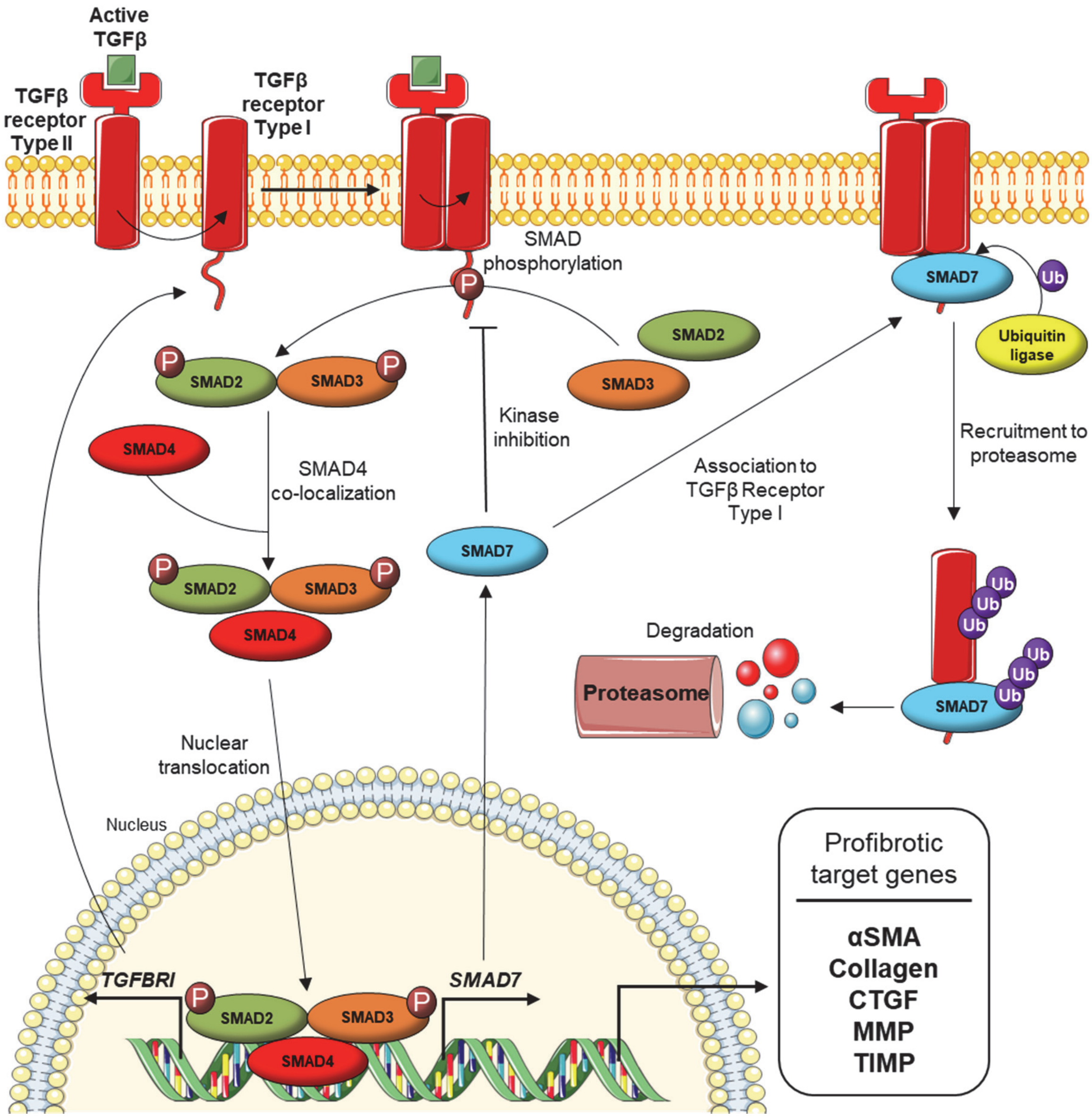

Figure 45: Canonical TGFβ/SMAD signaling and its negative/positive feedback loops

A distinct feature of fibroblast activation is the expression and *de novo* formation αSMA, considered the master marker of maturated myofibroblasts (Brown et al., 2005; Souders et al., 2009). A key finding of this work was that Rhein dose-dependently mitigated both TGFβ1-induced expression as well as protein abundance of αSMA in a dose-dependent matter. Furthermore, the present study demonstrated a similar pattern of dose responsiveness for other TGFβ1-stimulated gene targets including *CTGF*, *COL1A2* and *PAI1*, as potent reporter of TGFβ1 biological activity (He et al., 2010; Kawarada et al., 2016).

Altogether, these data present first hand findings that point towards Rhein-interceded abrogation of TGFβ/SMAD-signaling in the setting of cardiac fibrosis, which are in line with observations made in other tissues (Guo et al., 2002; Su et al., 2013; Tsang and Bian, 2015; Tsang et al., 2013b).

4.3.2 Rhein does not interfere with exogenous TGFβ1-mediated autoinduction

An interesting characteristic of TGFβ1 is its ability of transcriptional autoinduction thereby increasing its own synthesis and potential secretion (Kim et al., 1990; Kim et al., 1989). Confirmatively, in present experiments stimulation of HCF-v with exogenous TGFβ1 increased both mRNA and protein synthesis, and autoactivation persisted even when cells were exposed to Rhein in parallel. TGFβ1 transcriptional autoinduction is not only mediated by SMAD signaling, but also by other pathways like ERK and p38 (Flanders et al., 1995). While ERK signaling-mediated TGFβ1 transcription is directly linked to SMAD signaling, exogenous TGFβ1-induced autoinduction is independently mediated via p38 (Zhang et al., 2006a). The possible inability of Rhein to inhibit p38 in these experiments could provide an explanation, however this requires further analysis of the p38 phosphorylation state.

LTBP1 is co-regulated by TGFβ1 and is suggested to modulate the bioactivity of TGFβ1 (Miyazono et al., 1991; Taipale et al., 1994). Confirmative of the results obtained in the hypoxia experiments, where Rhein decreased LTBP1 protein and mRNA abundance, TGFβ1-induced LTBP1 mRNA synthesis was abrogated in the presence of Rhein. These findings suggest an independent pathway of LTBP transcriptional induction uncoupled from TGFβ1 autoactivation. Further, this allows for the speculation that although TGFβ1 autoinduction is not affected, secretion could be still defective in this context, associating to a TGFβ1 protein level-independent decrease of extracellular TGFβ1 activity (Tritschler et al., 2009).

4.3.3 Rhein reduces TGFβ-stimulated activation via inhibition of TGFβ/SMAD-signaling

Besides TGFβ1 autoactivation, another secondary mechanism in the adjustment of TGFβ response amplitude constitutes the positive feedback loop (Figure 45), which features the ligand-mediated upregulation of *TGFBR1* expression (Bloom et al., 1996), enhancing the mode of action after TGFβ receptor binding. Underlining previous key observations in hypoxia experiments, Rhein decreased both TGFβRI expression and even protein abundance, and abrogated TGFβ1-mediated upregulation. Reduced levels of TGFβRI have been reported in Rhein-treated mesangial cells (He et al., 2011), however the mechanism and its consequences were not further addressed. The present study demonstrates for the first time, that Rhein-mediated reduction of TGFβRI abundance was accompanied by obstructed levels of SMAD2 activation. In consent with the finding of impeded transcription of profibrotic genes, this evidently proves Rhein as TGFβ/SMAD signaling inhibitor by interfering with SMAD2/3/4 complex formation and nuclear transition. Apart from Rhein-mediated inhibition of *TGFBR1* transcription, a second mechanism can be postulated to be target to Rhein exposure. The

SMAD family not only comprises R- and co-SMADs, but also includes the inhibitory (I-)SMAD7 (Figure 45), as endogenous antagonist of the TGFβ-mediated SMAD-dependent signaling pathway (Hanyu et al., 2001). Herein, SMAD7 associates to TGFβRI, labeling it for recruitment of SMURF1/2 ubiquitin ligases and subsequent proteasomal degradation (Ebisawa et al., 2001; Suzuki et al., 2002), a process in which SMAD7 itself is also degraded (Kavsak et al., 2000).

4.3.4 Rhein posttranslationally stabilizes TGFβ-signaling inhibitor SMAD7 in a HDAC-dependent manner

The present thesis evidently identified a possible molecular mechanism of Rhein's pharmacological action in the inhibition of TGFβ/SMAD signaling by posttranslational stabilization of SMAD7. TGFβ/SMAD-signaling promotes the expression of SMAD7 (Stopa et al., 2000), which is able to inhibit TGFβRI kinase-mediated SMAD2/3 phosphorylation (Hayashi et al., 1997) and degradation of TGFβRI itself (Hanyu et al., 2001). Thus, TGFβ/SMAD-mediated activation of *SMAD7* mRNA constitutes a negative feedback loop capable of spatial and temporal fine-tuning of the intracellular TGFβ signal's magnitude. Confirming the presence of this negative regulatory element, exogenous TGFβ1 indeed stimulated the expression of *SMAD7* mRNA, however the hypothesized Rhein-mediated potentiation of SMAD7 was not observed in the present case.

According to literature, SMAD7 is constantly subjected to ubiquitination-mediated proteasome degradation and depletion is counteracted by competitive acetylation of lysine residues (Kavsak et al., 2000; Liu et al., 2008a). Herein, a balance between acetylation and deacetylation was proposed to regulate the stability of SMAD7 and hence, ultimately defining its abundance. As a novel finding in this thesis, SMAD7 protein was substantially increased in the presence of Rhein, even in the absence of TGFβ1, suggesting a TGFβ1-independent mechanism presumably involving the postulated posttranslational stabilization.

Interacting mediators regarding the acetylation status of SMAD7 lysine residues are SIRTs, HDACs and HATs (Gronroos et al., 2002; Kume et al., 2007; Simonsson et al., 2005). Inhibition of SIRT in the present experimental setting via NAM did not increase SMAD7 protein abundance and failed to mimic the Rhein effect. In contrast to that, SIRT knockdown was reported to stabilize SMAD7 (Kume et al., 2007). However, considering that Rhein effectively inhibited SIRT activity as previously demonstrated in this work, it seems likely that SIRT absence rather than SIRT inhibition plays a role, whilst excluding it as Rhein-mediated mechanism of posttranslational stabilization of SMAD7. HAT activity promotes the acetylation of lysine residues (Drazic et al., 2016), so that it was hypothesized that HAT inhibition-arbitrated hypoacetylation could reduce SMAD7 protein abundance due to failed protection from ubiquitination (Gronroos et al., 2002; Simonsson et al., 2005). In contrast to this assumption, AnA-driven inhibition of HAT did not affect SMAD7 protein stability at all. This finding, however, underlines the previously mentioned theory, that the observed reduced HAT activity in the hypoxia experiments, rather evolve from secondary mechanisms, as Rhein behaved fundamentally different from AnA.

In the present study, Rhein was already demonstrated to effectively diminish HDAC activity and promoting the posttranslational stabilization of p53. At this point, a second piece of evidence was determined, as HDAC inhibition using the reference inhibitor SB increased SMAD7 stability comparably to Rhein. Another interesting observation displays the amplitude of SMAD7 protein abundance, which seemed to correlate with the degree of inhibition according to SB and Rhein potency. Although, these findings increasingly support Rhein as valid HDAC inhibitor and suggest its effect to be HDAC-dependent, the present studies still harbor limitations. On the one hand, final proof of SMAD7's acetylation state after Rhein treatment in analogy to p53-acetylation would be required. Due to the inaccessibility of antibodies directed against acetylated SMAD7, this question could not be asked during this thesis.

4.3.5 Rhein functionally blocks TGFβ-induced collagen contraction in association with decreased αSMA expression

The present thesis delivered novel functional evidence for Rhein as anti-fibrotic agent *in vitro* in the context of cardiac fibrosis, demonstrated by fibroblast-populated collagen lattice (FPCL) contraction assays as a final proof-of-principle approach. The differentiation of fibroblasts to myofibroblasts is characterized by the *de novo* formation of αSMA fibers and the associated gain of contractile function (Brown et al., 2005; Souders et al., 2009). The presence of αSMA in myofibroblasts exerts higher tension forces effectuated on the ECM (Dahlmann-Noor et al., 2007; Wrobel et al., 2002), leading to condensation and stiffening of the tissue. Based on this procedure FPCL) contraction assays enable the investigation of FMT in a functional way, wherein the degree of contraction is directly proportional to the relative number of αSMA positive myofibroblasts (Bell et al., 1979). Thus, given that TGFβ induces collagen contraction (Montesano and Orci, 1988), FPCL assays constitute a reference *in vitro* model providing semi-quantitative assessment of FMT rates.

The key finding, providing final evidence of Rhein's anti-fibrotic properties was demonstrated by its dose-dependent inhibition of TGFβ1-stimulated, FMT-associated collagen contraction. In support of this observation and as proof-of-principle, the reduction of collagen contraction was attributed to the present levels of αSMA, displaying similar proportionate effect sizes in the context of Rhein dose and TGFβ1. Another noteworthy observation constitutes that Rhein treated FPCLs scored diminished basal contraction levels in comparison to unstimulated controls. This may be indicative of that Rhein administration even overcomes culture condition-driven basal FMT observed in unstimulated cells, thus, emphasizing its potency.

4.4 Conclusion and perspectives

The present thesis dealt with the exploration of the anthraquinone Rhein as potential anti-fibrotic agent in the context of cardiac fibrosis in an *in vitro* model of chronic hypoxia. Rhein, as a clinically relevant therapeutic compound in the treatment of osteoarthritis, has been previously reported to exert anti-fibrotic properties in relation to fibrotic pathologies of other organs, suggesting its pharmacological repurposing. In support of this, the present study provides evidence that Rhein indeed may contribute to the treatment of cardiac fibrosis, providing new insights and revealing novel underlying mechanisms of its mode of action.

The present study could show, that Rhein prevents the impact of chronic hypoxia as physiological effector in the pathological modulation of cardiac fibroblast behavior. In a holistic approach, using comprehensive secretome and transcriptome analysis combined with bioinformatic tools, the three upstream regulators TGFβ1, p53 and p21 were robustly predicted and identified. The presently detailed investigation of these regulators demonstrated the implication of Rhein in the decrease of active TGFβ1 bioavailability via mitigation of its secretion, reduction of cellular sensitivity to exogenous TGFβ1 and intracellular abrogation of TGFβ/SMAD-signaling. Furthermore, Rhein increased p53 and p21 associated to a prolongation of the G2/M cell cycle phase, in line with decreased proliferation. Mechanistically, for the first time Rhein-mediated effects were linked to the HDAC-dependent increase of p53 and SMAD7protein abundance.

Collectively, the present thesis identifies Rhein as a novel potent HDAC inhibitor linking anti-fibrotic treatment to HDAC inhibition. Pathophysiologically, these data clearly ascribe Rhein a pharmacological action to abrogate myofibroblast radiation and propagation, by impeding their ability to release paracrine and autocrine factors and decreasing their proliferative capacity. In the future, translation into long-term *in vivo* studies should be considered, investigating the potential prolongation of the life span in individuals at risk of premature and accelerated heart failure due to cardiac fibrosis. Concerning the specific targeting of Rhein action on designated cells or tissues, advancements in the use of nanoparticles will provide efficient delivery mitigating undesired side effects, a promising subject of current investigation.

From a clinical perspective, repurposing of Rhein, as readily available drug with approved safety, constitutes a promising potential therapeutic approach in the supplemental and protective intervention of cardiac fibrosis, preventing its propagation in high risk patients and aiding the preservation of cardiac function.

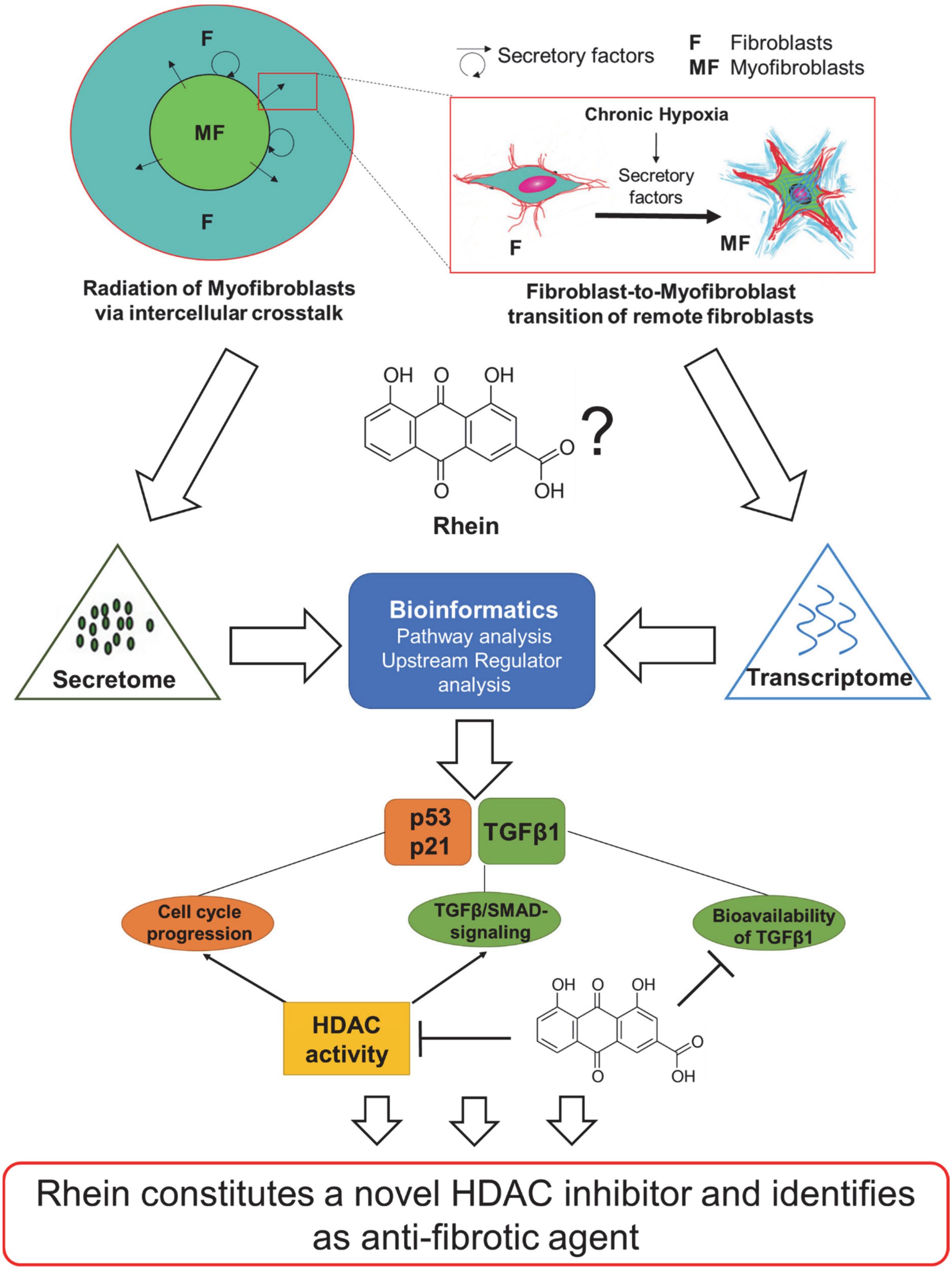

Figure 46: Graphical conclusion

List of References

Allfrey, V.G., Faulkner, R., and Mirsky, A.E. (1964). ACETYLATION AND METHYLATION OF HISTONES AND THEIR POSSIBLE ROLE IN THE REGULATION OF RNA SYNTHESIS. Proceedings of the National Academy of Sciences of the United States of America *51*, 786-794.

Aoyagi, T., and Matsui, T. (2011). The Cardiomyocyte as a Source of Cytokines in Cardiac Injury. Journal of cell science & therapy *2012*, 003.

Asby, D.J., Cuda, F., Hoakwie, F., Miranda, E., and Tavassoli, A. (2014). HIF-1 promotes the expression of its α-subunit via an epigenetically regulated transactivation loop. Molecular BioSystems *10*, 2505-2508.

Ask, K., Bonniaud, P., Maass, K., Eickelberg, O., Margetts, P.J., Warburton, D., Groffen, J., Gauldie, J., and Kolb, M. (2008). Progressive pulmonary fibrosis is mediated by TGF-beta isoform 1 but not TGF-beta3. The international journal of biochemistry & cell biology *40*, 484-495.

Asplund, A., Stillemark-Billton, P., Larsson, E., Rydberg, E.K., Moses, J., Hultén, L.M., Fagerberg, B., Camejo, G., and Bondjers, G. (2010). Hypoxic regulation of secreted proteoglycans in macrophages. Glycobiology *20*, 33-40.

Aviello, G., Rowland, I., Gill, C.I., Acquaviva, A.M., Capasso, F., McCann, M., Capasso, R., Izzo, A.A., and Borrelli, F. (2010). Anti-proliferative effect of rhein, an anthraquinone isolated from Cassia species, on Caco-2 human adenocarcinoma cells. Journal of cellular and molecular medicine *14*, 2006-2014.

Bagalad, B.S., Mohan Kumar, K.P., and Puneeth, H.K. (2017). Myofibroblasts: Master of disguise. Journal of Oral and Maxillofacial Pathology : JOMFP *21*, 462-463.

Banerjee, I., Fuseler, J.W., Price, R.L., Borg, T.K., and Baudino, T.A. (2007). Determination of cell types and numbers during cardiac development in the neonatal and adult rat and mouse. American journal of physiology Heart and circulatory physiology *293*, H1883-1891.

Bang, C., Antoniades, C., Antonopoulos, A.S., Eriksson, U., Franssen, C., Hamdani, N., Lehmann, L., Moessinger, C., Mongillo, M., Muhl, L., *et al.* (2015). Intercellular communication lessons in heart failure. European Journal of Heart Failure *17*, 1091-1103.

Bannister, A.J., and Kouzarides, T. (2011). Regulation of chromatin by histone modifications. Cell research *21*, 381-395.

Bartrons, R., and Caro, J. (2007). Hypoxia, glucose metabolism and the Warburg's effect. Journal of bioenergetics and biomembranes *39*, 223-229.

Baum, J., and Duffy, H.S. (2011a). Fibroblasts and myofibroblasts: what are we talking about? J Cardiovasc Pharmacol *57*, 376-379.

Baum, J., and Duffy, H.S. (2011b). Fibroblasts and Myofibroblasts: What are we talking about? Journal of cardiovascular pharmacology *57*, 376-379.

Beckerman, R., and Prives, C. (2010). Transcriptional regulation by p53. Cold Spring Harbor perspectives in biology *2*, a000935-a000935.

Bell, E., Ivarsson, B., and Merrill, C. (1979). Production of a tissue-like structure by contraction of collagen lattices by human fibroblasts of different proliferative potential in vitro. Proceedings of the National Academy of Sciences of the United States of America *76*, 1274-1278.

Bendtsen, J.D., Jensen, L.J., Blom, N., von Heijne, G., and Brunak, S. (2004). Feature-based prediction of non-classical and leaderless protein secretion. Protein Engineering, Design and Selection *17*, 349-356.

Benita, Y., Kikuchi, H., Smith, A.D., Zhang, M.Q., Chung, D.C., and Xavier, R.J. (2009). An integrative genomics approach identifies Hypoxia Inducible Factor-1 (HIF-1)-target genes that form the core response to hypoxia. Nucleic acids research *37*, 4587-4602.

Bhattacharyya, S., Ghosh, A.K., Pannu, J., Mori, Y., Takagawa, S., Chen, G., Trojanowska, M., Gilliam, A.C., and Varga, J. (2005). Fibroblast expression of the coactivator p300 governs the intensity of profibrotic response to transforming growth factor beta. Arthritis and rheumatism *52*, 1248-1258.

Birbrair, A., Zhang, T., Files, D.C., Mannava, S., Smith, T., Wang, Z.M., Messi, M.L., Mintz, A., and Delbono, O. (2014). Type-1 pericytes accumulate after tissue injury and produce collagen in an organ-dependent manner. Stem cell research & therapy *5*, 122.

Bloom, B.B., Humphries, D.E., Kuang, P.-P., Fine, A., and Goldstein, R.H. (1996). Structure and expression of the promoter for the R4/ALK5 human type I transforming growth factor-β receptor: regulation by TGF-β. Biochimica et Biophysica Acta (BBA) - Molecular Cell Research *1312*, 243-248.

Bomb, R., Heckle, M.R., Sun, Y., Mancarella, S., Guntaka, R.V., Gerling, I.C., and Weber, K.T. (2016). Myofibroblast secretome and its auto-/paracrine signaling. Expert review of cardiovascular therapy *14*, 591-598.

Bonnema, D.D., Webb, C.S., Pennington, W.R., Stroud, R.E., Leonardi, A.E., Clark, L.L., McClure, C.D., Finklea, L., Spinale, F.G., and Zile, M.R. (2007). Effects of age on plasma matrix metalloproteinases (MMPs) and tissue inhibitor of metalloproteinases (TIMPs). Journal of cardiac failure *13*, 530-540.

Bouche, M., Canipari, R., Melchionna, R., Willems, D., Senni, M.I., and Molinaro, M. (2000). TGF-beta autocrine loop regulates cell growth and myogenic differentiation in human rhabdomyosarcoma cells. FASEB journal : official publication of the Federation of American Societies for Experimental Biology *14*, 1147-1158.

Brown, R.D., Ambler, S.K., Mitchell, M.D., and Long, C.S. (2005). The cardiac fibroblast: therapeutic target in myocardial remodeling and failure. Annu Rev Pharmacol Toxicol *45*, 657-687.

Bruick, R.K., and McKnight, S.L. (2001). A conserved family of prolyl-4-hydroxylases that modify HIF. Science (New York, NY) *294*, 1337-1340.

Camelliti, P., Borg, T.K., and Kohl, P. (2005). Structural and functional characterisation of cardiac fibroblasts. Cardiovasc Res *65*, 40-51.

Caron, C., Boyault, C., and Khochbin, S. (2005). Regulatory cross-talk between lysine acetylation and ubiquitination: role in the control of protein stability. BioEssays *27*, 408-415.

Casamassimi, A., Federico, A., Rienzo, M., Esposito, S., and Ciccodicola, A. (2017). Transcriptome Profiling in Human Diseases: New Advances and Perspectives. International journal of molecular sciences *18*, 1652.

Chen, C., Li, R., Ross, R.S., and Manso, A.M. (2016). Integrins and integrin-related proteins in cardiac fibrosis. Journal of Molecular and Cellular Cardiology *93*, 162-174.

Chen, T., Li, J., Liu, J., Li, N., Wang, S., Liu, H., Zeng, M., Zhang, Y., and Bu, P. (2015a). Activation of SIRT3 by resveratrol ameliorates cardiac fibrosis and improves cardiac function via the TGF-beta/Smad3 pathway. American journal of physiology Heart and circulatory physiology *308*, H424-434.

Chen, Y., Du, J., Zhao, Y.T., Zhang, L., Lv, G., Zhuang, S., Qin, G., and Zhao, T.C. (2015b). Histone deacetylase (HDAC) inhibition improves myocardial function and prevents cardiac remodeling in diabetic mice. Cardiovascular diabetology *14*, 99.

Chevallet, M., Diemer, H., Van Dorssealer, A., Villiers, C., and Rabilloud, T. (2007). Toward a better analysis of secreted proteins: the example of the myeloid cells secretome. Proteomics *7*, 1757-1770.

Chu, P.-Y., Mariani, J., Finch, S., McMullen, J.R., Sadoshima, J., Marshall, T., and Kaye, D.M. (2010). Bone Marrow-Derived Cells Contribute to Fibrosis in the Chronically Failing Heart. The American Journal of Pathology *176*, 1735-1742.

Chu, W., Li, X., Li, C., Wan, L., Shi, H., Song, X., Liu, X., Chen, X., Zhang, C., Shan, H., *et al.* (2011). TGFBR3, a potential negative regulator of TGF-β signaling, protects cardiac fibroblasts from hypoxia-induced apoptosis. Journal of Cellular Physiology *226*, 2586-2594.

Clancy, R.M., Zheng, P., O'Mahony, M., Izmirly, P., Zavadil, J., Gardner, L., and Buyon, J.P. (2007). Role of hypoxia and cAMP in the transdifferentiation of human fetal cardiac fibroblasts: implications for progression to scarring in autoimmune-associated congenital heart block. Arthritis and rheumatism *56*, 4120-4131.

Clements, E.G., Mohammad, H.P., Leadem, B.R., Easwaran, H., Cai, Y., Van Neste, L., and Baylin, S.B. (2012). DNMT1 modulates gene expression without its catalytic activity partially through its interactions with histone-modifying enzymes. Nucleic Acids Research *40*, 4334-4346.

Condorelli, F., Gnemmi, I., Vallario, A., Genazzani, A.A., and Canonico, P.L. (2008). Inhibitors of histone deacetylase (HDAC) restore the p53 pathway in neuroblastoma cells. British journal of pharmacology *153*, 657-668.

Coronel, R., de Groot, J.R., and van Lieshout, J.J. (2001). Defining heart failure. Cardiovasc Res *50*, 419-422.

Cosme, J., Guo, H., Hadipour-Lakmehsari, S., Emili, A., and Gramolini, A.O. (2017). Hypoxia-Induced Changes in the Fibroblast Secretome, Exosome, and Whole-Cell Proteome Using Cultured, Cardiac-Derived Cells Isolated from Neonatal Mice. J Proteome Res *16*, 2836-2847.

Creemers, E.E., and Pinto, Y.M. (2011). Molecular mechanisms that control interstitial fibrosis in the pressure-overloaded heart. Cardiovasc Res *89*, 265-272.

Dahlmann-Noor, A.H., Martin-Martin, B., Eastwood, M., Khaw, P.T., and Bailly, M. (2007). Dynamic protrusive cell behaviour generates force and drives early matrix contraction by fibroblasts. Experimental Cell Research *313*, 4158-4169.

Dang, C.V. MYC, metabolism, cell growth, and tumorigenesis. Cold Spring Harbor perspectives in medicine *3*, a014217.

Darby, I.A., and Hewitson, T.D. (2016). Hypoxia in tissue repair and fibrosis. Cell and Tissue Research *365*, 553-562.

Das, C., and Kundu, T.K. (2005). Transcriptional regulation by the acetylation of nonhistone proteins in humans -- a new target for therapeutics. IUBMB life *57*, 137-149.

Das, M., Burns, N., Wilson, S.J., Zawada, W.M., and Stenmark, K.R. (2008). Hypoxia exposure induces the emergence of fibroblasts lacking replication repressor signals of PKCzeta in the pulmonary artery adventitia. Cardiovasc Res *78*, 440-448.

Davidson, S.M., Arjun, S., Basalay, M.V., Bell, R.M., Bromage, D.I., Bøtker, H.E., Carr, R.D., Cunningham, J., Ghosh, A.K., Heusch, G.*, et al.* (2018). The 10th Biennial Hatter Cardiovascular Institute workshop: cellular protection—evaluating new directions in the setting of myocardial infarction, ischaemic stroke, and cardio-oncology. Basic Research in Cardiology *113*, 43.

Deckx, S., Heymans, S., and Papageorgiou, A.-P. (2016). The diverse functions of osteoglycin: a deceitful dwarf, or a master regulator of disease? The FASEB Journal *30*, 2651-2661.

Dengler, V.L., Galbraith, M., and Espinosa, J.M. (2014). Transcriptional regulation by hypoxia inducible factors. Critical reviews in biochemistry and molecular biology *49*, 1-15.

Desmouliere, A., Geinoz, A., Gabbiani, F., and Gabbiani, G. (1993). Transforming growth factor-beta 1 induces alpha-smooth muscle actin expression in granulation tissue myofibroblasts and in quiescent and growing cultured fibroblasts. The Journal of cell biology *122*, 103-111.

Dickhuth, H.H., Rocker, K., Mayer, F., Konig, D., and Korsten-Reck, U. (2004). [Endurance training and cardial adaptation (athlete's heart)]. Herz *29*, 373-380.

Distler, J.H., Jungel, A., Pileckyte, M., Zwerina, J., Michel, B.A., Gay, R.E., Kowal-Bielecka, O., Matucci-Cerinic, M., Schett, G., Marti, H.H.*, et al.* (2007). Hypoxia-induced increase in the production of extracellular matrix proteins in systemic sclerosis. Arthritis and rheumatism *56*, 4203-4215.

Dobaczewski, M., Chen, W., and Frangogiannis, N.G. (2011). Transforming Growth Factor (TGF)-β signaling in cardiac remodeling. Journal of molecular and cellular cardiology *51*, 600-606.

Doe, M.R., Ascano, J.M., Kaur, M., and Cole, M.D. (2012). Myc posttranscriptionally induces HIF1 protein and target gene expression in normal and cancer cells. Cancer research *72*, 949-957.

Dorn, L.E., Petrosino, J.M., Wright, P., and Accornero, F. (2018). CTGF/CCN2 is an autocrine regulator of cardiac fibrosis. Journal of Molecular and Cellular Cardiology *121*, 205-211.

Doroudgar, S., and Glembotski, C.C. (2011). The cardiokine story unfolds: ischemic stress-induced protein secretion in the heart. Trends in Molecular Medicine *17*, 207-214.

Drazic, A., Myklebust, L.M., Ree, R., and Arnesen, T. (2016). The world of protein acetylation. Biochimica et Biophysica Acta (BBA) - Proteins and Proteomics *1864*, 1372-1401.

Dubois, C.M., Laprise, M.H., Blanchette, F., Gentry, L.E., and Leduc, R. (1995). Processing of transforming growth factor beta 1 precursor by human furin convertase. J Biol Chem *270*, 10618-10624.

Dutto, I., Tillhon, M., Cazzalini, O., Stivala, L.A., and Prosperi, E. (2015). Biology of the cell cycle inhibitor p21CDKN1A: molecular mechanisms and relevance in chemical toxicology. Archives of Toxicology *89*, 155-178.

Ebisawa, T., Fukuchi, M., Murakami, G., Chiba, T., Tanaka, K., Imamura, T., and Miyazono, K. (2001). Smurf1 interacts with transforming growth factor-beta type I receptor through Smad7 and induces receptor degradation. J Biol Chem *276*, 12477-12480.

Edgley, A.J., Krum, H., and Kelly, D.J. (2012). Targeting Fibrosis for the Treatment of Heart Failure: A Role for Transforming Growth Factor-β. Cardiovascular Therapeutics *30*, e30-e40.

Eichelbaum, K., and Krijgsveld, J. (2014). Rapid Temporal Dynamics of Transcription, Protein Synthesis, and Secretion during Macrophage Activation. Molecular & Cellular Proteomics *13*, 792.

Eickelberg, O., Centrella, M., Reiss, M., Kashgarian, M., and Wells, R.G. (2002). Betaglycan Inhibits TGF-β Signaling by Preventing Type I-Type II Receptor Complex Formation: GLYCOSAMINOGLYCAN MODIFICATIONS ALTER BETAGLYCAN FUNCTION. Journal of Biological Chemistry *277*, 823-829.

Ely, J.J., Bishop, M.A., Lammey, M.L., Sleeper, M.M., Steiner, J.M., and Lee, D.R. (2010). Use of biomarkers of collagen types I and III fibrosis metabolism to detect cardiovascular and renal disease in chimpanzees (Pan troglodytes). Comparative medicine *60*, 154-158.

Essop, M.F. (2007). Cardiac metabolic adaptations in response to chronic hypoxia. The Journal of physiology *584*, 715-726.

Estécio, M.R.H., and Issa, J.-P.J. (2011). Dissecting DNA hypermethylation in cancer. FEBS Letters *585*, 2078-2086.

Fan, D., Takawale, A., Lee, J., and Kassiri, Z. (2012). Cardiac fibroblasts, fibrosis and extracellular matrix remodeling in heart disease. Fibrogenesis Tissue Repair *5*, 15.

Flanders, K., G. Holder, M., and Winokur, T. (1995). Autoinduction of mRNA and protein expression for transforming growth factor-β S in cultured cardiac cells, Vol 27.

Frangogiannis, N.G. (2012). Matricellular proteins in cardiac adaptation and disease. Physiological reviews *92*, 635-688.

Frangogiannis, N.G. (2014). The inflammatory response in myocardial injury, repair, and remodelling. Nature Reviews Cardiology *11*, 255.

Frohlich, E.D. (1985). The heart: An endocrine organ (revisited). Archives of Internal Medicine *145*, 809-811.

Fu, X., Khalil, H., Kanisicak, O., Boyer, J.G., Vagnozzi, R.J., Maliken, B.D., Sargent, M.A., Prasad, V., Valiente-Alandi, I., Blaxall, B.C.*, et al.* (2018). Specialized fibroblast differentiated states underlie scar formation in the infarcted mouse heart. J Clin Invest *128*, 2127-2143.

Fulda, S., and Debatin, K.M. (2007). HIF-1-regulated glucose metabolism: a key to apoptosis resistance? Cell Cycle *6*, 790-792.

Gallinari, P., Marco, S.D., Jones, P., Pallaoro, M., and Steinkühler, C. (2007). HDACs, histone deacetylation and gene transcription: from molecular biology to cancer therapeutics. Cell Research *17*, 195.

Gao, Y., Chu, M., Hong, J., Shang, J., and Xu, D. (2014). Hypoxia induces cardiac fibroblast proliferation and phenotypic switch: a role for caveolae and caveolin-1/PTEN mediated pathway. J Thorac Dis *6*, 1458-1468.

Gartel, A.L., Serfas, M.S., and Tyner, A.L. (1996). p21--negative regulator of the cell cycle. Proceedings of the Society for Experimental Biology and Medicine Society for Experimental Biology and Medicine (New York, NY) *213*, 138-149.

Ghosh, A.K., Bhattacharyya, S., Lafyatis, R., Farina, G., Yu, J., Thimmapaya, B., Wei, J., and Varga, J. (2013). p300 is elevated in systemic sclerosis and its expression is positively regulated by TGF-beta: epigenetic feed-forward amplification of fibrosis. The Journal of investigative dermatology *133*, 1302-1310.

Grimaldi, V., De Pascale, M.R., Zullo, A., Soricelli, A., Infante, T., Mancini, F.P., and Napoli, C. (2017). Evidence of epigenetic tags in cardiac fibrosis. Journal of Cardiology *69*, 401-408.

Gronroos, E., Hellman, U., Heldin, C.H., and Ericsson, J. (2002). Control of Smad7 stability by competition between acetylation and ubiquitination. Molecular cell *10*, 483-493.

Guo, M.Z., Li, X.S., Xu, H.R., Mei, Z.C., Shen, W., and Ye, X.F. (2002). Rhein inhibits liver fibrosis induced by carbon tetrachloride in rats. Acta Pharmacol Sin *23*, 739-744.

Guo, W., Shan, B., Klingsberg, R.C., Qin, X., and Lasky, J.A. (2009). Abrogation of TGF-β1-induced fibroblast-myofibroblast differentiation by histone deacetylase inhibition. American Journal of Physiology-Lung Cellular and Molecular Physiology *297*, L864-L870.

Gurtner, G.C., Werner, S., Barrandon, Y., and Longaker, M.T. (2008). Wound repair and regeneration. Nature *453*, 314-321.

Hanahan, D., and Weinberg, Robert A. (2011). Hallmarks of Cancer: The Next Generation. Cell *144*, 646-674.

Hanyu, A., Ishidou, Y., Ebisawa, T., Shimanuki, T., Imamura, T., and Miyazono, K. (2001). The N domain of Smad7 is essential for specific inhibition of transforming growth factor-beta signaling. The Journal of cell biology *155*, 1017-1027.

Hasvold, G., Lund-Andersen, C., Lando, M., Patzke, S., Hauge, S., Suo, Z., Lyng, H., and Syljuåsen, R.G. (2016). Hypoxia-induced alterations of G2 checkpoint regulators. Molecular Oncology *10*, 764-773.

Hayashi, H., Abdollah, S., Qiu, Y., Cai, J., Xu, Y.Y., Grinnell, B.W., Richardson, M.A., Topper, J.N., Gimbrone, M.A., Jr., Wrana, J.L.*, et al.* (1997). The MAD-related protein Smad7 associates with the TGFbeta receptor and functions as an antagonist of TGFbeta signaling. Cell *89*, 1165-1173.

He, D., Lee, L., Yang, J., and Wang, X. (2011). Preventive Effects and Mechanisms of Rhein on Renal Interstitial Fibrosis in Obstructive Nephropathy. Biological and Pharmaceutical Bulletin *34*, 1219-1226.

He, W., Tan, R., Dai, C., Li, Y., Wang, D., Hao, S., Kahn, M., and Liu, Y. (2010). Plasminogen Activator Inhibitor-1 Is a Transcriptional Target of the Canonical Pathway of Wnt/β-Catenin Signaling. Journal of Biological Chemistry *285*, 24665-24675.

Heather, L.C., and Clarke, K. (2011). Metabolism, hypoxia and the diabetic heart. J Mol Cell Cardiol *50*, 598-605.

Heineke, J., and Molkentin, J.D. (2006). Regulation of cardiac hypertrophy by intracellular signalling pathways. Nature Reviews Molecular Cell Biology *7*, 589.

Henderson, N.C., Arnold, T.D., Katamura, Y., Giacomini, M.M., Rodriguez, J.D., McCarty, J.H., Pellicoro, A., Raschperger, E., Betsholtz, C., Ruminski, P.G.*, et al.* (2013). Targeting of αv integrin identifies a core molecular pathway that regulates fibrosis in several organs. Nature Medicine *19*, 1617.

Higgins, D.F., Biju, M.P., Akai, Y., Wutz, A., Johnson, R.S., and Haase, V.H. (2004). Hypoxic induction of Ctgf is directly mediated by Hif-1. American Journal of Physiology-Renal Physiology *287*, F1223-F1232.

Ho, Y.Y., Lagares, D., Tager, A.M., and Kapoor, M. (2014). Fibrosis—a lethal component of systemic sclerosis. Nature Reviews Rheumatology *10*, 390.

Hsia, T.C., Yang, J.S., Chen, G.W., Chiu, T.H., Lu, H.F., Yang, M.D., Yu, F.S., Liu, K.C., Lai, K.C., Lin, C.C.*, et al.* (2009). The roles of endoplasmic reticulum stress and Ca2+ on rhein-induced apoptosis in A-549 human lung cancer cells. Anticancer research *29*, 309-318.

Huntgeburth, M., Tiemann, K., Shahverdyan, R., Schlüter, K.-D., Schreckenberg, R., Gross, M.-L., Mödersheim, S., Caglayan, E., Müller-Ehmsen, J., Ghanem, A.*, et al.* (2011). Transforming Growth Factor β(1) Oppositely Regulates the Hypertrophic and Contractile Response to β-Adrenergic Stimulation in the Heart. PLoS ONE *6*, e26628.

Ichioka, S., Ando, T., Shibata, M., Sekiya, N., and Nakatsuka, T. (2008). Oxygen consumption of keloids and hypertrophic scars. Annals of plastic surgery *60*, 194-197.

Ip, S.W., Weng, Y.S., Lin, S.Y., Mei, D., Tang, N.Y., Su, C.C., and Chung, J.G. (2007). The role of Ca+2 on rhein-induced apoptosis in human cervical cancer Ca Ski cells. Anticancer research *27*, 379-389.

Jenkins, G. (2008). The role of proteases in transforming growth factor-β activation. The international journal of biochemistry & cell biology *40*, 1068-1078.

Ji, Z.Q., Huang, C.W., Liang, C.J., Sun, W.W., Chen, B., and Tang, P.R. (2005). [Effects of rhein on activity of caspase-3 in kidney and cell apoptosis on the progression of renal injury in glomerulosclerosis]. Zhonghua yi xue za zhi *85*, 1836-1841.

Kamura, T., Sato, S., Iwai, K., Czyzyk-Krzeska, M., Conaway, R.C., and Conaway, J.W. (2000). Activation of HIF1alpha ubiquitination by a reconstituted von Hippel-Lindau (VHL) tumor suppressor complex. Proceedings of the National Academy of Sciences of the United States of America *97*, 10430-10435.

Kane, C.J., Hebda, P.A., Mansbridge, J.N., and Hanawalt, P.C. (1991). Direct evidence for spatial and temporal regulation of transforming growth factor beta 1 expression during cutaneous wound healing. J Cell Physiol *148*, 157-173.

Kanekar, S., Hirozanne, T., Terracio, L., and Borg, T.K. (1998). Cardiac fibroblasts form and function. Cardiovascular pathology : the official journal of the Society for Cardiovascular Pathology *7*, 127-133.

Kavsak, P., Rasmussen, R.K., Causing, C.G., Bonni, S., Zhu, H., Thomsen, G.H., and Wrana, J.L. (2000). Smad7 binds to Smurf2 to form an E3 ubiquitin ligase that targets the TGF beta receptor for degradation. Molecular cell *6*, 1365-1375.

Kawaguchi, M., Takahashi, M., Hata, T., Kashima, Y., Usui, F., Morimoto, H., Izawa, A., Takahashi, Y., Masumoto, J., Koyama, J.*, et al.* (2011). Inflammasome activation of cardiac fibroblasts is essential for myocardial ischemia/reperfusion injury. Circulation *123*, 594-604.

Kawarada, Y., Inoue, Y., Kawasaki, F., Fukuura, K., Sato, K., Tanaka, T., Itoh, Y., and Hayashi, H. (2016). TGF-β induces p53/Smads complex formation in the PAI-1 promoter to activate transcription. Scientific reports *6*, 35483-35483.

Khan, S.A., Joyce, J., and Tsuda, T. (2012). Quantification of active and total transforming growth factor-β levels in serum and solid organ tissues by bioassay. BMC research notes *5*, 636-636.

Kim, J.-w., Tchernyshyov, I., Semenza, G.L., and Dang, C.V. (2006). HIF-1-mediated expression of pyruvate dehydrogenase kinase: A metabolic switch required for cellular adaptation to hypoxia. Cell Metabolism *3*, 177-185.

Kim, S.J., Angel, P., Lafyatis, R., Hattori, K., Kim, K.Y., Sporn, M.B., Karin, M., and Roberts, A.B. (1990). Autoinduction of transforming growth factor beta 1 is mediated by the AP-1 complex. Molecular and cellular biology *10*, 1492-1497.

Kim, S.J., Jeang, K.T., Glick, A.B., Sporn, M.B., and Roberts, A.B. (1989). Promoter sequences of the human transforming growth factor-beta 1 gene responsive to transforming growth factor-beta 1 autoinduction. Journal of Biological Chemistry *264*, 7041-7045.

Kischer, C.W., Thies, A.C., and Chvapil, M. (1982). Perivascular myofibroblasts and microvascular occlusion in hypertrophic scars and keloids. Human pathology *13*, 819-824.

Knittel, T., Janneck, T., Muller, L., Fellmer, P., and Ramadori, G. (1996). Transforming growth factor beta 1-regulated gene expression of Ito cells. Hepatology (Baltimore, Md) *24*, 352-360.

Kong, P., Christia, P., and Frangogiannis, N.G. (2014). The Pathogenesis of Cardiac Fibrosis. Cellular and molecular life sciences : CMLS *71*, 549-574.

Koritzinsky, M., Magagnin, M.G., van den Beucken, T., Seigneuric, R., Savelkouls, K., Dostie, J., Pyronnet, S., Kaufman, R.J., Weppler, S.A., Voncken, J.W.*, et al.* (2006). Gene expression during acute and prolonged hypoxia is regulated by distinct mechanisms of translational control. The EMBO journal *25*, 1114-1125.

Kukurba, K.R., and Montgomery, S.B. (2015). RNA Sequencing and Analysis. Cold Spring Harbor protocols *2015*, 951-969.

Kume, S., Haneda, M., Kanasaki, K., Sugimoto, T., Araki, S.-i., Isshiki, K., Isono, M., Uzu, T., Guarente, L., Kashiwagi, A.*, et al.* (2007). SIRT1 Inhibits Transforming Growth Factor β-Induced Apoptosis in Glomerular Mesangial Cells via Smad7 Deacetylation. Journal of Biological Chemistry *282*, 151-158.

Kuo, P.L., Hsu, Y.L., Ng, L.T., and Lin, C.C. (2004). Rhein inhibits the growth and induces the apoptosis of Hep G2 cells. Planta medica *70*, 12-16.

Lafleur, V.N., Richard, S., Richard, D.E., and Matera, A.G. (2014). Transcriptional repression of hypoxia-inducible factor-1 (HIF-1) by the protein arginine methyltransferase PRMT1. Molecular Biology of the Cell *25*, 925-935.

Layek, B., Kumar, T.S., Trivedi, R.K., Mullangi, R., and Srinivas, N.R. (2008). Development and validation of a sensitive LC-MS/MS method with electrospray ionization for quantitation of rhein in human plasma: application to a pharmacokinetic study. Biomedical chromatography : BMC *22*, 616-624.

Le, Q.-T., and Courter, D. (2008). Clinical biomarkers for hypoxia targeting. Cancer metastasis reviews *27*, 351-362.

Lee, A., Karamichos, D., Rich, C., Zieske, J.D., and Trinkaus-Randall, V. (2011). Hypoxia Modulates the Expression of Extracellular Matrix Proteins in a 3-D Primary Human Fibroblast Construct. Investigative Ophthalmology & Visual Science *52*, 3425-3425.

Lee, T.M., Lin, M.S., and Chang, N.C. (2007). Inhibition of histone deacetylase on ventricular remodeling in infarcted rats. American journal of physiology Heart and circulatory physiology *293*, H968-977.

Legendre, F., Heuze, A., Boukerrouche, K., Leclercq, S., Boumediene, K., Galera, P., Domagala, F., Pujol, J.P., and Ficheux, H. (2009). Rhein, the metabolite of diacerhein, reduces the proliferation of osteoarthritic chondrocytes and synoviocytes without inducing apoptosis. Scand J Rheumatol *38*, 104-111.

Li, Y.Y., McTiernan, C.F., and Feldman, A.M. (2000). Interplay of matrix metalloproteinases, tissue inhibitors of metalloproteinases and their regulators in cardiac matrix remodeling. Cardiovascular Research *46*, 214-224.

Lin, Y.-C., Sun, S.H., and Wang, F.-F. (2011). Suppression of Polo like kinase 1 (PLK1) by p21Waf1 mediates the p53-dependent prevention of caspase-independent mitotic death. Cellular Signalling *23*, 1816-1823.

Lipson, K.E., Wong, C., Teng, Y., and Spong, S. (2012). CTGF is a central mediator of tissue remodeling and fibrosis and its inhibition can reverse the process of fibrosis. Fibrogenesis & Tissue Repair *5*, S24.

Lisy, K., and Peet, D.J. (2008). Turn me on: regulating HIF transcriptional activity. Cell Death And Differentiation *15*, 642.

Liu, F.Y., Li, X.Z., Peng, Y.M., Liu, H., and Liu, Y.H. (2008a). Arkadia regulates TGF-beta signaling during renal tubular epithelial to mesenchymal cell transition. Kidney international *73*, 588-594.

Liu, G., Ma, C., Yang, H., and Zhang, P.-Y. (2017). Transforming growth factor β and its role in heart disease. Experimental and Therapeutic Medicine *13*, 2123-2128.

Liu, L., Cash, T.P., Jones, R.G., Keith, B., Thompson, C.B., and Simon, M.C. (2006). Hypoxia-induced energy stress regulates mRNA translation and cell growth. Molecular cell *21*, 521-531.

Liu, L., Marti, G.P., Wei, X., Zhang, X., Zhang, H., Liu, Y.V., Nastai, M., Semenza, G.L., and Harmon, J.W. (2008b). Age-dependent impairment of HIF-1alpha expression in diabetic mice: Correction with electroporation-facilitated gene therapy increases wound healing, angiogenesis, and circulating angiogenic cells. J Cell Physiol *217*, 319-327.

Lokmic, Z., Musyoka, J., Hewitson, T.D., and Darby, I.A. (2012). Hypoxia and hypoxia signaling in tissue repair and fibrosis. Int Rev Cell Mol Biol *296*, 139-185.

López-Casillas, F., Cheifetz, S., Doody, J., Andres, J.L., Lane, W.S., and Massague, J. (1991). Structure and expression of the membrane proteoglycan betaglycan, a component of the TGF-β receptor system. Cell *67*, 785-795.

Martin, G., Bogdanowicz, P., Domagala, F., Ficheux, H., and Pujol, J.P. (2003). Rhein inhibits interleukin-1 beta-induced activation of MEK/ERK pathway and DNA binding of NF-kappa B and AP-1 in chondrocytes cultured in hypoxia: a potential mechanism for its disease-modifying effect in osteoarthritis. Inflammation *27*, 233-246.

Martin, G., Bogdanowicz, P., Domagala, F., Ficheux, H., and Pujol, J.P. (2004). Articular chondrocytes cultured in hypoxia: their response to interleukin-1beta and rhein, the active metabolite of diacerhein. Biorheology *41*, 549-561.

Mathivanan, S., and Simpson, R.J. (2009). ExoCarta: A compendium of exosomal proteins and RNA. Proteomics *9*, 4997-5000.

Meng, X.-m., Nikolic-Paterson, D.J., and Lan, H.Y. (2016). TGF-β: the master regulator of fibrosis. Nature Reviews Nephrology *12*, 325.

Metes-Kosik, N., Luptak, I., DiBello, P.M., Handy, D.E., Tang, S.-S., Zhi, H., Qin, F., Jacobsen, D.W., Loscalzo, J., and Joseph, J. (2012). Both selenium deficiency and modest selenium supplementation lead to myocardial fibrosis in mice via effects on redox-methylation balance. Molecular Nutrition & Food Research *56*, 1812-1824.

Mewton, N., Liu, C.Y., Croisille, P., Bluemke, D., and Lima, J.A.C. (2011). Assessment of Myocardial Fibrosis With Cardiovascular Magnetic Resonance. Journal of the American College of Cardiology *57*, 891-903.

Miller, D.M., Thomas, S.D., Islam, A., Muench, D., and Sedoris, K. (2012). c-Myc and cancer metabolism. Clinical cancer research : an official journal of the American Association for Cancer Research *18*, 5546-5553.

Minet, E., Ernest, I., Michel, G., Roland, I., Remacle, J., Raes, M., and Michiels, C. (1999). HIF1A Gene Transcription Is Dependent on a Core Promoter Sequence Encompassing Activating and Inhibiting Sequences Located Upstream from the Transcription Initiation Site and cis Elements Located within the 5′UTR. Biochemical and Biophysical Research Communications *261*, 534-540.

Mirtschink, P., and Krek, W. (2016). Hypoxia-driven glycolytic and fructolytic metabolic programs: Pivotal to hypertrophic heart disease. Biochimica et Biophysica Acta (BBA) - Molecular Cell Research *1863*, 1822-1828.

Mishra, P.K., Givvimani, S., Chavali, V., and Tyagi, S.C. (2013). Cardiac matrix: a clue for future therapy. Biochim Biophys Acta *1832*, 2271-2276.

Misra, S., Fu, A.A., Misra, K.D., Shergill, U.M., Leof, E.B., and Mukhopadhyay, D. (2010). Hypoxia-induced phenotypic switch of fibroblasts to myofibroblasts through a matrix metalloproteinase 2/tissue inhibitor of metalloproteinase-mediated pathway: implications for venous neointimal hyperplasia in hemodialysis access. J Vasc Interv Radiol *21*, 896-902.

Miyazono, K., Hellman, U., Wernstedt, C., and Heldin, C.H. (1988). Latent high molecular weight complex of transforming growth factor beta 1. Purification from human platelets and structural characterization. J Biol Chem *263*, 6407-6415.

Miyazono, K., Olofsson, A., Colosetti, P., and Heldin, C.H. (1991). A role of the latent TGF-beta 1-binding protein in the assembly and secretion of TGF-beta 1. The EMBO journal *10*, 1091-1101.

Mizuno, S., Bogaard, H.J., Voelkel, N.F., Umeda, Y., Kadowaki, M., Ameshima, S., Miyamori, I., and Ishizaki, T. (2009). Hypoxia regulates human lung fibroblast proliferation via p53-dependent and -independent pathways. Respir Res *10*, 17.

Montesano, R., and Orci, L. (1988). Transforming growth factor beta stimulates collagen-matrix contraction by fibroblasts: implications for wound healing. Proceedings of the National Academy of Sciences of the United States of America *85*, 4894-4897.

Morris, M.J., and Monteggia, L.M. (2013). Unique functional roles for class I and class II histone deacetylases in central nervous system development and function. International journal of developmental neuroscience : the official journal of the International Society for Developmental Neuroscience *31*, 370-381.

Mukherjee, P., and Mani, S. (2013). Methodologies to decipher the cell secretome. Biochimica et biophysica acta *1834*, 2226-2232.

Muñoz-Fontela, C., González, D., Marcos-Villar, L., Campagna, M., Gallego, P., González-Santamaría, J., Herranz, D., Gu, W., Serrano, M., Aaronson, S.A.*, et al.* (2011). Acetylation is indispensable for p53 antiviral activity. Cell cycle (Georgetown, Tex) *10*, 3701-3705.

Murtha, L.A., Schuliga, M.J., Mabotuwana, N.S., Hardy, S.A., Waters, D.W., Burgess, J.K., Knight, D.A., and Boyle, A.J. (2017). The Processes and Mechanisms of Cardiac and Pulmonary Fibrosis. Front Physiol *8*, 777.

Nagaraj, N.S., and Datta, P.K. (2010). Targeting the transforming growth factor-beta signaling pathway in human cancer. Expert opinion on investigational drugs *19*, 77-91.

Nakayama, K., Frew, I.J., Hagensen, M., Skals, M., Habelhah, H., Bhoumik, A., Kadoya, T., Erdjument-Bromage, H., Tempst, P., Frappell, P.B.*, et al.* (2004). Siah2 regulates stability of prolyl-hydroxylases, controls HIF1alpha abundance, and modulates physiological responses to hypoxia. Cell *117*, 941-952.

Nguyen, M., Dougados, M., Berdah, L., and Amor, B. (1994). Diacerhein in the treatment of osteoarthritis of the hip. Arthritis & Rheumatism *37*, 529-536.

Nicolas, P., Tod, M., Padoin, C., and Petitjean, O. (1998). Clinical pharmacokinetics of diacerein. Clinical pharmacokinetics *35*, 347-359.

Nural-Guvener, H.F., Zakharova, L., Nimlos, J., Popovic, S., Mastroeni, D., and Gaballa, M.A. (2014). HDAC class I inhibitor, Mocetinostat, reverses cardiac fibrosis in heart failure and diminishes CD90+ cardiac myofibroblast activation. Fibrogenesis & Tissue Repair *7*, 10.

Panigrahi, G.K., Yadav, A., Srivastava, A., Tripathi, A., Raisuddin, S., and Das, M. (2015). Mechanism of rhein-induced apoptosis in rat primary hepatocytes: beneficial effect of cyclosporine A. Chemical research in toxicology *28*, 1133-1143.

Papageorgis, P. (2015). TGFbeta Signaling in Tumor Initiation, Epithelial-to-Mesenchymal Transition, and Metastasis. Journal of oncology *2015*, 587193.

Pazos-López, P., Peteiro-Vázquez, J., Carcía-Campos, A., García-Bueno, L., de Torres, J.P.A., and Castro-Beiras, A. (2011). The causes, consequences, and treatment of left or right heart failure. Vascular Health and Risk Management *7*, 237-254.

Peng, S.N., Zeng, H.H., Fu, A.X., Chen, X.W., and Zhu, Q.X. (2013). Effects of rhein on intestinal epithelial tight junction in IgA nephropathy. World journal of gastroenterology *19*, 4137-4145.

Petersen, T.N., Brunak, S., von Heijne, G., and Nielsen, H. (2011). SignalP 4.0: discriminating signal peptides from transmembrane regions. Nature Methods *8*, 785.

Pfander, D., Cramer, T., Schipani, E., and Johnson, R.S. (2003). HIF-1alpha controls extracellular matrix synthesis by epiphyseal chondrocytes. Journal of cell science *116*, 1819-1826.

Pinto, A.R., Ilinykh, A., Ivey, M.J., Kuwabara, J.T., D'Antoni, M.L., Debuque, R., Chandran, A., Wang, L., Arora, K., Rosenthal, N.A., *et al.* (2016). Revisiting Cardiac Cellular Composition. Circ Res *118*, 400-409.

Planavila, A., Fernández-Solà, J., and Villarroya, F. (2017). Chapter Nine - Cardiokines as Modulators of Stress-Induced Cardiac Disorders. In Advances in Protein Chemistry and Structural Biology, R. Donev, ed. (Academic Press), pp. 227-256.

Plotnikov, E.Y., Silachev, D.N., Popkov, V.A., Zorova, L.D., Pevzner, I.B., Zorov, S.D., Jankauskas, S.S., Babenko, V.A., Sukhikh, G.T., and Zorov, D.B. (2017). Intercellular Signalling Cross-Talk: To Kill, To Heal and To Rejuvenate. Heart, Lung and Circulation *26*, 648-659.

Polyakova, V., Loeffler, I., Hein, S., Miyagawa, S., Piotrowska, I., Dammer, S., Risteli, J., Schaper, J., and Kostin, S. (2011). Fibrosis in endstage human heart failure: Severe changes in collagen metabolism and MMP/TIMP profiles. International Journal of Cardiology *151*, 18-33.

Ponikowski, P., Anker, S.D., AlHabib, K.F., Cowie, M.R., Force, T.L., Hu, S., Jaarsma, T., Krum, H., Rastogi, V., Rohde, L.E., *et al.* (2014). Heart failure: preventing disease and death worldwide. ESC Heart Failure *1*, 4-25.

Pons, F., Lupón, J., Urrutia, A., González, B., Crespo, E., Díez, C., Cano, L., Cabanes, R., Altimir, S., Coll, R., *et al.* (2010). Mortality and Cause of Death in Patients With Heart Failure: Findings at a Specialist Multidisciplinary Heart Failure Unit. Revista Española de Cardiología (English Edition) *63*, 303-314.

Porter, K.E., and Turner, N.A. (2009). Cardiac fibroblasts: At the heart of myocardial remodeling. Pharmacology & Therapeutics *123*, 255-278.

Rabouille, C. (2017). Pathways of Unconventional Protein Secretion. Trends in Cell Biology *27*, 230-240.

Reed, S.M., and Quelle, D.E. (2014). p53 Acetylation: Regulation and Consequences. Cancers *7*, 30-69.

Remensnyder, J.P., and Majno, G. (1968). Oxygen gradients in healing wounds. Am J Pathol *52*, 301-323.

Rizk, S.M., El-Maraghy, S.A., and Nassar, N.N. (2014). A Novel Role for SIRT-1 in L-Arginine Protection against STZ Induced Myocardial Fibrosis in Rats. PLOS ONE *9*, e114560.

Robin, E.D., Murphy, B.J., and Theodore, J. (1984). Coordinate regulation of glycolysis by hypoxia in mammalian cells. J Cell Physiol *118*, 287-290.

Robinson, C.M., Neary, R., Levendale, A., Watson, C.J., and Baugh, J.A. (2012). Hypoxia-induced DNA hypermethylation in human pulmonary fibroblasts is associated with Thy-1 promoter methylation and the development of a pro-fibrotic phenotype. Respir Res *13*, 74.

Russo, I., and Frangogiannis, N.G. (2016). Diabetes-associated cardiac fibrosis: Cellular effectors, molecular mechanisms and therapeutic opportunities. J Mol Cell Cardiol *90*, 84-93.

Sanchez, C., Mathy-Hartert, M., Deberg, M.A., Ficheux, H., Reginster, J.Y., and Henrotin, Y.E. (2003). Effects of rhein on human articular chondrocytes in alginate beads. Biochemical pharmacology *65*, 377-388.

Sassi, Y., Ahles, A., Truong, D.-J.J., Baqi, Y., Lee, S.-Y., Husse, B., Hulot, J.-S., Foinquinos, A., Thum, T., Müller, C.E., *et al.* (2014). Cardiac myocyte–secreted cAMP exerts paracrine action via adenosine receptor activation. The Journal of Clinical Investigation *124*, 5385-5397.

Savarese, G., and Lund, L.H. (2017). Global Public Health Burden of Heart Failure. Cardiac Failure Review *3*, 7-11.

Schiller, M., Javelaud, D., and Mauviel, A. (2004). TGF-β-induced SMAD signaling and gene regulation: consequences for extracellular matrix remodeling and wound healing. Journal of Dermatological Science *35*, 83-92.

Schmid, T., Zhou, J., Köhl, R., and Brüne, B. (2004). p300 relieves p53-evoked transcriptional repression of hypoxia-inducible factor-1 (HIF-1). The Biochemical journal *380*, 289-295.

Schuetze, K.B., McKinsey, T.A., and Long, C.S. (2014). Targeting cardiac fibroblasts to treat fibrosis of the heart: focus on HDACs. Journal of molecular and cellular cardiology *70*, 100-107.

Schuetze, K.B., Stratton, M.S., Blakeslee, W.W., Wempe, M.F., Wagner, F.F., Holson, E.B., Kuo, Y.-M., Andrews, A.J., Gilbert, T.M., Hooker, J.M.*, et al.* (2017). Overlapping and Divergent Actions of Structurally Distinct Histone Deacetylase Inhibitors in Cardiac Fibroblasts. The Journal of pharmacology and experimental therapeutics *361*, 140-150.

Semenza, G.L. (1999). Regulation of Mammalian O2 Homeostasis by Hypoxia-Inducible Factor 1. Annual Review of Cell and Developmental Biology *15*, 551-578.

Semenza, G.L. (2012). Hypoxia-inducible factors: mediators of cancer progression and targets for cancer therapy. Trends in pharmacological sciences *33*, 207-214.

Senavirathna, L.K., Huang, C., Yang, X., Munteanu, M.C., Sathiaseelan, R., Xu, D., Henke, C.A., and Liu, L. (2018). Hypoxia induces pulmonary fibroblast proliferation through NFAT signaling. Sci Rep *8*, 2709.

Sharma, S., Gerke, D.S., Han, H.F., Jeong, S., Stallcup, M.R., Jones, P.A., and Liang, G. (2012). Lysine methyltransferase G9a is not required for DNMT3A/3B anchoring to methylated nucleosomes and maintenance of DNA methylation in somatic cells. Epigenetics & Chromatin *5*, 3.

Sheng-Nan, P., Hui-Hong, Z., Ai-Xiang, F., Xiao-Wen, C., and Qing-Xian, Z. (2013). Protection of rhein on IgA nephropathy mediated by inhibition of fibronectin expression in rats. Indian journal of pharmacology *45*, 174-179.

Shi, M., Zhu, J., Wang, R., Chen, X., Mi, L., Walz, T., and Springer, T.A. (2011). Latent TGF-β structure and activation. Nature *474*, 343.

Shi, Y., and Massague, J. (2003). Mechanisms of TGF-beta signaling from cell membrane to the nucleus. Cell *113*, 685-700.

Shimwell, N.J., Bryan, R.T., Wei, W., James, N.D., Cheng, K.K., Zeegers, M.P., Johnson, P.J., Martin, A., and Ward, D.G. (2013). Combined proteome and transcriptome analyses for the discovery of urinary biomarkers for urothelial carcinoma. British journal of cancer *108*, 1854-1861.

Shinde, A.V., and Frangogiannis, N.G. (2017). Mechanisms of Fibroblast Activation in the Remodeling Myocardium. Current Pathobiology Reports *5*, 145-152.

Simonsson, M., Heldin, C.-H., Ericsson, J., and Grönroos, E. (2005). The Balance between Acetylation and Deacetylation Controls Smad7 Stability. Journal of Biological Chemistry *280*, 21797-21803.

Snider, P., Standley, K.N., Wang, J., Azhar, M., Doetschman, T., and Conway, S.J. (2009). Origin of cardiac fibroblasts and the role of periostin. Circ Res *105*, 934-947.

Souders, C.A., Bowers, S.L., and Baudino, T.A. (2009). Cardiac fibroblast: the renaissance cell. Circ Res *105*, 1164-1176.

Spencer, C.M., and Wilde, M.I. (1997). Diacerein. Drugs *53*, 98-106.

Spinale, F.G. (2007). Myocardial matrix remodeling and the matrix metalloproteinases: influence on cardiac form and function. Physiological reviews *87*, 1285-1342.

Spriggs, K.A., Bushell, M., and Willis, A.E. (2010). Translational regulation of gene expression during conditions of cell stress. Molecular cell *40*, 228-237.

Stein, K.R., Giardina, B.J., and Hui-Ling Chiang (2014). - The Non-classical Pathway is the Major Pathway to Secrete Proteins in Saccharomyces cerevisiae. *- 4*, - 11.

Stine, Z.E., Walton, Z.E., Altman, B.J., Hsieh, A.L., and Dang, C.V. (2015). MYC, Metabolism, and Cancer. Cancer discovery *5*, 1024-1039.

Stopa, M., Anhuf, D., Terstegen, L., Gatsios, P., Gressner, A.M., and Dooley, S. (2000). Participation of Smad2, Smad3, and Smad4 in transforming growth factor beta (TGF-beta)-induced activation of Smad7. THE TGF-beta response element of the promoter requires functional Smad binding element and E-box sequences for transcriptional regulation. J Biol Chem *275*, 29308-29317.

Storey, K.B., and Storey, J.M. (2004). Metabolic rate depression in animals: transcriptional and translational controls. Biological reviews of the Cambridge Philosophical Society *79*, 207-233.

Stratton, M.S., and McKinsey, T.A. (2016). Epigenetic regulation of cardiac fibrosis. Journal of molecular and cellular cardiology *92*, 206-213.

Su, J., Yin, L.P., Zhang, X., Li, B.B., Liu, L., and Li, H. (2013). Chronic allograft nephropathy in rats is improved by the intervention of rhein. Transplantation proceedings *45*, 2546-2552.

Sun, H., Luo, G., Chen, D., and Xiang, Z. (2016). A Comprehensive and System Review for the Pharmacological Mechanism of Action of Rhein, an Active Anthraquinone Ingredient. Front Pharmacol *7*, 247.

Sutton, M.G., and Sharpe, N. (2000). Left ventricular remodeling after myocardial infarction: pathophysiology and therapy. Circulation *101*, 2981-2988.

Suzuki, C., Murakami, G., Fukuchi, M., Shimanuki, T., Shikauchi, Y., Imamura, T., and Miyazono, K. (2002). Smurf1 regulates the inhibitory activity of Smad7 by targeting Smad7 to the plasma membrane. J Biol Chem *277*, 39919-39925.

Taipale, J., Miyazono, K., Heldin, C.H., and Keski-Oja, J. (1994). Latent transforming growth factor-beta 1 associates to fibroblast extracellular matrix via latent TGF-beta binding protein. The Journal of cell biology *124*, 171-181.

Takeda, N., Maemura, K., Imai, Y., Harada, T., Kawanami, D., Nojiri, T., Manabe, I., and Nagai, R. (2004). Endothelial PAS Domain Protein 1 Gene Promotes Angiogenesis Through the Transactivation of Both Vascular Endothelial Growth Factor and Its Receptor, Flt-1. Circulation Research *95*, 146-153.

Takeda, N., and Manabe, I. (2011). Cellular Interplay between Cardiomyocytes and Nonmyocytes in Cardiac Remodeling. International Journal of Inflammation *2011*, 13.

Talasaz, A.H., Khalili, H., Jenab, Y., Salarifar, M., Broumand, M.A., and Darabi, F. (2013). N-Acetylcysteine Effects on Transforming Growth Factor-β and Tumor Necrosis Factor-α Serum Levels as Pro-Fibrotic and Inflammatory Biomarkers in Patients Following ST-Segment Elevation Myocardial Infarction. Drugs in R&D *13*, 199-205.

Tan, J., Gu, Y., Zhang, X., You, S., Lu, X., Chen, S., Han, X., and Sun, Y. (2013). Hypermethylation of CpG islands is more prevalent than hypomethylation across the entire genome in breast carcinogenesis. Clinical and Experimental Medicine *13*, 1-9.

Tan, L.B., Williams, S.G., Tan, D.K., and Cohen-Solal, A. (2010). So many definitions of heart failure: are they all universally valid? A critical appraisal. Expert Rev Cardiovasc Ther *8*, 217-228.

Tang, Y., Nyengaard, J.R., Andersen, J.B., Baandrup, U., and Gundersen, H.J. (2009). The application of stereological methods for estimating structural parameters in the human heart. Anatomical record (Hoboken, NJ : 2007) *292*, 1630-1647.

Tang, Y., Zhao, W., Chen, Y., Zhao, Y., and Gu, W. (2008). Acetylation Is Indispensable for p53 Activation. Cell *133*, 612-626.

Taniguchi, T., Iwashita, J., Murata, J., Ueda, K., and Abe, T. (2012). The histone deacetylase inhibitor trichostatin A induces cell cycle arrest and rapid upregulation of gadd45¦Â in LS174T human colon cancer cells. Advances in Biological Chemistry *Vol.02No.01*, 8.

Tao, H., Shi, K.-H., Yang, J.-J., Huang, C., Liu, L.-P., and Li, J. (2013). Epigenetic regulation of cardiac fibrosis. Cellular Signalling *25*, 1932-1938.

Taylor, W.R., and Stark, G.R. (2001). Regulation of the G2/M transition by p53. Oncogene *20*, 1803.

Tian, K., Liu, Z., Wang, J., Xu, S., You, T., and Liu, P. (2015). Sirtuin-6 inhibits cardiac fibroblasts differentiation into myofibroblasts via inactivation of nuclear factor kappaB signaling. Translational research : the journal of laboratory and clinical medicine *165*, 374-386.

Tirziu, D., Giordano, F.J., and Simons, M. (2010). Cell Communications in the Heart. Circulation *122*, 928-937.

Torina, A.G., Reichert, K., Lima, F., de Souza Vilarinho, K.A., de Oliveira, P.P., do Carmo, H.R., de Carvalho, D.D., Saad, M.J., Sposito, A.C., and Petrucci, O. (2015). Diacerein improves left ventricular remodeling and cardiac function by reducing the inflammatory response after myocardial infarction. PLoS One *10*, e0121842.

Townley-Tilson, W.H., Pi, X., and Xie, L. (2015). The Role of Oxygen Sensors, Hydroxylases, and HIF in Cardiac Function and Disease. Oxidative medicine and cellular longevity *2015*, 676893.

Travers, J.G., Kamal, F.A., Robbins, J., Yutzey, K.E., and Blaxall, B.C. (2016). Cardiac Fibrosis: The Fibroblast Awakens. Circ Res *118*, 1021-1040.

Tritschler, I., Gramatzki, D., Capper, D., Mittelbronn, M., Meyermann, R., Saharinen, J., Wick, W., Keski-Oja, J., and Weller, M. (2009). Modulation of TGF-beta activity by latent TGF-beta-binding protein 1 in human malignant glioma cells. International journal of cancer *125*, 530-540.

Tsang, S.W., and Bian, Z.X. (2015). Anti-fibrotic and anti-tumorigenic effects of rhein, a natural anthraquinone derivative, in mammalian stellate and carcinoma cells. Phytotherapy research : PTR *29*, 407-414.

Tsang, S.W., Zhang, H., Lin, C., Xiao, H., Wong, M., Shang, H., Yang, Z.-J., Lu, A., Yung, K.K.-L., and Bian, Z. (2013a). Rhein, a natural anthraquinone derivative, attenuates the activation of pancreatic stellate cells and ameliorates pancreatic fibrosis in mice with experimental chronic pancreatitis. PloS one *8*, e82201-e82201.

Tsang, S.W., Zhang, H., Lin, C., Xiao, H., Wong, M., Shang, H., Yang, Z.J., Lu, A., Yung, K.K., and Bian, Z. (2013b). Rhein, a natural anthraquinone derivative, attenuates the activation of pancreatic stellate cells and ameliorates pancreatic fibrosis in mice with experimental chronic pancreatitis. PLoS One *8*, e82201.

Uchida, T., Rossignol, F., Matthay, M.A., Mounier, R., Couette, S., Clottes, E., and Clerici, C. (2004). Prolonged Hypoxia Differentially Regulates Hypoxia-inducible Factor (HIF)-1α and HIF-2α Expression in Lung Epithelial Cells: IMPLICATION OF NATURAL ANTISENSE HIF-1α. Journal of Biological Chemistry *279*, 14871-14878.

Ugolini, G.S., Pavesi, A., Rasponi, M., Fiore, G.B., Kamm, R., and Soncini, M. (2017). Human cardiac fibroblasts adaptive responses to controlled combined mechanical strain and oxygen changes in vitro. eLife *6*.

Van Linthout, S., Miteva, K., and Tschöpe, C. (2014). Crosstalk between fibroblasts and inflammatory cells. Cardiovascular Research *102*, 258-269.

Vilahur, G., Juan-Babot, O., Pena, E., Onate, B., Casani, L., and Badimon, L. (2011). Molecular and cellular mechanisms involved in cardiac remodeling after acute myocardial infarction. J Mol Cell Cardiol *50*, 522-533.

Wang, H., Zhou, W., Zheng, Z., Zhang, P., Tu, B., He, Q., and Zhu, W.G. (2012a). The HDAC inhibitor depsipeptide transactivates the p53/p21 pathway by inducing DNA damage. DNA repair *11*, 146-156.

Wang, Q., Zhang, N.N., Li, H.Y., Jiang, M., Gao, J., and Bai, G. (2012b). [Active ingredients in rhubarb with anti-proliferative effects on scar fibroblasts]. Yao xue xue bao = Acta pharmaceutica Sinica *47*, 1618-1622.

Wang, Y., Miao, X., Liu, Y., Li, F., Liu, Q., Sun, J., and Cai, L. (2014). Dysregulation of histone acetyltransferases and deacetylases in cardiovascular diseases. Oxidative medicine and cellular longevity *2014*, 641979-641979.

Watson, C.J., Collier, P., Tea, I., Neary, R., Watson, J.A., Robinson, C., Phelan, D., Ledwidge, M.T., McDonald, K.M., McCann, A*., et al.* (2014). Hypoxia-induced epigenetic modifications are associated with cardiac tissue fibrosis and the development of a myofibroblast-like phenotype. Hum Mol Genet *23*, 2176-2188.

Watson, C.J., Horgan, S., Neary, R., Glezeva, N., Tea, I., Corrigan, N., McDonald, K., Ledwidge, M., and Baugh, J. (2016). Epigenetic Therapy for the Treatment of Hypertension-Induced Cardiac Hypertrophy and Fibrosis. Journal of Cardiovascular Pharmacology and Therapeutics *21*, 127-137.

Weber, K., Sun, y., Bhattacharya, S., Ahokas, R., and C Gerling, I. (2012a). Myofibroblast-mediated mechanisms of pathological remodelling of the heart, Vol 10.

Weber, K.T., and Diez, J. (2016). Targeting the Cardiac Myofibroblast Secretome to Treat Myocardial Fibrosis in Heart Failure. Circulation Heart failure *9*.

Weber, K.T., Sun, Y., Bhattacharya, S.K., Ahokas, R.A., and Gerling, I.C. (2012b). Myofibroblast-mediated mechanisms of pathological remodelling of the heart. Nature Reviews Cardiology *10*, 15.

Whitfield, M.L., George, L.K., Grant, G.D., and Perou, C.M. (2006). Common markers of proliferation. Nature Reviews Cancer *6*, 99.

Willems, I.E., Havenith, M.G., De Mey, J.G., and Daemen, M.J. (1994). The alpha-smooth muscle actin-positive cells in healing human myocardial scars. Am J Pathol *145*, 868-875.

Williams, S.M., Golden-Mason, L., Ferguson, B.S., Schuetze, K.B., Cavasin, M.A., Demos-Davies, K., Yeager, M.E., Stenmark, K.R., and McKinsey, T.A. (2014). Class I HDACs regulate angiotensin II-dependent cardiac fibrosis via fibroblasts and circulating fibrocytes. Journal of Molecular and Cellular Cardiology *67*, 112-125.

Wilson, K., Suveizdyt, K., Liles, J., Budas, G., Peacock, A., and Welsh, D. (2015). Hypoxia-induced pulmonary artery fibroblast proliferation and migration is prevented by ASK1 inhibition in an in vitro cellular model of pulmonary hypertension. European Respiratory Journal *46*.

Wipff, P.-J., Rifkin, D.B., Meister, J.-J., and Hinz, B. (2007). Myofibroblast contraction activates latent TGF-β1 from the extracellular matrix. The Journal of cell biology *179*, 1311-1323.

Wouters, B.G., van den Beucken, T., Magagnin, M.G., Koritzinsky, M., Fels, D., and Koumenis, C. (2005). Control of the hypoxic response through regulation of mRNA translation. Seminars in cell & developmental biology *16*, 487-501.

Wrobel, L.K., Fray, T.R., Molloy, J.E., Adams, J.J., Armitage, M.P., and Sparrow, J.C. (2002). Contractility of single human dermal myofibroblasts and fibroblasts. Cell motility and the cytoskeleton *52*, 82-90.

Yang, L., Besschetnova, T.Y., Brooks, C.R., Shah, J.V., and Bonventre, J.V. (2010). Epithelial cell cycle arrest in G2/M mediates kidney fibrosis after injury. Nature medicine *16*, 535-143.

Yang, Y., Nephew, K., and Kim, S. (2012). A novel k-mer mixture logistic regression for methylation susceptibility modeling of CpG dinucleotides in human gene promoters. BMC Bioinformatics *13*, S15.

Yao, H.-W., and Li, J. (2015). Epigenetic Modifications in Fibrotic Diseases: Implications for Pathogenesis and Pharmacological Targets. Journal of Pharmacology and Experimental Therapeutics *352*, 2-13.

Yoon, S., and Eom, G.H. (2016). HDAC and HDAC Inhibitor: From Cancer to Cardiovascular Diseases. Chonnam medical journal *52*, 1-11.

Yosef, R., Pilpel, N., Papismadov, N., Gal, H., Ovadya, Y., Vadai, E., Miller, S., Porat, Z., Ben-Dor, S., and Krizhanovsky, V. (2017). p21 maintains senescent cell viability under persistent DNA damage response by restraining JNK and caspase signaling. The EMBO journal *36*, 2280-2295.

Yu, L.M., and Xu, Y. (2015). Epigenetic regulation in cardiac fibrosis. World journal of cardiology *7*, 784-791.

Zeisberg, E.M., Tarnavski, O., Zeisberg, M., Dorfman, A.L., McMullen, J.R., Gustafsson, E., Chandraker, A., Yuan, X., Pu, W.T., Roberts, A.B.*, et al.* (2007). Endothelial-to-mesenchymal transition contributes to cardiac fibrosis. Nature Medicine *13*, 952.

Zhang, M., Fraser, D., and Phillips, A. (2006a). ERK, p38, and Smad signaling pathways differentially regulate transforming growth factor-beta1 autoinduction in proximal tubular epithelial cells. The American journal of pathology *169*, 1282-1293.

Zhang, M., Fraser, D., and Phillips, A. (2006b). ERK, p38, and Smad signaling pathways differentially regulate transforming growth factor-beta1 autoinduction in proximal tubular epithelial cells. Am J Pathol *169*, 1282-1293.

Zhao, X., Li, J., Zhu, S., Liu, Y., Zhao, J., Wan, M., and Tang, W. (2014). Rhein induces a necrosis-apoptosis switch in pancreatic acinar cells. Evid Based Complement Alternat Med *2014*, 404853.

Zhao, Y., Lu, S., Wu, L., Chai, G., Wang, H., Chen, Y., Sun, J., Yu, Y., Zhou, W., Zheng, Q.*, et al.* (2006). Acetylation of p53 at lysine 373/382 by the histone deacetylase inhibitor depsipeptide induces expression of p21(Waf1/Cip1). Molecular and cellular biology *26*, 2782-2790.

Zhou, B., and Pu, W.T. (2011). Epicardial epithelial-to-mesenchymal transition in injured heart. Journal of Cellular and Molecular Medicine *15*, 2781-2783.

Zhou, J., Hara, K., Inoue, M., Hamada, S., Yasuda, H., Moriyama, H., Endo, H., Hirota, K., Yonezawa, K., Nagata, M.*, et al.* (2008). Regulation of hypoxia-inducible factor 1 by glucose availability under hypoxic conditions. The Kobe journal of medical sciences *53*, 283-296.

Zhou, Y.X., Xia, W., Yue, W., Peng, C., Rahman, K., and Zhang, H. (2015). Rhein: A Review of Pharmacological Activities. Evid Based Complement Alternat Med *2015*, 578107.

Zhu, J., Liu, Z., Huang, H., Chen, Z., and Li, L. (2003). Rhein inhibits transforming growth factor beta1 induced plasminogen activator inhibitor-1 in endothelial cells. Chinese medical journal *116*, 354-359.

Zhuonan, Z., Sen, G., Zhipeng, J., Maoyou, Z., Linglan, Y., Gangping, W., Cheng, J., Zhongliang, M., Tian, J., Peijian, Z.*, et al.* (2015). Hypoxia preconditioning induced HIF-1α promotes glucose metabolism and protects mitochondria in liver I/R injury. Clinics and Research in Hepatology and Gastroenterology *39*, 610-619.

Zuo, C., Li, X., Huang, J., Chen, D., Ji, K., Yang, Y., Xu, T., Zhu, D., Yan, C., and Gao, P. (2018). Osteoglycin attenuates cardiac fibrosis by suppressing cardiac myofibroblast proliferation and migration through antagonizing lysophosphatidic acid 3/matrix metalloproteinase 2/epidermal growth factor receptor signalling. Cardiovasc Res *114*, 703-712.

Zymek, P., Bujak, M., Chatila, K., Cieslak, A., Thakker, G., Entman, M.L., and Frangogiannis, N.G. (2006). The role of platelet-derived growth factor signaling in healing myocardial infarcts. J Am Coll Cardiol *48*, 2315-2323.

Appendix

Table 27: Top 50 differentially secreted proteins (>1.5-fold, p-value< 0.05) in the comparison Normoxia vs Hypoxia.

		Normoxia vs. Hypoxia			
Genes	**ID**	**Protein Descriptions**	**Fold Change**	**q-value**	**Unique Peptides**
THBS3	P49746	Thrombospondin-3	-24.75	4.26E-02	19
FAM129B	Q96TA1	Niban-like protein 1	-15.44	3.70E-01	25
ANXA5	P08758	Annexin A5	-9.69	4.56E-05	22
NNMT	P40261	Nicotinamide N-methyltransferase	-9.57	3.83E-01	7
PFKL	P17858	ATP-dependent 6-phosphofructokinase, liver type	-8.77	2.37E-01	5
FABP3	P05413	Fatty acid-binding protein, heart	-8.38	1.23E-10	9
ACO1	P21399	Cytoplasmic aconitate hydratase	-7.88	5.11E-08	21
TMSB4X	P62328	Thymosin beta-4	-7.85	1.86E-01	1
ENO2	P09104	Gamma-enolase	-7.71	1.89E-05	17
MDN1	Q9NU22	Midasin	-7.35	3.72E-01	1
FTH1	P02794	Ferritin heavy chain	-7.3	5.19E-19	16
TTBK1	Q5TCY1	Tau-tubulin kinase 1	-7.13	4.47E-01	1
ANXA4	P09525	Annexin A4	-7.11	2.07E-01	6
STC1	P52823	Stanniocalcin-1	-6.65	1.87E-01	11
PPP2CB	P62714	Serine/threonine-protein phosphatase 2A catalytic subunit beta isoform	-6.32	4.04E-02	5
CFAP100	Q494V2	Cilia- and flagella-associated protein 100	-6.31	3.27E-01	1
VNN1	O95497	Pantetheinase	-6.29	2.94E-01	1
SPON1	Q9HCB6	Spondin-1	-6.22	1.98E-01	2
LMNB1	P20700	Lamin-B1	-6.14	3.27E-01	8
PPP1R12A	O14974	Protein phosphatase 1 regulatory subunit 12A	-5.94	3.07E-01	2
PDXK	O00764	Pyridoxal kinase	-5.54	1.28E-02	6
MYOM1	P52179	Myomesin-1	-5.5	2.04E-01	1
WASHC4	Q2M389	WASH complex subunit 4	-5.43	4.53E-01	1
TPBG	Q13641	Trophoblast glycoprotein	-5.43	1.33E-01	3

ADK	P55263	Adenosine kinase	-5.39	3.60E-01	4
ITGA3	P26006	Integrin alpha-3	-5.27	9.78E-02	6
CTNNA1	P35221	Catenin alpha-1	-5.24	1.49E-01	13
TNXB	P22105	Tenascin-X	-5.19	1.18E-01	3
GABARAP; GABARAPL 1	O95166; Q9H0R8	Gamma-aminobutyric acid receptor-associated protein;Gamma-aminobutyric acid receptor-associated protein-like 1	-5	1.41E-01	3
TPI1	P60174	Triosephosphate isomerase	-4.87	6.82E-13	22
FTL	P02792	Ferritin light chain	-4.69	1.29E-22	11
NUDC	Q9Y266	Nuclear migration protein nudC	-4.57	3.57E-01	6
NT5DC1	Q5TFE4	5'-nucleotidase domain-containing protein 1	-4.54	2.90E-01	3
EIF6	P56537	Eukaryotic translation initiation factor 6	-4.44	9.79E-02	6
CPS1	P31327	Carbamoyl-phosphate synthase [ammonia], mitochondrial	-4.4	3.54E-01	1
UBE2L3	P68036	Ubiquitin-conjugating enzyme E2 L3	-4.38	1.07E-03	10
NPC1	O15118	Niemann-Pick C1 protein	-4.35	3.63E-01	1
PIR	O00625	Pirin	-4.34	2.39E-01	1
PTMA	P06454	Prothymosin alpha	-4.27	2.93E-01	1
CPPED1	Q9BRF8	Serine/threonine-protein phosphatase CPPED1	-4.23	7.80E-02	7
ALB	P02768	Serum albumin	-4.2	3.88E-01	28
LDHAL6B	Q9BYZ2	L-lactate dehydrogenase A-like 6B	-4.14	1.05E-01	1
PPARD	Q03181	Peroxisome proliferator-activated receptor delta	-3.97	4.52E-01	1
IAH1	Q2TAA2	Isoamyl acetate-hydrolyzing esterase 1 homolog	-3.89	3.17E-01	3
ADH5	P11766	Alcohol dehydrogenase class-3	-3.82	1.79E-06	14
ENO3	P13929	Beta-enolase	-3.79	5.93E-03	6
TDRD15	B5MCY1	Tudor domain-containing protein 15	-3.77	3.76E-01	1
SH3BGRL3	Q9H299	SH3 domain-binding glutamic acid-rich-like protein 3	-3.76	3.85E-03	6
S100A13	Q99584	Protein S100-A13	-3.75	2.40E-01	4
FAM180A	Q6UWF9	Protein FAM180A	-3.75	9.68E-02	1
RPL18A	Q02543	60S ribosomal protein L18a	2.51	8.63E-02	2
NRP2	O60462	Neuropilin-2	2.51	1.52E-01	20
SLC39A10	Q9ULF5	Zinc transporter ZIP10	2.53	2.36E-01	1

RPS16	P62249	40S ribosomal protein S16	2.54	5.98E-07	9
CDH23	Q9H251	Cadherin-23	2.57	1.68E-01	1
CHST11	Q9NPF2	Carbohydrate sulfotransferase 11	2.64	2.94E-01	5
FLRT2	O43155	Leucine-rich repeat transmembrane protein FLRT2	2.65	1.12E-01	1
RPL30	P62888	60S ribosomal protein L30	2.66	3.88E-03	5
EIF2S1	P05198	Eukaryotic translation initiation factor 2 subunit 1	2.66	2.93E-01	5
SF3B1	O75533	Splicing factor 3B subunit 1	2.72	2.37E-01	2
JAG1	P78504	Protein jagged-1	2.75	2.55E-01	3
ACOT2;ACOT1	P49753;Q86TX2	Acyl-coenzyme A thioesterase 2, mitochondrial;Acyl-coenzyme A thioesterase 1	2.75	1.13E-01	5
LTBP4	Q8N2S1	Latent-transforming growth factor beta-binding protein 4	2.77	8.56E-02	2
COL14A1	Q05707	Collagen alpha-1(XIV) chain	2.78	4.79E-11	34
RPL3	P39023	60S ribosomal protein L3	2.79	8.52E-02	3
RPS13	P62277	40S ribosomal protein S13	2.79	2.16E-02	4
RPS8	P62241	40S ribosomal protein S8	2.8	2.73E-04	7
MMP1	P03956	Interstitial collagenase	2.81	1.89E-20	41
LXN	Q9BS40	Latexin	2.82	3.55E-01	3
RPS7	P62081	40S ribosomal protein S7	2.85	1.04E-04	7
ERH	P84090	Enhancer of rudimentary homolog	2.86	1.09E-01	1
KITLG	P21583	Kit ligand	2.88	6.36E-02	1
RPS14	P62263	40S ribosomal protein S14	2.89	9.67E-02	3
BLVRA	P53004	Biliverdin reductase A	2.93	1.54E-06	7
RPS10	P46783	40S ribosomal protein S10	2.93	1.73E-03	5
ADAMTS1	Q9UHI8	A disintegrin and metalloproteinase with thrombospondin motifs 1	2.98	3.99E-02	11
RPL14	P50914	60S ribosomal protein L14	2.98	1.27E-01	2
RPS6	P62753	40S ribosomal protein S6	3.05	2.67E-02	2
RPL7	P18124	60S ribosomal protein L7	3.06	8.93E-03	5
GDF15	Q99988	Growth/differentiation factor 15	3.13	4.89E-06	11
TFPI2	P48307	Tissue factor pathway inhibitor 2	3.13	7.88E-02	6
IFITM1;IFITM3;IFITM2	P13164;Q01628;Q01629	Interferon-induced transmembrane protein 1;Interferon-induced transmembrane protein	3.19	3.76E-01	1

		3;Interferon-induced transmembrane protein 2			
DBNL	Q9UJU6	Drebrin-like protein	3.27	2.78E-01	4
NRG1	Q02297	Pro-neuregulin-1, membrane-bound isoform	3.29	1.65E-01	1
SERPINA10	Q9UK55	Protein Z-dependent protease inhibitor	3.33	2.85E-01	1
RPL7A	P62424	60S ribosomal protein L7a	3.36	1.61E-01	4
RPL18	Q07020	60S ribosomal protein L18	3.56	5.90E-02	1
RPL27A	P46776	60S ribosomal protein L27a	3.71	8.53E-03	4
NPTX1	Q15818	Neuronal pentraxin-1	4.04	1.89E-01	2
RPS24	P62847	40S ribosomal protein S24	4.18	3.03E-02	2
RTCB	Q9Y3I0	tRNA-splicing ligase RtcB homolog	4.45	1.64E-01	2
NUCKS1	Q9H1E3	Nuclear ubiquitous casein and cyclin-dependent kinase substrate 1	4.75	2.26E-01	1
RPL4	P36578	60S ribosomal protein L4	4.85	2.10E-02	4
RPS15	P62841	40S ribosomal protein S15	5.41	2.49E-03	1
PSMD13	Q9UNM6	26S proteasome non-ATPase regulatory subunit 13	6.44	1.93E-01	9
CCL2	P13500	C-C motif chemokine 2	9.44	3.14E-01	5
HS1BP3	Q53T59	HCLS1-binding protein 3	19.47	2.93E-01	2
SNRNP200	O75643	U5 small nuclear ribonucleoprotein 200 kDa helicase	28.31	2.37E-01	6
PTPRF	P10586	Receptor-type tyrosine-protein phosphatase F	99.48	1.06E-01	14
ATP6V1B2	P21281	V-type proton ATPase subunit B, brain isoform	170.31	3.33E-01	19

negative value: more abundant in hypoxia, positive value: more abundant in normoxia

Table 28: Top 50 differentially secreted proteins (>1.5-fold, p-value< 0.05) in the comparison Normoxia vs Hypoxia.

Normoxia vs. Normoxia+Rhein					
Genes	**ID**	**Protein Descriptions**	**Fold Change**	**q-value**	**Unique Peptides**
CACNA2D1	P54289	Voltage-dependent calcium channel subunit alpha-2/delta-1	-91.9	8.56E-02	7
DBI	P07108	Acyl-CoA-binding protein	-43.88	9.60E-02	3
ATP6V1B2	P21281	V-type proton ATPase subunit B, brain isoform	-35.88	2.91E-01	19
PSMD13	Q9UNM6	26S proteasome non-ATPase regulatory subunit 13	-29.87	1.29E-01	9
CDK14;CDK1;CDK4;CDK2;CDK9;C	O94921;P06493;P11802;P24	Cyclin-dependent kinase 14;Cyclin-dependent kinase 1;Cyclin-dependent kinase	-23.11	1.63E-01	1

DK3;CDK6;CDK5;CDK16;CDK17;CDK18;CDK13;CDK15;CDK12	941;P50750;Q00526;Q00534;Q00535;Q00536;Q00537;Q07002;Q14004;Q96Q40;Q9NYV4	4;Cyclin-dependent kinase 2;Cyclin-dependent kinase 9;Cyclin-dependent kinase 3;Cyclin-dependent kinase 6;Cyclin-dependent-like kinase 5;Cyclin-dependent kinase 16;Cyclin-dependent kinase 17;Cyclin-dependent kinase 18;Cyclin-dependent kinase 13;Cyclin-dependent kinase 15;Cyclin-dependent kinase 12			
GDF15	Q99988	Growth/differentiation factor 15	-18.84	2.01E-19	11
LIF	P15018	Leukemia inhibitory factor	-9.99	6.80E-04	7
KRT19	P08727	Keratin, type I cytoskeletal 19	-9.83	4.05E-02	1
CPS1	P31327	Carbamoyl-phosphate synthase [ammonia], mitochondrial	-8.48	5.99E-02	1
MAPK14	Q16539	Mitogen-activated protein kinase 14	-8.27	1.05E-01	2
AGRN	O00468	Agrin	-7.79	4.09E-01	7
TRAPPC6B	Q86SZ2	Trafficking protein particle complex subunit 6B	-7.51	1.14E-01	1
COPE	O14579	Coatomer subunit epsilon	-7.35	9.82E-03	10
SLC44A1	Q8WWI5	Choline transporter-like protein 1	-7.14	1.60E-01	2
PPP2CB	P62714	Serine/threonine-protein phosphatase 2A catalytic subunit beta isoform	-7.13	2.92E-02	5
NUDC	Q9Y266	Nuclear migration protein nudC	-6.64	1.66E-01	6
JUP	P14923	Junction plakoglobin	-6.53	3.73E-01	2
SLC2A1	P11166	Solute carrier family 2, facilitated glucose transporter member 1	-6.39	1.64E-02	1
ANXA11	P50995	Annexin A11	-6.3	3.58E-02	2
KRT16	P08779	Keratin, type I cytoskeletal 16	-5.91	2.00E-11	17
SUSD2	Q9UGT4	Sushi domain-containing protein 2	-5.45	1.62E-01	4
LCN1	P31025	Lipocalin-1	-5.4	3.33E-01	5
DCD	P81605	Dermcidin	-5.28	1.73E-01	1
AZGP1	P25311	Zinc-alpha-2-glycoprotein	-5.22	2.72E-01	2
GPC1	P35052	Glypican-1	-5.14	6.18E-38	22
KRT17	Q04695	Keratin, type I cytoskeletal 17	-5.14	8.07E-06	12
LYZ	P61626	Lysozyme C	-5.13	2.83E-02	7
IL6	P05231	Interleukin-6	-5.1	5.80E-03	15
CTSL	P07711	Cathepsin L1	-5.05	1.51E-29	14
STOM	P27105	Erythrocyte band 7 integral membrane protein	-4.9	6.12E-11	8

ACAA1	P09110	3-ketoacyl-CoA thiolase, peroxisomal	-4.77	1.96E-02	4
MMP1	P03956	Interstitial collagenase	-4.66	2.30E-14	41
KRT14	P02533	Keratin, type I cytoskeletal 14	-4.53	1.54E-25	30
JRK	O75564	Jerky protein homolog	-4.46	2.12E-01	1
FLG2	Q5D862	Filaggrin-2	-4.44	1.90E-01	2
ZG16B	Q96DA0	Zymogen granule protein 16 homolog B	-4.42	4.82E-02	5
CSF1	P09603	Macrophage colony-stimulating factor 1	-4.36	2.78E-17	9
STO ml3	Q8TAV4	Stomatin-like protein 3	-4.32	9.43E-03	1
RPL35A	P18077	60S ribosomal protein L35a	-4.32	5.02E-03	3
CSTA	P01040	Cystatin-A	-4.31	2.68E-01	3
KRT2	P35908	Keratin, type II cytoskeletal 2 epidermal	-4.29	7.92E-36	44
SRSF1	Q07955	Serine/arginine-rich splicing factor 1	-4.26	4.44E-02	3
TGM3	Q08188	Protein-glutamine gamma-glutamyltransferase E	-4.15	2.82E-01	2
SLC3A2	P08195	4F2 cell-surface antigen heavy chain	-4.14	1.10E-10	15
KRT78	Q8N1N4	Keratin, type II cytoskeletal 78	-4.14	1.16E-01	1
PCOLCE2	Q9UKZ9	Procollagen C-endopeptidase enhancer 2	-4.12	8.44E-02	13
MMP10	P09238	Stromelysin-2	-4.1	1.84E-01	24
ULBP2	Q9BZM5	NKG2D ligand 2	-4.05	5.16E-03	5
VCP	P55072	Transitional endoplasmic reticulum ATPase	-4.04	7.20E-41	43
TGFB2	P61812	Transforming growth factor beta-2	-3.99	3.46E-01	7
HLA-A	P18462	HLA class I histocompatibility antigen, A-25 alpha chain	2.68	1.91E-01	5
XXYLT1	Q8NBI6	Xyloside xylosyltransferase 1	2.73	5.00E-02	3
CHPF	Q8IZ52	Chondroitin sulfate synthase 2	2.74	1.73E-01	2
PSG1	P11464	Pregnancy-specific beta-1-glycoprotein 1	2.78	4.77E-03	5
COL22A1	Q8NFW1	Collagen alpha-1(XXII) chain	2.91	3.08E-01	6
CLEC3B	P05452	Tetranectin	2.94	1.86E-10	11
DMKN	Q6E0U4	Dermokine	2.97	2.10E-01	5
COL1A2	P08123	Collagen alpha-2(I) chain	2.99	7.24E-72	97
AGT	P01019	Angiotensinogen	3.04	2.28E-04	11
SLIT3	O75094	Slit homolog 3 protein	3.05	6.95E-03	21
DCN	P07585	Decorin	3.12	5.29E-38	29

SNRNP200	O75643	U5 small nuclear ribonucleoprotein 200 kDa helicase	3.12	4.27E-01	6
DCUN1D1	Q96GG9	DCN1-like protein 1	3.14	4.50E-01	2
OLF ml3	Q9NRN5	Olfactomedin-like protein 3	3.15	1.48E-23	23
ADAMTS5	Q9UNA0	A disintegrin and metalloproteinase with thrombospondin motifs 5	3.18	5.00E-02	2
GALNT10	Q86SR1	Polypeptide N-acetylgalactosaminyltransferase 10	3.2	8.71E-04	12
LAMA5	O15230	Laminin subunit alpha-5	3.27	7.99E-02	4
CTHRC1	Q96CG8	Collagen triple helix repeat-containing protein 1	3.32	6.16E-04	8
FCGRT	P55899	IgG receptor FcRn large subunit p51	3.32	1.87E-01	1
CDH11	P55287	Cadherin-11	3.43	1.91E-08	19
AEBP1	Q8IUX7	Adipocyte enhancer-binding protein 1	3.44	4.96E-11	23
FAM20C	Q8IXL6	Extracellular serine/threonine protein kinase FAM20C	3.51	6.13E-02	6
MATN2	O00339	Matrilin-2	3.52	2.38E-06	10
MFAP5	Q13361	Microfibrillar-associated protein 5	3.64	1.49E-06	6
LAMA2	P24043	Laminin subunit alpha-2	3.7	1.43E-10	39
COL6A3	P12111	Collagen alpha-3(VI) chain	3.7	8.86E-239	217
LRRC17	Q8N6Y2	Leucine-rich repeat-containing protein 17	3.71	2.40E-06	14
PLTP	P55058	Phospholipid transfer protein	3.75	1.16E-12	17
IGFBP3	P17936	Insulin-like growth factor-binding protein 3	3.81	5.96E-13	12
THBS3	P49746	Thrombospondin-3	3.83	2.80E-12	19
COL5A3	P25940	Collagen alpha-3(V) chain	3.85	8.53E-03	8
GLT8D2	Q9H1C3	Glycosyltransferase 8 domain-containing protein 2	3.99	1.64E-01	2
C4A	P0C0L4	Complement C4-A	4.34	1.79E-01	1
LXN	Q9BS40	Latexin	4.41	3.20E-01	3
Ang	P03950	Angiogenin	4.48	3.47E-03	4
COL11A1	P12107	Collagen alpha-1(XI) chain	4.53	1.65E-01	7
SFRP4	Q6FHJ7	Secreted frizzled-related protein 4	4.58	1.05E-04	13
CXCL12	P48061	Stromal cell-derived factor 1	4.58	3.74E-03	3
FBLN5	Q9UBX5	Fibulin-5	4.76	3.31E-05	9
KDELC1	Q6UW63	KDEL motif-containing protein 1	5.01	1.43E-01	2

SRPX	P78539	Sushi repeat-containing protein SRPX	5.22	3.20E-05	23
ADAM15	Q13444	Disintegrin and metalloproteinase domain-containing protein 15	5.64	1.17E-01	4
ITGBL1	O95965	Integrin beta-like protein 1	5.96	1.87E-02	10
COL14A1	Q05707	Collagen alpha-1(XIV) chain	6.15	1.10E-04	34
NRP2	O60462	Neuropilin-2	6.36	1.78E-01	20
PCDH10	Q9P2E7	Protocadherin-10	7.33	1.27E-03	6
C7	P10643	Complement component C7	7.72	8.87E-07	28
CCL2	P13500	C-C motif chemokine 2	11.18	2.03E-01	5
UBA2	Q9UBT2	SUMO-activating enzyme subunit 2	22.37	2.93E-01	4
OGN	P20774	Mimecan	27.46	8.21E-02	8

negative value: more abundant in Normoxia+Rhein, positive value: more abundant in Normoxia

Table 29: Top 50 differentially secreted proteins (>1.5-fold, p-value< 0.05) in the comparison Normoxia vs Hypoxia.

Hypoxia vs. Hypoxia+Rhein					
Genes	**ID**	**Protein Descriptions**	**Fold Change**	**q-value**	**Unique Peptides**
ATP6V1B2	P21281	V-type proton ATPase subunit B, brain isoform	-1619,19	1,85E-01	19
PTPRF	P10586	Receptor-type tyrosine-protein phosphatase F	-54,65	2,68E-01	14
CDK14;CDK1;CDK4;CDK2;CDK9;CDK3;CDK6;CDK5;CDK16;CDK17;CDK18;CDK13;CDK15;CDK12	O94921;P06493;P11802;P24941;P50750;Q00526;Q00534;Q00535;Q00536;Q00537;Q07002;Q14004;Q96Q40;Q9NYV4	Cyclin-dependent kinase 14;Cyclin-dependent kinase 1;Cyclin-dependent kinase 4;Cyclin-dependent kinase 2;Cyclin-dependent kinase 9;Cyclin-dependent kinase 3;Cyclin-dependent kinase 6;Cyclin-dependent-like kinase 5;Cyclin-dependent kinase 16;Cyclin-dependent kinase 17;Cyclin-dependent kinase 18;Cyclin-dependent kinase 13;Cyclin-dependent kinase 15;Cyclin-dependent kinase 12	-14,72	2,88E-01	1
GOLGA6L4;GOLGA6L9;GOLGA6L3;GOLGA6L10;GOLGA6L19	A6NEF3;A6NEM1;A6NEY3;A6NI86;H0YKK7	Golgin subfamily A member 6-like protein 4;Golgin subfamily A member 6-like protein 9;Putative golgin subfamily A member 6-like protein 3;Golgin subfamily A member 6-like protein 10;Putative golgin subfamily A member 6-like protein 19	-11,68	1,84E-01	1
PSMD13	Q9UNM6	26S proteasome non-ATPase regulatory subunit 13	-6,41	1,86E-01	9

UAP1	Q16222	UDP-N-acetylhexosamine pyrophosphorylase	-5,56	1,39E-01	9
GDF15	Q99988	Growth/differentiation factor 15	-5,12	5,26E-04	11
KITLG	P21583	Kit ligand	-5,00	1,12E-01	1
ADAMTS1	Q9UHI8	A disintegrin and metalloproteinase with thrombospondin motifs 1	-4,82	3,09E-03	11
CFI	P05156	Complement factor I	-4,68	3,06E-01	5
NPTX1	Q15818	Neuronal pentraxin-1	-4,35	1,07E-01	2
NANS	Q9NR45	Sialic acid synthase	-4,30	4,20E-01	4
SLC44A1	Q8WWI5	Choline transporter-like protein 1	-4,24	1,82E-02	2
ASPH	Q12797	Aspartyl/asparaginyl beta-hydroxylase	-4,22	3,77E-01	6
HSPA9	P38646	Stress-70 protein, mitochondrial	-4,18	1,18E-03	18
JUP	P14923	Junction plakoglobin	-4,09	1,81E-01	2
TGM3	Q08188	Protein-glutamine gamma-glutamyltransferase E	-4,04	1,33E-01	2
NRG1	Q02297	Pro-neuregulin-1, membrane-bound isoform	-3,91	1,83E-01	1
CD93	Q9NPY3	Complement component C1q receptor	-3,81	3,78E-01	3
SLC2A1	P11166	Solute carrier family 2, facilitated glucose transporter member 1	-3,79	1,59E-02	1
NPTX2	P47972	Neuronal pentraxin-2	-3,74	4,23E-01	2
GC	P02774	Vitamin D-binding protein	-3,66	3,97E-07	6
IDUA	P35475	Alpha-L-iduronidase	-3,64	3,88E-01	4
KARS	Q15046	Lysine--tRNA ligase	-3,55	3,74E-01	17
HK1	P19367	Hexokinase-1	-3,47	3,39E-01	36
ATP1A1	P05023	Sodium/potassium-transporting ATPase subunit alpha-1	-3,44	5,41E-06	7
LRP10	Q7Z4F1	Low-density lipoprotein receptor-related protein 10	-3,41	4,69E-02	2
HNRNPL	P14866	Heterogeneous nuclear ribonucleoprotein L	-3,40	2,71E-01	5
FKBP2	P26885	Peptidyl-prolyl cis-trans isomerase FKBP2	-3,40	1,88E-01	4
JAG1	P78504	Protein jagged-1	-3,37	1,91E-01	3
ATP6V1A	P38606	V-type proton ATPase catalytic subunit A	-3,34	1,88E-02	26
IGKC	P01834	Immunoglobulin kappa constant	-3,24	1,47E-01	2
KRT17	Q04695	Keratin, type I cytoskeletal 17	-3,23	1,73E-07	12
NRDC	O43847	Nardilysin	-3,19	1,16E-01	10
SEMA4B	Q9NPR2	Semaphorin-4B	-3,18	1,67E-02	2

SYNCRIP	O60506	Heterogeneous nuclear ribonucleoprotein Q	-3,18	1,33E-02	14
MINPP1	Q9UNW1	Multiple inositol polyphosphate phosphatase 1	-3,17	9,61E-03	18
UBAC2	Q8NBM4	Ubiquitin-associated domain-containing protein 2	-3,14	9,01E-02	1
RPS10	P46783	40S ribosomal protein S10	-3,14	1,29E-02	5
GSDMA	Q96QA5	Gasdermin-A	-3,09	3,14E-01	1
EIF3H	O15372	Eukaryotic translation initiation factor 3 subunit H	-2,95	1,90E-01	5
TPM1	P09493	Tropomyosin alpha-1 chain	-2,94	4,03E-01	10
RPL30	P62888	60S ribosomal protein L30	-2,93	5,58E-02	5
AZGP1	P25311	Zinc-alpha-2-glycoprotein	-2,87	3,61E-02	2
AHSG	P02765	Alpha-2-HS-glycoprotein	-2,86	2,23E-02	3
HNRNPAB	Q99729	Heterogeneous nuclear ribonucleoprotein A/B	-2,84	4,13E-02	5
DBNL	Q9UJU6	Drebrin-like protein	-2,83	2,70E-01	4
MMP1	P03956	Interstitial collagenase	-2,83	8,45E-23	41
CA12	O43570	Carbonic anhydrase 12	-2,74	1,07E-02	10
NQO1	P15559	NAD(P)H dehydrogenase [quinone] 1	-2,73	3,19E-10	12
CFAP100	Q494V2	Cilia- and flagella-associated protein 100	2,65	4,37E-01	1
JAM3	Q9BX67	Junctional adhesion molecule C	2,66	3,03E-01	2
FRRS1	Q6ZNA5	Ferric-chelate reductase 1	2,70	2,69E-01	1
YWHAQ	P27348	14-3-3 protein theta	2,72	7,95E-02	10
NT5DC1	Q5TFE4	5'-nucleotidase domain-containing protein 1	2,73	4,27E-01	3
BCAM	P50895	Basal cell adhesion molecule	2,78	1,38E-01	2
ENO2	P09104	Gamma-enolase	2,79	1,63E-01	17
UBE2L3	P68036	Ubiquitin-conjugating enzyme E2 L3	2,80	1,14E-01	10
EIF6	P56537	Eukaryotic translation initiation factor 6	2,81	3,44E-01	6
ARSB	P15848	Arylsulfatase B	2,81	2,30E-02	8
NAXE	Q8NCW5	NAD(P)H-hydrate epimerase	2,96	1,88E-01	7
GABARAP; GABARAPL1	O95166; Q9H0R8	Gamma-aminobutyric acid receptor-associated protein;Gamma-aminobutyric acid receptor-associated protein-like 1	2,99	3,97E-01	3
ZBTB8OS	Q8IWT0	Protein archease	2,99	2,96E-01	1
ITGBL1	O95965	Integrin beta-like protein 1	3,08	2,73E-03	10

SERPINA3	P01011	Alpha-1-antichymotrypsin	3,08	9,06E-03	16
TPBG	Q13641	Trophoblast glycoprotein	3,12	4,54E-01	3
PTMA	P06454	Prothymosin alpha	3,12	3,81E-01	1
ABCF1	Q8NE71	ATP-binding cassette sub-family F member 1	3,13	2,98E-01	1
CTNNA1	P35221	Catenin alpha-1	3,16	1,32E-01	13
CTGF	P29279	Connective tissue growth factor	3,20	1,73E-04	14
WASHC4	Q2M389	WASH complex subunit 4	3,27	4,35E-01	1
HIST2H2AB	Q8IUE6	Histone H2A type 2-B	3,29	1,88E-01	2
C11orf54	Q9H0W9	Ester hydrolase C11orf54	3,31	2,82E-01	2
VNN1	O95497	Pantetheinase	3,31	4,08E-01	1
ANXA4	P09525	Annexin A4	3,34	6,20E-02	6
RBBP4	Q09028	Histone-binding protein RBBP4	3,46	1,53E-01	1
FTH1	P02794	Ferritin heavy chain	3,53	2,14E-06	16
LECT2	O14960	Leukocyte cell-derived chemotaxin-2	3,60	2,85E-01	1
PDCD1LG2	Q9BQ51	Programmed cell death 1 ligand 2	3,86	1,89E-01	1
MYOM1	P52179	Myomesin-1	4,11	3,01E-01	1
ANXA5	P08758	Annexin A5	4,27	1,04E-01	22
CYB5R2	Q6BCY4	NADH-cytochrome b5 reductase 2	4,34	3,08E-01	2
PGF	P49763	Placenta growth factor	4,46	7,89E-02	1
NPC1	O15118	Niemann-Pick C1 protein	4,55	3,48E-01	1
AMIGO2	Q86SJ2	Amphoterin-induced protein 2	4,83	3,51E-01	3
TTBK1	Q5TCY1	Tau-tubulin kinase 1	5,07	4,49E-01	1
CPPED1	Q9BRF8	Serine/threonine-protein phosphatase CPPED1	5,20	1,51E-02	7
JRK	O75564	Jerky protein homolog	5,33	3,25E-01	1
MDN1	Q9NU22	Midasin	5,51	3,59E-01	1
ADK	P55263	Adenosine kinase	7,32	2,30E-01	4
FGFR1	P11362	Fibroblast growth factor receptor 1	7,75	1,89E-01	2
ATP6V1H	Q9UI12	V-type proton ATPase subunit H	8,06	2,95E-01	4
OGN	P20774	Mimecan	8,67	1,99E-02	8
TMSB4X	P62328	Thymosin beta-4	8,81	1,26E-01	1
FAM129B	Q96TA1	Niban-like protein 1	10,79	8,26E-02	25

LMNB1	P20700	Lamin-B1	13,41	1,64E-01	8
PTMS	P20962	Parathymosin	15,93	3,23E-01	1
NNMT	P40261	Nicotinamide N-methyltransferase	16,36	3,90E-01	7
ACO1	P21399	Cytoplasmic aconitate hydratase	20,63	9,29E-03	21
THBS3	P49746	Thrombospondin-3	44,26	1,56E-04	19

negative value: more abundant in Hypoxia+Rhein, positive value: more abundant in Hypoxia

Table 30: Top 50 differentially secreted proteins (>1.5-fold, p-value< 0.05) in the comparison Normoxia vs Hypoxia.

		Normoxia+Rhein vs. Hypoxia+Rhein			
Genes	**ID**	**Protein Descriptions**	**Fold Change**	**q-value**	**Unique Peptides**
SFRP4	Q6FHJ7	Secreted frizzled-related protein 4	-7.97	1.98E-02	13
Ang	P03950	Angiogenin	-6.18	1.07E-03	4
OSBP	P22059	Oxysterol-binding protein 1	-5.13	3.07E-01	3
ADAM15	Q13444	Disintegrin and metalloproteinase domain-containing protein 15	-4.87	3.25E-02	4
CLEC3B	P05452	Tetranectin	-4.81	1.33E-02	11
COL5A3	P25940	Collagen alpha-3(V) chain	-4.62	6.95E-03	8
OPTN	Q96CV9	Optineurin	-4.28	3.54E-01	2
FABP3	P05413	Fatty acid-binding protein, heart	-4.14	1.10E-06	9
CXCL12	P48061	Stromal cell-derived factor 1	-4.1	7.45E-03	3
LXN	Q9BS40	Latexin	-3.78	1.49E-01	3
IGFBP3	P17936	Insulin-like growth factor-binding protein 3	-3.43	7.80E-14	12
STC1	P52823	Stanniocalcin-1	-3.39	2.50E-03	11
PLTP	P55058	Phospholipid transfer protein	-3.32	7.93E-09	17
COL6A3	P12111	Collagen alpha-3(VI) chain	-3.24	1.62E-196	217
GDF6	Q6KF10	Growth/differentiation factor 6	-3.2	2.76E-05	13
LRRC17	Q8N6Y2	Leucine-rich repeat-containing protein 17	-3.1	5.15E-03	14
CDH11	P55287	Cadherin-11	-3.1	4.16E-01	19
FBLN5	Q9UBX5	Fibulin-5	-3.07	2.70E-01	9
COL14A1	Q05707	Collagen alpha-1(XIV) chain	-3	3.31E-02	34

C7	P10643	Complement component C7	-3	1.99E-02	28
COL1A1	P02452	Collagen alpha-1(I) chain	-2.97	3.37E-28	89
RNASE4	P34096	Ribonuclease 4	-2.93	7.64E-03	7
COL1A2	P08123	Collagen alpha-2(I) chain	-2.9	4.54E-22	97
COLEC12	Q5KU26	Collectin-12	-2.83	6.96E-02	4
COL2A1	P02458	Collagen alpha-1(II) chain	-2.81	2.53E-03	6
GRN	P28799	Granulins	-2.8	1.23E-08	14
EPS15L1	Q9UBC2	Epidermal growth factor receptor substrate 15-like 1	-2.78	1.03E-02	2
SRPX	P78539	Sushi repeat-containing protein SRPX	-2.76	1.34E-03	23
SPON2	Q9BUD6	Spondin-2	-2.73	4.20E-03	11
VEGFA	P15692	Vascular endothelial growth factor A	-2.7	1.95E-02	4
GSN	P06396	Gelsolin	-2.64	3.66E-29	38
ITM2B	Q9Y287	Integral membrane protein 2B	-2.63	9.16E-04	8
SLIT3	O75094	Slit homolog 3 protein	-2.63	8.47E-02	21
PLAT	P00750	Tissue-type plasminogen activator	-2.57	3.79E-01	23
UAP1	Q16222	UDP-N-acetylhexosamine pyrophosphorylase	-2.56	3.35E-03	9
COL3A1	P02461	Collagen alpha-1(III) chain	-2.53	3.32E-29	75
DMKN	Q6E0U4	Dermokine	-2.5	1.48E-01	5
CSRP1	P21291	Cysteine and glycine-rich protein 1	-2.38	3.14E-01	8
MGAT2	Q10469	Alpha-1,6-mannosyl-glycoprotein 2-beta-N-acetylglucosaminyltransferase	-2.38	3.92E-02	5
ITGBL1	O95965	Integrin beta-like protein 1	-2.37	3.18E-02	10
APOE	P02649	Apolipoprotein E	-2.36	1.53E-07	19
EXT2	Q93063	Exostosin-2	-2.33	9.31E-09	23
FBLN7	Q53RD9	Fibulin-7	-2.32	1.05E-03	6
DCN	P07585	Decorin	-2.28	4.09E-22	29
LAMA1	P25391	Laminin subunit alpha-1	-2.27	4.67E-02	11
CLU	P10909	Clusterin	-2.25	2.89E-04	16
NOV	P48745	Protein NOV homolog	-2.24	3.68E-03	6
PCOLCE	Q15113	Procollagen C-endopeptidase enhancer 1	-2.19	1.92E-14	28
PAMR1	Q6UXH9	Inactive serine protease PAMR1	-2.18	5.75E-10	25

EXT1	Q16394	Exostosin-1	-2.18	3.66E-08	23
TGFBR3	Q03167	Transforming growth factor beta receptor type 3	3.27	4.02E-01	8
AK1	P00568	Adenylate kinase isoenzyme 1	3.29	1.13E-03	8
TPR	P12270	Nucleoprotein TPR	3.37	2.36E-01	4
PYGL	P06737	Glycogen phosphorylase, liver form	3.44	6.31E-02	17
RPS14	P62263	40S ribosomal protein S14	3.47	1.28E-02	3
C21orf33	P30042	ES1 protein homolog, mitochondrial	3.49	1.54E-01	2
LGMN	Q99538	Legumain	3.55	4.30E-02	19
COLGALT2	Q8IYK4	Procollagen galactosyltransferase 2	3.55	3.07E-01	1
H2AFZ;H2AFV	P0C0S5; Q71UI9	Histone H2A.Z;Histone H2A.V	3.63	1.52E-01	2
ADSL	P30566	Adenylosuccinate lyase	3.69	2.46E-02	6
GPC1	P35052	Glypican-1	3.71	4.72E-16	22
ATP6V1B2	P21281	V-type proton ATPase subunit B, brain isoform	3.77	1.43E-01	19
DCPS	Q96C86	m7GpppX diphosphatase	3.81	1.89E-01	3
RPL4	P36578	60S ribosomal protein L4	3.82	2.59E-01	4
GYG1	P46976	Glycogenin-1	3.86	4.43E-05	5
RPS6	P62753	40S ribosomal protein S6	3.9	1.46E-01	2
SHMT2	P34897	Serine hydroxymethyltransferase, mitochondrial	3.93	6.28E-02	6
BLVRA	P53004	Biliverdin reductase A	3.93	6.39E-05	7
CDH13	P55290	Cadherin-13	3.95	2.45E-01	6
MAPK14	Q16539	Mitogen-activated protein kinase 14	3.98	3.22E-01	2
RPL35A	P18077	60S ribosomal protein L35a	4.06	4.63E-02	3
RPL22	P35268	60S ribosomal protein L22	4.15	2.87E-01	3
RPL7	P18124	60S ribosomal protein L7	4.18	5.33E-03	5
RPL7A	P62424	60S ribosomal protein L7a	4.22	6.40E-02	4
IPO7	O95373	Importin-7	4.24	3.94E-02	9
RPS8	P62241	40S ribosomal protein S8	4.31	6.67E-03	7
RBM3	P98179	RNA-binding protein 3	4.33	4.34E-01	3
LRRC59	Q96AG4	Leucine-rich repeat-containing protein 59	4.42	2.11E-02	4
PTBP1	P26599	Polypyrimidine tract-binding protein 1	4.51	4.93E-02	10

RCC2	Q9P258	Protein RCC2	4.55	4.51E-03	2
MMP1	P03956	Interstitial collagenase	4.62	1.64E-16	41
COPE	O14579	Coatomer subunit epsilon	4.64	2.45E-02	10
TPP2	P29144	Tripeptidyl-peptidase 2	4.64	2.39E-04	25
ERH	P84090	Enhancer of rudimentary homolog	4.92	2.93E-01	1
HIST2H2AB	Q8IUE6	Histone H2A type 2-B	4.93	3.57E-02	2
ULBP2	Q9BZM5	NKG2D ligand 2	5.32	6.13E-04	5
RPL27A	P46776	60S ribosomal protein L27a	5.4	7.87E-02	4
LIF	P15018	Leukemia inhibitory factor	5.53	5.03E-04	7
MMP10	P09238	Stromelysin-2	5.76	4.45E-01	24
RPS15	P62841	40S ribosomal protein S15	5.84	7.23E-02	1
SRSF1	Q07955	Serine/arginine-rich splicing factor 1	5.9	8.15E-02	3
JRK	O75564	Jerky protein homolog	5.91	8.26E-02	1
TRAPPC6B	Q86SZ2	Trafficking protein particle complex subunit 6B	5.98	1.16E-01	1
TGFB2	P61812	Transforming growth factor beta-2	7	1.10E-01	7
TFPI2	P48307	Tissue factor pathway inhibitor 2	7.48	1.54E-01	6
IL6	P05231	Interleukin-6	7.91	1.25E-01	15
GDF15	Q99988	Growth/differentiation factor 15	11.51	6.26E-09	11
DBI	P07108	Acyl-CoA-binding protein	26.01	2.45E-01	3
PSMD13	Q9UNM6	26S proteasome non-ATPase regulatory subunit 13	30.01	1.77E-01	9
CACNA2D1	P54289	Voltage-dependent calcium channel subunit alpha-2/delta-1	61.15	3.17E-01	7

negative value: more abundant in Hypoxia+Rhein, positive value: more abundant in Normoxia+Rhein

Table 31: Top 50 up- and downregulated transcripts in the comparison Hypoxia vs Normoxia (1.5-fold, p-value < 0.05)

Hypoxia vs Normoxia			
Symbol	**ID**	**Expr Fold Change**	**Expr p-value**
SLC7A11	TC04001570.hg.1	-3.84	1.13E-02
NQO1	TC16001225.hg.1	-3.37	3.17E-02
EPHX1	TC01001856.hg.1	-3.15	1.97E-02
SLC2A12	TC06002124.hg.1	-3.09	8.00E-04
PGD	TC01000129.hg.1	-2.73	1.35E-02
ME1	TC06001912.hg.1	-2.7	3.20E-03
SNORD72	TC05001301.hg.1	-2.64	3.55E-02
GCLM	TC01002882.hg.1	-2.63	6.06E-05

ALDH1A1	TC09001211.hg.1	-2.51	2.31E-02
HTR1D	TC01002338.hg.1	-2.45	3.19E-02
MGST1	TC12000207.hg.1	-2.42	9.40E-03
TAF9B	TC0X001176.hg.1	-2.35	2.04E-02
SARS	TC01004603.hg.1	-2.14	3.12E-02
TALDO1	TC11000027.hg.1	-2.08	7.10E-03
G6PD	TC0X002294.hg.1	-2.05	1.18E-02
ASPH	TC08001264.hg.1	-2.04	1.03E-02
EPAS1	TC02000281.hg.1	-2	3.68E-02
HIPK2	TC07003195.hg.1	-1.99	3.29E-02
MFF	TC02001362.hg.1	-1.98	1.27E-02
LOC105370687	TC14001537.hg.1	-1.95	4.33E-02
CYB561A3	TC11001852.hg.1	-1.93	4.66E-02
MAGI1	TC03001529.hg.1	-1.92	8.50E-03
TXNRD1	TC12000810.hg.1	-1.92	2.50E-03
DPH5	TC01002924.hg.1	-1.91	4.00E-04
LOC100507599	TC22001045.hg.1	-1.9	1.62E-02
GABPB2	TC01004738.hg.1	-1.89	6.90E-03
TXN	TC09001473.hg.1	-1.88	2.20E-03
NABP1	TC02001128.hg.1	-1.87	1.50E-03
SDHC	TC01001386.hg.1	-1.87	3.18E-02
SNORD114-10	TC14000687.hg.1	-1.87	4.52E-02
FAM198B-AS1	TC04002938.hg.1	-1.83	4.73E-02
ZFAND5	TC09002594.hg.1	-1.83	3.40E-03
HIF1A	TC14002197.hg.1	-1.82	1.00E-03
TMEM138	TC11000530.hg.1	-1.82	6.40E-03
RRM2B	TC08001496.hg.1	-1.81	3.05E-02
ATP6V1A	TC03000583.hg.1	-1.79	4.21E-02
PELI2	TC14000332.hg.1	-1.78	4.64E-02
COPG2	TC07003379.hg.1	-1.77	4.77E-02
HADHB	TC02000149.hg.1	-1.77	1.60E-03
ERMARD	TC06003227.hg.1	-1.76	1.67E-02
NUDT16	TC03002549.hg.1	-1.76	1.20E-02
COX7C	TC05000427.hg.1	-1.75	3.50E-03
FMO4	TC01001490.hg.1	-1.75	4.10E-02
TRNT1	TC03002195.hg.1	-1.75	3.09E-02
BEX1	TC0X001233.hg.1	-1.74	5.50E-03
NKAPL	TC06000280.hg.1	-1.74	2.23E-02
SEC22B	TC01001086.hg.1	-1.74	9.60E-03
ACO1	TC09000128.hg.1	-1.73	4.91E-02
NOB1	TC16001226.hg.1	-1.73	1.53E-02
SLC48A1	TC12000340.hg.1	-1.73	7.50E-03
	TC21000768.hg.1		
SLC6A15	TC12001784.hg.1	2	4.20E-03
KDM3A	TC02000524.hg.1	2.01	2.09E-02
PRC1	TC15001858.hg.1	2.01	3.69E-02
RNY4	TC06000759.hg.1	2.02	1.77E-02
PLN	TC06003017.hg.1	2.03	1.34E-02
TICRR	TC15000850.hg.1	2.03	7.70E-03
CORIN	TC04001169.hg.1	2.05	1.50E-02

USP17L6P	TC04001892.hg.1	2.05	1.64E-02
MIR210HG	TC11001238.hg.1	2.06	6.00E-04
SUPT20H	TC13001019.hg.1	2.06	1.80E-03
ANKRD37	TC04000905.hg.1	2.1	5.96E-05
PDCD1LG2	TC09000038.hg.1	2.11	1.40E-02
KIF14	TC01003679.hg.1	2.12	2.40E-03
SLAMF7	TC01001372.hg.1	2.14	3.56E-02
CEP55	TC10000664.hg.1	2.21	8.50E-03
IGFBP3	TC07001355.hg.1	2.21	2.46E-02
OR5V1	TC6_mann_hap4000211.hg.1	2.24	1.05E-02
FAM212B-AS1	TC01004622.hg.1	2.26	3.11E-02
DEPDC1	TC01002766.hg.1	2.31	5.80E-03
LOXL2	TC08002613.hg.1	2.31	4.20E-02
TPI1	TC12000096.hg.1	2.31	9.22E-06
NUF2	TC01001430.hg.1	2.33	1.71E-02
NDRG1	TC08001659.hg.1	2.39	6.90E-03
PLOD2	TC03001866.hg.1	2.41	3.77E-02
BUB1	TC02002204.hg.1	2.43	5.50E-03
C5orf46	TC05001912.hg.1	2.44	1.40E-03
CENPF	TC01001791.hg.1	2.44	4.00E-03
PBK	TC08001086.hg.1	2.48	1.23E-02
PTPRB	TC12001718.hg.1	2.5	1.48E-02
EGLN1	TC01006192.hg.1	2.53	2.02E-05
GYS1	TC19002540.hg.1	2.54	3.08E-02
ESCO2	TC08000213.hg.1	2.55	2.12E-02
PDK1	TC02001031.hg.1	2.55	1.80E-03
P4HA1	TC10001398.hg.1	2.64	2.00E-04
PGK1	TC0X000425.hg.1	2.68	1.00E-04
ENO2	TC12000099.hg.1	2.72	3.10E-03
TOP2A	TC17002618.hg.1	2.73	3.31E-02
KIF20A	TC05000697.hg.1	2.74	1.70E-03
BHLHE40	TC03000015.hg.1	2.79	8.00E-03
BNIP3	TC10001769.hg.1	3.21	2.00E-04
SNORA23	TC11000172.hg.1	3.22	4.60E-03
PLK1	TC16000258.hg.1	3.45	1.50E-03
AK4	TC01004452.hg.1	3.62	2.16E-02
DLGAP5	TC14001155.hg.1	3.69	4.00E-03
ANLN	TC07000235.hg.1	4.24	2.60E-02
VEGFA	TC06002799.hg.1	4.34	6.00E-04
SLC2A1	TC01002578.hg.1	4.35	8.00E-04
NEK2	TC01006091.hg.1	4.96	4.00E-04
MKI67	TC10001756.hg.1	6.6	2.10E-03

negative value: more abundant in Normoxia, positive value: more abundant in Hypoxia

Table 32: Top 50 up- and downregulated transcripts in the comparison Normoxia vs Normoxia+Rhein (1.5-fold, p-value < 0.05)

Normoxia vs Normoxia+Rhein			
Symbol	**ID**	**Expr Fold Change**	**Expr p-value**
GDF15	TC19000356.hg.1	-133.8	8.02E-06
PTGS2	TC01003638.hg.1	-21.55	2.76E-05
NPTX1	TC17002817.hg.1	-18.39	1.45E-05
GDNF	TC05002960.hg.1	-17.7	1.40E-03
ULBP1	TC06001089.hg.1	-14.45	4.10E-03
ITGA2	TC05000218.hg.1	-14.28	2.00E-03
BMP2	TC20000067.hg.1	-13.46	6.76E-07
E2F7	TC12001756.hg.1	-12.61	1.00E-02
LIF	TC22000647.hg.1	-12.33	1.67E-06
ITGB3	TC17002878.hg.1	-11.62	5.28E-05
HSD11B1	TC01001750.hg.1	-9.99	1.70E-03
TBX2	TC17002307.hg.1	-9.45	1.00E-03
IL1A	TC02002218.hg.1	-9.12	7.00E-04
HMGA2	TC12002424.hg.1	-8.93	2.33E-06
ACER2	TC09001842.hg.1	-8.83	6.00E-06
CXCL8	TC04000408.hg.1	-8.79	1.25E-02
ANXA10	TC04000836.hg.1	-8.6	9.80E-06
MT2A	TC16002034.hg.1	-8.45	9.00E-04
PAQR5	TC15000635.hg.1	-8.16	1.50E-02
DUSP4	TC08002271.hg.1	-7.94	2.20E-03
HBEGF	TC05001854.hg.1	-7.66	2.98E-06
NPC1	TC18000413.hg.1	-7.41	7.99E-05
SLC7A11	TC04001570.hg.1	-7.39	4.00E-04
LOC100126784	TC11001483.hg.1	-7.25	1.52E-06
RNU11	TC01000388.hg.1	-6	1.20E-03
PLK3	TC01000566.hg.1	-5.91	4.05E-06
FOSL1	TC11001948.hg.1	-5.8	3.21E-09
TNFRSF10A	TC08001052.hg.1	-5.75	1.86E-07
DUSP5	TC10000801.hg.1	-5.64	4.82E-08
ZSWIM6	TC05000262.hg.1	-5.61	8.29E-05
DUSP6	TC12001796.hg.1	-5.58	8.36E-06
LINC00520	TC14001162.hg.1	-5.53	1.45E-05
AKR1B10	TC07002600.hg.1	-5.5	3.30E-03
CDK17	TC12001845.hg.1	-5.5	9.28E-05
EPGN	TC04000413.hg.1	-5.46	1.29E-05
DCLK2	TC04002263.hg.1	-5.41	2.96E-05
CCND1	TC11000718.hg.1	-5.34	1.90E-03
IRAK2	TC03000056.hg.1	-5.25	1.59E-05
OSGIN1	TC16000652.hg.1	-5.09	4.13E-08
RNVU1-15	TC01003152.hg.1	-4.96	7.07E-05
CSF1	TC01000955.hg.1	-4.93	2.00E-04
RND3	TC02002419.hg.1	-4.89	4.48E-05
MDM2	TC12002437.hg.1	-4.88	8.72E-07
PINCR	TC0X000205.hg.1	-4.85	2.30E-03
TMEM217	TC06001682.hg.1	-4.84	9.12E-05
DKK1	TC10000350.hg.1	-4.77	1.55E-02
PLIN2	TC09002418.hg.1	-4.76	1.20E-03

PSTPIP2	TC18000477.hg.1	-4.74	5.55E-05
TMEM171	TC05000345.hg.1	-4.7	1.98E-06
TNFRSF10B	TC08002257.hg.1	-4.63	9.47E-05
	TC01001686.hg.1		
SEMA5A	TC05002857.hg.1	7.98	1.50E-06
ADH1C	TC04001411.hg.1	8	2.97E-05
CPA4	TC07000810.hg.1	8.1	2.41E-02
COL14A1	TC08000700.hg.1	8.41	2.00E-04
PDE1A	TC02004734.hg.1	8.51	4.00E-03
ADAMTS5	TC21000892.hg.1	8.58	2.20E-02
CD248	TC11001962.hg.1	8.61	3.24E-02
OMD	TC09001335.hg.1	8.63	1.72E-05
LOC100507516	TC08002329.hg.1	8.65	1.00E-04
FMOD	TC01003722.hg.1	8.7	1.15E-02
SLC40A1	TC02002614.hg.1	8.7	3.80E-03
ZNF704	TC08002397.hg.1	8.86	3.40E-03
SLIT3	TC05002043.hg.1	8.92	7.04E-05
ALDH1L2	TC12003055.hg.1	9.02	2.00E-04
ITGBL1	TC13001260.hg.1	9.04	8.00E-04
SERPIng1	TC11002677.hg.1	9.06	3.32E-02
PLTP	TC20000893.hg.1	9.27	8.76E-06
TMEM119	TC12001937.hg.1	9.33	2.87E-05
GXYLT2	TC03003359.hg.1	9.34	3.17E-07
LGR5	TC12000624.hg.1	9.36	4.88E-05
TNNT2	TC01006036.hg.1	9.84	5.80E-03
STMN1	TC01005350.hg.1	9.88	8.01E-06
LAMA2	TC06000976.hg.1	10.11	4.85E-09
SOX4	TC06002615.hg.1	10.15	2.52E-02
MFAP4	TC17001243.hg.1	10.22	1.96E-06
OGN	TC09001334.hg.1	10.69	4.95E-05
PDE5A	TC04001504.hg.1	10.73	2.38E-05
LRRC17	TC07000668.hg.1	10.85	9.92E-05
FHL1	TC0X001889.hg.1	10.87	1.40E-03
SULF1	TC08000456.hg.1	11.06	2.51E-02
CTHRC1	TC08000646.hg.1	11.28	4.24E-06
RFTN2	TC02002649.hg.1	11.43	7.00E-04
MGP	TC12002778.hg.1	11.63	2.00E-04
EDNRA	TC04002255.hg.1	11.74	9.40E-03
OLF ml1	TC11000149.hg.1	11.85	2.90E-03
DMD	TC0X002026.hg.1	12.2	6.87E-06
ASPN	TC09001336.hg.1	12.47	2.43E-02
ABCA8	TC17001825.hg.1	13.48	1.72E-07
FMO2	TC01001488.hg.1	13.52	7.00E-04
ALPK2	TC18000542.hg.1	13.84	9.35E-07
SLC6A4	TC17001326.hg.1	15.53	5.50E-03
MYH10	TC17002479.hg.1	16.36	1.19E-06
CDON	TC11003400.hg.1	16.9	2.20E-03
SESN3	TC11003298.hg.1	19.37	6.00E-04
NAV2	TC11002591.hg.1	19.69	1.78E-06
CSRP2	TC12001755.hg.1	25.85	1.40E-06

C7	TC05000187.hg.1	47.35	3.68E-06
PTGIS	TC20000927.hg.1	54.83	3.42E-09
ADH1B	TC04001410.hg.1	203.57	3.95E-05

negative value: more abundant in Normoxia+Rhein, positive value: more abundant in Normoxia

Table 33: Top 50 up- and downregulated transcripts in the comparison Hypoxia vs Hypoxia+Rhein (1.5-fold, p-value < 0.05)

Hypoxia vs Hypoxia+Rhein			
Symbol	**ID**	**Expr Fold Change**	**Expr p-value**
HMOX1	TC22001089.hg.1	-6.55	3.50E-03
GDF15	TC19000356.hg.1	-6.1	4.01E-02
NPTX1	TC17002817.hg.1	-5.25	4.00E-03
PLIN2	TC09002418.hg.1	-4.5	8.70E-03
PTCH1	TC09002677.hg.1	-4.42	3.72E-05
NXPH4	TC12002397.hg.1	-3.92	2.50E-02
EPHX1	TC01001856.hg.1	-3.21	3.30E-03
CXCL12	TC10001212.hg.1	-3.2	4.95E-02
PTGR1	TC09001484.hg.1	-3.08	2.30E-03
SLC7A11	TC04001570.hg.1	-3.08	3.09E-02
TCF7	TC05002628.hg.1	-2.95	6.60E-03
CA12	TC15001541.hg.1	-2.93	2.00E-02
JADE2	TC05002634.hg.1	-2.93	3.00E-04
PIM1	TC06000541.hg.1	-2.93	4.70E-03
SMAD3	TC15002251.hg.1	-2.93	1.50E-03
FNDC10	TC01002103.hg.1	-2.91	5.73E-05
LOC730101	TC06000657.hg.1	-2.88	5.20E-03
ZCCHC14	TC16001332.hg.1	-2.79	4.00E-03
S1PR3	TC09002901.hg.1	-2.74	1.53E-02
NQO1	TC16001225.hg.1	-2.69	2.38E-02
GDF5	TC20000797.hg.1	-2.68	3.19E-02
HCN2	TC19000010.hg.1	-2.67	1.15E-05
NYNRIN	TC14000169.hg.1	-2.67	3.10E-02
ORAI3	TC16000363.hg.1	-2.61	1.60E-03
PFKFB3	TC10001860.hg.1	-2.6	1.50E-02
NDRG1	TC08001659.hg.1	-2.54	3.70E-03
TGFBR3	TC01005631.hg.1	-2.53	9.10E-03
TRIM52	TC05003395.hg.1	-2.52	2.49E-02
ABCC1	TC16000193.hg.1	-2.51	7.80E-03
REV3L	TC06002017.hg.1	-2.49	3.90E-03
TXN	TC09001473.hg.1	-2.49	1.20E-05
PGD	TC01000129.hg.1	-2.47	7.70E-03
MGAT5	TC02003597.hg.1	-2.4	4.01E-02
RPS19	TC19000587.hg.1	-2.4	1.03E-02
G6PD	TC0X002294.hg.1	-2.38	1.70E-03
MGST1	TC12000207.hg.1	-2.37	2.10E-03
PPM1D	TC17000739.hg.1	-2.37	4.10E-03
HIPK2	TC07003195.hg.1	-2.36	2.23E-02
ZNF426-DT	TC19001971.hg.1	-2.36	2.69E-05

ADNP2	TC18000268.hg.1	-2.33	8.00E-04
STOM	TC09001547.hg.1	-2.33	1.34E-02
LOC100507599	TC22001045.hg.1	-2.32	2.80E-03
FAM162A	TC03000631.hg.1	-2.31	4.00E-04
LPCAT2	TC16000455.hg.1	-2.31	1.36E-02
NMRAL2P	TC03001014.hg.1	-2.3	1.91E-02
BRI3	TC07000585.hg.1	-2.29	1.38E-02
NLGN2	TC17000093.hg.1	-2.29	9.60E-03
HMGA1	TC06002746.hg.1	-2.27	4.50E-03
NKAPL	TC06000280.hg.1	-2.27	1.20E-03
PHF1	TC06002739.hg.1	-2.27	7.10E-03
	TC08001432.hg.1		
ARHGDIB	TC12001278.hg.1	3.48	2.08E-02
MFAP5	TC12001181.hg.1	3.59	2.28E-02
SEMA3C	TC07001559.hg.1	3.61	4.19E-02
RHOJ	TC14000377.hg.1	3.73	1.68E-02
INHBA	TC07002911.hg.1	3.75	3.86E-02
LAMA2	TC06000976.hg.1	3.76	1.50E-05
CCDC71L	TC07003105.hg.1	3.77	8.40E-03
OLFM2	TC19001155.hg.1	3.87	4.19E-02
GNA14	TC09001226.hg.1	3.9	1.10E-03
DMD	TC0X002025.hg.1	3.91	3.60E-03
CCL2	TC17000383.hg.1	3.94	5.80E-03
PDCD1LG2	TC09000038.hg.1	3.98	2.00E-04
PTGIS	TC20000927.hg.1	4.02	9.90E-03
TOP2A	TC17001462.hg.1	4.02	2.30E-03
MYH11	TC16000898.hg.1	4.23	6.30E-03
ASPM	TC01003662.hg.1	4.29	3.00E-04
AEBP1	TC07000273.hg.1	4.34	3.00E-04
SORBS2	TC04002887.hg.1	4.37	6.30E-03
ALPK2	TC18000542.hg.1	4.47	9.00E-04
ITGBL1	TC13001260.hg.1	4.54	1.09E-02
RTKN2	TC10001324.hg.1	4.54	4.15E-02
TAGLN	TC11002894.hg.1	4.57	2.21E-02
MYH10	TC17002479.hg.1	4.58	7.10E-03
CNTNAP1	TC17000533.hg.1	4.63	5.25E-06
NPR3	TC05000144.hg.1	4.68	4.14E-02
ART4	TC12002777.hg.1	4.7	6.00E-04
PAK3	TC0X000544.hg.1	4.76	2.10E-03
CTHRC1	TC08000646.hg.1	4.78	1.90E-03
ALDH1L2	TC12003055.hg.1	4.81	4.40E-03
INMT	TC07003391.hg.1	4.84	1.00E-04
C7	TC05000187.hg.1	5.13	3.62E-02
NEK2	TC01006091.hg.1	5.22	1.30E-03
CNN1	TC19000202.hg.1	5.38	2.05E-02
COL12A1	TC06001879.hg.1	5.89	5.00E-04
OMD	TC09001335.hg.1	5.95	1.10E-03
FMO2	TC01001488.hg.1	6.08	3.71E-02
RASSF2	TC20000587.hg.1	6.18	6.43E-05
STMN1	TC01005350.hg.1	6.21	3.00E-04

ADGRF5	TC06003667.hg.1	6.28	4.95E-02
ANLN	TC07000235.hg.1	6.51	7.00E-04
PRPS1	TC0X000526.hg.1	6.69	1.70E-02
FMOD	TC01003722.hg.1	6.9	3.42E-02
TNC	TC09001517.hg.1	7.02	2.60E-03
MKI67	TC10001756.hg.1	7.29	1.00E-04
TNNT2	TC01006036.hg.1	7.62	1.23E-02
CTGF	TC06002112.hg.1	8.45	2.11E-02
ELN	TC07002404.hg.1	8.53	4.30E-03
OGN	TC09001334.hg.1	9.15	1.80E-03
PSAT1	TC09000358.hg.1	10.04	2.05E-02

negative value: more abundant in Hypoxia+Rhein, positive value: more abundant in Hypoxia

Table 34: Top 50 up- and downregulated transcripts in the comparison Hypoxia vs Hypoxia+Rhein (1.5-fold, p-value < 0.05)

Hypoxia+Rhein vs Normoxia+Rhein			
Symbol	**ID**	**Expr Fold Change**	**Expr p-value**
GDF15	TC19000356.hg.1	-33.22	4.00E-04
PSAT1	TC09000358.hg.1	-13.46	1.69E-02
CXCL8	TC04002067.hg.1	-12.92	1.63E-02
ITGA2	TC05000218.hg.1	-11.48	3.30E-03
ULBP1	TC06001089.hg.1	-10.01	1.30E-03
ANXA10	TC04000836.hg.1	-9.9	8.84E-07
PTGS2	TC01003638.hg.1	-9.55	7.00E-04
SLC7A11	TC04001570.hg.1	-9.22	1.00E-04
IL1A	TC02002218.hg.1	-8.86	8.00E-04
ITGB3	TC17002878.hg.1	-8.38	2.00E-04
ODC1	TC02001570.hg.1	-8.29	3.50E-05
BMP2	TC20000067.hg.1	-7.61	2.26E-05
TBX2	TC17002307.hg.1	-7.46	2.30E-03
TNFAIP6	TC02000937.hg.1	-7.33	1.00E-03
LIF	TC22000647.hg.1	-7.24	2.87E-05
NAV3	TC12000656.hg.1	-7	7.00E-04
HBEGF	TC05001854.hg.1	-6.95	8.40E-06
AKR1B10	TC07002600.hg.1	-6.68	2.60E-03
LOC100126784	TC11001483.hg.1	-6.63	8.57E-07
PAQR5	TC15000635.hg.1	-6.44	3.04E-02
MTHFD2	TC02003335.hg.1	-6.22	7.40E-03
HSD11B1	TC01001750.hg.1	-6.05	4.50E-03
NCEH1	TC03002008.hg.1	-5.97	1.00E-04
DUSP6	TC12001796.hg.1	-5.8	4.41E-05
NPC1	TC18000413.hg.1	-5.79	3.00E-04
TFPI2	TC07001611.hg.1	-5.53	3.99E-02
HMGA2	TC12002424.hg.1	-5.36	6.54E-05
PNP	TC14000056.hg.1	-5.28	2.14E-06
MET	TC07000722.hg.1	-5.23	3.07E-02
GDNF	TC05002960.hg.1	-5.2	2.62E-02
RND3	TC02002419.hg.1	-5.2	2.22E-05

IL1B	TC02002219.hg.1	-5.17	4.38E-02
SLC7A1	TC13000523.hg.1	-5.15	4.30E-03
CCND1	TC11000718.hg.1	-5.12	6.00E-04
TMEM38B	TC09000539.hg.1	-5.09	7.00E-04
EPGN	TC04000413.hg.1	-4.92	2.69E-05
CCL2	TC17000383.hg.1	-4.85	7.80E-03
CDK17	TC12001845.hg.1	-4.81	2.23E-05
TMEM171	TC05000345.hg.1	-4.62	3.45E-06
TMEM181	TC06003155.hg.1	-4.43	6.87E-07
TNFRSF10A	TC08001052.hg.1	-4.43	5.45E-06
XYLT1	TC16001788.hg.1	-4.41	4.70E-03
SLC3A2	TC11002708.hg.1	-4.35	2.10E-03
EVI2B	TC17001341.hg.1	-4.32	4.37E-02
GLA	TC0X001219.hg.1	-4.29	2.00E-04
DDX21	TC10000413.hg.1	-4.28	1.54E-06
DUSP4	TC08002271.hg.1	-4.23	1.37E-02
LINC00520	TC14001162.hg.1	-4.23	3.00E-04
ASNS	TC07001630.hg.1	-4.21	2.48E-02
PLA2G4A	TC01001607.hg.1	-4.19	8.99E-05
	TC22000248.hg.1		
MGP	TC12002778.hg.1	4.21	2.06E-02
LOC730101	TC06000657.hg.1	4.24	2.60E-03
SESN3	TC11002205.hg.1	4.24	4.85E-02
BNIP3	TC10001769.hg.1	4.29	1.29E-05
PLTP	TC20000893.hg.1	4.29	8.00E-04
CPA4	TC07000810.hg.1	4.33	2.14E-02
FHL1	TC0X001889.hg.1	4.38	2.36E-02
ACKR4	TC03000716.hg.1	4.39	2.46E-02
MASP1	TC03003257.hg.1	4.43	1.94E-02
PGK1	TC0X000425.hg.1	4.48	9.45E-08
CDH11	TC16001165.hg.1	4.5	2.00E-04
S100A10	TC01005824.hg.1	4.69	1.10E-03
COLEC12	TC18000273.hg.1	4.72	1.40E-03
SLC40A1	TC02002614.hg.1	4.76	1.47E-02
MUC1	TC01005848.hg.1	4.77	1.66E-02
ABCA8	TC17001825.hg.1	4.79	1.10E-03
MN1	TC22000620.hg.1	4.79	4.19E-06
COL4A4	TC02004836.hg.1	4.81	1.40E-03
ZNF704	TC08002397.hg.1	4.84	1.19E-02
FAXDC2	TC05001973.hg.1	4.85	4.83E-06
MYH10	TC17002479.hg.1	4.92	1.00E-04
NXPH4	TC12002397.hg.1	4.95	2.11E-02
IGHD3-22	TC14002222.hg.1	5.01	3.57E-02
IGFBP3	TC07001355.hg.1	5.03	4.49E-05
PCDH18	TC04001565.hg.1	5.18	4.00E-04
SOX4	TC06000135.hg.1	5.29	2.15E-02
PDK1	TC02001031.hg.1	5.47	2.86E-07
PDGFRB	TC05003303.hg.1	5.68	9.60E-03
CGNL1	TC15000437.hg.1	5.7	6.50E-05
P4HA1	TC10001398.hg.1	5.83	1.53E-07

SLIT3	TC05002043.hg.1	6.01	1.00E-03
ANOS1	TC0X000829.hg.1	6.02	8.30E-03
PPL	TC16000838.hg.1	6.1	1.14E-02
C7	TC05000187.hg.1	6.17	3.60E-03
NAV2	TC11002591.hg.1	6.52	2.00E-04
SYNPO2	TC04000609.hg.1	6.66	2.00E-04
AK4	TC01004452.hg.1	6.94	1.50E-03
GYS1	TC19002540.hg.1	7.31	6.23E-05
DACT1	TC14000353.hg.1	7.32	5.00E-04
COL14A1	TC08000700.hg.1	7.58	7.00E-04
LINC01151	TC08001572.hg.1	8.41	2.01E-05
LRRC17	TC07000668.hg.1	8.97	2.00E-04
GXYLT2	TC03003359.hg.1	9.53	2.38E-06
NDUFA4L2	TC12001622.hg.1	10.04	3.60E-03
PPP1R3C	TC10001522.hg.1	11.31	9.41E-05
CDON	TC11003400.hg.1	11.77	1.44E-02
ADH1B	TC04001410.hg.1	18.89	6.70E-03
CSRP2	TC12001755.hg.1	21.56	1.03E-05
PTGIS	TC20000927.hg.1	30.07	5.12E-08

negative value: more abundant in Normoxia+Rhein, positive value: more abundant in Hypoxia+Rhein

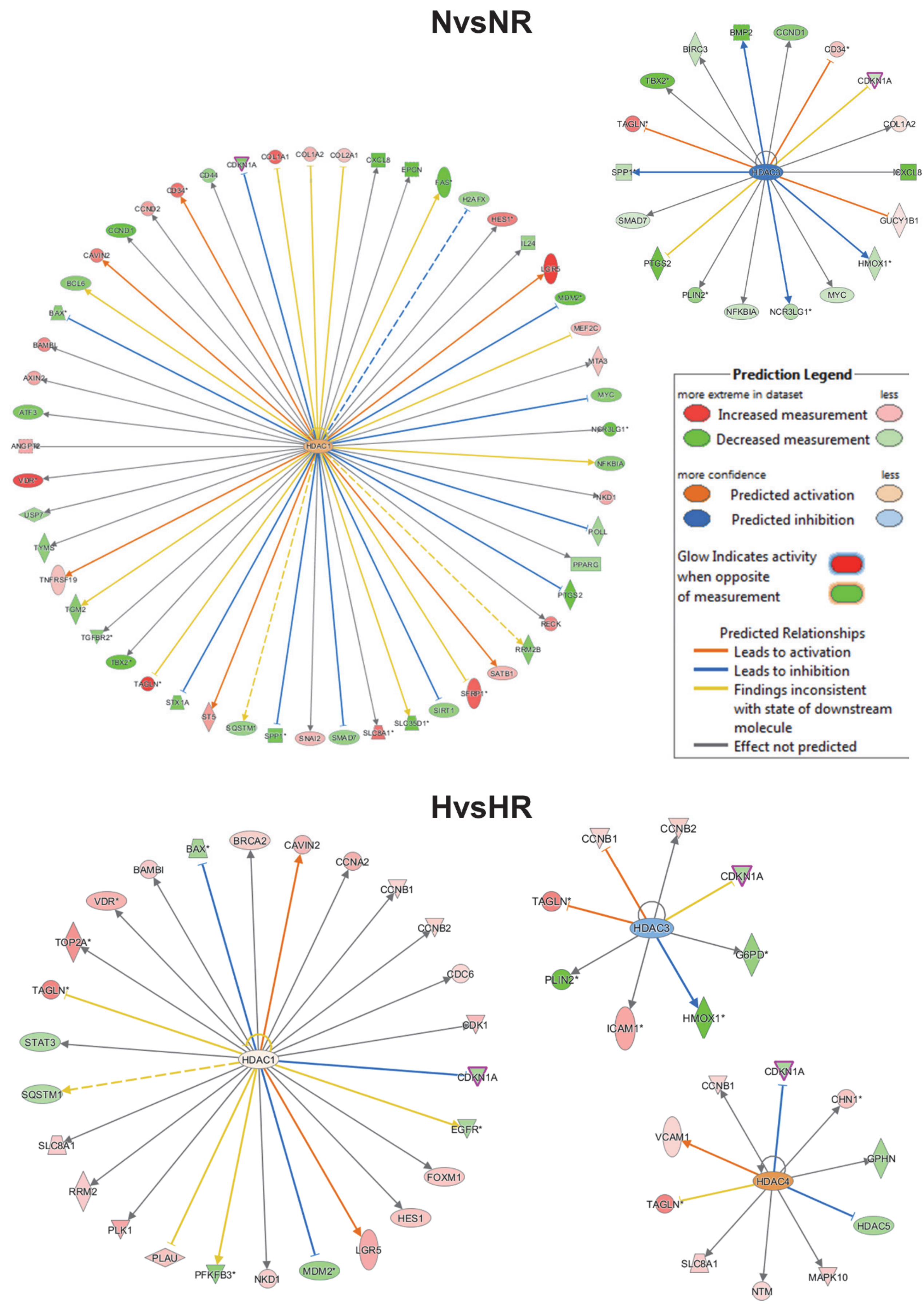

Figure 47: Upstream analysis of various HDACs and relation to CDKN1A in the transcriptomes of Rhein-treated vs untreated normoxic and hypoxic HCF-v

Eidesstattliche Erklärung

Ich versichere an Eides Statt, dass die Dissertation von mir selbständig und ohne unzulässige fremde Hilfe unter Beachtung der „Grundsätze zur Sicherung guter wissenschaftlicher Praxis an der Heinrich-Heine-Universität Düsseldorf“ erstellt worden ist. Die Dissertation wurde in der vorgelegten oder in ähnlicher Form noch bei keiner anderen Institution eingereicht. Ich habe bisher keine erfolglosen Promotionsversuche unternommen.

(Datum)	(David Monteiro Barbosa)